A low-cost photonic method for monitoring different production processes involving contaminating materials using Fourier-Transform Raman spectroscopy

Valentin Ortega Clavero

UNIVERSITÉ DE STRASBOURG

ÉCOLE DOCTORALE 269 MATHÉMATIQUES, SCIENCES DE L'INFORMATION ET DE L'INGÉNIEUR (MSII)

Laboratoire des sciences de l'ingénieur, de l'informatique et de l'imagerie (ICube) UMR7357

THÈSE présentée par:
Valentin ORTEGA CLAVERO

soutenue le : **11 juillet 2014**

pour obtenir le grade de : **Docteur de l'université de Strasbourg**
Discipline/ Spécialité : **Instrumentation et Procédés Photoniques**

TITRE de la thèse : A low-cost photonic method for monitoring different production processes involving contaminating materials using Fourier-Transform Raman spectroscopy.

THÈSE dirigée par:	
M. MEYRUEIS Patrick	Prof. Dr., Université de Strasbourg
RAPPORTEURS:	
M. SCHNECKENBURGER Herbert	Prof. Dr., Université Aalen (HS. Aalen)
M. GALAVIZ YAÑEZ Guillermo	Prof. Dr., Université Autonome de Basse-Californie
AUTRES MEMBRES DU JURY:	
M. SCHRÖDER Werner	Prof. Dr. rer.nat., Université de Offenburg (HS. Offenburg)
M. JAVAHIRALY Nicolas	Ass. Prof. Dr., Université de Strasbourg
M. CURTICAPEAN Dan	Prof. Dr., Université de Offenburg (HS. Offenburg)

[This page intentionally left blank]

TITLE:
A low-cost photonic method for monitoring different production processes involving contaminating materials using Fourier-Transform Raman spectroscopy

By ORTEGA CLAVERO, Valentin

Télécom Physique Strasbourg - Laboratoire des sciences de l'ingénieur, de l'informatique et de l'imagerie (ICube), Groupe EPhot

UNIVERSITÉ DE STRASBOURG

University of Strasbourg

in collaboration with the **University of Applied Sciences Offenburg**

Thesis submitted in partial fulfillment of the requirements for the degree of

Doctor of the University of Strasbourg

Members of the Committee:

THESIS DIRECTED BY:	
MEYRUEIS Patrick, Prof. Dr.	University of Strasbourg, Thesis Director
SCHRÖDER Werner, Prof. Dr. rer.nat.	Offenburg University of Applied Sciences, Thesis Co-Director
EXTERNAL REVIEWERS:	
SCHNECKENBURGER Herbert, Prof. Dr.	Aalen University
GALAVIZ YAÑEZ Guillermo, Prof. Dr.	Autonomous University of Baja California
CO-ADVISERS:	
JAVAHIRALY Nicolas, Ass. Prof. Dr.	University of Strasbourg, Thesis Co-Director
CURTICAPEAN Dan, Prof. Dr.	Offenburg University of Applied Sciences

Doctoral thesis publicly defended on July 11th, 2014

UNIVERSITÉ DE STRASBOURG

Valentin ORTEGA CLAVERO
A low-cost photonic method for monitoring different production processes involving contaminating materials using Fourier-Transform Raman spectroscopy

Hochschule Offenburg
University of Applied Sciences

Résumé

Dans ce travail de thèse, un spectomètre FT-Raman a été développé dans l'intention de mesurer les substances dangereuses de manière propre et durable permettant à l'utilisateur un cout d'utilisation réduit (approche low cost). Dans ce but, le système FT- Raman a été développé en utilisant une combinaison originale de composants conventionnels d'optoméchatronique avec laquelle nous proposons une méthode d'évaluation du spectre. Ce système FT-Raman proposé n'inclut aucun composants spécialisé coûteux et permet la détection de la diffusion Raman et le suivi du chemin optique.

Le dispositif a été testé lors d'analyses d'une série de composants chimiques standards largement utilisés dans la spectroscopie Raman (certains d'entre eux sont connus pour leur impact négatif sur la santé et l'environnement). Les résultats du spectre obtenus avec notre dispositif ont confirmé les valeurs signalées par le spectre Raman standar. Une comparaison des spectres avec des appareils commercialisés mesurants le FT-Raman a été également faite, et les résultats indiquent que notre combinaison de composants conventionnels et l'application de notre méthode d'évaluation peuvent être utilisées dans certaines surveillances d'applications demandant un haut degré de précision et la résolution sans toutefois présenter la charge financière que l'achat d'un instrument classique de mesure pourrait représenter.

Résumé en anglais

In this doctoral research project, a Fourier Trasform Raman spectrometer (FT-Raman spectrometer) instrument has been developed with the intention to perform the monitoring of certain materials having a contaminating and harmful nature, in a clean and sustainable manner, and without significantly affecting the financial aspect of the user (low-cost approach). For this purpose, the proposed FT-Raman system has been developed by using an original combination of conventional hardware (optomechatronics) parts and a method that we propose for spectral evaluations. In this FT-Raman system that we propose no specialized and costly hardware parts for optical path compensation, Raman scattering detection, optical path tracking, etc. have been used.

The proposed FT-Raman device has been tested by analyzing a series of chemical components widely used in Raman spectroscopy as standard reference materials (some of them are also known due to their negative impact on health or on environment). The resulting spectra obtained using our proposed device have greatly agreed with the values of the standard Raman spectra. A comparison with spectral outputs from state-of-the-art FT-Raman devices has been also performed. These results indicate that our "flexible" combination of conventional hardware parts and the applied evaluation method that we propose can be used in certain monitoring applications requiring a high degree of frequency accuracy and spectral resolution, without having the burden of a considerable expenditure that such a non-dispersive "classical" instrument might represent.

To my parents, my brothers, and my little Gaspar.

Planck, Fourier and Raman said:

$$E = h\nu = \frac{hc}{\lambda},$$

$$P = \alpha E,$$

$$P = \alpha_0 E_0 \cos 2\pi\nu_0 t + E_0 Q_j^\circ \left(\frac{\delta\alpha}{\delta Q_j}\right) \frac{\cos 2\pi(\nu_0 + \nu_j)t + \cos 2\pi(\nu_0 - \nu_j)t}{2},$$

$$E(\nu) = \int_{-\infty}^{\infty} I(x) e^{-i2\pi\nu x}\, dx,$$

$$\Delta\nu_j[cm^{-1}] = \left(\frac{1}{\lambda_0(\text{nm})} - \frac{1}{\lambda_j(\text{nm})}\right) \times \left(\frac{10^7\,\text{nm}}{\text{cm}}\right) ...$$

... and then there were spectra!

Acknowledgements

I would like to sincerely thank my directing advisers Prof. Patrick Meyrueis (University of Strasbourg) and Prof. Werner Schröder (Offenburg University of Applied Sciences) for all the support and trust that they have granted to me during the development of this doctoral project. I greatly appreciate this unique opportunity.

In the same manner, I would like to express my gratitude to Mr. Nicolas Javahiraly for guiding me into the researching and publishing world.

I also would like to thank Prof. Dan Curticapean (Offenburg University of Applied Sciences) for facilitating and guiding me in several of the practical matters concerning this research project during the last four years.

A very, very special thanks to Mr. Andreas Weber for all his invaluable, outstanding, detailed and precise support, in both technical and non-technical aspects, during the development of the present doctoral project. Merci vielmals!

Likewise, I would like to thank my two external reviewers Prof. Herbert Schneckenburger and Prof. Guillermo Galaviz Yañez for taking the time and for their commitment on the reviewing and evaluation of this doctoral thesis. I really appreciate your feedback and the constructive criticism that you have gave me.

During the development of the different stages of this research project, I received the kindly support from several persons to whom I am also very grateful:

- Mr. Stefan Staiger and Mr. Raimund Lehmann for their technical support on certain hardware and software components of our FT-Raman spectromenter.

- Prof. Klemens Lorenz, Prof. Bernd Spangenberg, Mrs. Regina Brämer, Mrs. Barbara Milz, and Mrs. Andrea Seigel from the *Chemie, Analytik, Umweltanalytik* laboratory from the Offenburg University of Applied Sciences for all the support on providing and storing the required chemical samples and laboratory material used to perform the presented Raman spectral analysis.
- Mr. Ernst Klausmann, Mr. Heiko Haufe, and Mr. Thomas Retzlik from the *Elektrowerkstatt/Mechanische Werkstatt* for providing the components for the proper functioning of the FT-Raman spectrometer.
- Prof. Christoph Nachtigall for all the feedback that I have received about my doctoral project.
- Mrs. Alexandra Raunig for her invaluable support collecting, storing and transporting the samples of commercial gasoline-ethanol blends.
- Mrs. Vera Vanié and Mrs. Richarde Clauss for their support on the proper edition of the sections of this document written in French language.
- Mr. Gernot Höhne, from Bruker Optik GmbH, and Mr. Andreas Schmid, from Thermo Fisher Scientific GmbH, for providing the Raman spectral measurements of the materials used for comparing the frequency accuracy of our FT-Raman device.
- My dear friends Dulce Carolina, Ursula, Elsa Daniela Guadalupe, Laura Angelica, Elvia, Razia (Rima), Matthias, and Jutta, for their outstanding cheering support during these last few years.

Finally, I would also like to extend my infinite appreciation to my dear friend Mrs. Carolina Alicia Islas Sedano for all her support on the financial aspect of the project, and for her long and sincere friendship. It also goes to Mrs. Aurea Miranda for her incredible and disinterested support representing me in certain bureaucratic formalities.

This doctoral project has been partially funded by the *Consejo Nacional de Ciencia y Tecnología* - CONACYT (National Council for Science and Technology), which is a decentralized agency of the Mexican Public Federal Administration. My most sincere recognition to all the personnel involved on the management of my specific case. It has been an excellent work!

Contents

List of figures

List of tables

Glossary

ADC	Analog-to-digital converter; device for extracting discrete samples from continuous signals.
APD	Avalanche photodiode; Highly sensitive semiconductor device with internal gain, that is widely used to perform photon counting.
ASTM	American Society for Testing and Materials.
DOF	Depth of field; distance, that defines where the portrayed object at the detector remains sharp.
FCS	Fluorescence correlation spectroscopy; Fluorescence spectroscopy-based measurement technique for the correlation analysis of the fluorescence intensities of materials in fluctuating state.
FFT	Fast Fourier transform; Algorithm widely used to compute the discrete Fourier transform.
FT-Raman	Fourier transform Raman spectroscopy; non-dispersive type of Raman spectroscopy that uses an interferometer in order to separate the different Raman lines in frequency.
FTIR	Fourier-Transform infrared spectroscopy.
FWHM	Full width at half maximum.
GAC	Green analytical chemistry; Philosophy inside green chemistry, that is *concerned with the development of analytical procedures that minimize consumption of hazardous reagents and solvents, and maximize safety for operators and the environment* [39].
HeNe-laser	Helium-neon laser; laser in the visible region of the spectrum (632.8 nm) commonly used in FT-Spectroscopy as reference, among several other applications.
IR	Infrared; region of the electromagnetic spectrum having larger wavelengths than those found in the visible region of the spectrum. The definition of this spectral region can vary depending on the author.
ISR	Interrupt service routine; callback subroutine running in the firmware of a microcontroller.

MTBE	Methyl tert-butyl ether; organic chemical compound mainly used as octave booster in fuel for gasoline engines.
NIR	Near infrared; region of the electromagnetic spectrum (region from 800 nm to 2500 nm). This region definition can vary depending on the author.
OPD	Optical path difference; difference in the optical path generated by the moving mirror inside the Michelson interferometer.
PCB	Printed circuit board; mechanical and electrical support for electronic circuits.
PID-controller	Proportional-Integral-Derivative controller; controller loop of negative feedback widely applied in control systems.
PMT	Photomultiplier tubes; Highly sensitive vacuum devices used to detect low intensities of light.
PWM	Pulse-width modulation.
RISC	Reduced instruction set computing; simplified instruction set for micro-controllers.
SERS	Surface-enhanced Raman spectroscopy; surface-sensitive method used to enhance the Raman scattering with small-size particles or metal.
SPAD	Single photon avalanche diode.
SPR-Spectroscopy	Surface Plasmon Resonance Spectroscopy; spectroscopic technique, that uses thin layers of metal (generaly Au and Ag) to improve the optical absorption.
SVD	Singular value decomposition; factorization method for real and complex matrices.
UV/VIS	Ultraviolet/Visible spectroscopy; instrumental analytical technique based on the absorption (or reflectance) of light in the range of 200 nm to 800 nm of the electromagnetic spectrum.

Extended summary in French (Résumé détaillé)

Introduction et le but de la recherche

Au cours des dernières années, l'importance du ≪développement écologiquement durable≫ a considérablement augmenté sous la pression de facteurs juridiques et sociaux. Des réglementations dans les différents domaines ont été mises en œuvre afin de réduire ou d'éliminer les effets nocifs des activités humaines, spécialement celles liées aux productions industrielles. En raison de ses propriétés inhérentes[1], la spectroscopie Raman répond à plusieurs des exigences du développement durable. Cette technique spectroscopique peut être utilisée pour le suivi de certains procédés chimiques utilisés dans l'industrie, d'une façon sûre et propre.

La spectroscopie FT-Raman a montré ses capacités et son efficacité dans un grand nombre de domaines d'études [93, 164, 38]. Aujourd'hui, la fabrication et la commercialisation de dispositifs FT-Raman sont devenus une niche de marché significative. Ces appareils sont fabriqués par une quantité réduite de fabricants dans le monde (par exemple Thermo Scientific, Bruker Optics et Jasco corporation). Cependant, les technologies intégrées dans ces instruments, la plupart du temps sont protegees par des brevets et sont considérablement spécialisés et très coûteuses. Le budget d'achat d'un tel dispositif commercial, ou des modules spécifiques, se situe entre 80,000 € et 125,000 €.

Dans ce travail de thèse, un spectomètre FT-Raman a été développé dans l'intention de mesurer les substances dangereuses présentes dans divers environnements de manière propre et durable tout en permettant à l'utilisateur un cout d'utilisation réduit (approche low cost adaptée notament à des pays à revenus faibles). Dans ce but, le système FT-

[1] La spectroscopie Raman est non destructive, non invasive, normalement il ne nécessite aucune préparation de l'échantillon, etc.

Raman que nous proposons a été développé en utilisant une combinaison originale de composants conventionnels d'optoméchatronique disponibles sur étagère à prix modérés. Nous proposons une méthode d'évaluation de spectre adaptée à un tel dispositif. Le système FT-Raman que nous proposons n'inclut aucun composant spécialisé coûteux et permet la détection de la diffusion Raman et le suivi du chemin optique de façon efficace.

L'importance de cette recherche s'appuie sur les besoins constants des méthodes de mesure efficaces de suivi. Dans les cas optimaux, une telle méthode devrait être aussi attractive en termes de ressources financières requises. Actuellement, ces méthodes ont tendance à être écologiquement durable en raison d'un ensemble de raisons, y compris les exigences sociales, politiques et juridiques. Spectroscopie FT-Raman est l'une des techniques d'analyse qui peuvent être appliqués à la réalisation de ces exigences, car il est propre, non-invasive et non destructive, et normalement il n'a pas besoin de préparation des échantillons avant la mesure. En outre, les utilisateurs potentiels prêts à appliquer cette technique, ne seraient pas accablés par les coûts élevés d'un tel dispositif et à l'impossibilité de modifier l'instrument à volonté en cas de processus de prototypage.

Il a été procédé en vertu de l'hypothèse que nous avons formulée, que certaines parties dédiées et complexes d'un spectromètre FT-Raman peuvent être enlevées ou remplacées par des composants génériques beaucoup plus simples et moins coûteux. Le système que nous proposons fonctionne en combinaison avec des algorithmes mathématiques, génériques afin de réduire considérablement les inconvénients financiers liés des dispositifs Raman sans affecter les capacités de mesure globale et la flexibilité nécessaire dans certaines applications d'analyse.

Les sections suivantes donnent un aperçu de la composition originale, et du fonctionnement spécifique du système FT-Raman que nous proposons. Un ensemble de principaux résultats obtenus à l'aide de l'instrument FT-Raman que nous avons conçu et réalisé est également fourni. Nous avons effectués quelques mesures, afin de valider la précision de notre méthode de mesure et caractérisation. Enfin, nous présentons quelques conclusions sur les résultats préliminaires que nous avons obtenu. Certains aspects originaux du système proposé et les résultats expérimentaux obtenus sont discutés.

Mise en oeuvre du système

Nous avons d'abord effectué des simulations d'évaluations spectrales en utilisant des effets non ideaux des composants méchaniques classiques. Après cela, nous avons fait la

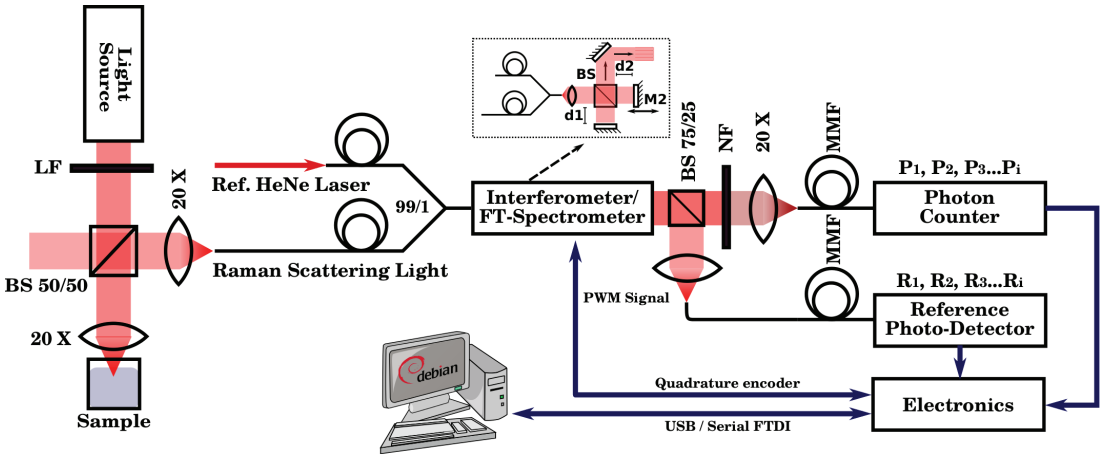

Figure 1: Schéma général du prototype proposé. Ce système FT-Raman se compose d'une combinaison originale de composants bon marché, aidé par une méthode d'exploitation fondée sur le ré-échantillonnage des signaux générés et diffusés en retour que nous recueillons.

simulation du procédé d'évaluation spectrale que nous proposons. Les résultats des simulations ont montré des valeurs de fréquence satisfaisants en comparaison avec les valeurs de référence dans la littérature. Nous avons également calculé la puissance lumineuse qui peut être acceptée par le système que nous avons proposé.

Le système FT-Raman qui est proposé est présenté dans la figure 1. Il se compose d'une combinaison de composants exploitée selon une méthode fiable d'évaluation spectrale (sur la base d'un ré-échantillonnage des données acquises) que nous avons développé. Les principaux composants de ce système sont: un interféromètre de Michelson, un photo-détecteur de référence (S5973-01 Hamamatsu) et une unité de comptage de photons . Le système FT-Raman que nous proposons a une configuration optique minimal, adaptée à l'excitation de l'échantillon analysé. La lumière Raman diffusée en retour de l'échantillon est couplée, dans l'interféromètre de Michelson de notre dispositif FT-Raman, par des fibres optiques multimodes.

La figure 2 montre la structure de base de l'unité de comptage de photons appartenant au système FT-Raman proposé. Cet appareil a été construit en utilisant une Si APD Excelitas Technologies C30921SH (0.25 mm de zone active) [1], un amplificateur de signal et un circuit de conditionnement de signal (Bascule de Schmitt). Un filtre réjecteur (NF) a été placé en face de la lentille d'entrée du dispositif de comptage de photons. Le but de

[1] Il s'agit d'un ancien appareil du fabricant Perkin-Elmer.

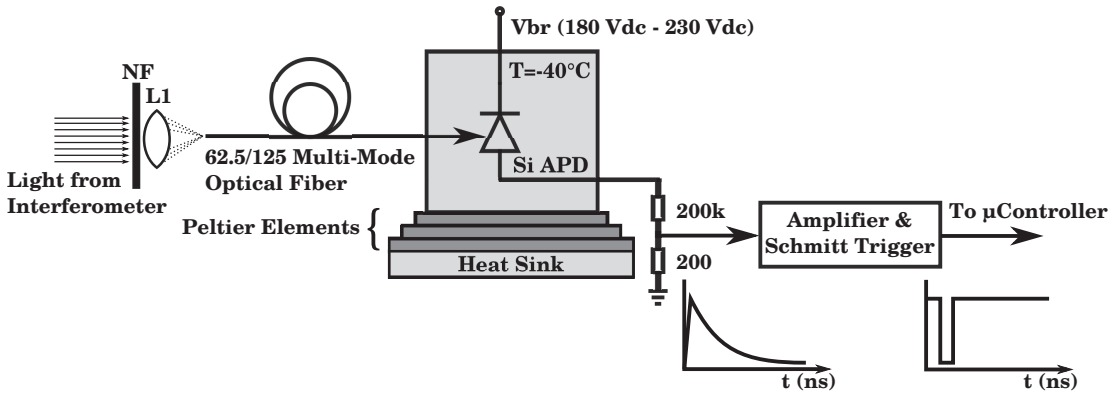

Figure 2: Schéma de l'unité de comptage de photons. Le signal obtenu juste après le circuit passif d'extinction du signal conditionné et connecté au micro-dispositif de commande de lecture peut également être observé.

notre choix est d'éliminer une grande proportion de la diffusion de Rayleigh de sorte que le dispositif de comptage de photons ne pénètre pas dans un état de saturation.

Afin de réduire le taux de ≪comptage noir≫ et d'améliorer la réceptivité de l'unité de comptage de photons, le Si APD est refroidi à l'aide d'un élément Peltier en trois étapes. La température de fonctionnement est comprise entre $-35\,°C$ et $-40\,°C$. On extrait la chaleur générée de l'élément Peltier aux trois étapes une pompe à chaleur; il est constitué d'un circulateur d'eau en aluminium (40 mm par 40 mm). Cette pompe à chaleur peut être facilement substituée par un air refroidi dissipateur de chaleur, si nécessaire. Dans notre développement de ce dispositif, il a également été évité l'incorporation d'éléments sophistiqués (par exemple système de refroidissement d'azote, circuits d'extinction actifs, pièces mécaniques, etc.)

Les effets indésirables des composants mécaniques non idéaux ont été surmontés en utilisant un procédé de ré-échantillonnage évaluation spectrale que nous avons adapté au système. Cette méthode d'évaluation est constitué d'un échantillonnage strictement simultanée de la lumière Raman et des signaux de référence monochromes au cours de la procédure de mesure.

Les échantillons distribués dans le temps, sont transformés en signaux de type distribués régulièrement dans l'espace, avant l'application de la transformation de Fourier. Ce type d'évaluation a donné un niveau élevé de précision de la fréquence detectée au spectromètre FT-Raman.

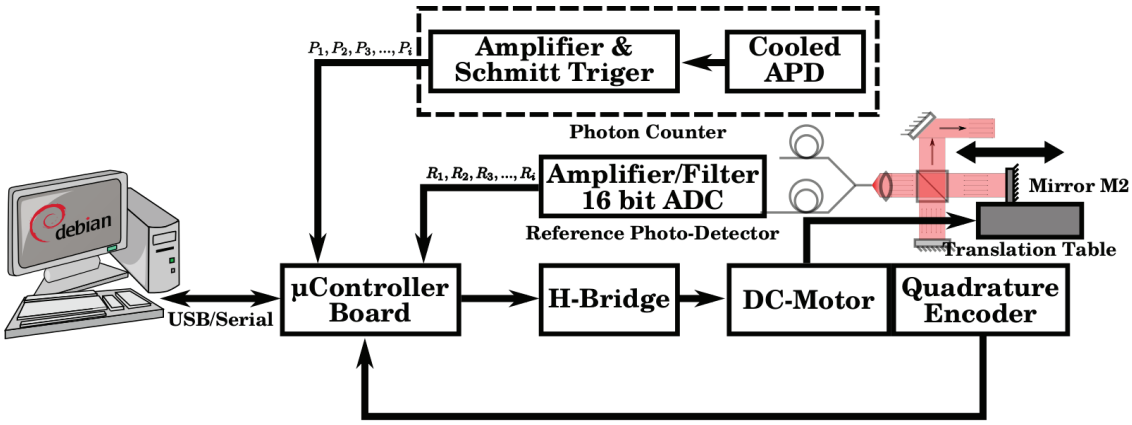

Figure 3: Schéma de l'interconnexion électrique du système FT-Raman.

Les trois composants principaux du système FT-Raman (l'interféromètre de Michelson, le dispositif de comptage de photons et le photodétecteur de référence) doivent interagir de telle sorte qu'un déplacement en douceur du miroir mobile M_2 de l'interféromètre de Michelson est effectuée, tandis que l'échantillonnage du dispositif de comptage de photons et le photo-détecteur de référence a lieu simultanément. Cela est nécessaire pour l'acquisition précise des échantillons temps également répartis pour notre méthode d'évaluation. En outre, le système doit être capable d'interpréter les commandes de l'interface utilisateur, et transmettre les données acquises au cours des processus de mesure.

Le noyau de bas niveau du système FT-Raman est un micro-contrôleur ATmega32 [10] d'Atmel®, qui est intégré dans une carte d'évaluation[1]. Les informations complémentaires à propos de cette carte d'évaluation peuvent être trouvées dans l'annexe B. Ce dispositif fournit la fonctionnalité de base requise pour entraîner tous les éléments du système FT-Raman d'une manière coordonnée. La figure 3 représente les différents dispositifs autour du micro-contrôleur avec les connexions électriques et logiques respectives nécessaires au bon fonctionnement du spectromètre FT-Raman que nous avons mis au point.

Le spectromètre FT- Raman proposé est contrôlé à l'aide de deux outils logiciels innovants que nous avons élaborés: une application d'interface utilisateur "personnalisée" et un logiciel de firmware pour le fonctionnement de bas niveau de l'instrument. L'évaluation des données collectées est également réalisé par un ensemble de scripts que nous avons spécialement adaptés à cet effet. Nous avons conçu ces outils en utilisant une plate-forme

[1]Carte d'évaluation mise au point à l'Université des Sciences Appliquées d'Offenburg sous le nom de *MK_Board*

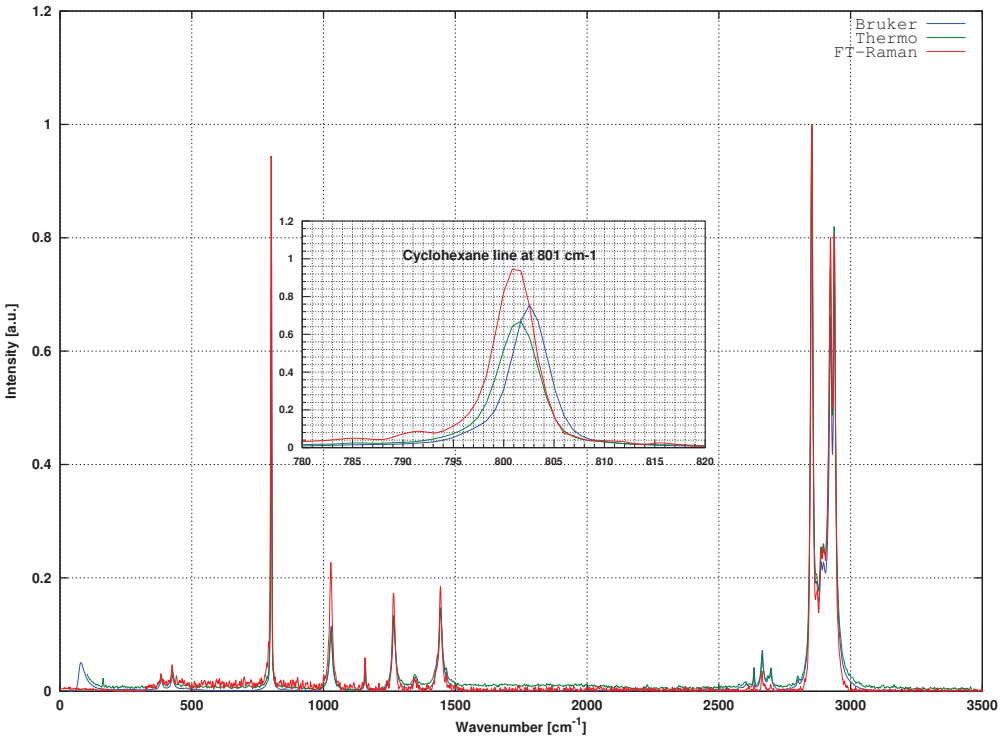

Figure 4: Spectres Raman de cyclohexane obtenus en utilisant le spectromètre FT-Raman prototype que nous proposons et les deux dispositifs commerciaux FT-Raman de Bruker Optik GmbH et Thermo Fisher Scientific GmbH.

GNU/Linux Debian (mais il peut être facilement porté sur d'autres plates-formes) en utilisant différentes GNU C/C++ compilateurs, les bibliothèques et le langage interprété GNU/Octave [42]. Outre un fonctionnement adéquat du système proposé , ces outils logiciels ont également permis de contribuer à la robustesse, à la flexibilité, à la sécurité et à la fiabilité de notre système [72, p. 395] [135, p. 8] [183, p. 63-64] . Tout cela a été accompli sans avoir à supporter la charge financière et la dépendance technique que les solutions commerciales pourraient comporter représenter [108, p. 3-4].

Validation expérimentale des résultats

Afin de valider la précision des spectres Raman obtenu avec le prototype FT-Raman que nous avons conçu et réalisé, une série de mesures se rapportant aux cyclohexanes, au toluène et au benzène ont été effectués. Les spectres collectés Raman de cyclohexane

Table 1: Pics Raman et intensités relatives de la norme [109] comparés à la simulation et spectre Raman observé dans le cyclohexane (C_6H_{12}) en utilisant la configuration que nous proposons dans la figure 1 et les deux appareils commerciaux.

Standard [cm^{-1}] / Rel. Int.	Simulation	FT-Raman	MultiRam	Nicolet iS50
384.1 ± 0.78 / 0.02	383.9 / 0.01	382.9 / 0.03	384.9 / 0.02	384.1 / 0.02
426.3 ± 0.41 / 0.03	425.6 / 0.02	425.8 / 0.04	427.3 / 0.02	426.6 / 0.03
801.3 ± 0.96 / 0.95	800.6 / 0.93	801.1 / 0.94	802.5 / 0.75	801.7 / 0.67
1028.3 ± 0.45 / 0.15	1027.3 / 0.12	1027.6 / 0.22	1028.8 / 0.11	1027.8 / 0.10
1157.6 ± 0.94 / 0.06	1157.3 / 0.05	1157.3 / 0.06	1158.9 / 0.04	1157.6 / 0.03
1266.4 ± 0.58 / 0.14	1265.6 / 0.13	1265.7 / 0.17	1267.3 / 0.13	1266.3 / 0.12
1444.4 ± 0.30 / 0.12	1443.9 / 0.11	1443.8 / 0.18	1444.6 / 0.14	1443.9 / 0.14
2664.4 ± 0.42 / 0.08	2664.0 / 0.07	2664.2 /0.03	2664.9 / 0.07	2664.1 / 0.06
2852.9 ± 0.32 / 1.00	2852.3 / 1.00	2852.8 / 1.00	2853.0 / 1.00	2852.3 / 1.00
2923.8 ± 0.36 / 0.58	2924.0 / 0.41	2923.7 / 0.80	2924.0 / 0.66	2923.2 / 0.74
2938.3 ± 0.51 / 0.67	2937.3 / 0.56	2938.3 / 0.80	2938.8 / 0.71	2937.9 / 0.81
Corr. coef.(freq.)	0.999999939	0.999999971	0.999999956	0.999999971
Euclidean dist.(freq.)	2.1354	1.7944	2.5338	1.3153

Table 2: Pics Raman et intensités relatives de la norme [109] comparés à la simulation et spectre Raman observé dans le toluène (C_7H_8) en utilisant la configuration que nous proposons dans la figure 1 et les deux appareils commerciaux.

Standard [cm^{-1}] / Rel. Int.	**FT-Raman**	**MultiRam**	**Nicolet iS50**
521.7 ± 0.34 / 0.10	521.1 / 0.18	522.2 / 0.17	521.4 / 0.22
786.6 ± 0.40 / 0.39	786.1 /0.54	787.1 / 0.54	786.3 / 0.59
1003.6 ± 0.37 / 1.00	1003.3 / 1.00	1004.2 / 1.00	1003.4 / 1.00
1030.6 ± 0.36 / 0.23	1030.1 / 0.27	1031.1 / 0.27	1030.4 / 0.28
1211.4 ± 0.32 / 0.26	1210.3 / 0.20	1211.2 / 0.21	1210.2 / 0.25
1605.1 ± 0.47 / 0.06	1604.8 / 0.12	1605.7 / 0.11	1604.7 / 0.14
3057.1 ± 0.63 / 0.30	3055.2 / 0.33	3055.6 / 0.40	3054.8 / 0.67
Corr. coef.(freq.)	0.999999911	0.999999897	0.999999898
Euclidean dist.(freq.)	2.4207	1.9391	2.6739

(C_6H_{12}) et du toluène (C_7H_8) ont été comparés aux spectres fondés sur la liste de la norme ASTM *Standard Guide for Raman Shift Standards for Spectrometer Calibration* [7], qui est largement utilisé dans ce domaine [109, 93, 181]. L'ASTM a rapporté des lignes Raman ayant une déviation de fréquence $\leq \pm 1.0\,cm^{-1}$. Le spectre Raman d'un troisième matériau, le benzène (C_6H_6), a été également recueilli en utilisant notre prototype.

Outre la comparaison des spectres fournis par notre méthode d'évaluation par rapport aux valeurs bien établies "classiques" de mesure Raman, nous avons également effectué l'analyse Raman de ces trois mêmes composés chimiques à l'aide de deux appareils FT-Raman disponibles dans le commerce (Bruker Optik GmbH MultiRAM et Thermo Fisher Scientific GmbH Nicolet iS50). Les spectres obtenus en utilisant notre dispositif prototype FT-Raman et la méthode d'évaluation que nous avons proposé, ont montré une bonne

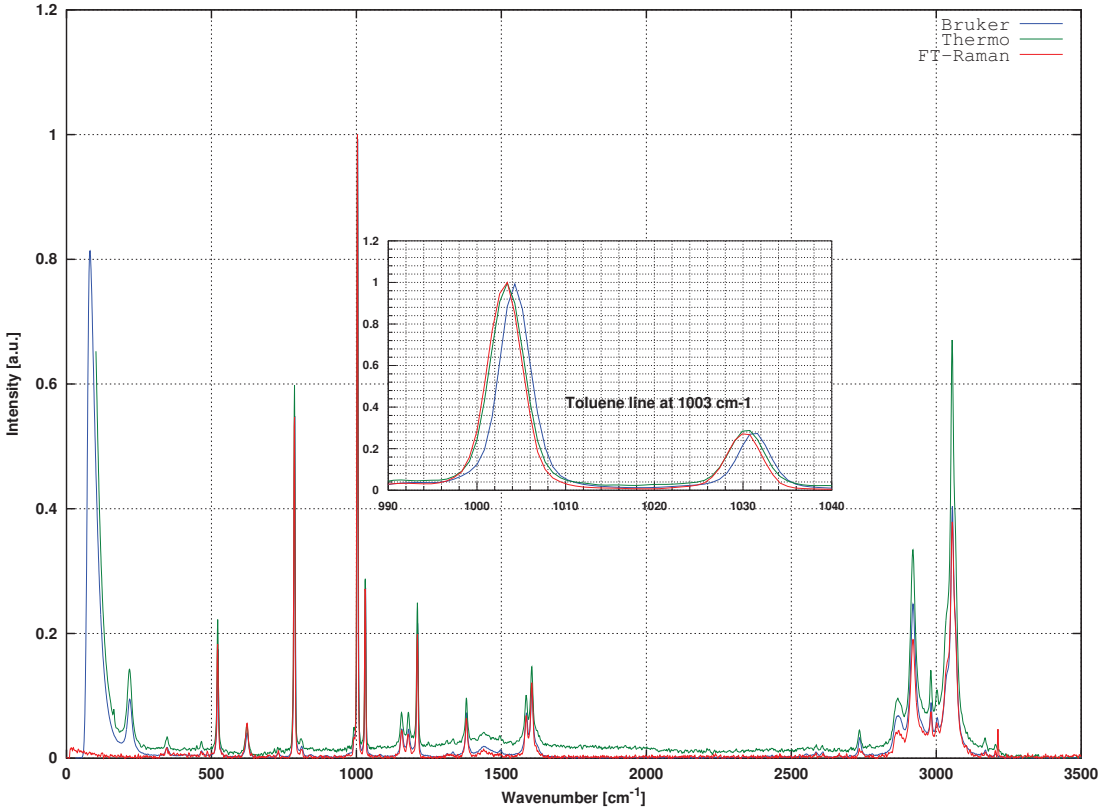

Figure 5: Spectres Raman de toluène obtenus en utilisant le spectromètre FT-Raman prototype que nous proposons et les deux dispositifs commerciaux FT-Raman de Bruker Optik GmbH et Thermo Fisher Scientific GmbH.

ressemblance des spectres obtenus avec le dispositif que nous proposons avec ceux obtenus en utilisant les dispositifs FT-Raman disponibles dans le commerce.

La figure 4 montre les spectres de cyclohexane, et un gros plan de la région autour de son pic de Raman caractéristique à $801\,\mathrm{cm}^{-1}$. Les trois spectres Raman ont montré une ressemblance remarquable avec les données standards. Les positions des fréquences et des intensités relatives ont également montrées un degré élevé de similitude. Le tableau 1 indique les positions des fréquences et les intensités relatives des raies principales Raman du cyclohexane. Des résultats similaires en termes de précision en fréquence et en intensité relative, ont été obtenus en utilisant les deux autres composés chimiques mentionnés.

La figure 5 montre les spectres de toluène, et un gros plan de la région autour de son pic de Raman caractéristique à $1003\,\mathrm{cm}^{-1}$. Les trois spectres Raman ont montré aussi

une ressemblance remarquable avec les données standards obtenues. Les positions des fréquences et des intensités relatives ont également montré un degré élevé de similitude. Le tableau 2 indique les positions de fréquences et les intensités relatives des raies principales de Raman du toluène.

Afin de déterminer certaines capacités techniques du système FT-Raman que nous avons conçu, un ensemble de mesure portant sur des échantillons chimiques impliquant des mélanges éthanol-carburant et leurs additifs connexes, les fluides hydrauliques, et les boissons alcoolisées ont été entreprises avec le dispositif et les methodes que nous proposons. Ces analyses Raman ont montré un degré remarquable de précision de la fréquence identifiée, et un niveau satisfaisant de succès sur la quantification et de détection des matériaux présents dans les échantillons.

Conclusions générales

La combinaison originale des composants bon marché et de la méthode d'évaluation spectrale que nous avons proposé a montré de bons résultats, en termes de précision de la fréquence mesurée (qui est d'une grande importance pour éviter les erreurs d'interprétation) et de l'intensité relative dans, la gamme comprise entre $0\,\mathrm{cm}^{-1}$ et $3500\,\mathrm{cm}^{-1}$. Les résultats obtenus à l'aide de l'instrument FT- Raman que nous avons conçu et réalisé sont totalement en accord avec les données Raman standards proposées par l'ASTM. Les spectres Raman des deux matériaux d'étalonnage que nous avons utilisés (cyclohexane et le toluène) ont montré un degré élevé de corrélation, et une quantité réduite de la distance euclidienne dans la comparaison aux valeurs des spectres Raman standard. Le dispositif que nous proposons utilisant des composants bon marchés classiques et des applications logicielles "open-source" complétés par la méthode d'évaluation spectrale par ré-échantillonnage que nous proposons, peut donc être utilisé pour l'analyse chimique des matériaux nocifs dans de composés, sans même avoir un contact direct avec les échantillons de ces composés.

Il n'est cependant pas possible de négliger certains artefacts et des inconvénients pratiques que l'instrument FT-Raman réalisé présente encore, notamment en raison de sa nature de prototype. Néanmoins, la comparaison des spectres de cyclohexane, du toluène et du benzène, obtenus à l'aide de notre appareil FT-Raman, comparés à ceux acquis à l'aide de deux instruments FT-Raman commerciaux suggère qu'il est possible d'effectuer une analyse spectrale FT-Raman exacte en réduisant significativement les coûts et la

complexité du dispositif Raman utilisé. Bien que certaines informations sur les aspects financiers des spectromètres FT-Raman disponibles dans le commerce puisse être obtenue, la comparaison directe liée aux coûts des dispositifs commerciaux par rapport au faible coût du dispositif que nous proposons ne peut être correctement réalisé. Toutefois, les paramètres de coûts de notre prototype FT-Raman indiquent une atténuation forte de l'impact financier que représente le prix des instruments commerciaux de marché dans les applications d'analyse Raman.

Bien que notre instrument FT-Raman a été développé sur une base à faible coût (les pièces de matériel coûtent environ entre 15000 € et 20000 € en fonction de la configuration du système FT-Raman), et que certaines données financières relatives aux différentes parties qui constituent notre système FT-Raman ont été obtenues, une évaluation correcte des paramètres financiers liés n'a pas puétre correctement réalisée. De même, nous avons été en mesure d'obtenir seulement des prix sur le marché de certains instruments FT-Raman disponibles dans le commerce. Cependant, une bonne approximation du prix de production ne peut pas être définie, car les fabricants ne divulguent pas ce type de données détaillées.

Pour les raisons mentionnées ci-dessus, nous n'avons pas été en mesure de fournir une comparaison fiable et précise des aspects financiers impliqués dans le développement de notre système FT-Raman et l'un des appareils disponibles dans le commerce FT-Raman. Néanmoins, en prenant simplement en compte les prix du marché (ou le coût général approchée de production décrits dans les rapports annuels de Bruker et Thermo Fisher Scientific [37, 194, 195]), on peut conclure que le dispositif Raman que nous proposons peut être un choix légitime pour certaines applications et d'environnements qui nécessitent une analyse FT-Raman à faible coût.

En résumé, notre système FT-Raman bon marché obtenu en utilisant une combinaison originale des matériaux classiques et de notre méthode d'évaluation, pourrait trouver sa place dans de nouveaux secteurs et domaines d'applications, où la spectroscopie Raman a seulement été que évoquée en théorie, mais pas mise en pratique, à cause de coûts d'acquisition, d'exploitation et d'entretien peu attractifs (spécialement dans le cas où les dispositifs Raman non dispersifs sont nécessaires).

Comme exemples de ces secteurs ou domaines d'applications où les dispositifs de Raman à faible coût peuvent être introduits, on peut citer les cas suivants:

- Petites et moyennes entreprises. Ces types d'entreprises sont généralement soumises à un contrôle strict de leurs budgets, spécialement dans les pays ayant des économies émergentes ou pauvres.

- Régions géographiquement isolées. Dans ces lieux, où aucun accès approprié à l'entretien ou de maintenance est disponible, notre dispositif peut être réparé ou exploité par l'utilisation de pièces classiques facilement disponibles.

- Environnements d'éducation. Une telle évolution permettrait un meilleur accès aux spectromètres Raman non-dispersifs dans les laboratoires de diplômés, de premier cycle et niveaux secondaire de scolarité, où l'entretien et le fonctionnement de l'appareil peut être effectué par un personnel technique qualifié sur place.

- Environnements non contrôlés et accessibles. Applications située dans des endroits où des installations spéciales pour le contrôle de certaines conditions ne sont pas disponibles (par exemple, les salles propres, contrôle de température et d'humidité, l'isolement de certains niveaux de vibrations mécaniques).

La liste des cas possibles, où ce prototype d'instrument FT-Raman pourrait être introduite, peut être étendue, ainsi que la combinaison de facteurs qui pourraient répondre aux besoins spécifiques d'une application de surveillance, y compris notre technologie. La décision finale sur cette question dépend directement du niveau des prestations que l'utilisateur peut obtenir dans son application à l'aide de ce type d'instrument que nous avons réalisé.

Plusieurs améliorations et adaptations, en fonction d'une application de contrôle plus généralisée, doivent être réalisées afin d'obtenir un appareil FT-Raman entièrement fonctionnel dans pratiquement tous les cas d'exploitation possible connus. En outre, le système FT-Raman que nous proposons peut être encore réduit en taille et en complexité (notamment par l'élimination des parties mécaniques mobiles, le remplacement du laser HeNe par un module de diode laser, etc), ce qui va contribuer à une réduction supplémentaire de des ressources financières dédiées a une tel dispositif qui deviendra ainsi une technologie à très faible coût.

Chapter 1. Introduction

The analysis of materials through Raman spectroscopy has found a variety of fields of study and this technique is not longer exclusively used under laboratory environments. Several of the technical drawbacks that Raman spectroscopy faced in the past two decades have been overcome. This vibrational technique is nowadays applied in fields like pharmaceutics, art conservation, forensic science, material science, biology, diagnostics, nanotechnology, etc. We have witnessed an increasing number of applications involving the use of Raman analysis in the last few years. This has been the result of several technical improvements of some components that are normally embedded in these type of instruments (e.g. optical components, the excitation light sources, and the light detectors).

In recent years the importance of the so called "ecologically sustainable development" has grown dramatically under the pressure of legal and social factors. Regulations in different areas of interest have been implemented in order to reduce, or eliminate, the harmful effect of human activities, specially the ones related to industrial productions. Due to its inherent properties[1], Raman spectroscopy matches several of the requirements of these types of sustainable development policies. This spectroscopic technique can be applied for the monitoring of certain chemical processes used in the industry in a safe and clean manner.

Some industrial processes apply already some type of chemical analysis methods using Raman spectroscopy [93, 181, 181], and the amount and types of applications are constantly increasing. There are two types of Raman spectrometer devices: dispersive (gratings/CCD) and non-dispersive (FT-Raman) Raman spectrometers. The application requirements dictate the type of device that must be employed. McCreery [109, p. 149, p. 221] has given a wide technical explanation about these two types of instruments, and he has also included some typical applications examples for each type of device. Lewis and Edwards [93] also mention different fields of application of Raman spectroscopy and different instrumental implementations. Despite the similarity of the information extracted from a sample using any of these two types of Raman spectrometers, certain applications

[1] Raman spectroscopy is non-destructive, non-invasive, normally it requires no sample preparation, etc.

requiring better fluorescence avoidance, frequency accuracy, and higher resolution values, must rely on non-dispersive spectrometers or commonly known as Fourier transform Raman spectrometer (FT-Raman spectrometer).

Nowadays the fabrication of FT-Raman devices has turned into a market niche and these devices are manufactured by a reduced amount of companies around the world. By performing a quick research, we can verify that companies as Thermo Scientific, Bruker Optics and Jasco corporation are part of this compact group of producers of FT-Raman spectrometers. They also provide the software applications required for the operation of the FT-Raman instruments. The capabilities of these instruments can easily be ported to laboratories and, up to some extent, to production processes. However, the technology embedded in these instruments (e.g. optical path system tracking, moving mirror systems, light detectors, etc.), are most of the time under the protection of patents and tend to be greatly specialized and highly-priced. The cost range of such devices, or special modules, lies between 80,000 € and 125,000 €[1].

As a consequence, the aforementioned issues impact unfavorably on a potential user that would intend to implement FT-Raman spectroscopy in different ways: firstly, the variety and amount of devices available are rather limited; a second aspect is directly related to the financial capacity of the user, since the initial cost of the device, and sometimes the expenses generated by the maintenance of the device too, can result in a drawback. A third aspect is the lack of accessibility and flexibility of both hardware and software due to the encapsulation nature of such a devices. As it normally occurs with commercial instruments, the warranty is void if the hardware is modified in any way. Furthermore, the proprietary software for operating these types of devices is designed to accomplish certain specific tasks and the behavior of such end-user programs cannot be adapted at will.

The purpose of this research project is *to provide a low-cost FT-Raman system that achieves spectral measurements having similar (or better in an ideal case) frequency accuracy characteristics in comparison with those obtained by using the commercially-available counterparts*. This FT-Raman system that we propose must be accomplished without substantially affecting the financial capacities of the end user, and allowing an easy and low cost maintenance. The system must also offer certain level of flexibility that allows changes in order to adapt the FT-Raman device to the requirements of certain specific measurements.

[1] Approx. prices as of April 2014

The hardware of this prototype consist, basically, of the following parts: a conventional Michelson interferometer (used as FT-spectrometer), a self-developed photon counter and a photo-detector for optical accurate optical path extraction. There exist several literary sources from different authors describing the general aspects of interferometry in which this project relies on. Hariharan, Saleh and Teich offer a general description about the interferometric techniques applied in the proposed FT-Prototype [68, 67, 160]. These authors have made a clear reference to the physical effects of both coherent and partially coherent light inside interferometers without providing additional information about the instrumentation issues present in interferometric devices.

Some of the essential aspects of Fourier transform spectrometry have been explained by Kauppinen and Partanen[84]. The authors have provided the mathematical background required when real applications based on interferometry are used (e.g. instrumental and sampling effects, optical path calculations, truncating of interferograms, etc.). Similar material by Sumner P. Davis and Brault can be found in [187]. Unlike Kauppinen and Partanen, Sumner P. Davis and Brault have concentrated on Fourier transform spectroscopy in general, and on the application of digital signal processing methods on the data obtained in order to achieve better performance. Griffiths and De Haseth cover some technical details about Fourier transform infrared spectroscopy in [62] (also applicable to FT-Raman spectroscopy) that can be applied not only to high-cost instruments but also to less expensive devices (therefore it has been considered as very suitable for the purposes of this project). They have also included extensive explanations about the main three instrumental advantages of Fourier transform spectrometers: Multiplex advantage (Fellgett's advantage), Connes advantage and Throughput advantage (Jacquinot's advantage). Some specific application cases according to the measurement requirements are presented for each of these advantages. A complete chapter has been devoted to FT-Raman spectroscopy and some references to more concrete problems that can be found too.

Introductory literature about Raman spectroscopy can be found in [50] by Ferraro et al.. These authors have described the basic theory, the instrumental techniques normally used in Raman spectroscopy and some of the applications for this vibrational spectroscopic technique. A distinctive feature of this source can be observed in the detailed literary reference they offer for every section presented. McCreery has large experience in the field of Raman spectroscopy, with more than 200 publications. Different important aspects of

modern Raman spectroscopy (clearly differentiating between dispersive and non-dispersive spectroscopy), specially for chemistry applications, can be found in [109], which has been widely used as reference. In this work McCreery has exhibited a practical combination of historical background, basic theory, technical analysis of instruments and some of the application fields of Raman spectroscopy. Sasic had recently published, in [165], material concerning Raman spectroscopy from the pharmaceutical perspective. The basic theory and additional material have been partially taken from McCreery and Ferraro et al. among others. Larkin has made a suitable description of the complementary nature of infrared and Raman spectroscopy and its implications in [92]. This text offers a practical guide to properly interpret and understand the different vibrational groups among chemical compounds in Raman and infrared spectroscopy.

Specific issues affecting the spectral data obtained from FT-Raman spectrometers have been discussed in two different papers by Bowie et al. in [16, 17]. Both, the effects of the instruments and the effects of the analyzed sample on the spectrum, are broadly described. Additionally, Bowie et al. have included these materials in a deeper way as part of a well known handbook dedicated to vibrational spectroscopy [18].

In this thesis project, it has been proceeded under the hypothesis that certain dedicated and complex parts of a FT-Raman spectrometer can be removed or replaced by generic components and mathematical algorithms in order to significantly reduce the cost-related drawbacks without affecting the overall measurement capabilities and the flexibility required for prototyping purposes in certain monitoring applications.

The significance of this research relies on the constant needs of efficient measurement methods for process monitoring. In the optimal cases, such a method should be also attractive in terms of the required financial resources. At the present time, these methods tend to be ecologically sustainable due to a set of reasons, including social, political and legal demands. FT-Raman spectroscopy is one of the analytical techniques that can be applied for accomplishing these requirements, since it is clean, non-invasive, non-destructive, and normally it does not need sample preparation prior to the measurement. Furthermore, potential users willing to apply this technique, would not be burdened with high costs for such a device and with the impossibility of modifying the instrument at will in case of prototyping processes.

Chapter 2 provides an overview about different technical aspects of some of the most used spectroscopic techniques, including Raman spectroscopy. In this chapter we have

also justified the reasons supporting our decision to concentrate our efforts in this type of instrumentation.

In chapter 3 we have shown the different types of spectral evaluation that can be employed in order to extract FT-Raman spectra, as well as the issues that might appear when these type of evaluations are performed in systems having no-specialized hardware parts (with no ideal linear properties). We also present in this chapter the evaluation method that we propose in order to support the use inexpensive and conventional hardware parts in our FT-Raman design.

Chapter 4 presents the different conforming parts of the practical implementation of the proposed FT-Raman system. This part of the research report also offers an overview about the functioning and control of the FT-Raman system that we have developed.

Chapter 5 offers the first set of validating Raman measurements that we have obtained by using our FT-Raman spectrometer. These frequency accurate and precise validating measurements obtained (compared to the standard Raman spectra from the literature), have been performed by analyzing three different chemical compounds that possess well-known and highly defined Raman spectra. Two of these chemical compounds (cyclohexane and toluene) belong to the calibration materials reported by the American Society for Testing and Materials (ASTM). The third material (benzene) also has a suitable Raman spectrum that permits the verification in frequency of the obtained Raman lines. Additionally, the Raman spectra of these three materials, obtained by using our implemented FT-Raman devices, have been also compared to the Raman spectra obtained by using two different commercially-available and last generation FT-Raman spectrometers.

Chapter 6 reports some results related to the use of our FT-Raman spectrometer for the spectral monitoring of different materials that involve potentially harmful properties, such as gasoline-ethanol blends, hydraulic fluids, and some agave-derived alcoholic beverages. These measurements have helped in determining some of the measurement capacities and also some of the limitations of our FT-Raman system.

Finally, chapter 7 presents the general conclusions that have been able to be drawn during the conception, realization and validation of this research project. We also offer an outlook for the possible further developments of the type of technical solution that we propose.

Additionally, a listing of the publications generated during this research project, and two appendixes about certain technical aspects of our FT-Raman device have been in-

cluded. Appendix A reports the expected amount of Raman scattered light in our theoretical photon counting device. This information has been referenced in section 3.3. Appendix B shows additional information about the different comprising stages of the implemented FT-Raman system, that has been reported in chapter 4.

Chapter 2. Literature review

As previously stated in chapter 1, our work addresses certain aspects of Raman spectroscopy in a non-dispersive arrangement for its application on the monitoring of certain materials. The arguments for choosing this type of analytical technique and this specific type of instrumental arrangement relies on the analysis of different factors (including technical, financial and practical reasons). Some of these arguments will be introduced in the next subsections.

In the instrumental chemistry analysis there are a vast amount of methods of analysis. Furthermore, the quantity of bibliographic data in this field is large and it constantly increases. Our review has been focused on some of the most used instrumental methods based on the interaction of molecules with electromagnetic radiations in the infrared, the near infrared, the visible and the ultraviolet spectrum. These techniques share some common features, and are widely used in analytical chemistry. Raman spectroscopy and infrared spectroscopy have received special emphasis as they are considered to be complementary measurement techniques. In the literature these two measurement techniques can be found in a variety of contexts. Nevertheless, we have limited our review to the cases of monitoring processes applications.

In recent years the environmental consciousness has taken an important role in our society organizations and it has strongly affected the way instrumental chemistry is applied. Nowadays it is rather difficult to find human activities that are not affected by this trend. In the case of industrial processes it is required to observe certain regulations that are related to the ecological aspects of its surrounding environment. Nevertheless, it is important not to disregard, that the ultimate goal of any industrial process is to generate products or provide services in a cost-efficient fashion.

A philosophy that tries to include all the aforementioned aspects (including the ecological, the economical, the educational and the ethical aspects) is the so called green analytical chemistry (GAC). In [39] edited by de la Guardia and Garrigues it is possible to find the main concepts of this philosophy. GAC strategies, similarly to the environmental-friendly processes required by legal authorities and other institutions, are concerned with

the reduction or complete substitution of hazardous materials and with the direct measurement of untreated samples, as in the case of Raman spectroscopy (in [39, ch. 6] several contact-less techniques examples are also described).

2.1 Ultraviolet/Visible spectroscopy

Ultraviolet/Visible spectroscopy (UV/VIS) is an instrumental analytical technique based on the absorption (or reflectance) of light in the range of 200 nm to 800 nm of the electromagnetic spectrum. Table 2.1 shows the spectral ranges of the UV/VIS and NIR spectroscopies. The definition of these values can vary and they depend on the author and in the field of study. UV/VIS spectroscopy plays an important role in different research fields, including environmental analysis where measurements with low concentrations (higher than 0.5 mg/L) can be performed [221].

In this analytical technique, the absorbed energy generate electronic transitions of the materials (with σ, π and n electrons) contained in the sample under observation. These transition occur because the UV/VIS radiation has enough energy to promote the change of electronic state of the absorbing molecule or ion [9]. In figure 2.1 a diagram with the possible electronic transitions can be observed. In the electronic energy transitions there are also a large number of rotational and vibrational energy states. A direct consequence of this is the generation of broad bands in the spectrum (spectral low resolution), which lead to severe drawbacks when complex chemical compounds are analyzed, e.g. sample separation or preparation prior to the measurement.

The quantitative absorbance in UV/VIS spectroscopy is calculated by using Beer-Lambert law. This provides a non-complex method to determine the type of molecule or ion in a specific sample. However, the Beer-Lambert law can be used linearly only under certain circumstances, since different effects appear when the concentration of analyte increases. In these cases additional calibration curves must be applied.

The instrumental setup for a UV/VIS spectrometer or spectrophotometer consists of a light source (e.g. tungsten or xenon lamp and more recently LED in the visible region), a monochromator for light separation and a light detector. Additionally these type of setups are equipped with samples and references holders. The configuration can differ from one setup to another: single-beam, double-beam, etc. Modern instruments are provided with a computer terminal in order to provide signal processing capabilities and the storage of the data. In certain cases, it also provides the measurement control sequence.

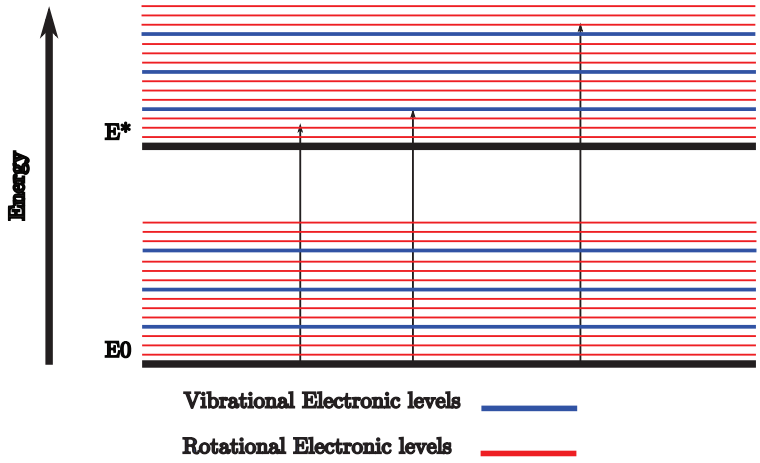

Figure 2.1: Energy levels of the electronic transitions in UV/VIS spectroscopy.

Although UV/VIS spectroscopy has been substituted by newer techniques, it can be consider as an *"old-fashioned"* well established analytical method. UV/VIS spectroscopy finds application in several modern fields of study, specially with liquid samples and solutions. For instance, UV/VIS is widely used in the analysis of pharmaceutical preparations[9] and as complementary analysis of separation methods, e.g. thin layer chromatography [221].

Nowadays this spectral technique is rather well suited and applied in the laboratory analysis of metals ions and macro-molecules due to the electronic transitions they present when absorbing electromagnetic radiation in the UV/VIS region. Due to preparation requirements, and to some of the characteristics of this analytical technique it is uncommon to find it as an in-line monitoring element at automated production processes.

At research level Robinson et al. have recently reported experimental results related to complex anions of ruthenium ([Ru(ttpy$(CN)_3$]) [156], where the metallochromism effects

Table 2.1: Spectral range for UV, VIS and NIR spectroscopy [169].

Range	in nm	cm^{-1}
UV	200-400	50000-25000
VIS	400-800	25000-12500
NIR	800-2500	12500-4000

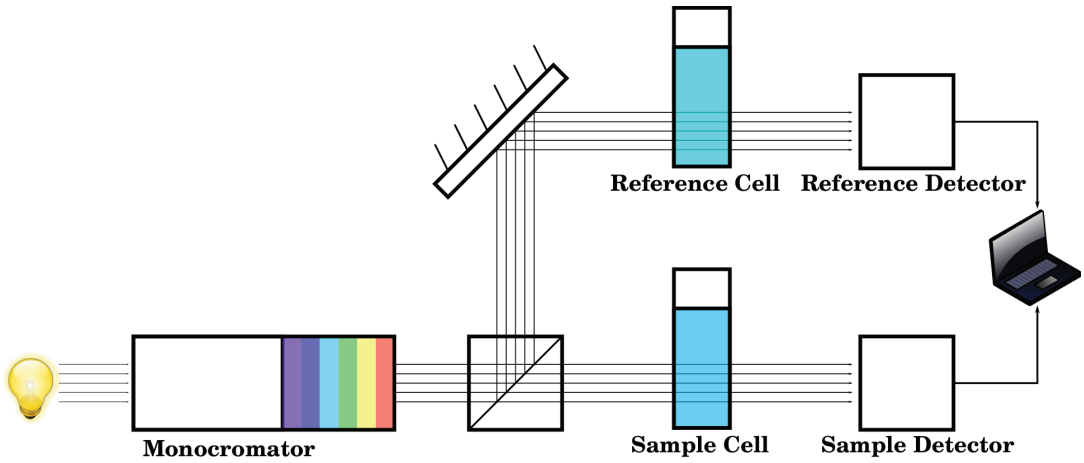

Figure 2.2: Diagram of a double-ray UV/VIS spectrometer setup.

of this material are described. Chi-Ming Che has been using UV/VIS spectroscopy in order to characterize inorganic chemical compounds, mostly ruthenium and ruthenium complexes and its oxidation states [27, 25]. This material can be used in oxygen sensors, in biological staining additives or in electrical and electronic parts. He has also performed a similar study in order to obtain certain properties of ruthenium/osmium-carbon [28] and gold nano-particles [188]. In the latter he has tried to verify the anti-cancer properties of the gold nano-particles. Similarly, V. Amendola and M. Meneghetti have published several documents related to the analysis of gold nano-particles for different purposes. They have included some works where they have evaluated the size of the gold nano-particles based on the fitting of the spectra, by the Mie model, for spheres [5, 114, 6]. They have also determined light localization effects in opals.

2.2 Fluorescence Spectroscopy

Fluorescence spectroscopy is an electromagnetic emission technique that can be regarded as complementary to UV/VIS spectroscopy. This technique is highly sensitive and it is applied in many disciplines, and it is one of the main analytical tools in biotechnology. Furthermore this technique is one of the most used method to study the behavior of biological macromolecules, membranes tissues and living cells [19]. Both organic and inorganic materials can be analyzed using this spectroscopic technique, although the latter present normally a lesser degree of fluorescence. Some materials present fluorescence effects

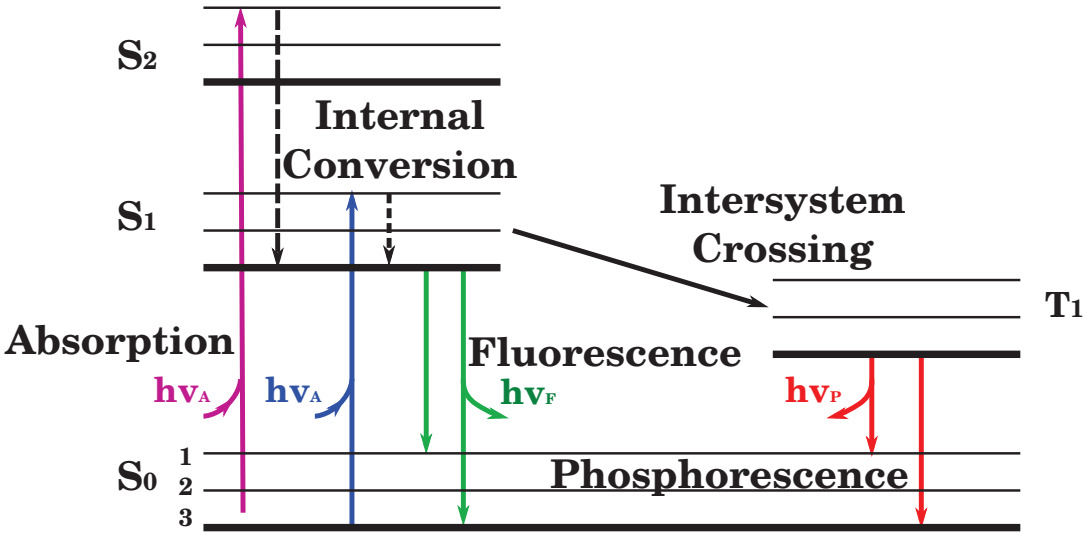

Figure 2.3: Jablonski diagram. It represents the electronics transitions affecting the molecule in fluorescence spectroscopy .

that can be directly monitored (intrinsic fluorophores). With materials lacking of this effect, it is necessary prepare the sample prior to the measurement by generating a reaction with a reagent or by mixing with fluorescence materials (extrinsic fluorophores) [69], [4, p. 102-104].

In fluorescence spectroscopy, the electronic and vibrational states of an analyzed sample are involved. Initially this sample absorbs a photon (excitation from the ground state E_0 to some vibrational state at the excited state E_*). From the vibrational state, the molecule returns to the lowest vibrational state of the excited state E_*. In this process the energy difference is released in form of photons with longer wavelengths (lower energy). Figure 2.3 shows the Jablonski diagram with the possible electronic transitions an excited molecule can experiment. S_0, S_1 and S_2 represent the electronic states and every electronic state can have several vibrational states. Due to the nuclear properties of the atoms, the emission spectra of the transitions $S_1 \rightarrow S_0$ are almost mirror-similar to the absorption spectra [90, 167, 4]. Figure 2.4 shows a conventional excitation and emission spectra of calcein.

The fluorescence spectrometers (or spectrofluorometer) are generally complex instruments capable of recording both excitation and emission spectra [90]. The environmental influences in this type of measurements must be taken into account in order to correct

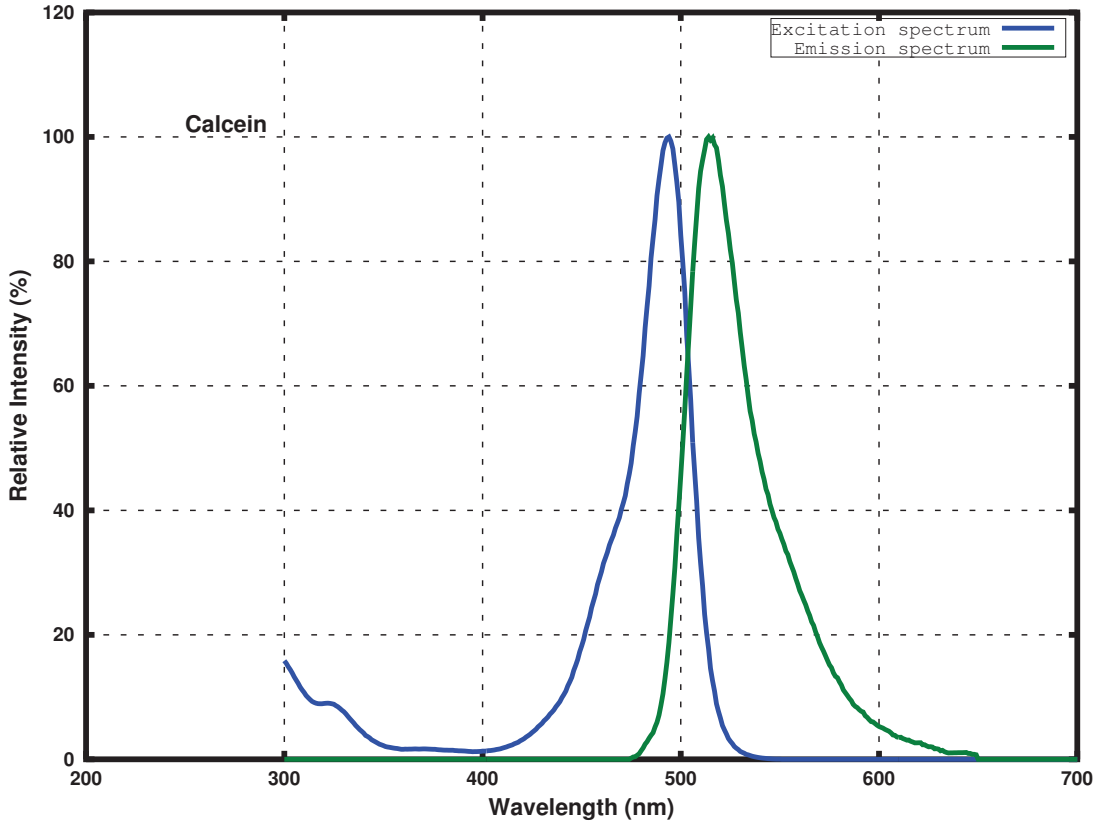

Figure 2.4: Excitation and emission spectra in fluorescence spectroscopy.

them and avoid corrupting the results. Such an instrument have an xenon lamp as exciting source. These lamps are normally operating under a high pressure (approx. 10 atmospheres) and therefore they must be placed in proper casing to avoid physical damages. The instruments also have monochromators for selecting excitation and emission wavelengths. The light is normally detected with a photomultiplier and the resulting data is evaluated and stored in a computer terminal. Several additional optical elements, including sample holder, filters, polarizers, shutters, etc., are present, as well, in this type of equipments.

Lakowicz has been very active in the field of fluorescence spectroscopy. He has been reporting recently studies about the photo-induced electron transfer (PET) quenching reaction of metal-ligand-complex Ru(II). One of the key findings is that a drastic change in the fluorescence intensity has been observed as the amount of quenchers have increased. This effect can lead to a new optical and ratio metric methods for the analysis of sugar molecules

using MLC probes containing the boronic acid group [201]. He has been also actively working with some metal-enhanced samples mostly related to biology in order to determine the biochemical and optical properties of the imaging agents(fluorophores) [223, 54]. Some of the efforts have also covered experiments in order to achieve some improvements in the emission coupling with silver nano-particles [31, 222].

Wöll et al. have been leading a research group in the field of single molecule fluorescence spectroscopy in soft matter. One of the main topics covered by this research group is the characterization of polymers. An example of this type of experiments can be found in [216, 217]. Here the dynamics of thin polymer films using a single molecule approach have been investigated. Wöll et al. have also reported the diffusion coefficients of perylene diimide dies by combining fluorescence correlation spectroscopy and wide-field fluorescence microscopy [218].

In recent years, the fluorescence spectroscopy-based technique named fluorescence correlation spectroscopy (FCS) has been used for analyzing a wide variety of physical phenomena in biology. A recent overview about the advances of this type of analysis has been reported by Thompson et al. [198]. Additionally Ries et al. have published material with several technical aspects and practical considerations that must be taken into account when applying FCS [154]. This analytical technique is subject to diverse artifacts (optical, photo-bleaching, saturation, etc.) that can affect negatively the resulting data of the experiments. Nevertheless, this approach, with the proper conditions, enables the study of cells distributions and the detection of single molecule in biology.

The Horiba group offers an up to date and wide review about different methods applied using fluorescence spectroscopy [75]. These data include applications for different fields of study including food technology, biotechnology, water quality, determination of pigments, oxygen measurements, etc.

2.3 Infrared Spectroscopy

Infrared spectroscopy (IR spectroscopy) is a measurement technique, which is used in a wide type of applications. It is based on the absorption of electromagnetic radiation in the region adjacent to the visible part of the electromagnetic spectrum ($0.8\,\mu$m - $1000\,\mu$m). By convention and due to the type of physical effect on the sample under observation, IR spectroscopy is divided into three main regions: near-, mid- and far infrared. Table 2.2

Table 2.2: Infrared regions and the related type of excitations.

IR Region	Spectral Range	Type of associated excitation
Near-Infrared	0.8 - 2.5 μm (14000 - 4000 cm^{-1})	overtones vibrations
Mid-Infrared	2.5 - 25 μm (4000 - 400 cm^{-1})	rotational-vibrational structures
Far-Infrared	25 - 1000 μm (400 - 10 cm^{-1})	rotational spectroscopy

shows the spectral range of the three IR spectroscopic regions and the associated effect involved in the method.

Unlike UV/VIS spectroscopy, where the UV/VIS light excites the electronic states of the analyte, in IR spectroscopy the exciting IR source promote changes in the vibrational or rotational state of molecules, since the lower energy radiation fits their resonance frequencies (energies in the order of 8 kJ/mol to 40 kJ/mol) [137]. The absorbed energy is directly related to the structure of the molecule being analyzed and therefore the identification of the material is possible. The relation of the incident light from the source, the transmitted light and the concentration of analyte is given by the Lambert-Beer law [92] as in UV/VIS spectroscopy.

IR spectroscopy is one of the most applied analytical methods for several reasons: it can be applied for several type of materials, IR spectra are rich in information and it offers a high selectivity, etc. Furthermore, this technique is quite inexpensive, and the only few drawbacks can be described (water absorption, poor performance with complex mixtures) [180]. Another important factor for the popularity of IR spectroscopy instruments has been the increasing demand for quality control improvement and production rationalization in several production activities that has led to the gradual substitution of time-consuming analytical techniques [175].

The IR spectroscopic setups can be found in mainly two different of arrangements: dispersive IR spectrometers and Fourier-Transform IR spectrometers (FTIR). The former consist of light source for excitation, entrance slit, diffraction gratings, mirrors, output slit and a light detector. The FTIRs have an interferometer instead of a diffraction grating and they tend to be highly costly devices. Additionally a separate holder for a reference sample must be present on the setup. If this is not the case, the measurement must be followed by the measurement of the background in order to subtract the spectral difference.

This analytical technique enjoys a high level of popularity due to its reliability, its relative low-cost requirements, and its versatility. Nevertheless, in order to apply this instrumental methodology it is necessary to collect reference measurements so that the final results do not suffer alterations. Moreover, the technique encounters certain difficulties with solid samples, and with liquid samples in aqueous mediums, as water that absorbs also IR light strongly so it can smear the spectrum of interest.

The measurements obtained from infrared (mid-IR) spectroscopy are complementary to the information obtained from Raman spectrometers. Both measurements methods extract data about the molecular vibration of the sample, but in two different physical phenomenas and different selection rules. Moreover, IR spectroscopy has a higher occurrence probability and it is more efficient with molecules of asymmetric vibrations of polar groups. Larkin in [92, p. 2] offers a structured comparison of these two spectroscopic techniques. Similar information has been presented by McCreery in [109, p. 11].

As mentioned previously, IR spectroscopy is nowadays applied in several fields: Pharmaceutical, food industry, polymers, oil industry, etc. Garrigues and de la Guardia have been focusing on this instrumental technique, as they consider it as a clean tool for chemical analysis. One of the main concerns they have recently pointed out is the improvement of sensibility levels of the measurements in order to perform trace analysis [61]. It is of great importance, since IR spectroscopy is not well suited for environmental analysis due to its limited sensibility. An improvement on the technologies used in IR spectroscopy could also benefit other spectroscopic techniques. These authors also have reviewed the existing alternatives, for the analysis in a non-invasive fashion way, of solid samples [57], as it is one of the precepts in the green analytical analysis paradigm [39].

Information about some industries where IR spectroscopy is applied can be found in [186, p. 172]. In this text by Stuart, different industrial applications are exposed, including pharmaceutical (ingredients properties), food (quality control), agriculture (grains structure) and paper. The environmental aspect is also covered and some specific examples are shown. Stuart has been working also in the study of soil properties. Several of these studies rely on IR spectroscopy.

2.4 Surface Plasmon Resonance Spectroscopy

Surface plasmon resonance spectroscopy (SPR spectroscopy) is a high sensitivity, surface analytical technique that is being applied mainly for analysis of proteins and similar bi-

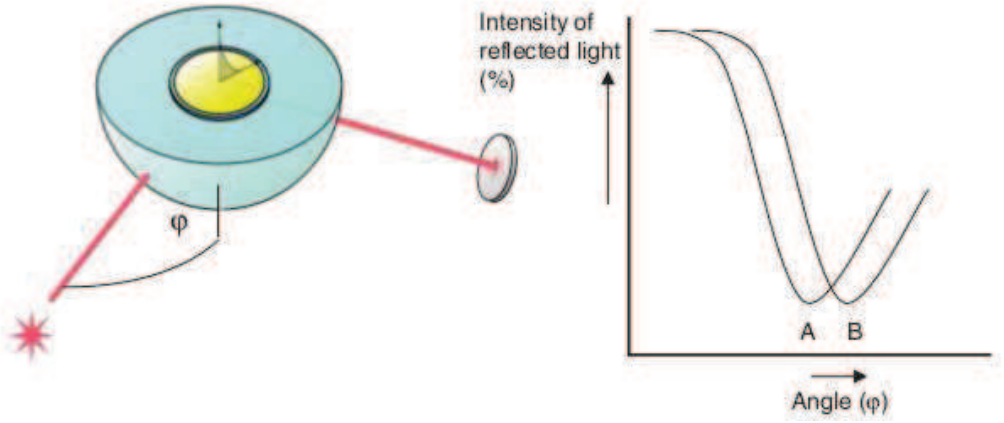

Figure 2.5: Schematic experimental set-up of surface plasmon resonance excitation. Image taken from [168].

ological samples. This technique relies on the resonance of charge density oscillations under the influence of evanescence electromagnetic waves along a metallic-dielectric interface [220, 20, 168].

This relative new technique (it has been under constant development since the last 20 years) can be used independently or it can be applied in combination with other measurement techniques in order to improve the analyzed signal, as in the case of Raman and fluorescence spectroscopy. The devices based on this analytical technique employ thin metallic films of mainly gold (Au) and silver (Ag) in combination with a prism. In SPR spectroscopy the light beam having a certain angle φ is shone to the prism with the sample. A light detector observe the intensity changes vs. the angle of the incoming light due to the change of refractive index (which corresponds to the material inside the prism). When the incidence angle match the excitation, the light detector observes a decrement of intensity. In figure 2.5 a basic setup used in SPR spectroscopy is shown. Curve A, in figure 2.5, shows the intensity of the light observed by the detector against the angle of incidence φ, when the prism cell of the arrangement is empty. Curve B is obtained after the sample has been injected into the cell. The time required for the curve for going from A to B is also observed and it is sample dependent.

SPR require a rather elaborated measurement system with three essential units, that

includes specialized sample cells with thin films of noble metals and and small optical arrangement. SPR can be used in a wide variety of configuration, but the most common SPR setup is the so called Kretschmann configuration [168]. In recent years Homola has published papers about the application of the SPR spectroscopy principles, including some devices fabricated on modified waveguides [73, 144, 74]. The use of surface plasmon resonance sensors constructed on optical fibers have been recently reported by Perrotton et al. for the remote detection of hydrogen (H), which seems to be one of the options for future clean energy, but it is linked to certain level of danger [142, 141, 140]. Similarly, Gupta has recently presented similar applications using SPR sensors using fiber optics [191, 113, 178, 182]. The sensor have been applied for mainly gas detection (e.g. hydrogen sulphide). Similar to Perrotton et al., the metal used for the sensors have differ from the conventional layers of gold and silver (e.g. Al, Cu−ZnO). These types of configurations contribute to reduce the size and the complexity of the measurement systems.

SPR spectroscopy does not require a label additive. Nevertheless it requires a specific layer for target recognition and several preparation steps for a single measurement (including some level of sample preparation). Additionally a constant size of the nano-particles on the thin film layer is required in order to avoid shifts of the spectrum [207]. In [207] Van Duyne et al. have mentioned how the size and the shape of the nano-particles used in SPR may affect the measurements using this technique. Similar data has been reported in [45]. A direct assumption from this fact, is that the thin films, which are not necessary cost extensive, must accomplish certain quality level in order to provide a reliable result.

Besides the conventional applications in some biology laboratories, SPR spectroscopy is nowadays applied in the food and beverage industry [168, ch. 11]. The type and number of analysis performed with SPR in the food industry is large: quality control, gene mutation of the supply chain, level of vitamins, detection of allergens, pathogens [87, 15, 212], etc. Pharmaceutics and life science have also profited from this measurement methods in the development of drugs and diagnostic tests. An extended description about the application of SPR spectroscopy, and some other surface sensors, in food biotechnology and food processing has been reported by Simpson [177].

2.5 Raman Spectroscopy

Raman spectroscopy is a measurement technique based on the inelastic scattering (Raman scattering) of light from a sample, which is excited with a monochromatic light (usually

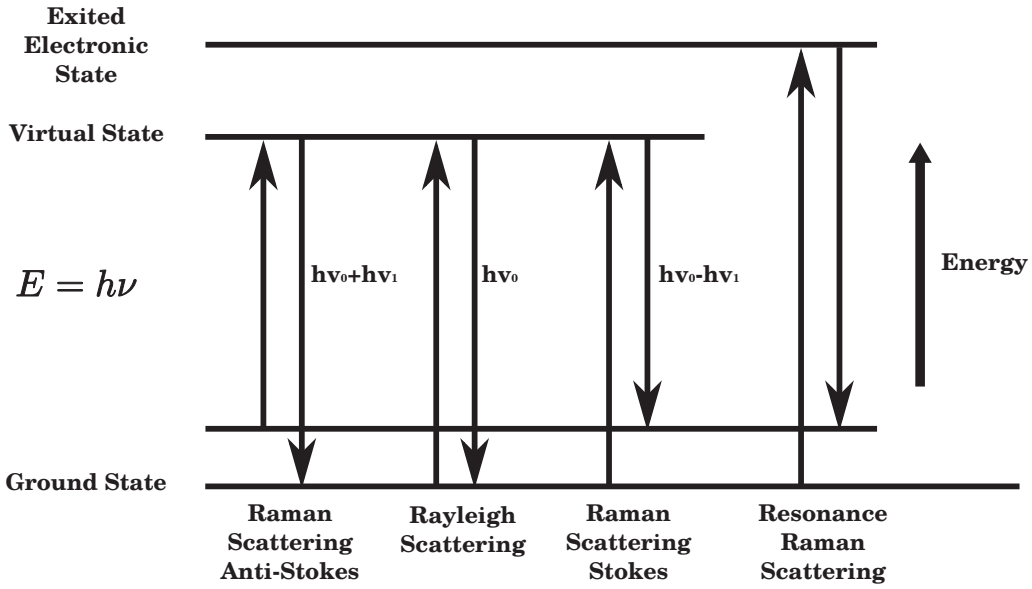

Figure 2.6: Transitions underlying different types of vibrational spectroscopic techniques.

a laser in the visible range up to the near infrared region) in the visible and near infrared region. Raman spectroscopy and IR spectroscopy, as already mentioned in section 2.3, are complementary analytical methods. Although Raman scattering (named after Sir Chandrasekhara V. Raman) has been experimentally observed in 1928 [152, 153], Raman spectroscopy has been successfully established in the late 1980's with the development of the laser. Ever since, Raman spectroscopy has experimented a gradual transition from the laboratory to the practical applications[109].

In Raman scattering photons from a light source interact with the molecular bonds of the sample under observation. The Raman effect is an inelastic scattering process where molecules or atoms are excited and taken to higher vibrational or rotational virtual energy states, when they return from these levels, a small energy difference can be absorbed or released. This effect is observed at the wavelength of the emitted photon (spectrum), since it differs from the wavelength of the incident light source. The amount of Raman scattering light is reduced (depending on the molecule, some hundreds of photons per second) and therefore an adequate light sensor and an excellent filtering of Rayleigh scattering is required in order to obtain the spectral information of the molecule analyzed. Figure 2.6 presents the spectroscopic transitions involved in Raman and Rayleigh scattering. In Rayleigh scattering the energy transition begins at ground level and ends at the same

place. In Raman scattering the transition begins or ends at different energy levels. The shifted value depends on the nature of the molecular bonds and it is unique for every compound, which makes it suitable for analysis and monitoring applications. More details about the Raman effect can be found in[50, 109]. The frequency of the shifted energy can be approximately calculated with both classical and quantum mechanics. For a bi-atomic molecule with a single degree of freedom (the simplest case) the vibration frequency, $\overline{\nu}$, can be calculated using the classical harmonic oscillator with:

$$\overline{\nu} = \frac{1}{2\pi}\sqrt{\frac{k}{\mu}}, \tag{2.1}$$

where μ represents the reduced mass of the atoms involved in the molecule and k is a force constant, which depends on the type of molecular bond (e.g. C−C, C=O, C=N,etc.). In quantum mechanics the frequency ν of a specific bond vibration is found by solving the Schödinger wave equation:

$$E_n = h\left(n + \frac{1}{2}\right)\nu = h\left(n + \frac{1}{2}\right)\frac{1}{2\pi}\sqrt{\frac{k}{m}}, \tag{2.2}$$

where n is a quantum number that can take specific values (e.g. n=1, 2, 3,...,) and h is the Planck's constant. The same evaluation can be applied for the vibrations of IR spectroscopy.

Similar to IR spectroscopy, the instrumentation of a Raman setup can be done using dispersive or non-dispersive (FT spectrometer) arrangements (see figure 2.7). The later offers certain advantages over the former (e.g. higher resolution, frequency precision, etc.), however the availability and the costs related aspects of such devices are still an important issue, which is covered in this research report.

The intrinsic characteristics of the Raman scattering (which offers the vibrational information about the molecules of the sample) allows this spectroscopic technique to find applications in a large variety of fields of study (e.g. pharmaceutical industry, geology, forensic, art, bio-sciences, etc.). Raman spectroscopy can be applied without having contact with the sample and normally no preparation is required prior to the measurement. Furthermore, this technique is water-complatible in comparison to infrared spectroscopy. This allows the use of this analytical technique in a highly versatile, clean and efficient fashion. Table 2.3 presents the comparison of some parameters from the main vibrational

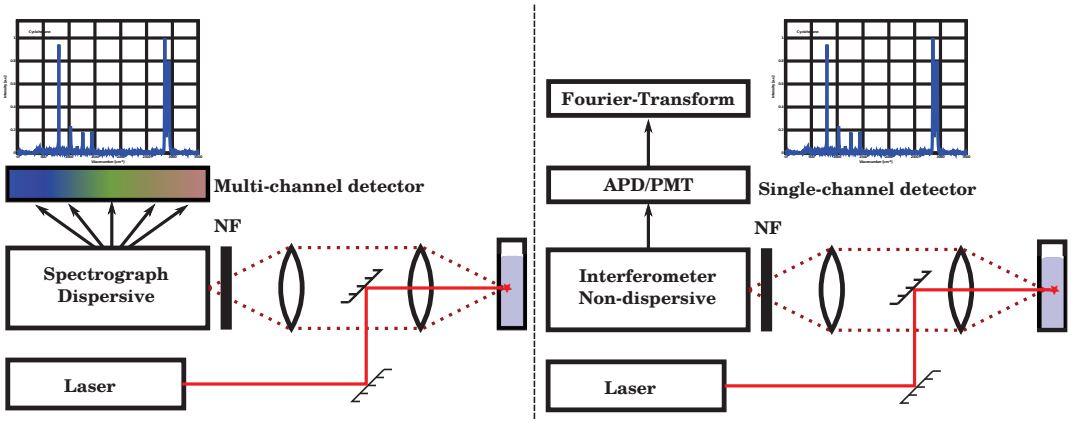

Figure 2.7: Dispersive and non-dispersive configurations of Raman spectrometer devices.

spectroscopic techniques. Additionally, it can be mentioned, that Raman spectroscopy offers high sensitivity to molecular geometry changes (polymorphism) [210, 165] in comparison with the other analytical techniques, which is relevant for some areas like in the pharmaceutical industry.

Although Raman spectroscopy offers a great deal of advantages compared to other spectroscopic techniques, some aspects of this analytical tool, mostly inherent to the intensity of the Raman scattering, are considered inconvenient for certain applications. One of the most drastic drawbacks lies in the extremely low amount of photons available from the Raman scattering effect. This property limits the sensibility of the measurements and hence the capability for tracing applications. A second aspect is the fluorescence that certain samples may generate. This effect can be avoided by increasing the wavelength of the excitation source, but with a severe reduction of the Raman scattered light as a consequence [109, p. 18-21].

Raman spectroscopy and some of it variants are nowadays being used in a wide range of fields of study, and in some production activities. HORIBA Scientific [76] has provided a detailed catalog with several notes and articles about the possible applications of Raman spectroscopy. Similar material has been produced by Kaiser Optical Systems, Inc. [82]. Another manufacturers (e.g. Bruker Optics, Renishaw, etc.) also offer similar informative materials.

Lewis and Edwards have edited a compendium with several of the applications of Raman spectroscopy nowadays including research laboratories and industrial environ-

Table 2.3: Comparative aspects of Raman, Mid-IR and Near-IR Spectroscopy [92, p. 2]. Some of the parameters show clearly the complementary nature of the three analytical techniques.

	Raman	Infrared	Near-IR
Ease of sample preparation	Very simple	Variable	Simple
- Liquids	Very simple	Very simple	Very simple
- Powders	Very simple	Simple	Simple
- Polymers	Very simple*	Simple	Simple
- Gases	Simple	Very simple	Simple
Fingerprinting	Excellent	Excellent	Very good
Best vibrations	Symmetric	Asymmetric	Comb/overtone
Group Frequencies	Excellent	Excellent	Fair
Aqueous solutions	Very good	Very difficult	Fair
Quantitative analysis	Good	Good	Excellent
Low frequency modes	Excellent	Difficult	No

* True for FT-Raman at 1064 nm.

ments [93]. Besides the basic theoretical background, this material includes fields of studies such as gemmology, semiconductors, chemical catalysis, study of gases, in vivo research, environmental applications, etc. An additional rewarding aspect of this material can be found in some of the technical considerations offered about the systems and the processes involved in the use of Raman spectroscopy.

Although Raman spectroscopy can be applied in a wide number of applications, only a few have been taken into considerations for illustration purposes in the present section. Pharmaceutics, fuel industry and food chemistry are fields that can be considered as representative in the application of Raman spectroscopy, since they cover a large amount of possible applications. In recent years, fields like material science, nanotechnology (including studies of graphene) and semiconductors are making use of Raman spectroscopy in order to analyze the chemical composition and other characteristics of the samples in these areas of study [38].

As previously mentioned, Raman spectroscopy is widely applied in the pharmaceutical industry. The control requirements in this industry is a crucial point in order to detect counterfeiting, deteriorations or to ensure the right dosages of active components even if the final products are inside the package. A clear example of this type of applications has been provided by Lyndgaard et al. with a study on paracetamol [103]. Baeyens et al. have shown additional analytical examples about this type of applications in the

pharmaceutical industry [11, 12, 13]. Sasic has provided bibliographical material, that covers several aspects of the pharmaceutical applications of Raman spectroscopy [165]. Besides the basic theory of Raman spectroscopy, he has included certain general aspects of the instrumental requirements. Some of these information and additional ones can also be found, in more details, in the material provided by McCreery [109], which can be considered as a relevant reference in the field of Raman spectroscopy in recent years.

Raman spectroscopy is commonly used in the fuel industry. The potential use of this analytical technique in the fuel industry has been explored extensively again after some issues in the initial years of this technique mainly due to the effects of fluorescence. One of the first proposals for analyzing fuel and some other related chemical compounds using Raman spectroscopy has been made by Rosenbaum in the late 50s using lower wavelengths in the excitation source [157]. Nowadays in this field the Raman devices can be employed, with excitation sources of larger wavelengths, for determining the blending composition, authenticity (gasoline adulteration), octane number, etc [50, p. 334].

Choquette et al. have proposed on the late 90s the use of Raman spectroscopy (combined with FT-NIR spectroscopy) for the identification and quantification of oxygenates in gasoline samples using commercial non-dispersive devices (Bruker RFS-100, 1064 nm) [29, 30]. In these experiments, some specific drawbacks related to the measurements of the encapsulated samples performed using mid and near infrared spectroscopy have been described. Similar experiments using a self-constructed dispersive Raman device have been reported by Cooper et al.. Besides the detection of some oxygenates, these measurements have been focused on determining the octane number of different samples of gasoline by applying multivariate analysis to the spectral information [35, 34]. At that time the costs for the construction of the Raman prototype has been presented as an important issue, as it was comparable to the near IR devices and significantly less expensive than the commercial FT-Raman spectrometers. This later subject has not significantly changed in recent years.

More recently, the environmental and health concerns have added terms like “safety” and “sustainability” to the intrinsic analytical properties of Raman spectroscopy (and some other techniques) at the fuel industry. The volatile nature of fuels in combination with the harmful characteristics of some of their additives makes Raman spectroscopy a suitable option for remotely perform different types of analysis without any contact or sample preparation [39, 109, 50].

For instance, the use of fuel-ethanol-methanol blends has been gradually introduced in recent years in order to reduce the amount of air pollutants from internal combustion vehicles [203, 22]. Nevertheless, these fuel blends still contain additives that are often associated to ground water contamination and to serious health issues, including cancers (e.g. toluene, MTBE, benzene, etc.) [83, 100].

Using a dispersive setup Qing Ye et al. have reported qualitative and quantitative analysis of gasoline-ethanol and gasoline-methanol blends [149, 150]. Although the frequency precision and the resolution of the resulting Raman spectra obtained at these experiments have not shown a high degree of accuracy, the ratio of the gasoline blends has been successfully calculated (a similar method has been reported by Larkin [92, p. 44-47]). These results can be considered suitable for the analysis of laboratory blends under optimal circumstances. Nevertheless, for practical purposes additional consideration must be taken into account , since commercial fuel blends contain several additives and they vary significantly depending on the manufacturer (e.g. toluene and benzen are normally present in commercial E10 gasoline blends and their characteristic Raman lines are separated by only a few cm^{-1}).

Similar analysis on laboratory-prepared and on commercial gasoline-blends have been conducted using a self-designed and cost-efficient FT-Raman spectrometer [127, 133, 131]. The spectra from these analysis have shown a reduced frequency deviation compared to the values proposed by McCreery [109, 111] and the values found at the database from the National Institute of Advanced Industrial Science and Technology (AIST / SDBS) [119]. This frequency accuracy helps to avoid interpretation errors in the spectra obtained. Additional details about the behavior and the use of toluene as a frequency calibrating material in the analysis of gasoline is proposed, as this chemical compound is normally present in commercial fuels in order to improve the octane number (between 5% to 11% (v/v) [44, 47]).

Researchers at the institute of chemistry at the University of Brasilia have reported several studies on bio diesel and ethanol fuels. These studies have been focused on the detection of adulterated diesel and bio-diesel blends, as they had not been analyzed previously at the time. They also have made a detailed comparison of the different evaluation methodologies of the data (principal component regression, partial last square regression and artificial neural network) obtained with Raman spectroscopy and IR spectroscopy [126, 1, 158]. All these experimental procedures have been carried out using

commercial FT-spectrometers.

Another sector that has been making use of Raman spectroscopy is the food industry. In this widespread field there are several aspects that must be carefully inspected in order to assure the quality and safety of food and beverages from different points of view (chemical, physical and nutritional). The increasing use of Raman in food industry in recent years can be explained by the overcoming of several deficiencies on this technique, particularly fluorescence, that is caused by several of the organic chemical compounds that are present in food.

Li-Chan, Chalmers, and Griffiths have gather and edited a large amount of material about the application of the different vibrational spectroscopic techniques including Raman in the analysis of food [95]. The section contributed by Pudney and Hancewicz offers an extensive description, from different points of view (including some instrumental factors) of confocal Raman spectroscopy applied in food science [148]. Viereck et al. have also collaborate in the redaction of a full chapter dedicated to the application of Raman in the analysis of food [208]. They have recognized in this text the intrinsic characteristic of Raman spectroscopy as well as the complementary nature of this technique and IR spectroscopy and its potential use for in-line monitoring applications.

Li-Chan has also published since the late 90s different studies about the the characteristics proteins from plant and animal origin (lysozyme, R-lactalbumin and β-lactoglobulin) [94, 98, 99, 96]. Her studies comprises the interaction of ingredients of certain foodstuff and the development of strategies for the isolation of certain materials at lower costs [97]. Although several of the experimental procedures, she has reported, have been made using a JASCO NR 1100 spectrometer some of the experimental data have been also collected using different FT-Raman spectrometers.

The adulteration of food and some of its repercussions have been explained by Ellis et al. [43]. Although this review lacks of information at instrumental level, several of the characteristics and capabilities of vibrational spectroscopy, including Raman spectroscopy, in the food industry have been described. In this bibliographical material it can be observed the emphasis that the portability and the ability of Raman for perform analysis of different nature of foodstuff inside the package.

In the particular case of beverages, it is worth mentioning that Raman spectroscopy can be applied easily, since this technique allows the analysis of aqueous samples with a reduced or nonexistent effect from water [39, p. 92] even if the samples are inside the

Table 2.4: Modern FT-Raman spectrometers models and their approximated price according to the respective manufacturer.

Manufacturer	Bruker	Thermo Fisher	JASCO
Model	MultiRam	Nicolet iS50	FT-Raman RFT-6000
Approx. Price*	from 100,000 €	$\simeq$ 85,000 €	$\simeq$ 90,000 €+Tax

* Prices between April and Sept. 2013

containers. Raman spectroscopy has been applied for the observation of several alcoholic beverages, including vodka, tequila, wines and beer [53, 166, 192]. Besides quality control in beverages, Raman spectroscopy can be applied as well for the detection of drugs and harmful chemical compounds like methanol and aldehyde-like materials, that can inflict severe damage in humans.

As already covered, the non-dispersive Raman arrangements can be applied in order to perform highly frequency accurate Raman analysis and to avoid certain undesirable effects, like fluorescence. Contrary to the dispersive Raman devices, commercial FT-Raman devices are only available from rather a reduced number of manufacturers. This represents certain level of drawback for some users in technical and economic terms. The devices are in several cases only available as additional modules for its coupling into a IR spectrometer system. Table 2.4 contains information about some state-of-the-art FT-Raman devices from the main manufacturers and their respective approximated values on the market. The charges for maintenance, service and accessories have not been taken into account.

2.6 Summary and conclusion of the chapter

All the analytical tools mentioned previously are suited for optimal results in specific areas and for using specific materials. Raman spectroscopy can be used in similar cases where infrared spectroscopy is applied as a complementary analytical tool. Unlike infrared spectroscopy, the spectral analysis performed using Raman spectroscopy is normally compatible with water; it can be achieved without contact and in remote locations. In terms of flexibility and applicability these characteristics are relevant.

Despite certain pitfalls and drawbacks, mainly lower sensibility (with SERS and similar techniques Raman scattering can be significantly improved), this analytical technique also

Table 2.5: Performance of some of the characteristics of the different spectroscopic techniques [197].

Parameter	UV/VIS	Fluoresc.	IR	SPR	Raman
Selectivity	below avg.	good	excellent	excellent	excellent
Calibration	average	average	good	regular	good
Accuracy	very good	good	very good	very good	good
Precision	average	average	very good	good	good
Limit of quantification	excellent	excellent	below avg	excellent	below avg
Limit of detection	excellent	excellent	average	excellent	average
Ruggedness	good	average	good	good	good

offers certain advantages over other spectroscopic methodologies (e.g. measurement of packaged samples). The overcoming of fluorescence and the optimization of the optical elements and light detectors have given Raman spectroscopy the opportunity to penetrate in newer fields of study.

The commercial aspect of Raman spectroscopy is still a topic to be attended. The collection of spectral Raman information using dispersive devices can be costly if the equipment contains several technical features. This factor depends strongly on the model required and on the manufacturer. It is also possible to find dispersive devices at reasonable prices as these devices are less complex and there exist a larger amount of manufacturers compared to the non-dispersive devices (e.g. Ocean Optics, Bruker, Jasco, Horiba, Renishaw).

In the case of the FT-Raman devices, due to different factors (the highly-sensitive character of the interferometric system and the hardware requirements) only few manufacturers offer these types of devices and the cost-related requirements are prohibitive for several users. The literature does not addresses this type of subjects broadly as it is not a technical-scientific matter. Only a few comments have been founded in this particular case. The cost-related information can basically be found directly through the manufacturers. As in any commercial device, commercial FT-Raman devices can be operated with a set of software tools that are enclosed and they cannot be modified if any special adjustment or configuration is desired.

Table 2.5 summarizes some of the performance of different parameters of the spectroscopic techniques mentioned in this chapter. A certain level of subjectivity exists in the contents of this table, since all this parameters depends strongly in the type of material

Table 2.6: Parametric benchmark of some of the practical considerations from different spectroscopic technologies.

Parameter	UV/VIS	Fluoresc.	IR	SPR	Raman
Sample preparation	2	2	3	2	4
Sample state					
- Solid	3	4	5	3	4
- Liquid	5	5	5	5	5
- Gas	1	3	5	3	2
Water influence	3	4	1	4	4
Time of measurement	4	4	4	2	4
Non-contact	2	3	2	4	5
Non-destructive	1	2	5	2	5
Waste generation	4	3	4	4	5
Amount of sample	4	5	5	4	4
Evaluation *	29	35	39	33	42

*1 lowest value, 5 max. value

under observation. Additionally it is worth mentioning that the evaluation has been made from the Raman spectroscopy point of view.

Table 2.6 contains the scores of different practical consideration for each of the measurement techniques mentioned in this chapter. The scores have been assigned again taking as reference FT-Raman spectroscopy and partially IR spectroscopy.

The determination of further exploring FT-Raman as analytical tool for monitoring certain processes that involve harmful materials has relied mainly in its unique combination of intrinsic characteristics that helps in performing remote chemical anaylsis of harmful materials in a clean, simple and selective way.

Moreover, the potential reduction in complexity and in the cost-related factors might enable the applications of this analytical methodology in additional fields of studies and to a larger amount of users. It cannot be disregarded, that in the near future, different issues, like the sensibility of Raman detectors among other subjects, could be improved and/or optimized.

As a consequence, such an advance might allow the fabrication of FT-Raman spectrometers without moving parts (e.g. all-fiber FT-Raman spectrometer) at even lower-costs, since these complex mechanical parts and some special optical components increase the financial requirements of such devices.

Chapter 3. Instrumental requirements, considerations and constrains

In this chapter, the main requirements for the proper acquisition of spectral Raman information, needed for the monitoring of certain production processes, are described. Although several parameters must be observed in order to successfully extract Raman spectra from the materials under observation, the present chapter covers the effects of the conventional mechanical parts on the optical path, the evaluation requirements, some instrumental effects (e.g. finite path, source size, etc.) and the detection of the back-scattered Raman light. For that purpose we have included a modeling of the possible impact, that the mechanical components and the optical parts used in the arrangement might have on the evaluated Raman spectrum. This modeling has provided data on the drawbacks and the issues that the FT-Raman system we have proposed must overcome in order to be functional.

As already explained in chapter 1, the purpose of this research project is to explore the possibility of low cost proposed methodologies for the chemical analysis of certain harmful materials (e.g. cyclohexane, toluene, benzene [116, 117, 118]) in a sustainable manner based on FT-Raman spectroscopy. It has also been already alluded, that certain aspects of the commercial FT-Raman devices can result unsuitable for users having limited economical resources (as in emerging economy countries) and having also further interest to explore unorthodox measurements and configurations of the instrumental arrangement. Therefore, this process must be achieved without affecting, or affecting to a lesser extent, the financial involvement of the end user, as well as the flexibility of the instrument and its controlling and evaluating software performances.

In order to accomplish this objective on a low-budget basis, without losing resolving power and frequency accuracy, the instrumental arrangement that we propose, requires to leave aside sophisticated and expensive pieces of hardware and software that are commonly used by the manufacturers of commercial FT-Raman devices. However, replacing these parts by inexpensive and conventional ones might generate undesirable effects on the quality of the evaluation of the Raman spectra of the material analyzed (e.g. fre-

quency deviation, shift-lines broadening, etc.) and therefore it is compulsory to find a compensating process having at the same time low cost and spectral evaluation quality.

Some of the characteristics of the FT-Raman spectroscopy are, among some other ones, frequency precision, frequency accuracy, and high resolution. These parameters are relevant as they can help avoiding interpretation errors on the analysis of complex chemical mixtures, that can emerge in highly selective measurement methodologies as in the case of some specific polluting materials. The American Society for Testing and Materials (ASTM) has proposed a value of $\pm$ 1.0 cm^{-1} of spectral deviation for the calibration of the FT-spectrometers using the spectrum of certain well-known materials [7][109, p. 267]. This value is also used by the main manufacturers of commercial FT-Raman devices.

The main aspects of the specific instrumental arrangement covered in this chapter to accomplish the proper extraction of the Raman spectral information of the materials under observation, are the following:

- Raman spectrum evaluation under non-optimal conditions due to the irregular nature of the hardware components.
- Instrumental effects due to the optical components.
- Detection of the Raman scattering light.

The analysis and the understanding of these aspects have assisted us in the achievement of a new measurement system that is able to deliver Raman spectra having high resolution and frequency precision, as recommended by the ASTM. This analysis has also revealed the physical limitations of the system, so that we avoid performing measurements leading to erroneous results or to false interpretations of the collected data.

Section 3.1 presents the consequences of different disturbing effects, mainly of mechanical nature, on the estimation of the Raman spectrum by using different evaluation schemes. This section (specifically subsection 3.1.4) also describes the method that we have proposed and that we consider to be the most appropriate for the spectral evaluation of the Raman scattered light collected by using a low-budget-based spectrometer. Section 3.2 contains some of the instrumental effects, such as Raman shift and resolution limitation, generated by the main optical components of the FT-Raman system. Finally, section 3.3 describes the possible amount of useful Raman scattering light that can be observed on a photon counter system with the optical parts analyzed in the previous sections.

3.1 Implications of eliminating sophisticated and dedicated hardware on the spectral evaluation

A key component of the FT-Raman systems is the interferometer (generally a Michelson interferometer or a variation of this device), which is required for modulating the different wavelengths from the Raman shifts. These devices serve inside FTIR and FT-Raman spectrometers by generating an interference signal as a function of the scanned optical path. Interferometers are sensitive devices that are easily disturbed by external factors, specially mechanical vibrations and thermal drifts. In order to perform Raman measurements using non-dispersive means, it is necessary to have an accurate knowledge about the optical path that the light follows inside the interferometer of a FT-Raman device. An oversight in the acquisition of the optical path may result in a significant deterioration of the spectrum obtained.

Commercial devices and researchers rely on different systems and methods in order to evaluate the Raman spectra obtained from FT-Raman systems. Bruker optics has a patented pendulum-type of mirror system for both arms in the Michelson interferometer [176, 85][62, p. 117], which is known as RockSolid^{TM}. Thermo Scientific makes extensive use of a patented frictionless electromagnetic drive system, that keeps the moving mirror pointing into the reference detector, with some control routines and software modules [32]. These two systems allow the extraction of highly accurate Raman spectra using these special components and methodologies.

For the spectral evaluation, the interference pattern (Raman scattering light of the analyzed sample) in most commercial devices is collected at the so called zero-crossing points from a well known monochromatic wavelength (usually from a helium-neon laser) [161, p. 95] [211, p. 40]. This method allows to generate highly frequency-precise Raman spectra, when the deviations of the optical path are inside a certain range (generally up to some μm). A broader description of the applicability of this method in the proposed FT-Raman system is provided in subsection 3.1.3.

Griffiths and De Haseth have reported about the frequency accuracy of the HeNe laser used inside the FTIR spectrometers as a reference signal[62, p. 108-109]. This principle is also used in commercial FT-Raman devices in order to obtain outstanding frequency accuracy. In extreme cases, deviation values of about $0.3\,\mathrm{cm}^{-1}$ in the spectrum could be observed due to mode hopping and to changes in the cavity length of the laser. However,

modern FT-Instruments usually have specifications that allow a frequency accuracy of $0.01\,\mathrm{cm}^{-1}$. Even for unstabilized HeNe lasers (Frequency f =473.6127 THz, wavelength λ_{vacuum} =632.9901 nm, operating in the $3s_2 \rightarrow 2p_4$ transition), it is possible to expect a relative standard uncertainty of only 1.5×10^{-6} [184].

3.1.1 Effects of equally distributed mechanical deviations on the spectral evaluation

Under optimal circumstances, where the trajectory of the movable mirror of the Michelson interferometer displays an optical path equivalent to a linear function without abnormalities, the evaluation of the Raman spectrum would rely only in the application of the Fourier transform function. In the commercial applications, the interferometric systems inside the FT-Raman devices are affected by several factors. That is the main reason why commercial devices are built with the use of highly sophisticated scanning hardware parts.

If these special parts are replaced by common standard components (e.g. simple translations tables, DC motors, micro-controllers, etc.), it is likely to reduce significantly the related cost of such a devices, which is one of the aims of this research project. Nevertheless, objectionable effects on the FT-Raman devices are also to be expected if no proper replacement or evaluation methodologies are used for the device. The most common artifact in these cases is the distortion of the optical path. Additional anomalies affecting the quality of a Raman spectra have been described by Bowie et al. [18].

Assuming an ideal and continuous optical path difference (OPD), the spectrum from the sample under observation would be calculated by applying the Fourier transformation, which is represented by the following equation [84, p. 82]:

$$E(\nu) = \int_{-\infty}^{\infty} I(x) e^{-i2\pi\nu x}\, dx, \tag{3.1}$$

where $I(x)$ is the interferogram and x is the optical path difference traced by the movable mirror around the balance position of the interferometer. In the cases where the optical path difference x is influenced by some non-linearities, eq. 3.1 can only be applied directly if the spectral structure of the material is well-defined and the optical path deviation remains within a narrow range. As the error affecting the optical path difference increases, the amplitude of the Raman peaks decreases. Furthermore, the Raman lines having lower spectral amplitudes would fade under the effects of these disturbances.

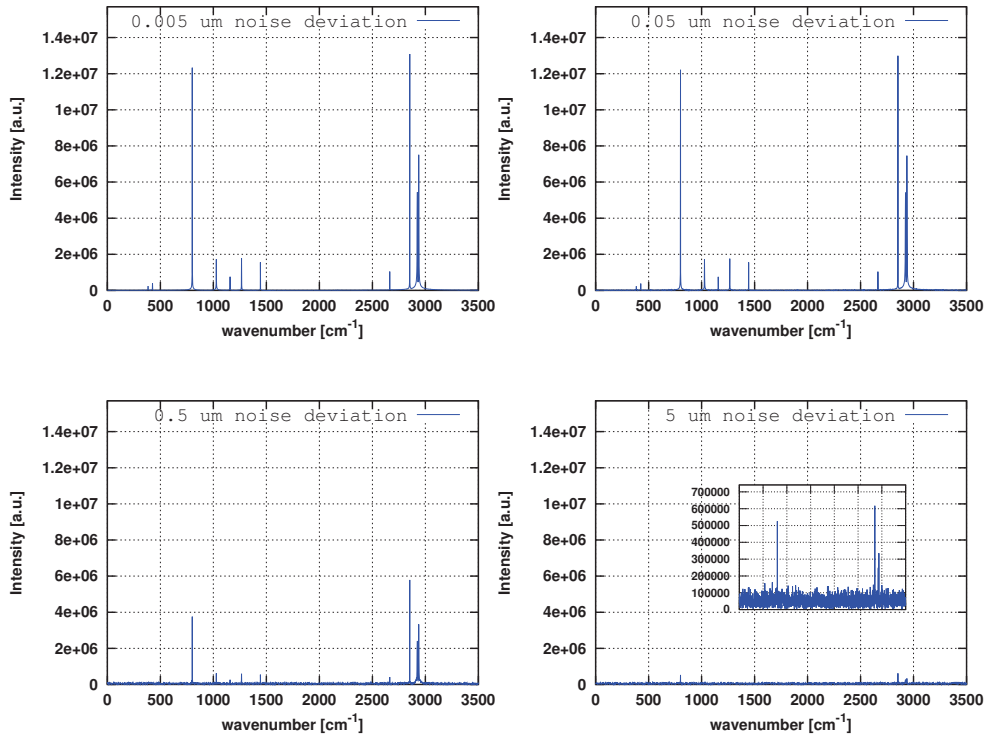

Figure 3.1: Simulated Raman spectrum of cyclohexane evaluated under the influence of non-ideal optical paths having different magnitudes of equally distributed deviations.

The magnitude of optical path deviation that the spectral evaluation can tolerate varies according to the nature of the spectral characteristics of the sample under observation. A simulation using a synthetic spectrum with the ideal spectral characteristics of cyclohexane (C_6H_{12}, table 3.1), which is a well-known material with highly defined frequencies and is used for frequency calibration purposes in Raman spectroscopy, has shown that the spectral evaluation can be seriously affected when the magnitude of the equally distributed noise added to the optical path exceeds some tenths of μm. The simulated interferogram signal $I(x)$ has a theoretical optical path length of 6 mm and the reference wavelength is $\lambda = 632.8$ nm. Figure 3.1 depicts some of the results of simulations with different magnitudes of optical path deviation.

Table 3.1: Frequency and amplitude characteristics of the Raman spectrum of cyclohexane. The Raman shift in nm is given for an excitation wavelength of λ=632.8 nm. This data has been used to generate the simulation signal. Data taken from [109, p. 262].

Raman shift [cm^{-1}]	Raman shift [nm]	Rel. intensity [%]
384.1	648.56	2
426.4	650.35	3
801.3	666.60	95
1028.3	676.84	15
1157.6	682.82	6
1266.4	687.93	14
1444.4	696.46	12
2664.4	761.13	8
2852.9	772.21	100
2923.8	776.46	58
2938.3	777.33	67

3.1.2 Effects of the mechanical deviations of oscillating nature on the spectral evaluation

The translation table for the movable mirror of a conventional Michelson interferometer, which has been used for the development of a FT-spectrometer for prototyping purposes, presents mechanical characteristics that heavily influence the spectral evaluation. Moreover, rather than having equally distributed abnormalities, the non-perfect mechanical properties of this translation table generates an oscillating deviation around the optimal optical path. This deviation can be observed in figure 3.2. This graph presents the effects of the mechanical error of the movable mirror along the optical axis. Figure 3.3 depicts the repeatability of the mechanical deviation generated at the translation table. This mechanical error is dominated by the oscillation at 1.0 mm (corresponding to one turn of the shaft at the translation table). This figure also presents several components of higher frequencies (they appear at lower values of the distance traveled) with far lower amplitudes.

The oscillating behavior deployed by the mechanics of the translation table incorporates an additional adverse factor to the evaluation of the Raman spectrum. Besides the deviations in the optical path x, the interferogram signal $I(x)$ is modulated by a quasi-sinusoidal function (true only if we neglect the effect of the higher frequencies in figure 3.3). This modulating function widens the Raman peaks and distributes the magnitude of the signal in broader spectral ranges, so that the Raman spectrum would disappears rapidly in

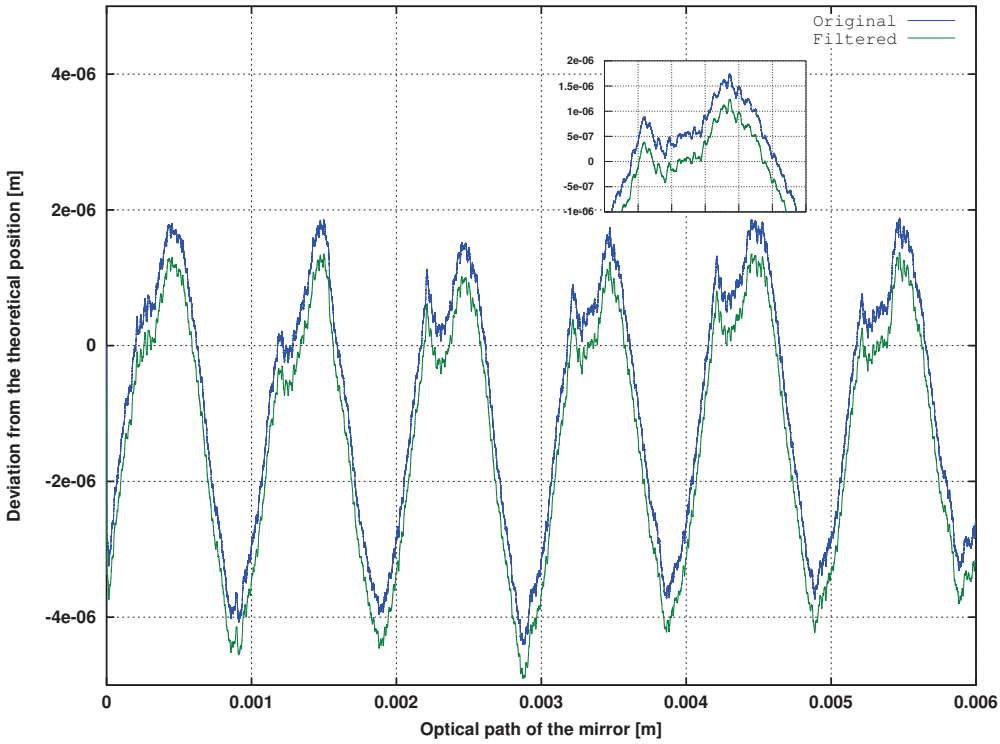

Figure 3.2: Mechanical deviation from the ideal optical path of the movable mirror inside the Michelson interferometer generated by the shaft of the translation table. The recording of the reference signal has been performed around the position of balance (Around approx. 3 mm).

comparison with the spectral signal affected by only uniformly distributed noise deviation. Assuming an oscillating mechanical error having a continuous and sinusoidal function, the expected enlargement of the spectral signal would be described by the modulation theorem of the Fourier transform [84, p. 26]:

$$\mathcal{F}\{I(x)\cos(2\pi\nu_0 x)\} = \int_{-\infty}^{\infty} I(x)\cos(2\pi\nu_0 x)e^{-i2\pi\nu x}\,dx, \tag{3.2}$$

$$= \frac{1}{2}E(\nu+\nu_0) + \frac{1}{2}E(\nu-\nu_0), \tag{3.3}$$

$$I(x) = \cos[2\pi\nu x + \Delta\nu\cos(2\pi\nu_0 x)] \tag{3.4}$$

The approximation of the modulation theorem from eq. 3.3 implies, that every peak of the Raman spectrum $E(\nu)$ will be broadened by $\pm\nu_0$. Here ν_0 represent each of the frequencies affecting the mechanics of the translation table. As a consequence of this

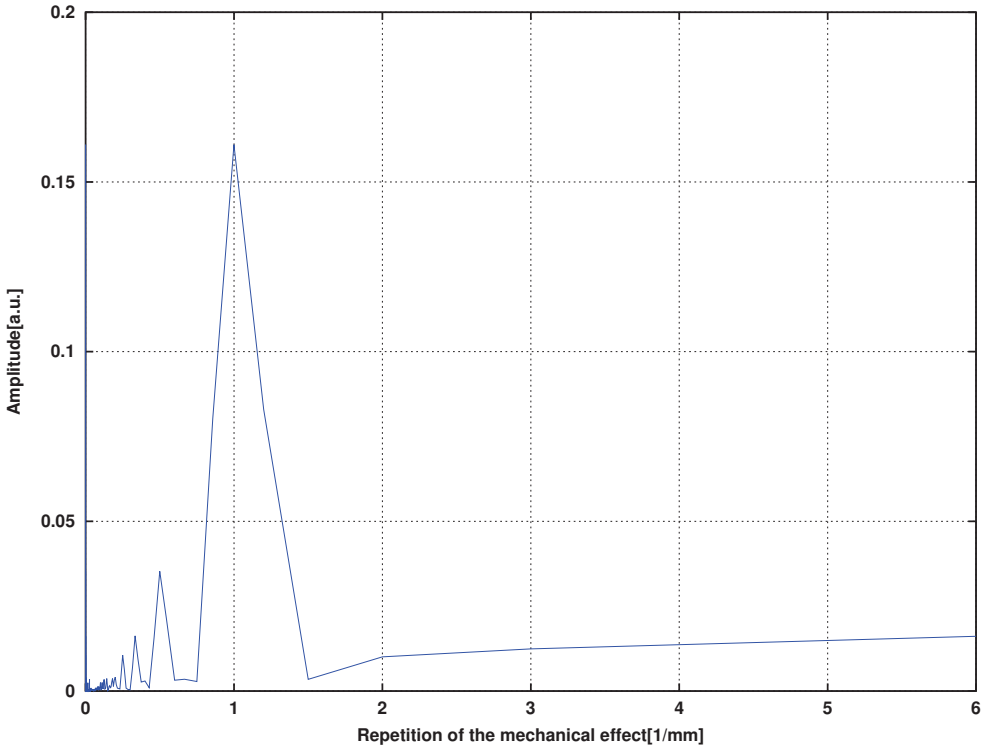

Figure 3.3: Fourier transform of the mechanical error present at the translation table of the Michelson interferometer. The mechanical error oscillation is dominated by the peak at 1.0 mm.

spectral spreading, the lower Raman peaks can be obscured by spectral noise; the frequency and the amplitude of the larger Raman peaks would also be distorted by this modulating effect.

A set of simulations using the interferogram signal $I(x)$ of cyclohexane from table 3.1 have helped to determine the magnitude of the mechanical distortion that can be tolerated at the spectral evaluation. In this simulation, instead of equally distributed mechanical noise, different increasing levels of the mechanical distortion of the translation table (see figure 3.2) have been added to the ideal optical path. Figure 3.4 shows the results of the simulation of the spectral evaluation of cyclohexane. The results of this simulation suggest that already by 1.0% the base of the Raman lines enlarge but the overall figure of the Raman spectrum can be identified. 10% of this oscillating mechanical distortion in the optimal optical path is enough to importantly deform the the Raman spectrum of cyclohexane. The spectral information under the influence of low magnitudes of the oscillating mechanical distortion have remained without relevant deformations.

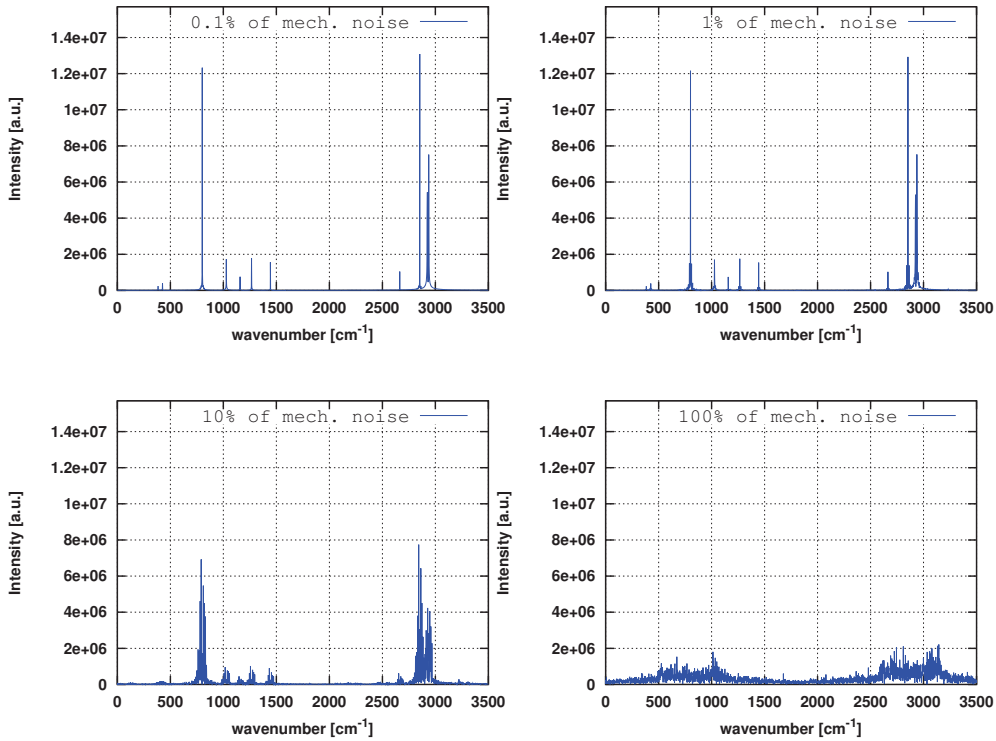

Figure 3.4: Simulated Raman spectrum of cyclohexane evaluated under the influence of different levels of the oscillating mechanical distortion present at the translation table of the Michelson interferometer.

3.1.3 Limitations of the zero-crossing evaluation method

Modern FTIR and FT-Raman commercial spectrometers make extensive use of the zero-crossing evaluation method. In this method an internal referencing system generates a monochromatic (usually HeNe laser light at λ =632.8 nm) interference pattern in order to accurately detect the position of the movable mirror [211, 193, 139, 155]. The interferogram $I(x)$ (Raman scattering light) must be sampled at exactly the zero-crossing points of the monochromatic interference pattern. The frequency accuracy of the spectrum depends basically on the spectral stability of the laser [62]. As stated before, the commercial devices using this type of evaluation method achieve frequency precisions around 0.01 cm^{-1}. This frequency accuracy characteristic of the Fourier transform devices is known as *Connes Advantage*.

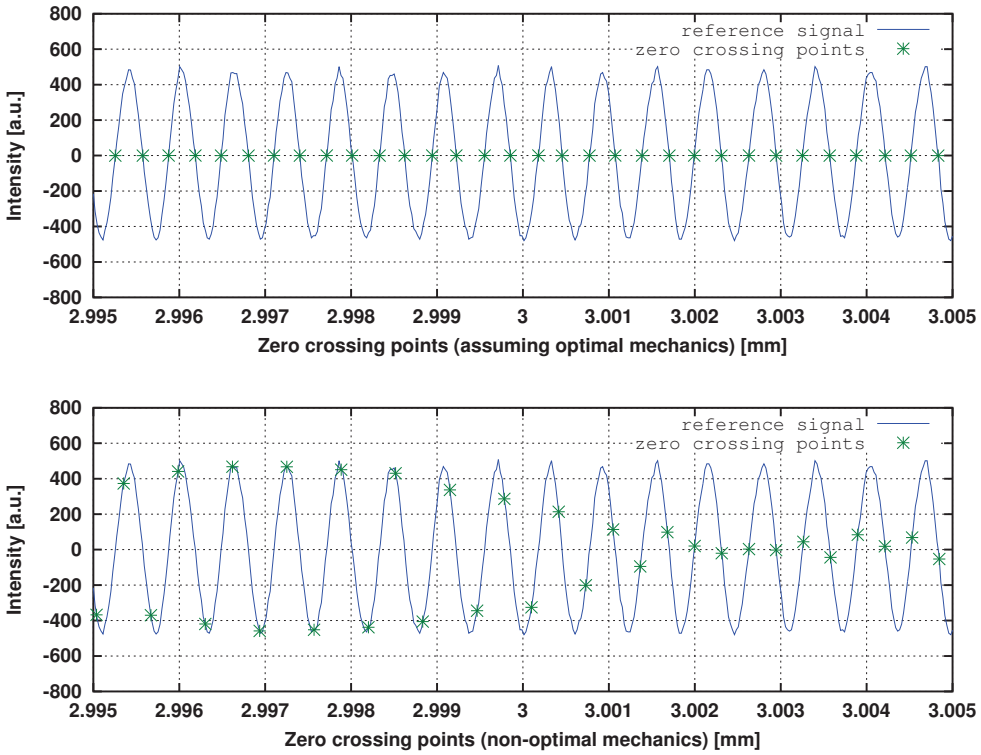

Figure 3.5: Calculated zero-crossing points of the reference assuming ideal optical path without distortions from the mechanical irregularities vs. the zero-crossing points of the reference under the influence of the mechanical distortions.

Nevertheless, in this evaluation methodology for the acquisition of the interferogram, the information between the zero-crossing points is completely neglected. Changes in the average of the reference signal (where the zero-crossing point are normally calculated) may get distorted due to effects from the acquisition system or from the mechanical system. These effects can only be tolerated in certain low ranges in the measurements. If the disturbances outside this limit are neglected, it would certainly lead to an erroneous and undesired outcome.

The zero-crossing method for the accurate acquisition of the interferogram is reliable only if the monochromatic reference displays a sinusoidal shape with a reduced deviation. This method cannot be applied when the optical path of the interference pattern is affected by non-linearities outside certain range. Furthermore, the monochromatic interference

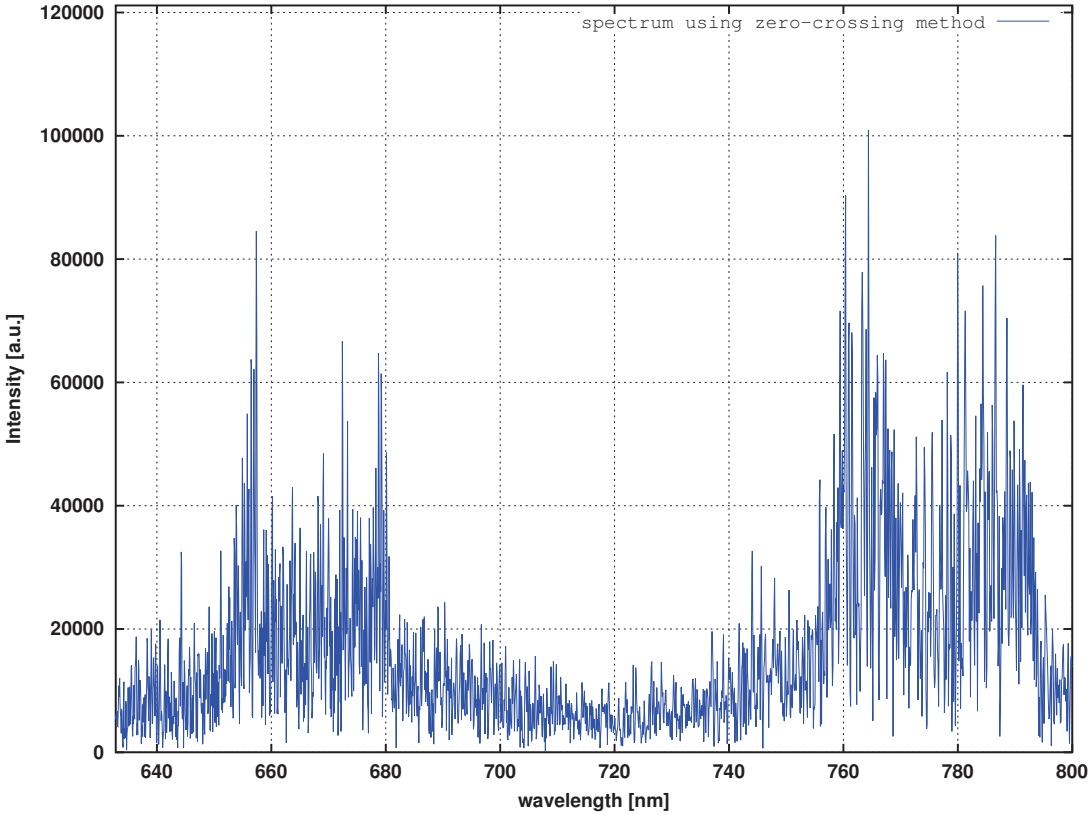

Figure 3.6: Raman spectrum of the simulated cyclohexane signal using the distorted optical path and applying the zero-crossing method.

pattern affected by strong deviations and oscillating behavior on the mechanical system yields to erroneous positions of zero-crossing points. Figure 3.5 shows the difference in the position of the zero-crossing points in the interference pattern used for reference using the ideal optical path and using the real optical path. There it can be observed how the position of such points change every period when the real optical path is used.

The spectral evaluations using the zero-crossing method without taking into account the influence of the mechanical distortions on the optical path difference lead to undesirable results. The extremely distorted spectrum obtained under this circumstances are difficult to interpret or definitely inadequate for analytical purposes. Figure 3.6 portraits the spectral result of the evaluation of the simulated signal of cyclohexane using the zero-crossing method under the influence of the mechanical deviations of the translation table.

3.1.4 Proposed method for the proper extraction of the Raman spectrum collected by using a conventional FT-spectrometer

The incorporation of less complex and conventional elements into the FT-Raman spectrometer, as the one described previously, in order to reduce the cost-related and the complexity factors, implicates the possible appearance of strong and undesirable influences on the interferogram, and hence on the final spectrum. This is one of the main reasons justifying the use of specialized interferometric hardware in this type of in commercial devices. Moreover, even the incorporation of special parts can lead to unsatisfactory results if the system is not properly built [163, p. 59]. In our approach, these effects have been carefully assessed prior to the computation of the Raman spectrum of the material under observation.

It has been also demonstrated in subsections 3.1.1, 3.1.2 and 3.1.3, that the direct evaluation of the Raman spectrum of the interferometric information using a Michelson interferometer with mechanical characteristics similar to those depicted in figure 3.2 is not feasible, as the mechanical irregularities of the system impact negatively in the final result. Furthermore, the zero-crossing evaluation method, which is commonly applied in commercial FT-spectrometers, only take three samples per period of the reference signal. This method disregards the non-optimal nature of conventional mechanical parts and also lead to unfavorable results.

In order to overcome the aforementioned and undesired issues generated by the elimination of the non-conventional hardware parts, we propose the use of a spectral evaluation method that properly supports the development of an inexpensive FT-Raman prototype. In this scheme that we propose, the incorporation of a highly monochromatic reference signal (e.g. HeNe laser), with certain similarity as in the commercial FT-Raman devices, should help to achieve accurate evaluations of a Raman spectrum within the $\pm 1\,\mathrm{cm}^{-1}$ of spectral deviation, as proposed by the American Society for Testing and Materials (ASTM) [109, p. 267] [7]. However, this proposed evaluation method requires a reference signal having extremely low levels of optical power (some nW) in order to avoid the interference of the weak Raman signals. The corresponding detector must also be able to react properly to these low levels of the reference signal.

Our proposed and analyzed approach for the proper calculation of the Raman spectrum, collected by using an inexpensive arrangement of conventional parts, relies on the meticulously simultaneous sampling of the HeNe laser reference and the back-scattered

Raman signals during the scanning process, so that we obtain the following arrays after the scanning procedures:

$$P_i = \{P_0, P_1, P_2..., P_n\}, \tag{3.5}$$

$$R_i = \{R_0, R_1, R_2..., R_n\}, \tag{3.6}$$

where P_i is an array generated by sampling the back-scattered Raman light and R_i is a quasi-sinusoidal interference pattern signal generated by the reference HeNe laser. Both arrays are collected at specific sampling times $i = 0 \ldots n$.

The sampling rate applied in this evaluation method that we propose, must surpass the rate suggested by the Nyquist-Shannon theorem and the sampling rate used conventionally in FT-spectrometers (zero-crossing method, typically $\lambda/2$ [175, p. 95]). As a consequence, the quantization errors from the analog-to-digital converter (ADC), used to register the reference signal, can be significantly reduced [26, p. 442-443] and the irregularities influencing the real optical path in the Michelson interferometer can be effectively registered.

After the scanning procedures, the time-equidistant back-scattered Raman light, which is irregularly spaced due to the mechanical imperfections, can be transformed into a corrected and equally-spaced distributed re-sampled interferogram by taking into account the phase information extracted from the monochromatic reference signal, and by applying some mathematical methodologies (e.g. different interpolation schemes). This phase information allows an accurate retrieval of the relative position of the movable mirror along the scanned optical path by applying different mathematical methods (e.g. the Fourier Transform, or the Hilbert transform). Figure 3.7 depicts graphically the basic concept of the methodology that we propose for the spectral evaluation.

An interpolation method for the spectral evaluation of irregular-spaced samples, similar to the foretold above, has been described by Naylor et al. [121] for the evaluation of certain type of spectral data. However, this method involves the use of elaborated iterative operations and FFT subroutines that may significantly raise the complexity of the spectral evaluation, in comparison with our evaluation approach.

In this approach that we propose, the simultaneous scanning is performed under the assumption that the inherent change in phase ϕ_i of the monochromatic reference

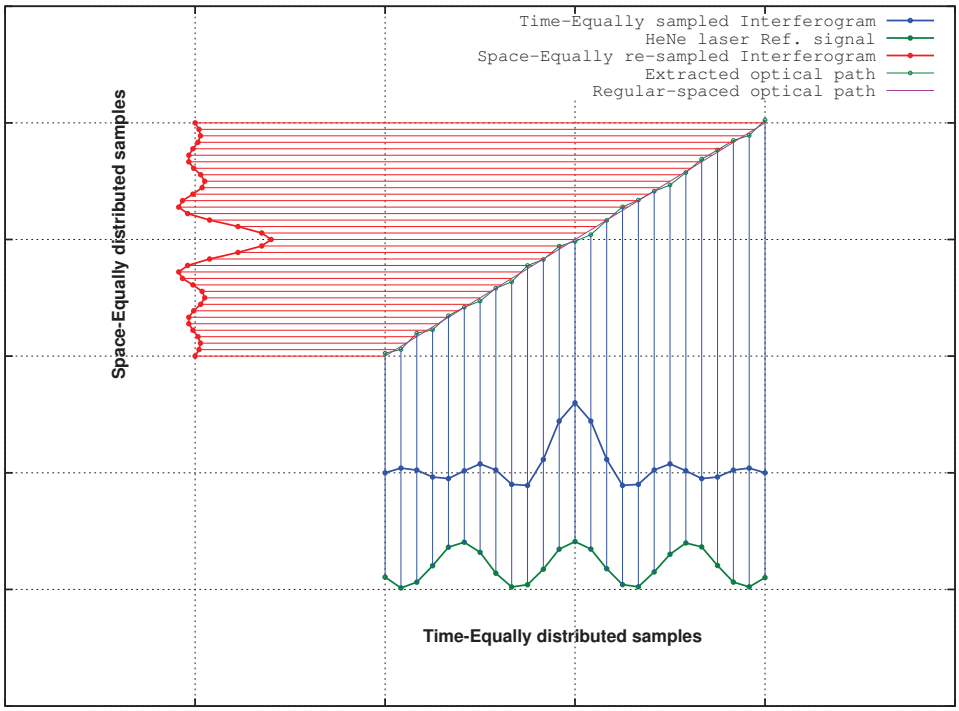

Figure 3.7: Graphical representation of the re-sampling evaluation methodology proposed for evaluating the Raman spectrum collected with the FT-Raman with conventional components. The equidistant-time sampled Raman back-scattered light is transformed into a regularly-spaced inteferogram by exploiting the information of the observed optical path from the reference signal.

signal, generated by the optical path difference, strictly increases monotonically ($\phi_i = \phi_0, \phi_2, \phi_3 \ldots \phi_n$). In the cases where this condition is not fulfilled, the complexity of the readout system of the reference signal increments, as additional efforts are necessary so that the phase information can be recovered.

For the monochromatic reference signal, we have considered a low power HeNe laser as a suitable device. HeNe lasers are light sources widely used in metrology, with a demonstrated effectiveness in the FTIR and FT-Raman spectroscopy, due to their low cost and due to their well-defined and stable wavelength [104, p.326]. Besides that, these lasers are available from a large number of manufacturers at reasonable prices. Furthermore, as already mentioned in the first part of this chapter, the accepted relative standard uncertainty for an unstabilized HeNe laser is about 1.5×10^{-6} [184] [66, p.165], which would represent only a few fractions of cm^{-1} of spectral deviation under critical conditions.

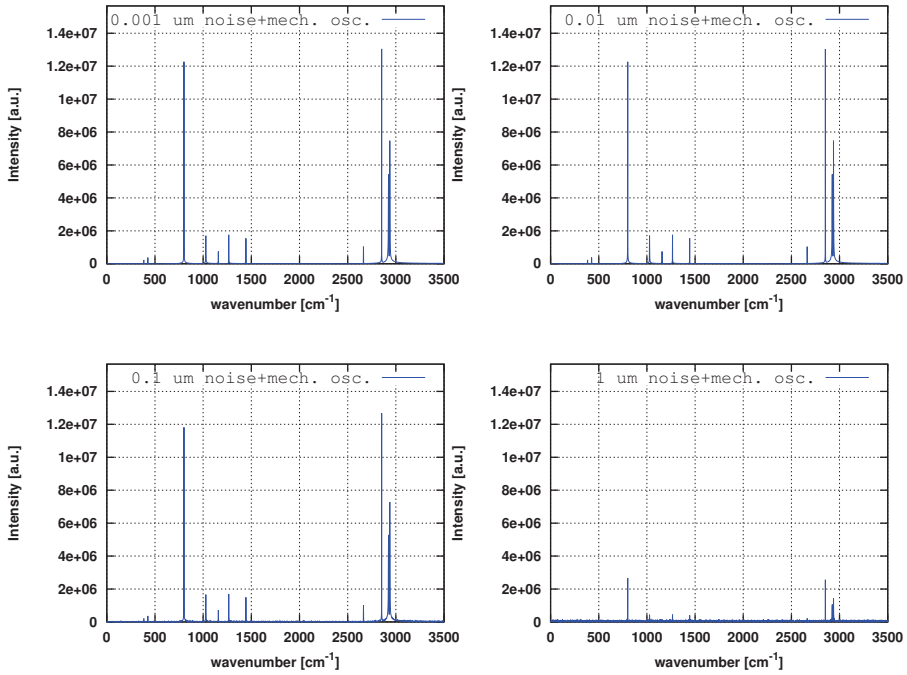

Figure 3.8: Simulated Raman spectrum of the synthetic signal of cyclohexane under the effect of the mechanical oscillations and different levels of equally distributed mechanical noise applying the re-sampling evaluation method.

A simulation of this re-sampling evaluation method, that we propose, using the same synthetic cyclohexane signal having the effects of the oscillating mechanical properties of the same Michelson interferometer, as in the previous subsections, has demonstrated that the Raman information obtained under the influence of different additional levels of equally distributed noise can be recovered without major impact on the frequency accuracy of the final Raman spectrum. The calculation of the corrected interferogram I_j (space-equally distributed) has been accomplished as follows:

$$I_j = \frac{j - O_i}{O_{i+1} - O_i}[P_{i+1} - P_i] + P_i, \tag{3.7}$$

where O_i represents the irregular-spaced optical path (or time-equally distributed), that has been extracted from the reference signal R_i (eq. 3.6), and it is calculated using the following equation:

$$O_i = \frac{\phi_i}{2\pi}\lambda, \tag{3.8}$$

Table 3.2: Main Raman shift peaks of standard vs. simulated Raman spectrum from the synthetic signal of cyclohexane (C_6H_{12}) applying the spectral evaluation method that we propose.

Standard spectrum[cm^{-1}]	Simulated spectrum [cm^{-1}]
384.1 ± 0.78	383.9
426.3 ± 0.41	425.6
801.3 ± 0.96	800.6
1028.3 ± 0.45	**1027.3**
1157.6 ± 0.94	1157.3
1266.4 ± 0.58	1265.6
1444.4 ± 0.30	1443.9
2664.4 ± 0.42	2664.0
2852.9 ± 0.32	2852.3
2923.8 ± 0.36	2924.0
2938.3 ± 0.51	2937.3

where ϕ_i is the phase information obtained from the reference signal R_i, and λ is the wavelength of the reference signal (e.g. HeNe laser).

Table 3.2 shows the main peaks of the standard Raman spectrum compared against the resulting peaks from the simulated Raman spectrum obtained by using our spectral evaluation method. The largest difference has been found at the Raman line of 1028.3 cm^{-1}, whereas the rest of the lines have shown only smaller fractions of spectral deviations. The characteristic Raman peak of cyclohexane at 801.3 cm^{-1} has shown a deviation of about 0.7 cm^{-1}, which is still within the margin recommended by the ASTM. Figure 3.8 shows the simulated Raman spectrum of the synthetic signal of cyclohexane under the influence of the mechanical oscillating irregularities and additional equally-distributed noise.

3.2 Étendue vs. spectral resolution, and the instrumental effects

The interferometers used in FT-Raman and in FTIR spectroscopy have certain advantages compared to the dispersive systems: wavenumber stability (or Connes advantage), Fellgett's advantage (or Multiplex advantage) and Jacquinot's advantage (or throughput advantage) [62, p. 171-172, 387] [211, p. 37-40]. The later is a relevant parameter that defines the amount of Raman scattering light that is going to pass through the FT-Raman system.

The Jacquinot's advantage or throughput advantage, also known as *"étendue"*, describes how a larger energy throughput in an interferometer can be achieved compared

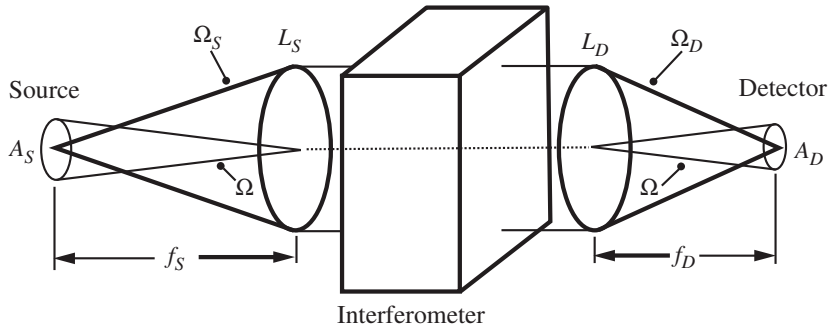

Figure 3.9: Representation of the étendue of an interferometer. Taken from [67].

to a dispersive system having the same resolution. As a result, it is possible to achieve values of signal-to-noise ratios as in the dispersive arrangements in shorter periods of time. However, there are several factors attached to this parameter that can influence the final spectral evaluation.

The throughput of the interferometer or étendue is defined by the size of the input source of the interferometer and its collimation optics. Figure 3.9 shows the general diagram of these parameters along the interferometer. The étendue of the interferometer is defined as [67, 157-158]:

$$E = A_s\Omega_s = A_D\Omega_D, \tag{3.9}$$

where Ω_s is the solid angle of the collimator lens observed from the source and it is defined as:

$$\Omega_s = A/f_s^2, \tag{3.10}$$

The larger the area A of the collimator lens and the area A_s of the interferometer source, the larger is the resulting étendue. However, this value has to be carefully observed and limited as it is also responsible for certain instrumental effects on the interferometer. The instrumental effects related to the optical properties of the interferometers and the tradeoffs attached to these parameters have been reported by Griffiths under the term *trading rules* [62, 63]. Figure 3.10 shows the influence of an increment of source size on several parameters of the Michelson interferometer.

Besides Griffiths, the instrumental effects and the tradeoffs of the interferometers have also been widely reported by Hariharan, Kauppinen and Partanen, and Sumner P. Davis

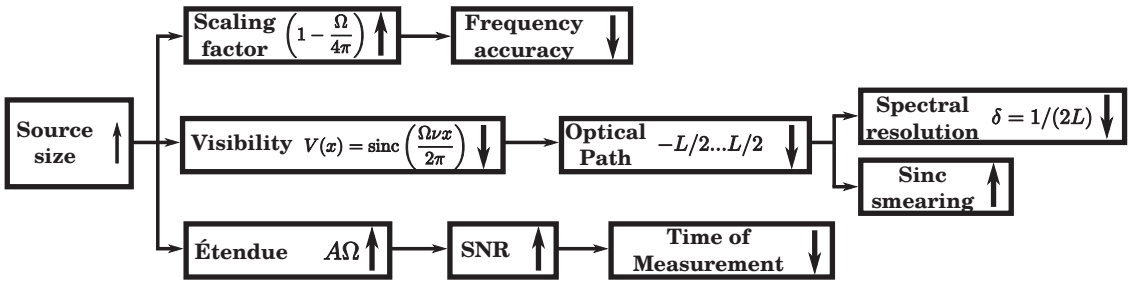

Figure 3.10: Tradeoff of the involved parameters of the interferometer as function of an increasing source size. The symbol ↑ represents an increment of the effect of the parameter; the symbol ↓ represents a decrement.

and Brault. The understanding of these parameters allows the optimal combination of the involved parameters in the interferometer in order to gather the largest possible amount of Raman light without affecting the accuracy of the spectral signal.

Under ideal conditions, the interferograms recorded by using an interferometer are produced by dividing and recombining waves from a single point source of ideal area $A = 0$, and for every component having a frequency ν present in the recombined signal, an intensity $I(x) = (1 + \cos 2\pi\nu x)$ can be observed.

In the commercial applications, this point source has a finite size area (A_S in the present case in figure 3.9) that defines the aforementioned optical properties of the interferometer. The finite size of the area of the entrance source of the interferometer, besides the limited amount of gathered light, has two main effects on the spectral informations:

- Scaling of the spectral shift axis by $\left(1-\frac{\Omega}{4\pi}\right)$
- Limitation of the spectral resolution through a limited visibility $V(x) = \mathrm{sinc}\left(\frac{\Omega\nu x}{2\pi}\right)$

These two effects modified substantially the intensity of the interferogram as a function of the optical path scanned and turn it into a signal of the form:

$$I(x) = 1 + \mathrm{sinc}\left(\frac{\Omega\nu x}{2\pi}\right)\cos(2\pi\nu x[1-\frac{\Omega}{4\pi}]) \tag{3.11}$$

It can be observed in eq. 3.11 that as the solid angle increases, the frequency of the sinc function increases too, and it forces the function $I(x)$ to go negative at some points

of the optical path x. Similarly, as the solid angle Ω grows, so does it the frequency of the cos function, generating a spectral deviation of the signal.

In order to efficiently radiate light into the interferometer, minimizing the instrumental effects on the spectral information, it has been necessary to investigate and optimize the combination of the optical parts and the entrance source of the interferometer of our proposed FT-Raman system. Additional optical effects can also be encountered such as line broadening (due to truncation, sampling and short finite path lengths), overfilling or under filling the entrance of the interferometer. However, these effects can be effortless overcome by scanning an adequate optical path lengths ($1/L \ll 2\nu_{max}$) and by properly adjusting the optical parts of the system.

The use of single-mode waveguides for the coupling of light into the Michelson interferometer would appear at first glance as an acceptable choice, as they have reduced diameter size (less than $10\,\mu$m). This would affect minimally the axis shift scaling of the spectrum and would allow large values of optical path lengths. However, these type of waveguides have the disadvantage of low acceptance angles and they are also difficult to adjust. In the case of multi-mode waveguides (with larger core diameters between $50\,\mu$m to $62.5\,\mu$m), the coupling procedure can be achieved in a less complex manner and it can keep low the levels of the scaling on the Raman shift. However, the larger core diameters of the multi-mode waveguides would have the drawback of smaller optical path lengths, in comparison with the single-mode waveguides.

Defining a multi-mode fiber (core diameter $62.5/125\,\mu\text{m} \pm 3.0\,\mu$m, NA=0.275 $\pm$0.0015) as the primary unit at the entrance of the Michelson interferometer, in combination with a collimation lens (focal length f =8.0 mm and a diameter ø=6.0 mm), the scaling factor $\left(1 - \frac{\Omega}{4\pi}\right)$ and the visibility envelope of the interference pattern $V(x) = \text{sinc}(\Omega\nu x/2\pi)$ have been simulated in order to verify the physical limits that would constrain our proposed instrumental arrangement.

In figure 3.11 it is possible to observe the spectral deviations generated by the scaling value $\left(1 - \frac{\Omega}{4\pi}\right)$, using different multiplication factors of the core of the multi-mode waveguide. Waveguides having diameters larger than 2.5 times the core of a $62.5\,\mu$m multi-mode fiber would produce spectral deviations larger than $0.1\,\text{cm}^{-1}$, which we consider already as significant (this represents 1/10 of the recommended values suggested by the ASTM). The diameter of one time the diameter core of the multi-mode fiber would generate a spectral

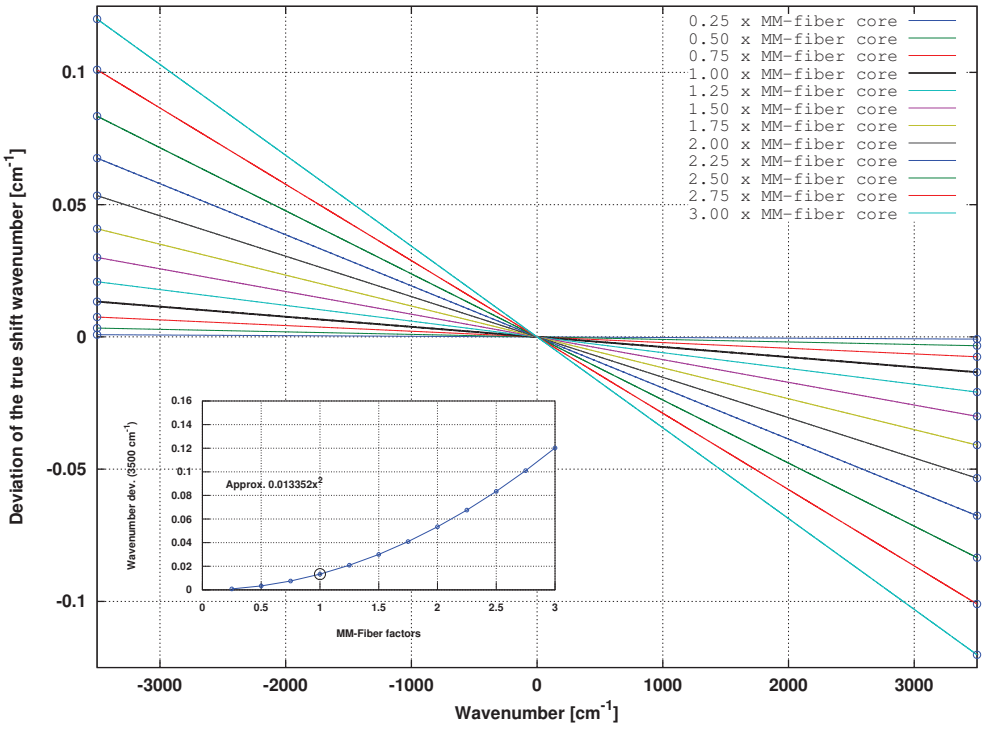

Figure 3.11: Effects of the finite source size at the interferometer input aperture along the Raman shift axis. Using different multiplicating factors of the 62.5 um fiber, it is possible to determine at which size of the diameter core the effect on the wavenumber axis the system is limited at the largest region of interest ($3500\,\mathrm{cm}^{-1}$).

deviation at $3500\,\mathrm{cm}^{-1}$ (largest possible value of interest) of about $0.013\,\mathrm{cm}^{-1}$. Two times the diameter of the multi-mode would generate a deviation of about $0.053\,\mathrm{cm}^{-1}$.

The effect of the sinc function ($\mathrm{sinc}(\Omega\nu x/2\pi)$) on the interference pattern, caused by the solid angles of the different light-guides, can be observed in figure 3.12 for the interference pattern generated with a HeNe laser ($\lambda = 632.8\,\mathrm{nm}$). For this specific wavelength, it is possible to confirm only reduced amounts of influence of the sinc function for core diameters smaller than $62.5\,\mu\mathrm{m}$. An optical path of 6.00 mm can be scanned without suffering major change on the visibility of the interference pattern. It does not occur in the case of the larger core diameters. The simulated core diameter of two times the multi-mode fiber caused a decay on the visibility of the signal of about 5%. A core diameter of three times the size of the multi-mode fiber generates a decay of almost 20% for the same scanned optical path.

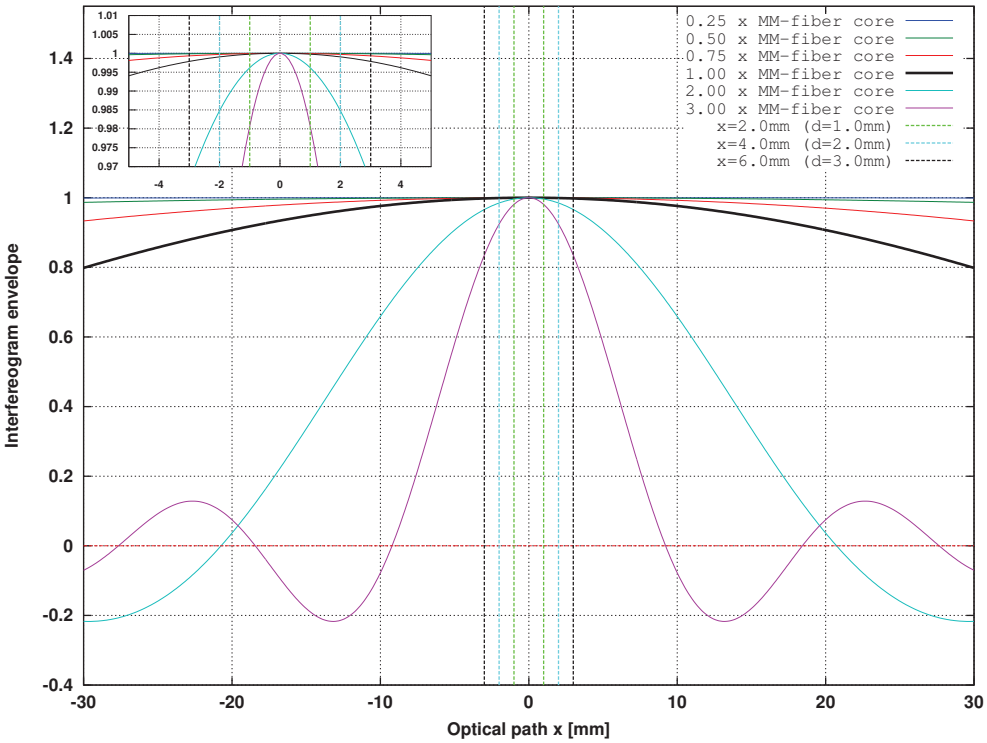

Figure 3.12: Envelope of the interferometric data collected as a function of the scanned optical path. The amplitude of the interference would decay significantly and turn negative when optical paths larger than 25 mm are used with the proposed optical arrangement.

Figure 3.12 has also shown the limit of the possible optical path for this theoretical arrangement with different optical fibers. In contradistinction to the wavenumber scaling $\left(1 - \frac{\Omega}{4\pi}\right)$ effect, that can be compensated, the effect of the sinc signal must be taken more seriously into account, as it defines plainly the possible path length that the system can scan before the interference pattern diminishes significantly or disappears entirely.

The emphasis on the optical path length $x = 6.00\,\text{mm}$ stated so far, obeys to the theoretical spectral resolution ($\delta\overline{\nu} = 1/(\Delta x_{max})$) of about 1.66 mm that can be achieved. The resolution required by most liquid and solid samples is around $3.0\,\text{cm}^{-1}$ to $10.0\,\text{cm}^{-1}$ [109, p.91].

3.3 Detection of the Raman scattering

A major concern in Raman spectroscopy is the reduced amount of generated Raman scattering available from the excited sample. For detecting the low levels of inelastic Raman scattering light from the materials under observation, two main conditions must be accomplished:

1. Effective suppression of Rayleigh scattering.
2. Adequate single photon counting capabilities.

There are several choices for eliminating the wavelengths of the so called Rayleigh scattering (which belong to the exciting light source in Raman spectroscopy). The most important and widely commercial available options are:

- Optical filters (Long pass or edge filters and notch filters).
- Tunable spectrometers.

The former consists of a single optical element that can be incorporated in an effortless manner (which is not the case with a tunable spectrometer) into the system. These optical filters are available for most conventional excitation wavelengths and they can be acquired from different vendors. In recent years, the notch filters have dominated the market due to their efficiency suppressing (values of optical density $OD \geq 6$ or values in transmission $T \leq 1 \times 10^{-6}$ for a specific wavelength) the Rayleigh light and due to its reduced size [181, p. 26]. The proper rejection of this specific wavelength is essential, as the amount of Raman light available for measurement is extremely low in relation to the Rayleigh scattering light.

In the non-dispersive systems, the detection of the back-scattered Raman light is provided by the so called single channel detectors [109, p. 180-183]. The available options for Raman scattering detection are basically the photomultiplier tubes (PMT) and the avalanche photodiodes (APD). The former have been gradually replaced by the detectors based on semiconductors due to several reasons: price, size, robustness, quantum efficiency, etc. Additionally, the PMTs devices with higher wavelengths detection capabilities are rather scarce. PMTs required high voltage levels and they are also affected by magnetic fields, even at small magnitudes of exposure [214, p. 259], [3, p. 403], so additional shielding might be necessary [173, p. 162].

Table 3.3: Common specifications of the most used single-channel detectors. Information taken from [109].

Parameter	Photomultiplier tube (PMT)	Avalanche Photodiode (APD)
Maximum Q	25%	90%
Response Range	185 - 930 nm	$<$ 300 -1050 nm
Photosensitive area	3 $\times$ 10 mm	5 - 20 mm
Dark signal	$<$10/s	$<$ 25/s
Maximum count rate	$> 10^5$ /s	$> 10^6$/s

Combining some of its characteristics (see table 3.3), it seems more affordable and favorable to our goals the use of a low-cost and compact APD in the so called *Geiger-mode*[1] than the use of a PMT. APDs are small devices with high quantum efficiency, that require almost no maintenance, and can operate with a simple circuitry. Moreover, the external circuitry of the detector with an APD could be adapted in order to match certain requirements of the FT-Raman system. An important weakness of the APD in Geiger-mode is the cooling system required for the reduction of the dark counting rate. This could potentially increase the expenses of the photon detection system at the levels of a conventional PMT.

Excelitas Technologies offers low-noise silicon APDs having high sensitivity in the range from 400 nm to 1000 nm (C30902 series) that can be conveniently incorporated as a photon counting device into our FT-Raman system. Similar devices have been found from manufacturers like Hamamatsu, and ID Quantique. The spectral coverage, the technical specifications and the low price range of these three manufacturers linked to this type of semiconductor devices, also support the conception of a photon counting device based on an APD in order to serve as a detector in the FT-Raman prototype that we propose.

As already mentioned at the beginning of this section, the intensity of the Raman scattering generated from a specific sample is significantly lower than the Rayleigh scattering. The Raman intensity depends directly on the so-called Raman cross section, the amount of excitation energy applied and on the amount of molecules excited in the sample. McCreery has reported, in a highly descriptive way, the intensity of a variety of chemical compounds for the 180° geometry arrangement [109, p. 31]. The Raman intensity values for these materials are between 8.9×10^5 and 1.0×10^{13} photons/cm^2/sr/s.

[1] APD with applied bias above the breakdown voltage, typically a couple hundreds of volts.

The amount of the detected Raman scattering light depends on factors such as the geometry of the collecting optics, the transmission of the system, the quantum efficiency of the detector, etc. However, determining the expected amount of Raman light from a sample is not a trivial process, since several parameters are involved in this process and occasionally certain characteristics of the system are not completely determined. Nevertheless, under the assumption of a 180° geometry and using as an excitation light source a helium-neon laser (HeNe laser, 632.8 nm, P=10 mW, beam diameter ø=1.0 mm), we would expect to generate 5.6×10^{11} photons/cm^2/sr/s in a pure sample of cyclohexane (C_6H_{12})[1] at 802 cm^{-1}. From this generated Raman light, our proposed photon detecting system would detect at least approximately between 16.3×10^3 and 94.5×10^3 photons/s of this specific Raman line by using a conventional 20x microscope objective and assuming a system transmission of 50%, and a quantum efficiency of 70% (see appendix A for a detailed description of this evaluation).

This value might fluctuate according to the changes in the optics, the overall transmission of the system, and the quantum efficiency of the detector. However, this only Raman line of cyclohexane could already surpass the amount of dark counts from the APD at room temperature (the C30902SH APD from Excelitas Technologies[2] has dark counts rates from 5×10^3 to 15×10^3 photons/s with a probability detection of about 5% [48]). Lower temperatures could help to reduce these noise figures.

3.4 Summary and conclusion of the chapter

We have demonstrated the inconveniences of extracting Raman spectra by applying common evaluating methods used in FT-spectroscopy when using specific engineering conventional and inexpensive hardware parts, being under the influence of certain amounts of equally distributed deviations of the optical path, and other mechanical disturbances. Nevertheless, the simulations performed for the spectral evaluation have confirmed that the re-sampling method that we are proposing might successfully assist on the extraction of Raman spectra having high frequency accuracy and precision. The instrumental effects that such a device might have on the resulting spectra, due to the optical properties of the Michelson interferometer, has shown that the Raman spectrum of a calibrating material

[1] Cyclohexane is a well known material in spectroscopy and it has well documented Raman cross section values for different Raman lines and using different sources of excitation.

[2] Formerly produced by PerkinElmer.

could be extracted without suffering relevant frequency deviations. The analysis of the instrumental arrangement has been performed considering an optical path that allows an adequate frequency resolution of the Raman spectra.

Additionally, under the constraints of the physical limits of the Michelson interferometer, described in sections 3.1 and 3.2, it has been found out that even under severe conditions, the possible amount of detectable Raman light from the chemical compound cyclohexane could easily exceed the dark counting rate of both photomultiplier tubes (PMT) and avalanche photodiodes (APD).

Chapter 4. Implementation of the FT-Raman system and its functionality

In chapter 3, some of the undesirable effects on the spectral evaluation have been shown. We have also provided an overview about the solutions that we propose in order to overcome these artifacts. These unwanted effects emerge when the collected data of a FT-Raman device, fabricated by using non-sophisticated mechanical parts, are evaluated applying the methods traditionally used in the commercial FT-Raman spectrometers. However, the accurate extraction of the optical path and the subsequent re-sampling of the Raman scattering light might enable the calculation of the Raman spectrum having an adequate spectral resolution and frequency accuracy, as in commercial FT-Raman devices. In the present chapter, the basic composition and functionalities of the FT-Raman system that we propose are introduced. This system has been built by using mostly usual, affordable and conventional parts, and it is supported by software modules that we have developed by using only open-source programming tools.

Section 4.1 describes, in four different subsections, the general physical arrangement of the FT-Raman system that we propose, including the interconnection of all its components. Section 4.2 is divided into three subsections that contain information about the software tools that support the functionality of the FT-Raman instrument that we have realized. Finally, section 4.3 describes in shorthand the basic procedures (e.g. calibration, measurements, adjustments, etc.) that are required by the validating prototype that we have developed in order to acquire the Raman spectrum of a specific material under observation.

4.1 Instrumental setup

The implementation of the FT-Raman system for validating the design and the method that we propose has been achieved by the following main hardware components: a Michelson interferometer, a self-designed photon counter and a Si photo-detector for reference recording. Figure 4.1 shows a general diagram of the main setup of the FT-Raman prototype that we propose. This instrument has been used by us to validate certain aspects

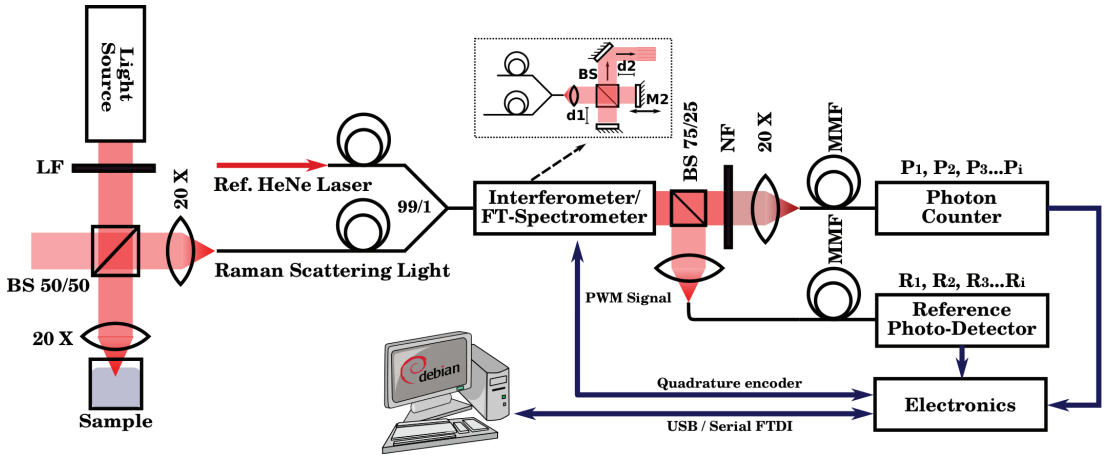

Figure 4.1: General diagram of the FT-Raman spectrometer prototype proposed. This FT-Raman device consists of an original combination of conventional and inexpensive hardware parts that are supported by our spectral evaluation method.

of the evaluation methodology that we proposed in subsection 3.1.4 and in subsection 3.3. A wider description of the different parts of this system can be found in the subsequent sections of this chapter, and also in appendix B.

Our FT-Raman system is characterized, from its basic concept, by the absence of sophisticated parts (for easing an industrial process of production) that are usually included in these type of commercial instruments for different purposes (e.g. for optical path tracking, photo-detectors cooling systems, optical corrections, photon counting units, etc.). The Raman light, from the excited sample, is guided to the FT-Raman system using a coupling ratio 99/1 coupler (62.5/125 μm multi-mode optical fiber). This coupler is also used to transmit the low-power monochromatic light used as a reference, so it follows the same path as the Raman scattering light inside the Michelson interferometer. The FT-Raman system also incorporates a micro-controller board, and some readout circuitry that allow the basic functions of this device. The software layer, used to control the FT-Raman spectrometer and to evaluate the data collected, is a combination of three main interconnected components: a PC application, firmware for the micro-controller and some custom evaluation scripts.

4.1.1 Michelson interferometer as spectrometer

The modulation of the different wavelengths generated from the sample under observation is achieved with a Michelson interferometer that we choose. This type of devices has been selected since its construction, operation and adjustment demands little efforts [68, p. 18] [175, p. 66], while the acquisition of its components is rather straightforward. Moreover, this type of instrument allows the modulation and the detection of the different wavelengths from the Raman scattering by using only a single detector (a photon counter in our case, which is described in subsection 4.1.2). The Raman information retained in a complex interferogram can be separated in the different components afterward by computing through a Fourier Transformation [109, p. 225].

The Michelson interferometer of the system consists in a robust aluminum case, which holds a collimator lens (f=8.0 mm, ø=6.0 mm) at the entrance, a 50/50 beam-splitter BS, and a fixed mirror M_1. Outside the aluminum case there is a moving mirror M_2. Both mirrors, M_1 and M_2, are assembled on tilt-inserts so that the XY angles can be manually adjusted. The moving mirror M_2 is mounted on top of a linear stage (0.5 mm per turn). This linear stage has a DC-motor (driven by a H-Bridge circuit), a gearing system, and an optical quadrature encoder. The combination of these components allows the linear stage to reach a mechanical resolution of approximately 22.9 nm per step.

The output of the Michelson interferometer is sectioned by a SiO_2 75/25 beam-splitter. This optical component transmits 75% of the intensity of the outgoing beam from the interferometer to the photon counting device, and reflects only 25% of the light to the photo-detector for the optical path recording.

4.1.2 Single photon counting system

It has been previously described that the Raman back-scattered light produced by a sample is, in general, significantly smaller than the light produced by the Rayleigh scattering[1]. In order to detect efficiently this reduced amount of Raman light, it is necessary to suppress the greatest possible amount of Rayleigh scattering light, and to set an adequate device with single photon counting capabilities. From the available choices, we have proposed and justified in section 3.3, both technically and financially, the use of a single photon counting system based on an avalanche photodiode (APD).

[1]The probability for a **strong** Raman scatterer is approx. 10^{-6} of the incident light [92, p. 17].

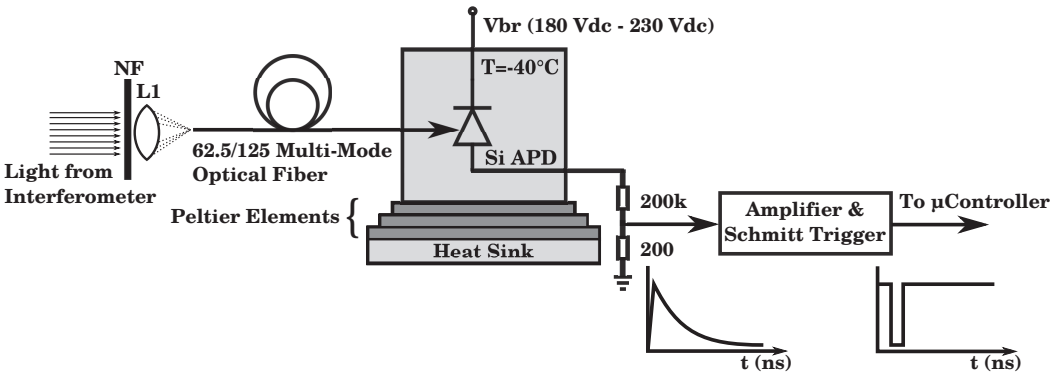

Figure 4.2: Diagram of the single photon counting unit. The signal obtained right after the passive-quenching circuit and the conditioned signal connected to the readout micro-controller can also be observed.

Figure 4.2 shows the basic structure of the photon counting unit belonging to the proposed FT-Raman system. This device has been built by using an Excelitas Technologies C30921SH (0.25 mm active area) Si APD[1], a signal amplifier and a signal conditioning circuit (Schmitt trigger). A notch filter (NF) has been placed in front of the entrance lens of the photon counting device. The purpose of our choice is to eliminate a large proportion of the Rayleigh scattering so that the photon counting device does not enter into a state of saturation.

We operate the C30921SH APD [48] of the photon counter device in the so called Geiger mode[2] using a passive quenching circuit, which consist of two resistors connected in serial configuration. This operation mode allows the Si APD to detect single photons in the visible and near infra-red regions of the spectrum with convenient values of quantum efficiency (up to 90%). When a photon reaches the Si APD (through the 62.5/125 multi-mode optical fiber and the light-pipe of the APD case) and generates a pulse, it is amplified and conditioned to the TTL level at the Schmitt trigger. The Schmitt trigger output can be directly read by the micro-controller during the measurement process. The applied voltage at the Si APD, for Geiger mode operation, is calculated according to the Si APD temperature in such a way that photon detection probability achieves a value of at least 50 %.

In order to reduce the dark counting rate and improve the responsivity of the photon

[1]This is a former device from the manufacturer Perkin-Elmer.
[2]The Si APD must be biased above the breakdown voltage $Vbr + V$.

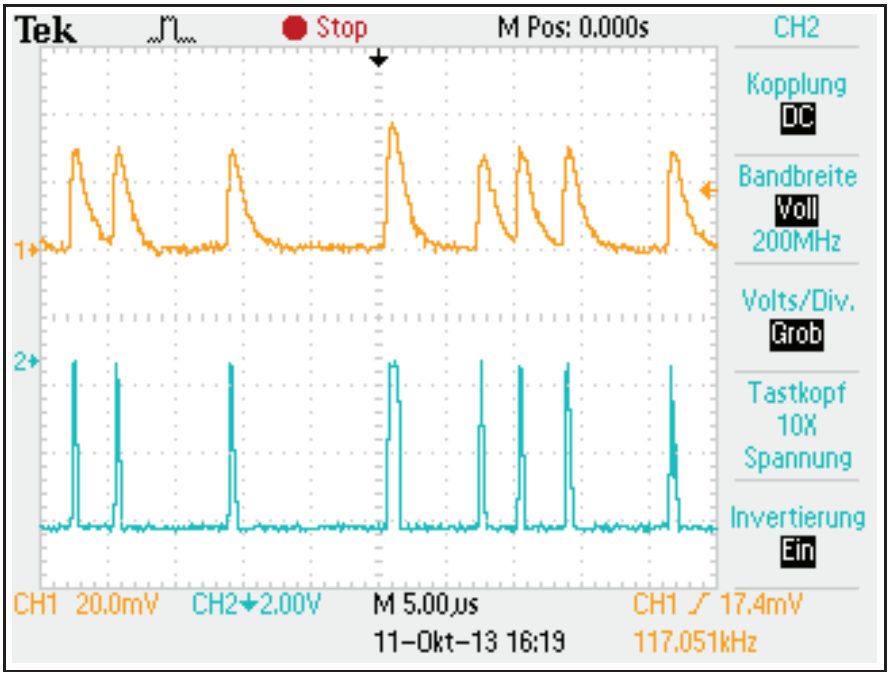

Figure 4.3: Signals of the photon counter device from an oscilloscope during a measurement procedure. Channel 1 (orange) shows the analog output from the Si APD. Channel 2 (blue) shows the inverted output of the signal conditioning circuit, which is connected to the micro-controller.

counting unit, the Si APD is cooled down using a three-stage Peltier element. The operative temperature ranges from $-35\,^{\circ}\mathrm{C}$ to $-40\,^{\circ}\mathrm{C}$. We extract the generated heat of the three-stage Peltier element cooling system with a heat pump; it consists of a 40 mm by 40 mm aluminum water circulator.

This heat pump can be easily substituted by an air cooled heat sink if required. In our development of this device it has also been avoided the incorporation of sophisticated elements (e.g. nitrogen cooling system, active quenching circuits, mechanical parts, etc.).

Under this conditions the photon counting device has achieved dark counting rates in the range from 150 to 200 counts per second. We have observed counting rates of some hundreds up to 150,000 photons per second with this photon counter setup. Higher counting rates have been also tested although these quantities tend to be not reliable for a proper analysis. Figure 4.3 shows the output signals of the photon counter unit that we acquired by using a digital oscilloscope.

4.1.3 Reference photo-detector

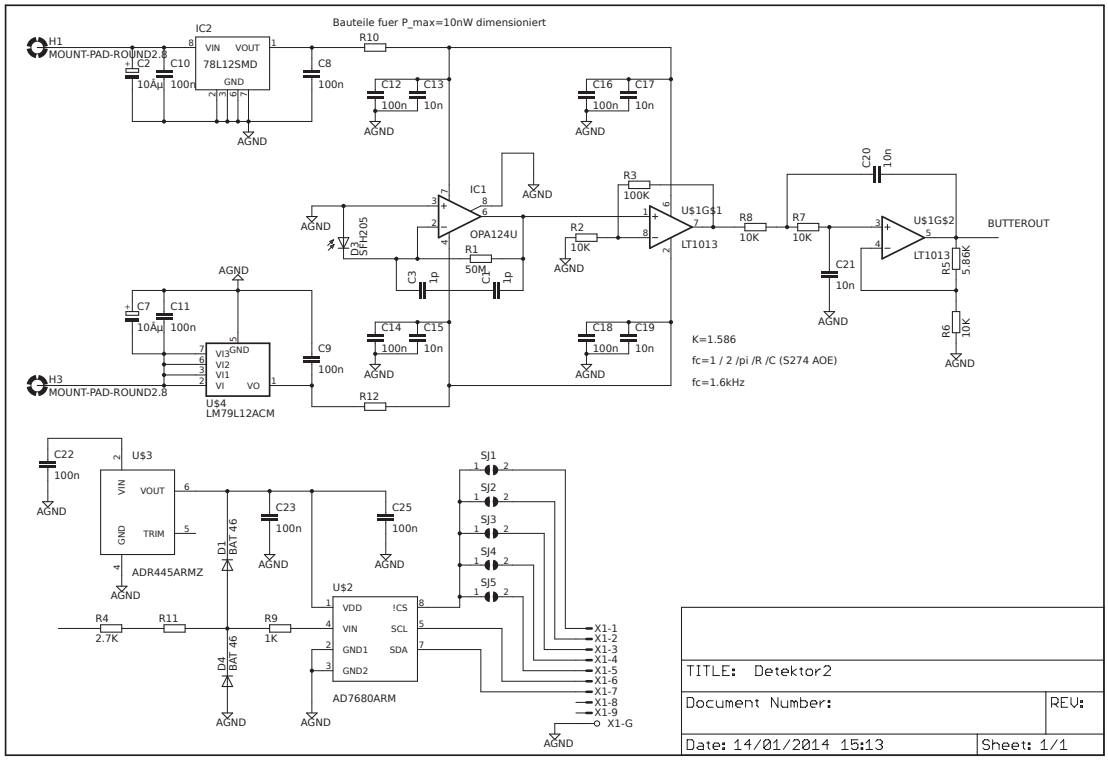

Figure 4.4: Schematic of the internal structure of the reference photo-detector used to extract the optical path information. Image taken from [213].

A critical process in the evaluation method we proposed relies in the accurate extraction of the optical path described by the movable mirror of the Michelson interferometer during the scanning process. The optical path in this case is obtained by sampling an additional interference reference pattern, generated by a monochromatic light source, with a photo-detector unit. However, since the reference light is coupled with the Raman back-scattered light from the sample, it is mandatory to apply only reduced intensity levels (some nW) for this reference signal. Reference signals having higher intensities would cause similar effects on the photon counting process than those produced by the Rayleigh scattering light (saturate the photon counter device), therefore an adequate circuitry that can register properly the reference interference pattern is required.

The photo-detector we developed used for the extraction of the optical path has been developed by using a Si PIN photodiode S5973-01 from Hamamatsu in combination with

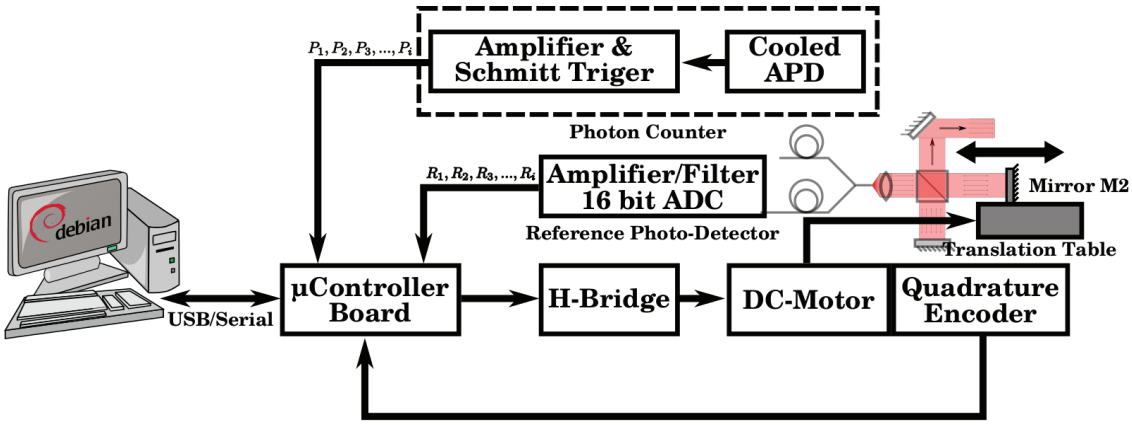

Figure 4.5: Diagram of the electrical interconnection of the FT-Raman system.

a transimpedance amplifier and a second order Butterworth low-pass filter (Sallen-Key topology [21, p. 380-381] on the upper right part of figure 4.4). The selected cut-off frequency is tuned at approximately 1.6 kHz. The photo-detector includes an A/D converter (16bit SAR AD7680ARM, SPI interface, from Analog Devices) right after the amplification and the filter stages. Figure 4.4 shows the schematic representation of design of the photo-detector unit that we propose. This arrangement has been successfully tested in the detection of low-power signals [213] and is able to register optical power levels of about 10 nW. Additionally, this same photo-detector is used to locate the balance position of the Michelson interferometer and to adjust the values of visibility of the reference during the calibration procedures.

4.1.4 Electrical interconnection of the system

The three main components of the FT-Raman system (Michelson interferometer, photon counter device and reference photo-detector) must interact in such a way that a smooth displacement of the movable mirror M_2 of the Michelson interferometer is carried out, while the sampling of the photon counter device and the reference photo-detector takes place simultaneously. This is required for an accurate acquisition of the time-equally distributed samples for our evaluation method, which has been already described in subsection 3.1.4. Besides that, the system must be able to interpret the commands from the user interface, and to transmit the data acquired during the measurement processes.

The low-level core of the FT-Raman system is an ATmega32 micro-controller [10] from

Atmel®, which is embedded in a locally-developed evaluation board[1]. This device provides the basic functionality required for driving all the components of the FT-Raman system in a coordinated manner. Figure 4.5 depicts the different devices around the micro-controller with the respective electrical and logical connections required for the proper operation of the FT-Raman spectrometer.

This micro-controller performs the main following tasks in the FT-Raman spectrometer:

- Receiving and converting the commands transmitted by the user interface.
- Acting as PID controller loop in order to provide a highly smooth and constant displacement of the movable mirror $M2$ of the Michelson interferometer (on the linear translation table) during the scanning process.
- Reading the feedback signals from the quadrature encoder, which is embedded in the DC-motor that drives the translation table.
- Receiving the sampled data from the photon counter and from the reference photo-detector devices.
- Transmitting the measurement and the status data to the user interface.

As the measurements take place, the control loop evaluates the output signal, which is then transmitted to a H-bridge circuit. The H-bridge is an electronic circuit that allows the operation of the DC-motor of the translation table in both directions. As a result of the motor operation, the quadrature encoding device, embedded in the DC-motor, changes its state and it can be used as the feed-back for the control loop. As this operation is performed, the micro-controller collects the data from the photon counter and from the reference photo-detector, which are then transmitted to the user interface for further evaluation and visualization.

4.2 Control and operation of the FT-Raman system

The instrumental arrangement, described previously in section 4.1, specially the interaction of low-level components described in subsection 4.1.4, requires an operative set of

[1]Evaluation board developed at the University of Applied Sciences Offenburg under the name of *MK_Board*. Additional information about this evaluation board can be found in appendix B.

software modules for different purposes: communication between the user and the system, scanning of a specific optical path, sampling of the sensors, etc. Commercial FT-Raman devices use proprietary closed-source software interfaces (mainly for Windows platforms) like the OMNIC^{TM}Series (Thermo Scientific) or the OPUS suite developed by Bruker Optik GmbH [211, p. 1-2]. These software packages enable, among other things, the operation of the instrument, the collection of data, and the visualization and evaluation of the spectra. However, these kind of products cannot be integrated in our FT-Raman system due to the intrinsic characteristics of the instrumental implementation of our system and the proprietary nature of these commercial software suites.

The proposed FT-Raman spectrometer presented in this chapter operates with the support of two self-developed software tools: custom user interface application and a firmware software for the low-level operation of the FT-Raman instrument. The evaluation of the collected data is likewise performed by a set of scripts specially tailored for this purpose. We have conceived these tools under the platform GNU/Debian Linux (although it can be easily ported to other Unix-like platforms or another conventional operative systems) using different GNU C/C++ compilers, libraries and the high-level interpreted language GNU/Octave [42]. Besides an adequate operation of the proposed system, these software tools also permit achieving a great deal of robustness, flexibility, security and reliability in our system [72, p. 395] [135, p. 8] [183, p. 63-64]. All this can be achieved without having the financial and dependency burden that commercial solutions might represent [108, p. 3-4].

At the highest level of the system is the user interface, which is incorporated in a single PC application. This application provides visual aid and communication capabilities with the micro-controller firmware of the FT-Raman system. The firmware is in charge of the reception and interpretation of the commands from the user interface, the performing of the measurements, and the collection and transmission of the collected data. The next three subsections describe some additional details about the main tasks and composition of each of the software modules of the FT-Raman system that we proposed.

4.2.1 User interface application

Since the amount of possible combinations of the parameters that can be adjusted is high, before a Raman measurements can take place, it is necessary to adjust and combine in an optimized way several parameters. Therefore, it is necessary to establish a mechanism

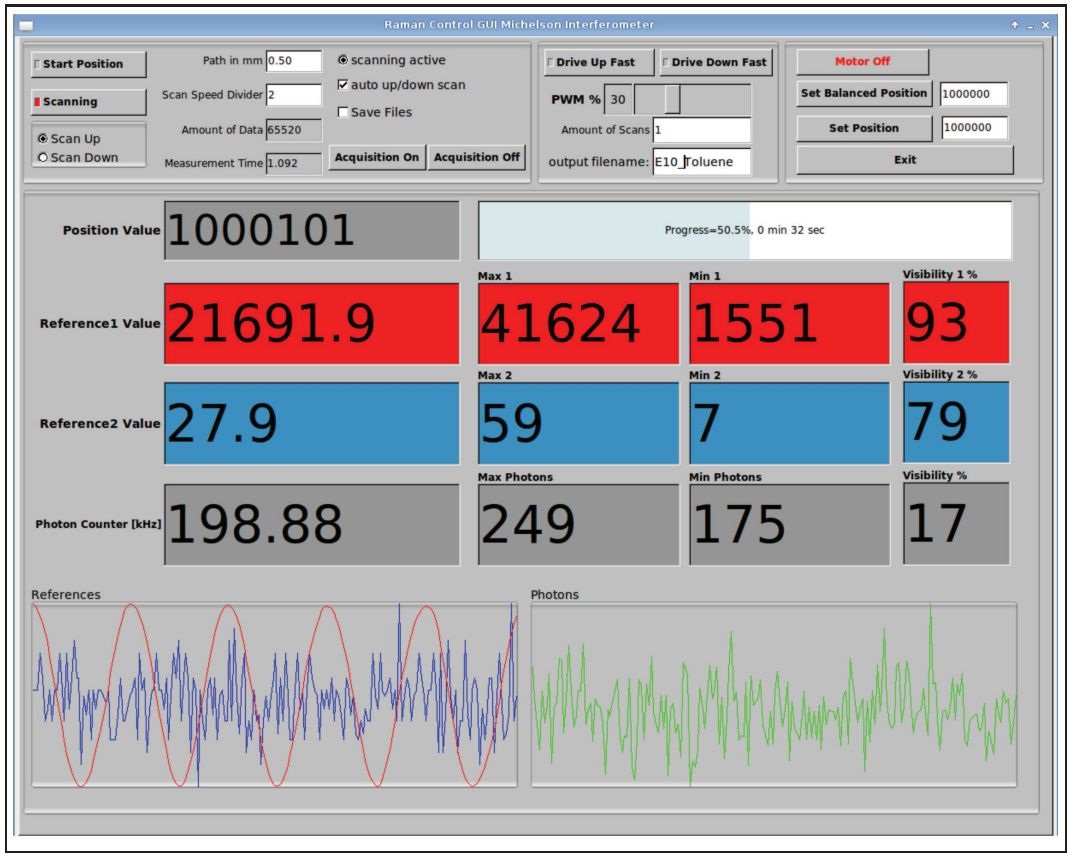

Figure 4.6: Graphical user interface used to perform tasks such as calibration and measurements with the FT-Raman spectrometer.

that allows the system user to interact with this system during the whole measurement procedure: pass the measurement parameters to the instrument, verify the actual state of a running measurement, receive and save data transmitted by the Ft-Raman spectrometer, etc.

In order to accomplish all the tasks mentioned previously, we have developed a set of applications that allow the interaction required between the user and the FT-Raman system. The user interface application is the most original piece of this software package of the system. This application allows the user to run the necessary commands to calibrate the FT-Raman spectrometer, perform measurements, save the data collected, etc. It also offers the user visual support about values like time to complete the scanning or values of visibility, reference levels, position, etc. can be also displayed. Figure 4.6 shows the application used to carry out a measurement on the FT-Raman spectrometer that we

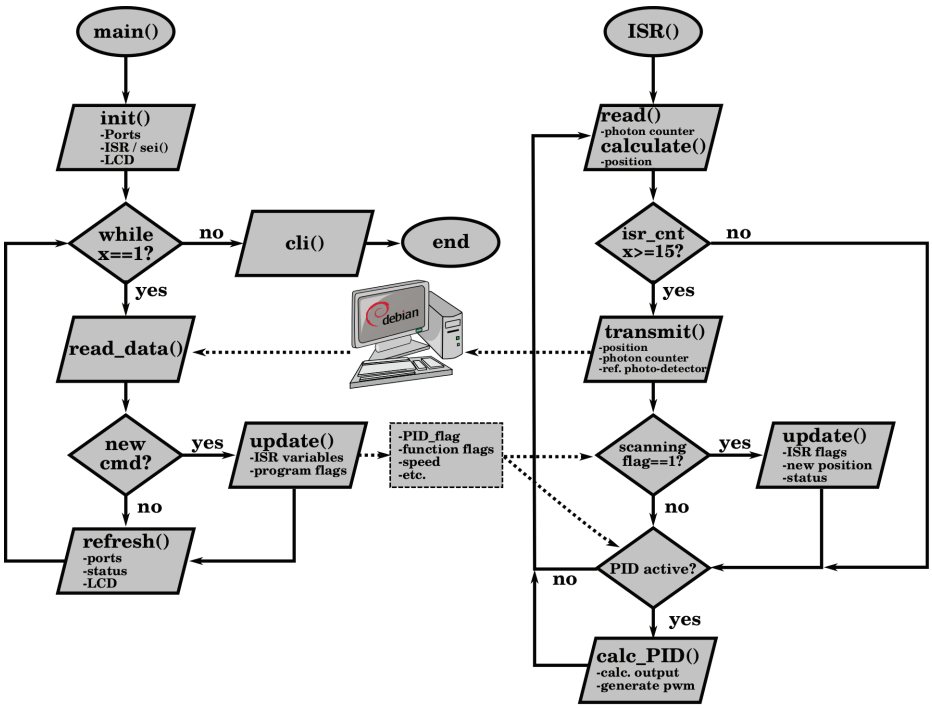

Figure 4.7: Flowchart of the most representative functions performed by firmware embedded in the ATmega32 micro-controller. The left part represents the main loop of the program, whereas the right part represents the interrupt service routine (ISR) that performs the equally-time distributed sampling of the detectors.

propose. In the cases where no visual assistance is required, the measurements can be performed by using a console application, which requires less memory resources from the PC terminal.

This user interface application has been developed with the GNU C++ compiler and it is distributed in several classes. Additionally, different libraries have been used to accomplish all the features of the applications: FLTK (development of the graphical interface), FFTW3 (fast Fourier transform), libftdi1 (USB-Serial communication between PC application/micro-controller).

4.2.2 System firmware

As previously described, the low-level capabilities, required for the application of the evaluation methodology that we have proposed, are carried out by an evaluation board with an embedded ATmega micro-controller. The functionality of this part of the system

has been implemented using the AVR Libc packages, which are the most extended and documented for the Atmel AVR micro-controllers. These packages provide a subset of the standard C library for the ATmega32 and other AVR 8-bit RISC (*Reduced instruction set computing*) devices from Atmel.

The coordinated reception, interpretation and transmission of the data in the micro-controller is achieved with basically two relevant functions: a main function, and an interrupt service routine (ISR). The function "main" of the micro-controller is in charge to initiate the proper status of all the ports and interfaces. It also starts all the flags necessary to run the ISR used to control the measurements. Once the variables and conditions are set, the micro-controller reach an infinite loop, where it "listens" and interprets the commands transmitted by the user interface. Figure 4.7 shows a representative flowchart of the firmware software that resides in our micro-controller.

The interrupt service routine (ISR) is the most important part of the program running inside the micro-controller. This ISR is called every 62.5 μs (f_{ISR} = 16 kHz), in order to detect the small changes in optical path so the system accomplishes a highly smooth displacement of the translation table in which the movable mirror is mounted. The ISR transmits to the PC user interface the sampled values of the reference photo-detector and the photon counting device with a frequency of 1.0 kHz (or every ms). The output value of the controller is also updated at this same frequency. The ISR function also allows the user to calibrate the FT-Raman spectrometer prior to the measurements.

4.2.3 Evaluation scripts

The commercial FT-Raman devices, which normally apply the zero-crossing evaluation method, acquire only three data points per period of the monochromatic interference pattern used as a reference. For example, if a spectral measurement is having an optical path length O_{length} of 6.0 mm, the amount of collected data would be approximately:

$$AmountOfData = 3 \times \frac{O_{length}}{\lambda_{ref}} = 28445 \tag{4.1}$$

28445 data points per parameter, assuming that a HeNe laser (λ_{ref}=632.8 nm) is used as a monochromatic reference signal. The amount of resulting data gathered during the measurements carried out with our proposed methodology is substantially higher (up to approximately 262000 data points per parameter for an optical path of approx. 6.0 mm)

due to the higher sampling ratio required for the accurate estimation and correction of the optical path. Therefore, besides an evaluation tool, a suitable mean of data handling also was required for our FT-Raman system.

We have chosen GNU/Octave [42] to be the evaluating software for the collected data from the measurements. GNU/Octave is an high-level scripting software intended for numerical calculations (similar to MATLAB) that provides a large set of functions packages and is well-suited for the digital processing of information and for prototyping purposes. Furthermore, the amount of collected data from every scan can be easily handled in fractions of seconds in a conventional PC terminal having a 64-bit processor (e.g. a dual core AMD64). Additionally, the size of the scripting programs can be kept short, highly readable and in text-format only, which make its maintenance and management less complex.

Under the GNU/Debian Linux platform, the combination of the evaluation scripts and the user interface applications can be achieved through the command interface offered by this UNIX-like operative system (basically with the C++ *system()* function). In that case, an automatic evaluation of the spectra can be accomplished just after the corresponding file of a specific scan has been generated, otherwise the evaluation can be performed after a whole set of scans has been completed.

Several GNU/Octave scripts have been developed for handling the data acquired during the Raman measurements. The main scripts are used for the initial extraction of the spectral information contained in the collected interferograms from every single scan of the measurement. In this GNU/Octave script, the accurate extraction of the optical path has been implemented. Another script contains the algorithms required to generate a final version of a specific Raman spectrum, including peak position labeling, averaging of the numerous spectra from the scans, applying different filtering techniques, baseline corrections, saving the final spectrum, generating the proper plots, etc.

4.3 FT-Raman system operation and evaluation procedures

The original operation of the FT-Raman system that we propose, as presented in this chapter, substantially differs from the operation of the commercial FT-Raman devices. Our FT-Raman spectrometer has to accomplish several steps before the monitoring of certain harmful materials is performed. This section describes briefly the common sequence

that must be followed during a spectral measurement using the FT-Raman system that we have conceived.

The initial procedure is the calibration of the Michelson interferometer. This is accomplished by successively sampling the light from the Michelson interferometer output with both a white light source (a red super-luminescence light-emitting diode with a coherence length of about 30 μm) and a monochromatic light source (HeNe laser). The white light allows to find the balanced point ($d_1 - d_2 = 0$) of the Michelson interferometer. Once the balanced position is found, the visibility around the calibrated position has to be optimized by scanning the interference pattern from the monochromatic light. It is accomplished by carefully overlapping the reflected light of mirrors M_1 and M_2. A proper adjustment allows to achieve visibility values of about 93 % to 96 %. The cooling stage of the photon counting unit and the warming-up of the lasers are performed in parallel.

Once the calibration procedures have been carried out, the parameters required for the measurement (e.g. optical path difference d, scanning speed, file location, etc.) are configured in the PC application, and transmitted to the micro-controller. The micro-controller receives all the needed parameters, interprets them and proceeds with the measurement. During this measurement the movable mirror M_2 travels on the optical path from $-d/2$ to $d/2$ around the calibrated position, at typically 23 μm/s. Simultaneously, the photon counter, the reference photo-diode and the DC-motor encoder are sampled at a frequency of 1.0 kHz. All the sampled data are transmitted back to the PC application through an universal serial bus (USB) for later evaluation.

For each measurement scan, one text file is created containing the data from the time-equally distributed samples of the photon counting device, and the reference photo-detector. Additionally, the file contains the relative position of the moving mirror M_2, which is obtained from pulses given by the quadrature encoder. This information helps to verify the proper adjustment of the gain parameters of the control loop. The PC application can automatically evaluate the collected data from the FT-Raman measurement after every scan is completed or it can be evaluated subsequently using additional GNU/Octave script programs. Figure 4.8 shows the evaluation diagram that has been implemented in this GNU/Octave script in order to extract the Raman spectrum after every scan during a measurement while using our FT-Raman spectrometer.

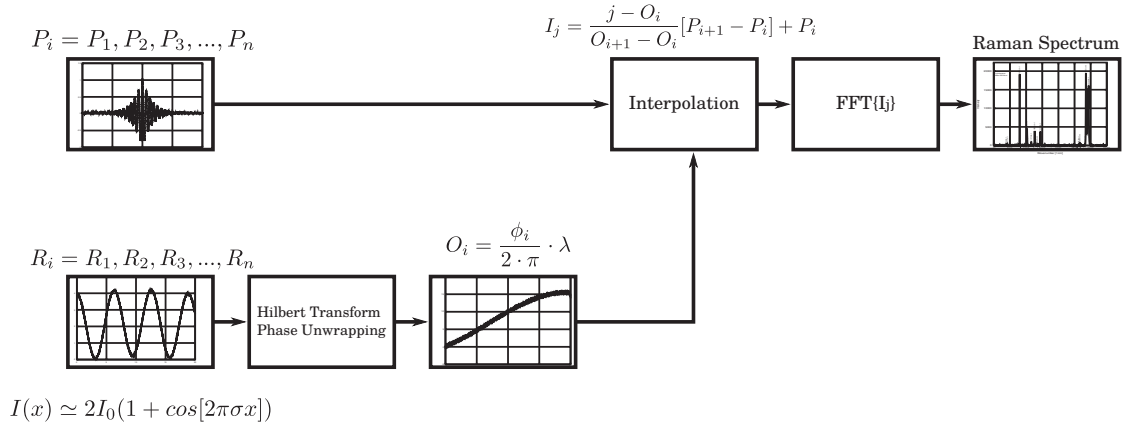

Figure 4.8: Evaluation diagram of the Raman spectrum after every scan. This evaluation procedure has been implemented on GNU/Octave.

4.4 Summary of the chapter

The implementation of the instrumental setup that is required for validating the evaluation method that we have proposed has been presented in this chapter. It has been shown how the system and its interconnection were achieved by combining mostly conventional parts and open-source software tools. Although the original operation of this FT-Raman prototype requires certain additional adjustments prior to the measurements (in several cases also required by the commercially-available FT-Raman devices), the overall flexibility of our FT-Raman system gives the user an outstanding platform for exploring non-conventional configurations of the instrumental arrangement and the experimental procedures.

Some of the validation results obtained can be found in chapter 5. Chapter 5 shows parameters such as frequency accuracy and precision, as well as the relative intensity obtained from certain calibration materials (e.g. cyclohexane, toluene, benzene). The first two materials are included in the ASTM list of calibration materials and as previously mentioned, the spectral deviation of the characteristic main peaks of these materials must be less than $\pm 1.0\,\mathrm{cm}^{-1}$.

Chapter 5. System validation

A convenient measurement system must deliver consistent, reliable and accurate information in order to avoid possible interpretation mistakes of the analytical data, specially in systems where sensitive instrumentation is used (e.g. optical interferometers). The validation of a method can be used to judge the level of reliability of the measurement technique [2].

This chapter present a series of spectral measurements and comparisons intended to validate and verify certain capabilities of the system and the evaluation methodology that we have proposed, specially the spectral frequency accuracy. This chapter also includes an approximate evaluation of the financial resources devoted to the development of the FT-Raman system, and an indirect comparison with the expenses that a commercial FT-Raman device would require.

5.1 Validation of the frequency accuracy using calibration materials

Different authors[109, 93, 181] agree in the usefulness of validating the frequency accuracy using the data offered by the American Society for Testing and Materials (ASTM) [7]. The document that contains the data required for the frequency validation can be found under the title of *Standard Guide for Raman Shift Standards for Spectrometer Calibration*. Besides the wavenumber values, the relative intensity of the characteristic Raman peaks of the calibration materials are also revealed in this guide. Eight different materials (naphthalene, 1,4-Bis[2-methylstyryl]-benzene, sulfur, toluene, acetamidophenol, benzonitrile, cyclohexane and polystyrene) have been added to this list. The Raman spectra of these materials were collected by using instruments having a reported maximum deviation of less than $1.0\,\mathrm{cm}^{-1}$. McCreery, Lewis and Edwards also offer a description of the steps to follow in order to calibrate and validate the measurements obtained with Raman spectroscopy and in the use of the values provided by the ASTM.

In order to validate the frequency accuracy of the resulting Raman spectra obtained with the FT-Raman spectrometer that we propose, a series of measurements related to

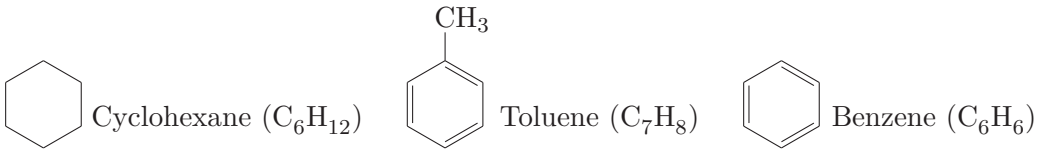

Figure 5.1: Structure representation of the chemical compounds used as additives in commercial gasoline. The Raman spectra of these material have been also investigated using the setup in figure 4.1.

cyclohexane, toluene and benzene have been performed. Figure 5.1 shows the structural representation (or skeletal formula) of these three chemical compounds. The collected Raman spectra of cyclohexane (C_6H_{12}) and toluene (C_7H_8) have been compared to the standard spectra found in the ASTM list. The Raman spectrum of a third material, benzene (C_6H_6), has also been collected using the FT-Raman prototype for validation purposes. Although benzene is not widely used as a calibration material, its Raman spectrum has been compared to the spectral values suggested by McCreery, the National Institute of Standards and Technology (NIST), and the National Institute of Advanced Industrial Science and Technology (AIST / SDBS) [110, 119, 120]. Besides their spectral characteristics and inherent volatile nature, these three chemical compounds are relevant for the purposes of this research project, since they are commonly found in products often related to certain harmful effects, specially toluene and benzene.

Besides the comparison of the spectra provided by our evaluation method against well-established values of Raman shifts, we have also performed the Raman analysis of these three chemical compounds (cyclohexane, toluene and benzene) using two commercially available FT-Raman devices. For this purpose, we have arranged three sets (all samples are from the same source to reduce the possibility of any additional measurement errors) of pure cyclohexane (Carl Roth, anhydrous $\geq$ 99.9%), toluene (Sigma-Aldrich, anhydrous $\geq$ 99.8%), and benzene (Sigma-Aldrich, anhydrous, $\geq$99.8%). One of the samples set has been analyzed using our FT-Raman spectrometer. The remaining two sets have been analyzed separately using state-of-the-art commercial FT-Raman devices from Bruker Optik GmbH (MultiRAM, excitation source at 1064 nm) and Thermo Fisher Scientific GmbH (Nicolet iS50, excitation source at 1064 nm). The exact conditions of the Raman analysis performed with these two commercial devices have not been disclosed. According to their specification sheets, these commercial devices combine high quality optics, advanced

electronics and software controls in order to deliver accurate Raman spectra.

The spectral information of the calibration materials provided by the ASTM serves to validate the frequency accuracy and relative intensity of certain given Raman spectrum. This information can also be used to determine the wavelength accuracy and stability of the excitation light source [93, p. 100] [109, p. 251-253]. However, values like the wavelength accuracy and wavelength stability of the laser embedded in our setup have not been validated. This is because, as it has been previously alluded, HeNe lasers are highly stable devices that only show insignificant values of wavelength deviation from its main oscillating frequency [184].

5.1.1 Validation by measuring cyclohexane (C_6H_{12})

Cyclohexane (C_6H_{12}) is a chemical component widely used in industrial environments, e.g. textile industry, fuel production, etc. It can be obtained by the catalytic hydrogenation of benzene (C_6H_6) [189, p. 413] and therefore cyclohexane has a slightly tied higher price than benzene [179, p. 141]. Although certain environmental risks and health harms, besides its volatility, are reported [117] for this particular material, the fact that toluene derives from benzene would also pose a sensitive danger during its production.

The chemical composition of this material offers a unique feature in Raman spectroscopy that can be exploited as a reliable standard spectrum. Cyclohexane is one of the materials included in the ASTM E1840 list for Raman calibration and it has highly defined Raman lines. Moreover, the Raman line of cyclohexane around $801\,\mathrm{cm}^{-1}$ has a full width at half maximum (FWHM) of about $4.0\,\mathrm{cm}^{-1}$ [109, p. 93] and also helps to determine the amount of broadening the instrument generate on the spectral information.

As an initial step, for validation purposes a set of three samples of cyclohexane have been observed using the FT-Raman prototype and the other two last generation FT-Raman spectrometers. In the case of our FT-Raman prototype, the final spectrum is the result of averaging 30 successive scans with a spectral resolution of about $1.66\,\mathrm{cm}^{-1}$. For the measurements with the MultiRam spectrometer the configuration information or similar data were not disclosed. Nevertheless, according to the technical specifications, this instrument can achieve measurements having spectral resolutions better than 0.5 nm and wavenumber accuracy better than $0.1\,\mathrm{cm}^{-1}$. The Raman spectrum from the Nicolet iS50 instrument has been obtained by averaging 64 scans with a spectral resolution of about $4.0\,\mathrm{cm}^{-1}$.

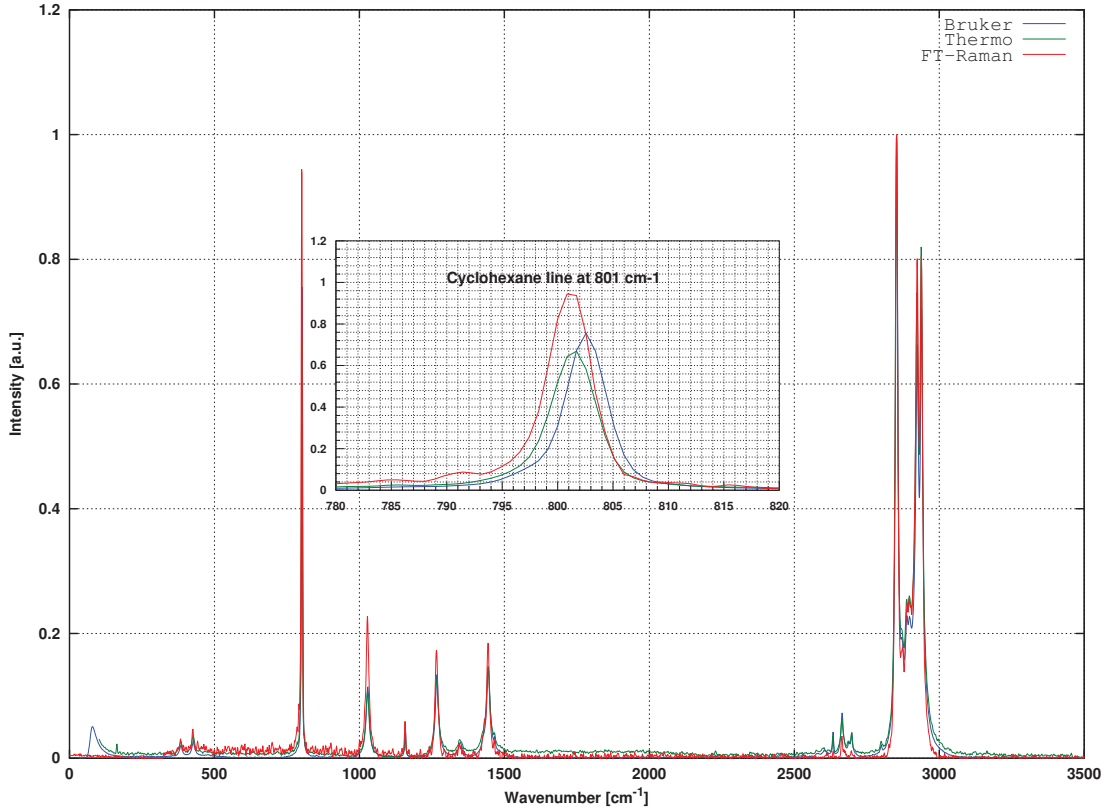

Figure 5.2: Raman spectra of cyclohexane using the FT-Raman spectrometer prototype and the two commercial FT-Raman devices.

During the acquisition of the Raman spectrum of cyclohaxane, the maximum counting rate registered by the photon counting device, oscillated between approximately 100 kcps to 120 kcps. The fixed applied electrical tension above the breakdown level of the APD (photon counter device) has allowed to achieve detection probabilities of about 50% to 70%. From the total counting rate range, the amount of Raman scattering light (obtained by observing the counting rate while repeatedly placing and removing the cyclohexane sample from the FT-Raman spectrometer and by subtracting the dark counting rate) has been found out to be in the range of 65 kcps to 75 kcps. In section 3.3 it has been suggested that a counting rate between 16 kcps to 94.5 kcps would be expected, assuming an overall system transmission of 50% (suitable value of transmission considering that a 62.5/125 multi-mode optical fiber can achieve values of coupling efficiency between 80% to 90% [196, p. 190] [209, p. 386]). These observed counting rates are at least 13 times larger than

Table 5.1: Main Raman shift peaks and relative intensities of standard [109] vs. the simulated and the observed Raman spectrum from cyclohexane (C_6H_{12}) using the FT-Raman setup in figure 4.1 and two commercial devices.

Standard [cm^{-1}] **/ Rel. Int.**	**Simulation**	**FT-Raman**	**MultiRam**	**Nicolet iS50**
384.1 ± 0.78 / 0.02	383.9 / 0.01	382.9 / 0.03	384.9 / 0.02	384.1 / 0.02
426.3 ± 0.41 / 0.03	425.6 / 0.02	425.8 / 0.04	427.3 / 0.02	426.6 / 0.03
801.3 ± 0.96 / 0.95	800.6 / 0.93	801.1 / 0.94	802.5 / 0.75	801.7 / 0.67
1028.3 ± 0.45 / 0.15	1027.3 / 0.12	1027.6 / 0.22	1028.8 / 0.11	1027.8 / 0.10
1157.6 ± 0.94 / 0.06	1157.3 / 0.05	1157.3 / 0.06	1158.9 / 0.04	1157.6 / 0.03
1266.4 ± 0.58 / 0.14	1265.6 / 0.13	1265.7 / 0.17	1267.3 / 0.13	1266.3 / 0.12
1444.4 ± 0.30 / 0.12	1443.9 / 0.11	1443.8 / 0.18	1444.6 / 0.14	1443.9 / 0.14
2664.4 ± 0.42 / 0.08	2664.0 / 0.07	2664.2 /0.03	2664.9 / 0.07	2664.1 / 0.06
2852.9 ± 0.32 / 1.00	2852.3 / 1.00	2852.8 / 1.00	2853.0 / 1.00	2852.3 / 1.00
2923.8 ± 0.36 / 0.58	2924.0 / 0.41	2923.7 / 0.80	2924.0 / 0.66	2923.2 / 0.74
2938.3 ± 0.51 / 0.67	2937.3 / 0.56	2938.3 / 0.80	2938.8 / 0.71	2937.9 / 0.81
Corr. coef.(freq.)	0.999999939	0.999999971	0.999999956	0.999999971
Euclidean dist.(freq.)	2.1354	1.7944	2.5338	1.3153

the simulated expected counting rates under the worst conditions for only the Raman line of cyclohexane at 802 cm^{-1}(see figure A.2), and just about the half of the expected value under ideal conditions (having a 100% transmission of the system, which is not plausible).

Figure 5.2 shows the resulting spectra of cyclohexane and a close-up of the region around its characteristic Raman peak at 801 cm^{-1}. The three Raman spectra have shown a remarkable resemblance to the standard value at this particular line. The frequency positions and the relative intensities have also shown a high degree of similarity.

The FWHM of this particular Raman line, obtained using the FT-Raman prototype, has shown a value of about 4.3 cm^{-1}, which is only 0.3 cm^{-1} wider than the theoretical value proposed by the ASTM; however this value is the closest of the three observed Raman spectra to the theoretical one. For instance, the MultiRam Raman spectrometer has shown a FWHM of about 3.2 cm^{-1}, and 3.1 cm^{-1} has been obtained from the Nicolet iS50 device. These resulting values having a smaller value of FWHM than the 4.0 cm^{-1} reported by the ASTM might be the result of applying certain functions (e.g. Happ-Genzel apodization function in the Nicolet iS50) that are not applied in the spectral data collected from our FT-Raman prototype.

Table 5.1 shows a spectral comparison of the standard Raman lines of cyclohexane against the observed values of this material with the three FT-Raman devices. The resulting deviation in the Raman lines for this particular material can be regarded as low. The correlation of the peaks position with the standard values is larger than 0.9999999 in

Table 5.2: Resulting statistic data obtained by repeatedly measuring a sample of cyclohexane.

Standard [cm^{-1}]	**Mean**	**Median**	**Mode**	**Min.**	**Max.**	σ_{std}
384.1 ± 0.78	383.70	383.76	383.76	379.49	388.89	2.63838
426.3 ± 0.41	425.88	425.64	424.79	422.22	430.77	2.51681
801.3 ± 0.96	801.40	801.71	801.71	800.85	801.71	0.41383
1028.3 ± 0.45	1027.98	1028.21	1028.21	1023.93	1032.48	1.60585
1157.6 ± 0.94	1157.88	1157.26	1157.26	1152.99	1162.39	2.32572
1266.4 ± 0.58	1265.94	1265.81	1265.81	1262.39	1269.23	1.69392
1444.4 ± 0.30	1443.59	1443.59	1443.59	1440.17	1446.15	1.39572
2664.4 ± 0.42	2664.79	2664.96	2664.96	2659.83	2669.23	2.50560
2852.9 ± 0.32	2852.77	2852.99	2852.99	2851.28	2853.85	0.51523
2923.8 ± 0.36	2923.81	2923.93	2923.93	2922.22	2925.64	0.74570
2938.3 ± 0.51	2938.15	2938.46	2938.46	2936.75	2940.17	0.60502
Corr. coef.(freq.)	0.999999946	0.999999930	0.999999877	0.999999028	0.999998845	-
Euclidean dist.(freq.)	1.2959	1.5312	2.0911	11.8991	11.1731	-

the three cases, which are in agreement with the expected results. The overall euclidean distances to the values of the standard spectrum of cyclohexane have shown reduced amounts of wavenumbers in the three cases. The behavior of the relative intensity of the Raman lines are also highly similar, except for the region of larger wavenumbers.

The simulated data from the proposed spectral evaluation method have been also included in table 5.1. The synthetic signal of cyclohexane and the observed Raman spectrum obtained with the FT-Raman spectrometer showed a high level of correlation in frequency. However, the relative intensity of these two signals differs significantly at higher wavenumbers.

More satisfactory values of correlations and euclidean distances, can be observed in the Raman spectrum obtained by using the FT-Raman prototype that we propose rather than at the simulated one, which at first might appear unusual. Nevertheless, this effect is the result of using only one scanned optical path at the simulations instead of several scans, as in the real measurements, that might help to average the error of the mechanical properties and noise from the system.

Table 5.2 contains some statistical data obtained on a set of around 50 spectra of cyclohexane. These spectra have been collected by repeatedly scanning the Raman backscattered light of cyclohexane with our FT-Raman spectrometer. This statistical analysis has shown the efficiency of the evaluation method that we have proposed. The Raman lines having the largest amplitudes of relative intensity, have shown estimated values of

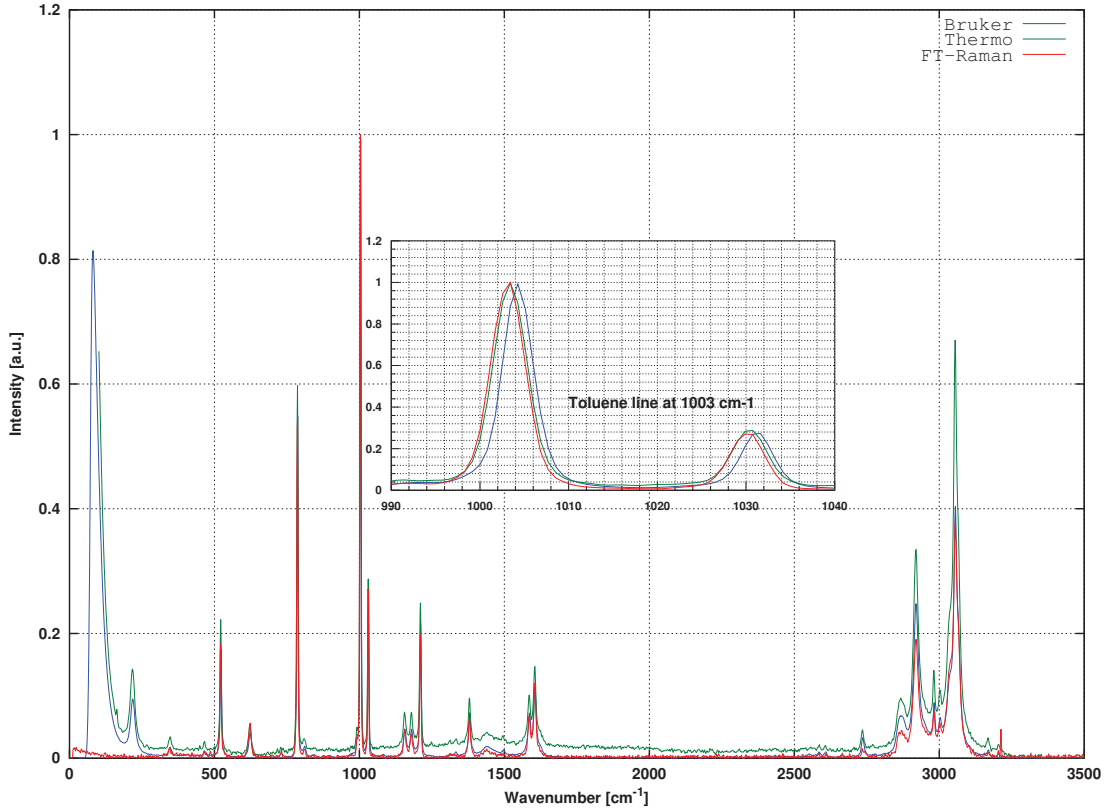

Figure 5.3: Raman spectra of toluene using the FT-Raman spectrometer prototype and the two commercial FT-Raman devices.

mean, mode and median very close to the standard value reported by the ASTM. Even the minimum and maximum values founded in this estimation are located within the allowed interval. In the case of the smaller Raman lines (384 cm^{-1} and 426 cm^{-1}), larger values of spectral deviation has been registered due to the smearing influence of the background noise. However the mean, mode and median values are also within required limits.

5.1.2 Validation by measuring toluene (C_7H_8)

Toluene (C_7H_8) is a flammable aromatic commonly used as solvent and several other industrial applications [70, p. 714]. However toluene is mainly used in the fuel industry for octane number improvement [205]. The chemical properties, and the related hazards and risks associated to toluene (e.g. nervous system impairment, renal damage, etc.), in health and in environment, can be easily found in several agencies such as the US

Table 5.3: Main Raman shift peaks and relative intensities of standard [109] vs. the observed Raman spectrum from toluene (C_7H_8) using the FT-Raman setup in figure 4.1 and two commercial devices.

Standard [cm^{-1}] / **Rel. Int.**	**FT-Raman**	**MultiRam**	**Nicolet iS50**
521.7 ± 0.34 / 0.10	521.1 / 0.18	522.2 / 0.17	521.4 / 0.22
786.6 ± 0.40 / 0.39	786.1 /0.54	787.1 / 0.54	786.3 / 0.59
1003.6 ± 0.37 / 1.00	1003.3 / 1.00	1004.2 / 1.00	1003.4 / 1.00
1030.6 ± 0.36 / 0.23	1030.1 / 0.27	1031.1 / 0.27	1030.4 / 0.28
1211.4 ± 0.32 / 0.26	1210.3 / 0.20	1211.2 / 0.21	1210.2 / 0.25
1605.1 ± 0.47 / 0.06	1604.8 / 0.12	1605.7 / 0.11	1604.7 / 0.14
3057.1 ± 0.63 / 0.30	3055.2 / 0.33	3055.6 / 0.40	3054.8 / 0.67
Corr. coef.(freq.)	0.999999911	0.999999897	0.999999898
Euclidean dist.(freq.)	2.4207	1.9391	2.6739

Environmental Protection Agency (EPA) [47, 205].

Despite the harmful aspects of this chemical compound, toluene is also part of the calibration list provided by the ASTM since its chemical structure allows the extraction of well-defined Raman lines [7, 14]. The most intense Raman line of toluene can be found around 1003 cm^{-1}. Right beside this intense Raman line we can find a tight-located Raman line at 1030 cm^{-1}. This is an interesting feature of this material that offers a convenient way to assess the spectral resolving capacity of the FT-Raman prototype.

In order to confirm the values obtained about frequency accuracy, we have also performed similar measurements as in subsection 5.1.1, however by using the set of three samples of toluene. For comparison purposes, the two additional samples from the same source have been analyzed using the two commercial FT-Raman spectrometers. Cyclohexane is up to certain extent more documented than any other material here deployed, including toluene, and hence the larger amount of information shown in the previous subsection in comparison with the present and the subsequent subsection.

Figure 5.3 depicts the Raman spectra from the set of three samples of toluene that have obtained from the three FT-Raman devices. The enlarged section in this figure belongs to the Raman peaks at 1003 cm^{-1} and 1030 cm^{-1}. Both Raman lines have been correctly resolved and can be clearly distinguished. The FWHM of the former Raman line has shown a value of about 4.65 cm^{-1}. The MultiRam Raman instrument has shown a FWHM of about 4.19 cm^{-1} and the the Nicolet iS50 device 4.62 cm^{-1}. As of the beginning of 2014, the value of FWHM for the main Raman line of this chemical compound has not been found in the literature, and therefore, it has not been possible to compared our

Table 5.4: Resulting statistic data obtained by repeatedly measuring a sample of toluene.

Standard [cm^{-1}]	**Mean**	**Median**	**Mode**	**Min.**	**Max.**	σ_{std}
521.7 ± 0.34	521.03	521.37	521.37	520.51	522.22	0.50258
786.6 ± 0.40	785.91	786.32	786.32	785.47	786.32	0.43072
1003.6 ± 0.37	1003.15	1003.42	1003.42	1002.56	1004.27	0.43072
1030.6 ± 0.36	1030.14	1029.91	1029.91	1029.91	1030.77	0.38115
1211.4 ± 0.32	1210.28	1210.26	1210.26	1209.40	1211.11	0.44416
1605.1 ± 0.47	1604.93	1605.13	1605.13	1600.85	1609.40	1.40192
3057.1 ± 0.63	3055.00	3054.70	3054.70	3052.14	3057.26	0.88775
Corr. coef.(freq.)	0.999999876	0.999999822	0.999999822	0.999999519	0.999998215	-
Euclidean dist.(freq.)	2.6262	2.7764	2.7764	7.1178	4.4047	-

observed values against those obtained by using the commercially-available FT-Raman spectrometers.

Table 5.3 contains the Raman shift positions of the standard spectrum of toluene, as well as the spectral shifts of this material that have been observed with the three FT-Raman spectrometers. The values of the spectral deviation can also be regarded as low and with a high value of correlation in the three cases of the observed spectra with the standard values suggested by the ASTM.

In terms of intensity, only the last two lines of the spectrum have shown a rather larger mismatch of the values of relative intensity in comparison with the values from the standard Raman spectrum. However, the first five Raman lines soundly coincide with the values of relative intensity suggested by the ASTM.

Table 5.4 contains similar statistical data as the one obtained by using cyclohexane (see table 5.2). A set of around 50 spectra of toluene has been analyzed in order to verify the spectral variations, and some additional statistical values, that occur during the Raman analysis of toluene. These spectra have been too acquired by repeatedly scanning the Raman back-scattered light of a sample of toluene with our proposed FT-Raman prototype. The statistical analysis of this material has shown even less deviation than those found by using cyclohexane. The Raman lines having the largest amplitudes of relative intensity, have shown once again estimated values of mean, mode and median close to the standard Raman values reported by the ASTM. The largest deviation on the Raman lines of toluene has been found at $1605\,cm^{-1}$. Although this specific Raman vibration has the smallest relative intensity of this spectrum, the center values obtained for this line also agreed with the one reported in the literature.

5.1.3 Validation by measuring benzene (C_6H_6)

Benzene (C_6H_6) is an aromatic hydrocarbon commonly found in gasoline (1% to 2% v/v) and it is used a intermediate precursor for different chemical components and materials, including cyclohexane [80, p. 210-211]. Benzene is considered as a harmful material that must be handled carefully. Several agencies and authors have reported different effects of this particular material on public health and on the environment [116, 83, 206, 204, 46]. The most serious cases related to benzene exposure include renal failures and severe types of cancer [88, p. 58] [58, p. 203].

Although benzene does not belong to the calibration list provided by the ASTM, the chemical structure of this material makes it suitable for our validation purposes. Moreover, different agencies such the National Institute of Standards and Technology (NIST) and the National Institute of Advanced Industrial Science and Technology (AIST / SDBS) have provided a decent approximation of the frequencies of the main Raman lines of this chemical compound. McCreery also suggested that the main Raman band of benzene is located at $992\,\mathrm{cm}^{-1}$ [109, 110]. The main characteristic Raman line of benzene, at around $992\,\mathrm{cm}^{-1}$ (fairly close to the characteristic Raman line of toluene around $1003\,\mathrm{cm}^{-1}$), can be used for frequency comparison and for the estimation of cross section values of unknown samples in Raman spectroscopy [109, p. 288].

Similarly as in the previous two validation experiments using cyclohexane and toluene, the three samples of benzene have been observed using the FT-Raman prototype and the two commercial FT-Raman spectrometers from Bruker and Thermo Fisher. The resulting Raman spectra have been contrasted and the frequency values of the Raman lines have shown a high degree of resemblance. The comparison of the observed spectra with values obtained from the agencies mentioned previously also agree. The most recent data is the one suggested by McCreery at $992\,\mathrm{cm}^{-1}$ and the measurements, specially those collected with the FT-Raman prototype and the FT-Raman spectrometer from Thermo Fisher, have shown only a reduced amount of spectral deviation.

Figure 5.4 shows the Raman spectra of the three samples of benzene. In this particular case, the Raman spectra of the commercial FT-Raman devices have shown Raman spectra having an evident reduced amount of noise than the one obtained with our FT-Raman prototype, although the measuring conditions were not modified at all. Figure 5.4 also shows the close-up of the $992\,\mathrm{cm}^{-1}$, $3046\,\mathrm{cm}^{-1}$ and $3062\,\mathrm{cm}^{-1}$ Raman lines. These last two lines are generated by two different adjacent CH stretch modes. However, the $3046\,\mathrm{cm}^{-1}$

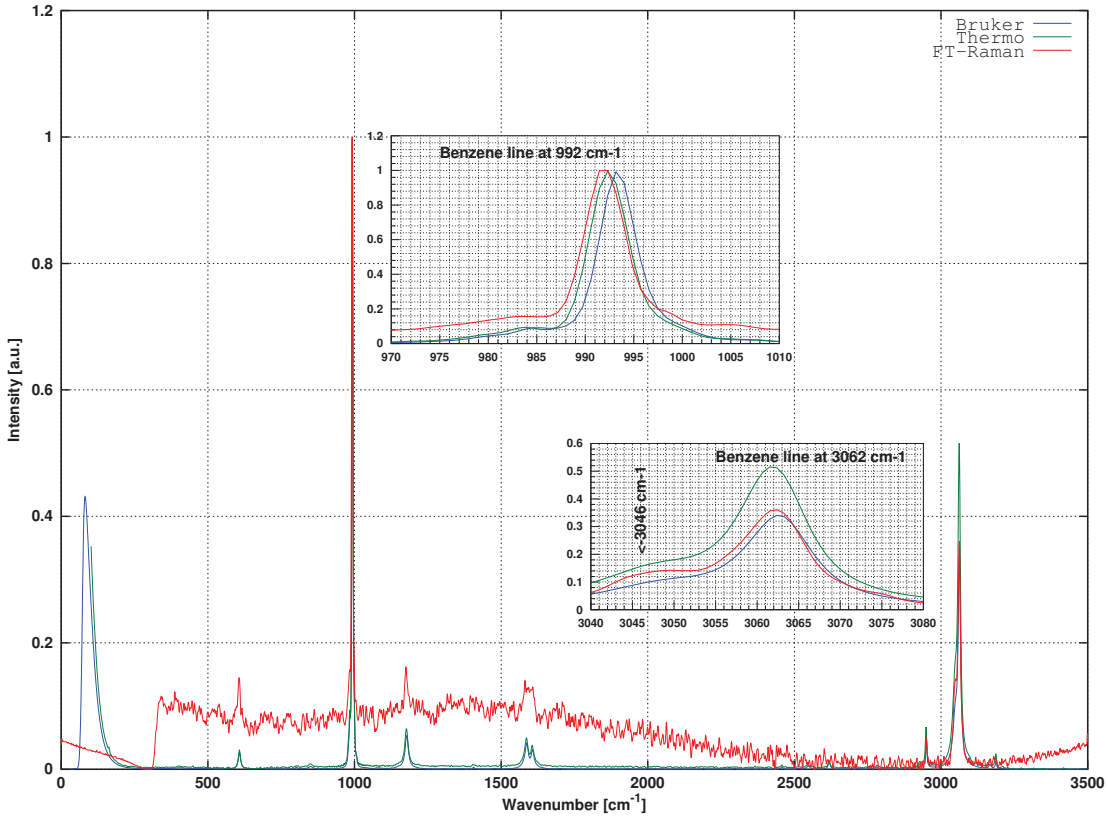

Figure 5.4: Raman spectra of benzene using the FT-Raman spectrometer prototype and the two commercial FT-Raman devices.

Raman line can be better distinguished from the line at 3062 cm^{-1} using the FT-Raman prototype. At least in this set of measurements, the two commercial devices were not able to resolve correctly this specific Raman band.

Despite the greater levels of noise observed in the Raman spectrum of benzene collected by using our FT-Raman prototype, the frequency values of the Raman lines are comparable to those obtained with the two commercial devices. Table 5.5 contains the resulting frequency position of the main Raman lines of benzene of all three FT-Raman devices. The first column of figure 5.5 presents the data suggested by the NIST, which happen to be the most complete and reliable source founded for this material. Once more, the three resulting Raman spectra of benzene coincide to a large degree among them and with the values proposed by the NIST. Nevertheless the values of the correlation and the euclidean distances of the observed Raman spectra are less satisfactory than those

Table 5.5: Observed main Raman peaks from benzene (C_6H_6) using the FT-Raman setup in figure 4.1 and two commercial devices. The Raman shift values of benzene suggested by the NIST, SDBS and from McCreery [110] have been included for comparison purposes (vs = very strong, s = strong).

NIST[cm^{-1}] [**120**]	**FT-Raman**	**MultiRam**	**Nicolet iS50**	**SDBS / Rel. Int.**	**McCreery**
605.6 s	606.45	608.14	607.41	-	-
991.6 vs	991.83	993.17	992.31	996 / 0.96	992
1178.0 s	1175.72	1178.24	1176.80	-	-
1584.6 s	1581.13	1587.40	1586.13	-	-
1606.4 s	1606.06	1607.14	1605.81	-	-
3046.8 s	3049.14	3049.72	3047.38	-	-
3061.9 vs	3062.22	3062.55	3061.34	3063 / 0.14	-
Corr. coef.(freq.)	0.999998249	0.999999333	0.999999372	-	-
Euclidean dist.(freq.)	4.8691	5.1294	2.9256	-	-

observed using cyclohexane and toluene. This effect can be explained due to the out-of-date values founded at the NIST, and to the fact that these come from a lesser number of laboratories in contrast to the information offered by the ASTM.

By taking as a reference the widely accepted Raman band value of $992\,cm^{-1}$ suggested by McCreery, the resulting Raman spectrum collected with our FT-Raman device would be the most accurate with a spectral deviation of only $0.17\,cm^{-1}$. The values of the largest Raman peaks suggested by the SDBS differ to a greater extent when compared against the three measurements of benzene. No additional technical details about the acquisition of this Raman spectrum were disclosed by the SDBS.

5.2 Financial impact/requirements on the deployment of the FT-Raman system

The information provided in the previous section only constituted an experimental validation of the implemented FT-Raman system and the evaluation method proposed throughout this document. One of the aims of this research project is strongly related with the technical capacities of the FT-Raman system in the monitoring of hazardous materials. However, these technical capacities must be achieved without significantly affecting the financial aspects of a specific monitoring arrangement.

In other words, the instrumental simplification of the FT-Raman system ought to reduce the implicit costs of the instrumental setup, without undermining the capacities

(frequency accuracy and precision, flexibility, robustness, etc.), of the FT-Raman device. As already presumed and exposed, this is accomplished by replacing complex and dedicated hardware by a more colloquial one, and by carefully extracting the optical path and using the re-sampling method prior to the spectral transformation of the Raman interferometric information.

In this section an approximate assessment of the materials used in the construction of our FT-Raman system is presented. The resources devoted to each stage of the FT-Raman spectrometer have been adjusted to the inflation of the last four years in order to obtain a final value of the expenditures involved in the development, as accurate and actual as possible. However, we have not been able to obtain a proper benchmarking of our FT-Raman prototype against commercial devices due to the lack of accurate financial information from the manufacturers. A serious comparison requires the incorporation a large amount of parameters that are difficult to obtain, even if the manufacturer agrees to disclose such a type of information.

It has been already mentioned throughout this document that most of the materials and components used in the development of the FT-Raman prototype that we propose are from conventional sources, so that the final spending could be kept as low as possible. Only certain pieces of hardware (e.g. the aluminum case of the Michelson interferometer, the water circulator of the photon counter, holders for optics, etc.) have been specially tailored in-house. Additionally, the translation table of the Michelson interferometer (including the gearing system and the quadrature encoder) had been acquired from Physik Instrumente GmbH & Co. KG. for previous optical experimental setups prior to its inclusion into the FT-Raman spectrometer.

Table 5.6 contains the description and the corresponding final market price of the components included in the construction of the FT-Raman instrument. The required expenditures in materials and hardware parts used for the development of the FT-Raman spectrometer, as listed in table 5.6, rounds the 20,000 € as of January 2014. However, certain parts of this prototype (e.g. excitation laser and high voltage power supply) can be easily replaced by more costs-accessible components that would still maintain the overall performance of the instrument undistorted.

For example, a laser diode and a high voltage module could be used instead of the Melles-Griot HeNe laser and the high power voltage supply. As a result the budget of the system could be brought down to an amount of approximately 15,000 €. Furthermore, a

Table 5.6: List of material used in the construction of the FT-Raman spectrometer and their corresponding approximated prices as of January 2014.

Material	Approx. market price (€)
Excitation and reference light sources	
HeNe Laser Melles-Griot (632.8 nm, P=35 mW)	4500
Laser diode 785nm @ 600mW	1600
HeNe Laser 632.8 nm @ 2mW (Ref. Sys)	2000
Optics	
5X Microscope objectives (20x/160)	525-640
3X Beamsplitter + mirrors	300
1X Notch filter	400
2X Laser line filter	240
3X Cuvettes (plastic + SiO2)	250
1X 62.5/125 MM Fiber coupler	50
Electronics	
2X Transimpedance amplifiers	200
ATMEGA microcontroller board	30
1X H-Bridge	20
Seriel to USB interface	20
4X Power supply	1000
High voltage power supply	2500
Photon counter	
Excelitas Technologies Corp C30902 APD	400
3 Stage cooling system	300
Photon counter signal conditioning	70
Mechanics	
15X dia=20mm OWIS optics holder	500
8X OWIS sys 40 tracks	300
4X XY tilt adjusting units	200
Physik Instrumente translation stage	1600
4X 3Axis adjusting units	2000

low-cost photon counter device (around 400 € in material) can be obtained by including generic APD (e.g. the S12060-02 APD from Hamamatsu, which has similar characteristics as the C30921SH APD from Excelitas Technologies), including electronics for temperature sensing and control, signal conditioning and data transfer.

As it can be observed, the direct expenditures on material and components dedicated to set up the FT-Raman prototype have resulted significantly lower than any of those required by the commercial FT-Raman devices reported in this document (see table 5.7). Table 5.7 contains the market cost-related information of three different state-of-the-art FT-Raman spectrometers. This information has been obtained by directly making an inquiry to the respective manufacturer during the second part of 2013.

Table 5.7: Modern FT-Raman spectrometers models and their approximated market price according to the respective manufacturer. This information have been obtained by a direct inquiry to the corresponding distributor or manufacturer.

Manufacturer	Bruker	Thermo Fisher	JASCO
Model	MultiRam	Nicolet iS50	FT-Raman RFT-6000
Approx. Price (€)	$\geq$ 100,000	$\simeq$ 85,000	$\geq$ 90,000

Bruker Optik GmbH offers a modern complete set with several options, services and external accessories that includes a MultiRAM FT-Raman spectrometer (which is a stand-alone and high performance Fourier transform Raman spectrometer[59]), an excitation light source (Nd:YAG-Laser, diode-pumped, P=1000 mW), a Ge detector (cooled with N_2), optical arrangements, cuvette cell, software for the system and libraries, as well as a PC terminal for a total amount of 122,550 €. Depending on the configuration of the desired system, this value can change. However, the basic functionality can be achieved with an expense of at least 82,000 €.

In the case of the device from Thermo Fisher (Nicolet iS50), a setup having the basic configuration would required spending 84,990 €. The FT-Raman offered by JASCO (RFT-6000, which is used in conjunction with a FT/IR-6300 spectrometer) has a market price of about 90,000 €. Furthermore, the corresponding value added tax (VAT) of these two FT-Raman devices must still be added to the final price. The older immediate previous generation of non-dispersive Raman spectrometers from these main manufacturers does not represent a significant improvement in the cost-related factor. Even costs reductions of 50% for such a device would lead to expenditures that are still three to four times larger compared to the FT-Raman prototype.

Even the wide range of commercial available Raman spectrometers based on dispersive arrangements, having far less mechanical disadvantages but lower frequency accuracy and resolution, can be financially compared with our FT-Raman spectrometer. Ocean optics is a well-known manufacturer of optical sensing products that offers a variety of dispersive Raman devices having prices between approximately 15,000 € and 26,000 € [124]. Another example would be Horiba [77], which also offers complex and sophisticated Raman devices such as the LabRAM HR Evolution, the XploRA or the XploRA invers. For these type of devices a customer must be ready to invest between 99,500 € and 175,000 €[1].

[1]Information provided by the sales office of HORIBA Jobin Yvon GmbH in Germany

As already alluded, we have not been able to properly perform an accurate comparison of the financial-related aspects of the FT-Raman devices. However, by using the information obtained from the annual reports from Bruker Optiks and Thermo Fisher (gross profit margins[1] between about 42 % and 47 % in the last years) [36, 37, 194, 195], we can presume that the overall cost of our FT-Raman device is significantly lower than the commercial counterparts by taking the upper overall value obtained in our calculations.

5.3 Conclusion of the chapter

In the previous two sections of this chapter, the capacities of the proposed FT-Raman system and the efficiency of evaluation method that we have proposed have been demonstrated. The financial resources required for the construction of such an instrument have been likewise approximately estimated.

Our FT-Raman prototype has been able to extract the Raman spectra of two chemical compounds (cyclohexane and toluene), which are included in the list of calibration materials provided by the American Society for Testing and Materials (ASTM). The observed spectra of these two calibration materials obtained using the FT-Raman prototype have shown frequency deviations that are mostly within the limits suggested by the ASTM of $\pm 1.0\,\mathrm{cm}^{-1}$.

The FT-Raman instruments has been also used to collect the Raman spectrum of benzene, which is not included in the calibration standard provided by the ASTM, but this material possesses a distinctive Raman line that is also used for comparison purposes in Raman spectroscopy, and it is a relevant chemical compound in the field of toxicology. The observed spectral information of benzene has also shown similar values of the Raman lines to those proposed by McCreery, the National Institute of Standards and Technology (NIST) and the National Institute of Advanced Industrial Science and Technology (AIST / SDBS).

Another relevant outcome of the spectral data obtained from the three chemical compounds, is that the instrumental effects generated by our FT-Raman spectrometer do not contribute significantly to the overall Raman spectra. Furthermore, the effects of truncation (sinc ripples), finite size entrance or wavenumber shifting cannot be observed in the

[1] gross profit: difference between revenue and the cost of making a product or providing a service, before deducting overheads, salaries, taxes, and interest payments.

Raman spectra of these chemical samples, although we have not applied any compensation for these type of physical effects.

The resulting spectra of these three chemical compounds, observed with our FT-Raman instrument, have been closely compared to the Raman spectra collected with two modern commercially-available FT-Raman spectrometers from the manufacturers Bruker Optik GmbH, and Thermo Fisher Scientific GmbH. In the three cases the spectra information has shown a remarkable resemblance in both frequency accuracy and relative intensity values. In some cases, the overall sum of errors (euclidean distances) obtained by using our FT-Raman spectrometer have resulted in more satisfying values than those obtained by using the two commercial FT-Raman devices.

Although our FT-Raman spectrometer prototype has caused a slight widening (fractions of cm^{-1}) of the Raman spectra, the bandwidth value that we have found is the most similar to the theoretical value reported by the ASTM and by McCreery (in the specific case of cyclohexane) than those values obtained by using the commercial FT-Raman spectrometers, which generally apply functions such as the Happ-Genzel apodization.

Since our self-designed FT-Raman spectrometer has been assembled by using mostly widely available conventional parts and it is operated by open source software applications, the financial resources dedicated to the development and operation of such a prototype can be significantly reduced in comparison with the commercial FT-Raman instruments. Moreover, the financial resources devoted to the FT-Raman spectrometer that we have developed can be financially compared to some of the well-known dispersive Raman systems.

The next chapter describes some practical applications and capabilities that can be performed by using the FT-Raman system that we propose in certain processes. These processes generally involve harsh and harmful-related environments having materials that by nature are considered dangerous, harmful or toxic.

Chapter 6. Monitoring applications

The FT-Raman spectrometer that we propose has shown satisfactory validation results, in form of highly accurate and precise Raman spectra, when compared to the standard Raman spectra of certain calibration materials and to the observed spectra obtained with commercial FT-Raman spectrometers. Moreover, being given the assessment of the materials included in the FT-Raman prototype, the development of this system can be accomplished using only a fraction of the financial resources required by a commercially available FT-Raman device.

Nevertheless, our practical aim for this research project is to use our Raman instrumental low-cost setup in the monitoring of certain processes that involve contaminating and harmful materials. Therefore, different Raman analysis have been performed in order to determine the capabilities, advantages, drawbacks and restrictions that such an instrument might have in a specific field.

Since the amount of possible monitoring applications that can be performed by using the FT-Raman spectrometer designed and the method that we propose is substantially large, we have concentrated our validation efforts in the following main fields: gasoline-ethanol blends, hydraulic fluids, and some agave-derived alcoholic beverages. These specific fields of study have been selected, as the harmful materials involved in such processes can be safely handled under the present technical conditions of the FT-Raman spectrometer that we have elaborated.

6.1 Experiments using different gasoline blends

Just after the discovery of the Raman effect, researchers involved in the petroleum industry have attempted to use this technique in the analysis of the chemical properties of different oil-based fuels. This interest on the Raman analysis quickly vanished as the fluorescence problem seemed to be unresolvable at the time [50, p. 334-337]. The FT-Raman devices have allowed to overcome the fluorescence problems and nowadays this technique can be used efficiently in the petroleum industry. Moreover, Raman spectroscopy is more sensitive than infrared spectroscopy to unsaturated hydrocarbons in the fuels.

Some environmental guidelines and geopolitical rules, implemented during the last years, have also influenced the production of fuels for internal combustion machines. The commercial use of oil-based fuels combined with materials such as ethanol (C_2H_6O) in order to reduce CO_2 emissions have been increasing since its implementation, a couple decades ago [8, 65]. Nowadays, gasoline blends are relevant from the commercial, environmental and technical perspectives. The oil-based gasoline is still one of the main fuels used by internal combustion machines. Moreover, there are also predictions that place the gasoline-ethanol blends on a relevant position on the future of energy [86, p. 205-208]. Although a forecast predicts an increment in the production of electric cars to 800,000 units, the actual facts strongly differs from these data and it is highly probable that internal combustion vehicles will dominate the market in the next decade [136, p. 271-272].

Despite the efforts on regulating and eliminating several substances from oil-based fuels, the commercial available gasoline-ethanol blends, found in most gas stations, also contain different additives, e.g. toluene (C_7H_8), benzene (C_6H_6), methyl-tert-butyl ether (MTBE), etc. for octane improvement. These materials can inflict harm to our environment or to our public health and therefore a proper control and monitoring of these blends is required[81].

There are several reasons justifying the relevance and the interest in fuels in this research project. Fuels are commercially important and also have a environmental component that must be carefully attended. Oil-based fuels have several chemical compounds that strongly differs from one manufacturer to another. e.g. the chemicals inside, ethanol, toluene, etc. that must be identified by appropriate tools. In most of the cases the use of such tools has to be environmentally-friendly and non-polluting. This is the case, as the required information is obtained optically.

6.1.1 Monitoring of laboratory-prepared gasoline-ethanol blends

In order to determine some of the basic measuring capabilities of our FT-Raman prototype and method in validating practical applications, a series of laboratory-prepared samples of gasoline blends have been qualitatively and quantitatively analyzed [127, 133]. For this purpose, detailed Raman spectral information from some binary gasoline-ethanol blends having different proportions have been collected. In the same fashion a Raman measurement of a tertiary gasoline-ethanol-methanol blend has been performed. These measurements have been performed without any additional chemical markers.

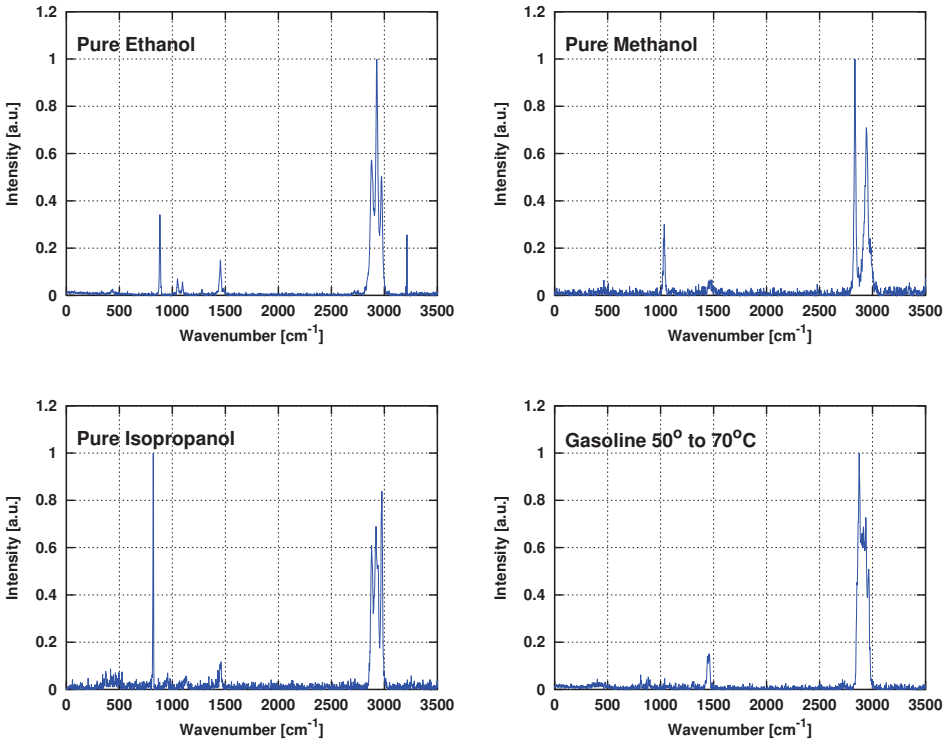

Figure 6.1: Raman spectra from the different pure chemical compounds used during the experimental procudures using laboratory-prepared samples.

The samples for the Raman analysis have been realized by using pure ethanol (C_2H_6O), pure methanol (CH_4O), and gasoline (petroleum ether from Riedel-De Haën AG) with a boiling range between 50 °C to 70 °C, with approx. 0.02% of water content. Four samples of gasoline-ethanol blends having defined proportions of ethanol (5%, 10%, 15%, 20% and 50%, v/v) have been prepared for initial experiments. For the second fuel experiments a sample having equal amounts of gasoline, ethanol and methanol has been prepared. Figure 6.1 shows the Raman spectra of the pure materials prior to the preparation of the gasoline-ethanol and gasoline-ethanol-methanol mixtures. An additional sample of isopropanol (C_3H_8O) has been portrayed for illustrations purposes only, although this material is commonly used in the automotive industry as an additive.

For the Raman measurement the liquid samples have been poured into a 5 mL quartz cuvette, and placed in front of a 20X microscope objective of the FT-Raman spectrometer

Table 6.1: Chemical samples used for the Raman measurements and their different proportions. Data taken from [127].

	Chemical samples					
Material in sample	E05	E10	E15	E20	E50	ME33
Gasoline (mL)	4.75	4.50	4.25	4.00	2.50	1.50
Ethanol (mL)	0.25	0.50	0.75	1.00	2.50	1.50
Methanol (mL)	0.00	0.00	0.00	0.00	0.00	1.50

(see figure 4.1). The observed samples have been mixed using an *Eppendorf Research*® plus adjustable pipette holder (0.5 mL to 5.0 mL with a maximum measurement inaccuracy of ±2.4%). The Raman spectra of these samples have been collected at room temperature.

Figure 6.2 shows the resulting Raman spectra of the gasoline-ethanol blends having 15%, 20% and 50% v/v proportion of ethanol. A qualitative analysis of these samples permits to distinguish relevant features of the different gasoline-ethanol samples. The samples, as it can be observed, exhibit an increasing behavior of the characteristic Raman peak of ethanol at 882 cm^{-1} according to its proportion present in each of the samples. Figure 6.2 also shows the Raman spectrum of the tertiary blend (gasoline-ethanol-methanol sample). In this Raman spectrum, the two characteristic peaks of ethanol at 882 cm^{-1} and methanol at 1034 cm^{-1} can be also observed.

Contrary to the rate method in binary blends, where two characteristic Raman peaks of two chemical compounds of interest are compared [92, 149], the approximated quantitative analysis of the binary ethanol-gasoline blends and the gasoline-ethanol-methanol blend have been performed using most of the spectral information by solving the $Ax = b$ matrix system having the following characteristics:

$$A = \begin{bmatrix} a_{11} & a_{12} & \cdots & a_{1n} \\ a_{21} & a_{22} & \cdots & a_{2n} \\ \vdots & \vdots & \ddots & \vdots \\ a_{m1} & a_{m2} & \cdots & a_{mn} \end{bmatrix}, \quad \mathbf{x} = \begin{bmatrix} x_1 \\ x_2 \\ \vdots \\ x_n \end{bmatrix}, \quad \mathbf{b} = \begin{bmatrix} b_1 \\ b_2 \\ \vdots \\ b_m \end{bmatrix}, \tag{6.1}$$

where A is a m x n matrix containing the Raman spectral information of the pure chemical compounds (e.g. ethanol, methanol, petroleum ether), x is an n column vector with the unknown proportions present in the blend, and b is a column vector of m entries holding the experimental Raman spectrum obtained for each of the blends. The quantitative analysis is performed under the assumption that the changes in the Raman signal

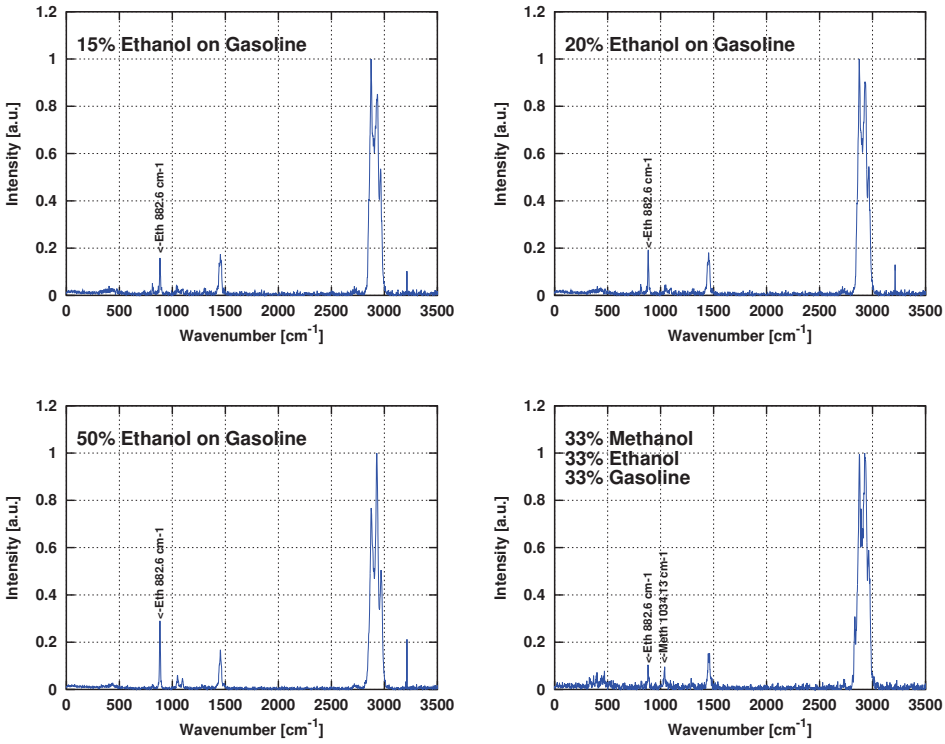

Figure 6.2: Raman spectra from three of the binary gasoline-ethanol blends and the gasoline-ethanol-methanol blend.

coupled into the Raman spectrometer oscillates around a certain average value and therefore using several consecutive scans can help to reduce the effects of such a oscillations. This data arrangement is over-determined and therefore it can be also solved by using QR decomposition in order to accomplish additional improvement on computing time. The resulting calculated proportions obtained using QR decomposition leads to similar results as those obtained by solving the $Ax = b$ system.

The outcome of the quantitative analysis of the blends has allowed an approximated calculation on the proportion of ethanol and methanol in the gasoline mixtures despite the molecular complexity of these samples. This has been achieved without adding any Raman marker or by executing any complex calibration method. Table 6.2 presents the obtained proportions from the gasoline-ethanol blends and the equally proportioned gasoline-ethanol-methanol blend. Figure 6.3 depicts the linear regression obtained from the quan-

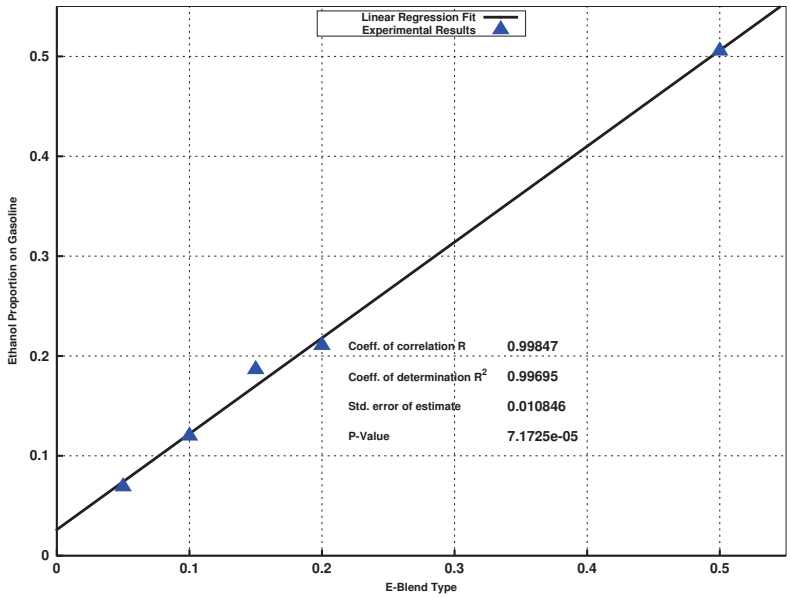

Figure 6.3: Linear regression calculated for the observed spectra of the gasoline-ethanol blends.

titative evaluation of the gasoline-ethanol binary blends. This result has demonstrated a fairly linear response of the gasoline-ethanol mixtures, with a coefficient of determination of $R^2 = 0.99695$. Although Raman spectroscopy is not a tracing sensitive measurement technique and makes it difficult to detect reduced amounts of molecules without special configurations or enhancements, smaller amounts of ethanol are likely to be quantified and detected (0.5% to 1.0%) by prolonging the measurement time of each sample or the by increasing the power level of the excitation light source. This type of measurement can be used in cases where the peak ratio analysis induces inconvenient due to the poor signal of the ethanol in the gasoline blends or other samples having more molecules of complex structure.

Table 6.2: Calculated proportion values from the observed binary ethanol-gasoline blends, and the equally proportioned 33% gasoline-ethanol-methanol blend. Data taken from [127].

Materials	E05	E10	E15	E20	E50	ME33
Gasoline	0.93118	0.88029	0.81380	0.75986	0.49470	0.33030
Ethanol	0.06881	0.11971	0.18620	0.24014	0.50530	0.35030
Methanol	-	-	-	-	-	0.31940

6.1.2 Monitoring of commercial gasoline-ethanol blends

The previous subsection described a Raman analysis that has been performed to laboratory-prepared gasoline blends using ethanol and methanol, and our device and technology. A laboratory-prepared sample is, up to a certain extent, an ideal material in terms of chemical content and spectral figure. However, our FT-Raman system is intended for "real-world" applications. For that purpose, different commercially-available gasoline-ethanol blends have been acquired, and analyzed by using the FT-Raman spectrometer that we propose. These types of oil-based fuels are mixtures of a large amount of chemical compounds [138, 185] and its chemical analysis becomes more elaborated in comparison with the laboratory-prepared samples. For instance, the characteristic Raman line of ethanol around $882\,\mathrm{cm}^{-1}$ might not be observed in certain cases due to stronger Raman signals from the additives present in such a blends [50, p. 337-339].

For the Raman analysis three commercially-available gasoline-ethanol blends (E10) randomly selected have been acquired in three different service stations from the companies Esso, Shell and Aral [128, 130, 129]. These gas stations are located in the urban area of Offenburg (Ortenaukreis), Germany. The three companies claim to deliver gasoline-ethanol fuel having up to 10% content of ethanol v/v. The samples were obtained in a short period of time (less than 45 min.) and were stored in brown glass laboratory bottles at room temperature. No additional chemical treatment has been applied in this procedure, and no prior knowledge about the exact chemical composition of the samples was available.

As in the previous subsection, for the spectral monitoring each liquid sample has been poured into a 5 mL quartz cuvette. The cuvette with the sample has then been placed in front of a 20X microscope objective in the FT-Raman spectrometer, which has been already described in chapter 4 (Figure 4.1). All the aforementioned samples have been measured at room temperature and without performing any additional preparation.

Figure 6.4 illustrates the resulting Raman spectra from the three commercial samples of E10 gasoline-ethanol blends in the range from $0\,\mathrm{cm}^{-1}$ to $3500\,\mathrm{cm}^{-1}$. An additional spectrum of laboratory-prepared E10 (as in subsection 6.1.1) is presented for comparison purposes. This laboratory E10 sample can be qualitatively distinguished with ease from the spectra of the three commercial samples due to the reduced amount of chemical compounds present in this mixture. Unlike the laboratory-prepared E10 sample that offers a

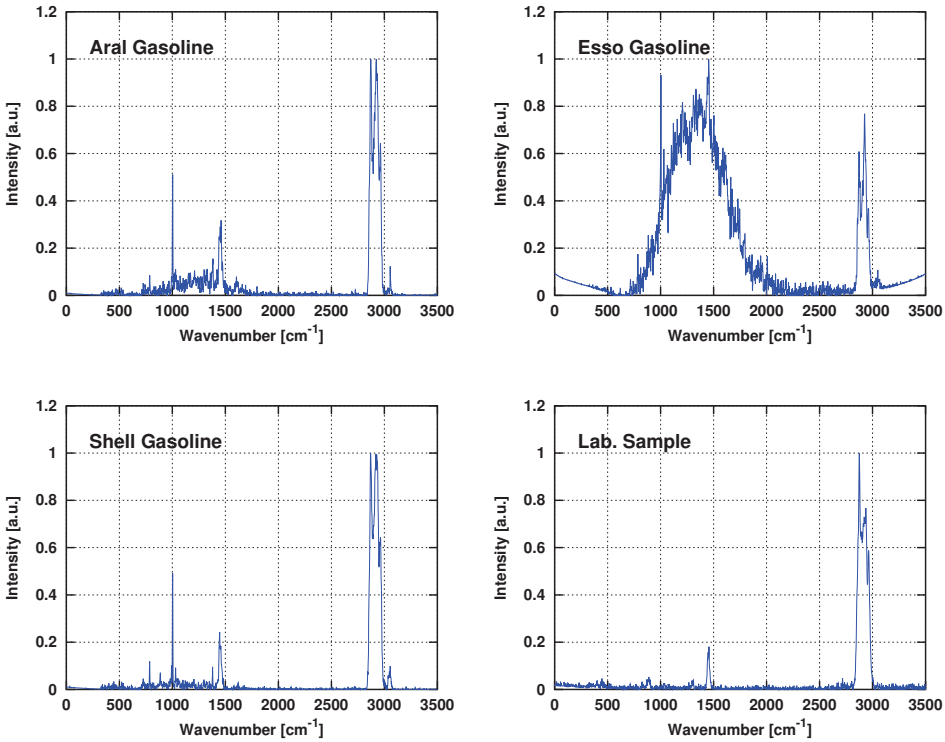

Figure 6.4: Raman spectra obtained from the three commercially-available E10 gasoline-ethanol blends. A sample of a laboratory-prepared E10 gasoline-ethanol sample is also presented (bottom right).

rather regular behavior across the entire spectrum, the Raman spectra from the commercial gasoline-ethanol blends have shown stronger levels of noise and a wide band spectral component in the region between $700\,\mathrm{cm}^{-1}$ to $2100\,\mathrm{cm}^{-1}$, despite the baseline correction applied to the three spectra. This effect is more notorious in the spectrum of the gasoline obtained at the Esso gas station. The sample from the Shell gas station has shown the smallest wide band component.

The Raman line at $1450\,\mathrm{cm}^{-1}$ (from the CH_3 out-of-plane bend of heptane [92, p. 140]) was present in all the gasoline-ethanol samples, including the laboratory-prepared sample, it has shown a constant relative amplitude, despite the chemical complexity of the gasoline blends. This feature can be further explored in the quantification of certain materials of these gasoline-ethanol mixtures.

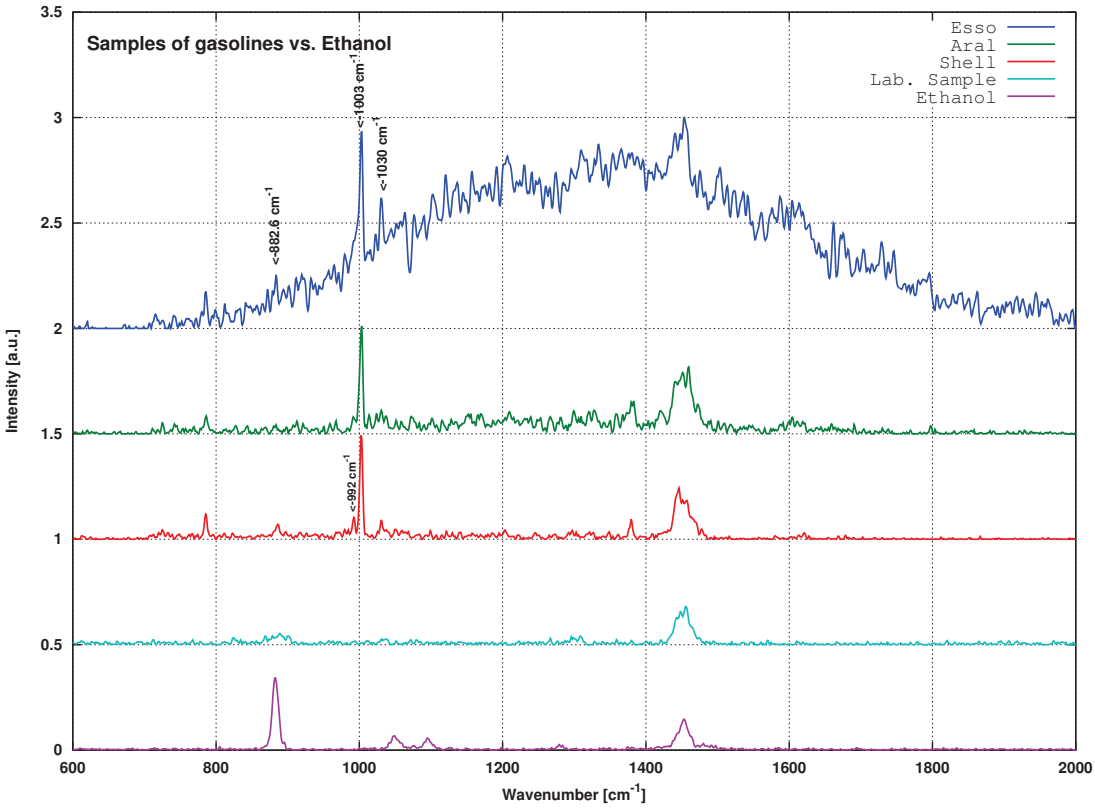

Figure 6.5: Close up to the Raman spectra from $600\,\mathrm{cm}^{-1}$ to $2000\,\mathrm{cm}^{-1}$ obtained from the three commercially-available E10 gasoline-ethanol blends, the laboratory prepared E10 and a pure sample of ethanol.

Figure 6.5 shows the Raman spectra from the gasoline-ethanol binary blends and the Raman spectra of pure ethanol in the range from $600\,\mathrm{cm}^{-1}$ to $2000\,\mathrm{cm}^{-1}$. The samples from the gas stations Esso and Shell show clearly the characteristic Raman shift peak at $882.6\,\mathrm{cm}^{-1}$ from ethanol. In minor proportion the same Raman shift peak appears in the E10 sample from Aral.

Besides the characteristic Raman line of ethanol in the gasoline samples, additional features can be observed in the Raman spectra of the three commercial samples that are not present in the laboratory-prepared sample. For instance, the spectral information obtained (see figure 6.4) shows that these three commercial gasoline samples also exhibit strong Raman bands from at least three gasoline additives: toluene ($1003\,\mathrm{cm}^{-1}$ and $1030\,\mathrm{cm}^{-1}$), benzene ($992\,\mathrm{cm}^{-1}$) and methyl-tert-butyl ether ($724\,\mathrm{cm}^{-1}$).

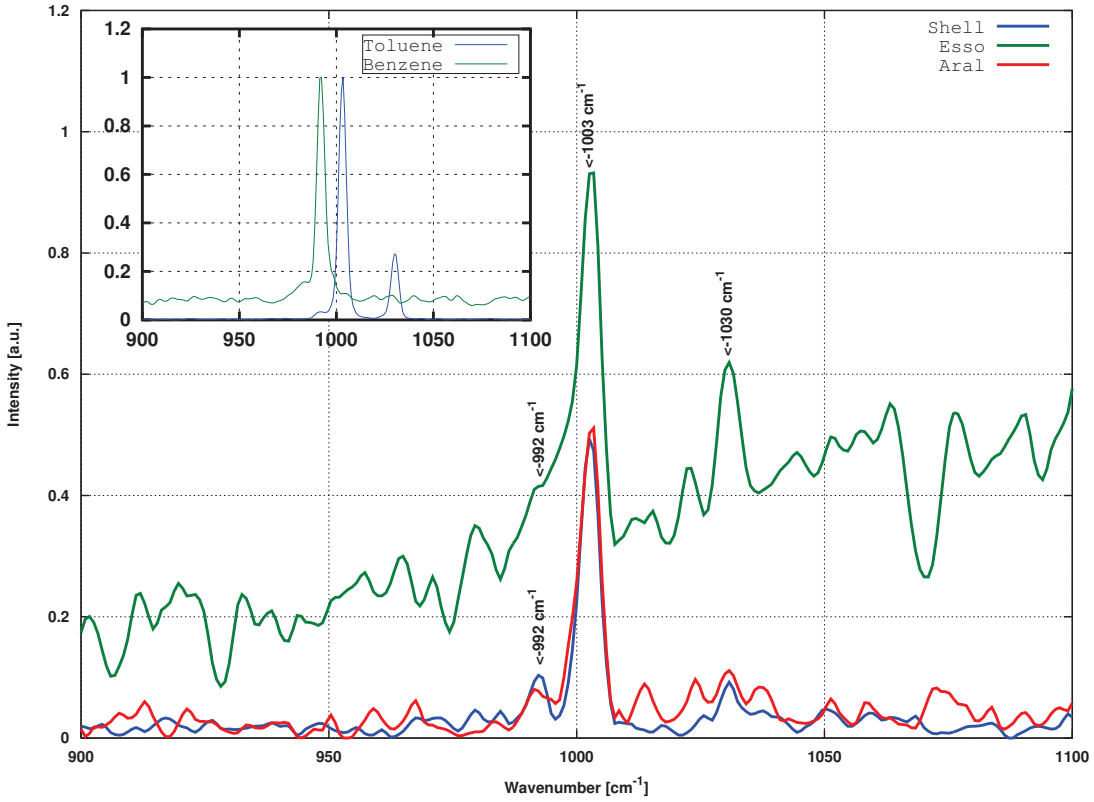

Figure 6.6: Closeup of the gasoline samples around $1000\,\mathrm{cm}^{-1}$. For comparison purposes the upper left plot presents a detail of the normalized Raman spectra of non-combined toluene and benzene in the same spectral region. Image taken from [130].

From the different materials found in these commercially-acquired gasoline samples, toluene has shown the strongest and most well-defined Raman lines of the spectra. Table 6.3 shows, with a reduced frequency deviation despite the complex chemical content of these samples, the main Raman shift peaks of toluene observed in the three commercial E10 gasoline-ethanol blends. This reduced deviation values can be compared with the standard Raman shift suggested in the literature.

Figure 6.6 shows the spectral region from $900\,\mathrm{cm}^{-1}$ to $1100\,\mathrm{cm}^{-1}$. This region contain relevant information about the gasoline-ethanol samples. For instance, the two characteristic Raman lines of toluene ($1003\,\mathrm{cm}^{-1}$ and $1030\,\mathrm{cm}^{-1}$) and the Raman line of benzene ($992\,\mathrm{cm}^{-1}$), which is tightly located beside the aforementioned mentioned Raman lines of toluene, have been plainly resolved in the samples of Shell and Aral. The Esso sample

Table 6.3: Main Raman shift peaks of standard vs. observed Raman spectrum from toluene (C_7H_8), found in the three commercial gasoline-ethanol samples, using the FT-Raman setup in figure 4.1. The observed Raman spectrum has not been compensated for instrumental effects.

Spectrum Type	Toluene Main Characteristic Raman Shift Peaks (cm^{-1})				
Standard [109]	786.6±0.40	1003.6±0.37	1030.6±0.36	1211.4±0.32	3057.1±0.63
Observed	785.8	1002.5	1030.7	1210.3	3054.7

Table 6.4: Chemical compounds found in the commercial samples of gasoline-ethanol blends. For every chemical compound the characteristic Raman shift position and the normalized amplitude are given. Wavenumbers values marked with "*" are tight adjacent Raman lines of toluene and benzene. The fields values NC represent the no-conclusive amplitude values in the Raman spectrum of Esso. Data taken from [130].

Additive	**Wavenumber** (cm^{-1})	**Shell**	**Esso**	**Aral**
Toluene	786	0.11	0.17	0.083
	1003*	0.49	0.61	0.51
	1030*	0.089	0.2	0.1
	1604	0.01	NC	0.07
	3055	0.09	0.06	0.12
Benzene	992*	0.10	NC	0.07
Cyclohexane	801	-	0.09	-
MTBE	725	0.044	0.036	0.051
Naphthalene	1380	0.091	NC	0.14

have only shown a reduced inflection mark at 992 cm^{-1} due to the overlapping wide-band affecting its spectral information. The effect of the wide-band in the Esso sample has as a consequence a lower normalized amplitude of the Raman peaks of the different additives in some spectral regions.

Table 6.4 contains a list with the most visible materials found inside the three samples of the commercially-acquired gasoline-ethanol samples. Beside toluene, benzene and MTBE, these gasoline-ethanol samples might contain low proportions of cyclohexane and naphthalene.

6.1.3 Monitoring of laboratory-prepared gasoline-ethanol blends having different proportions of toluene

Due to different factors, like the instrumental effects and coupling, in quantitative Raman analysis it is sometimes necessary to incorporate additional materials having well-known

and defined Raman peaks into the sample of interest. Another approach is the analysis of an external reference in order to asses the amount of a specific analyte [123, 122, 166, 190]. However, certain spectral properties of the chemical compounds contained in some samples, like toluene or benzene in commercial-available gasoline blends, can be used to quantify the concentration of certain material present on the sample analyzed.

In the particular case of the gasoline-ethanol blends, the proportions of toluene that can be found in gasoline-ethanol blends vary according to the producer. However, the European Commission and the Environment Agency[1] [47, 44] have reported an average of about 11% v/v content of toluene in the gasoline consumed in Europe. We have also repeatedly observed a large spectral component of these material during the Raman analysis of the commercial-available gasoline-ethanol blends.

For the monitoring procedures presented in this subsection, samples of laboratory-prepared binary gasoline-ethanol blends (additives-free, 10% ethanol v/v) having different amounts of toluene have been mixed for a subsequent Raman analysis [132].

The Laboratory-prepared E10 samples have been obtained by mixing petroleum ether (Riedel-De Haën AG, DAB 6, boiling range of 50 °C to 70 °C, approx. 0.02% of water content) and pure ethanol (C_2H_6O). Six different samples having proportions of toluene in the range from 1% to 6% v/v have been mixed using the binary E10 blend. Table 6.5 shows the composition of the samples used for these experimental procedures. As in subsection 6.1.1, these samples have been mixed by using two *Eppendorf Research*® variable pipette holders (0.5 mL to 5.0 mL with a maximum measurement deviation of ±2.4%, and 0.03 mL to 0.3 mL with a maximum measurement deviation of ±2.5%).

The Raman spectra of these samples have then been collected and evaluated by using the FT-Raman spectrometer and the methodologies that we have proposed, as in the previous subsections. Every resulting spectrum is the average of about 30 scans, having a spectral resolution of approximately 1.66 cm^{-1}. At first glance, the Raman spectra of the samples can be qualitatively distinguished by observing a fast-changing of intensity in some of the characteristic Raman lines of toluene.

Figure 6.7 shows the characteristic Raman peaks of toluene at 1003 cm^{-1} and 1030 cm^{-1} found in the different samples of gasoline-ethanol blends. The Raman spectra from the six gasoline-ethanol samples, as we have expected, have shown a monotonically increasing

[1] Executive non-departmental public agency responsible to the Secretary of State for environment, food and rural affairs in the United Kingdom

Table 6.5: Composition of the laboratory-prepared E10 gasoline-ethanol blends having different proportions of toluene. An initial sample of 50 mL of E10 has been prepared for a subsequent incorporation of different v/v proportions of toluene between 1.0 % to 6.0 %.

Lab.-Prepared E10 Composition		**Lab. E10+Toluene Comp.**		
Petroleum Ether (mL)	**Ethanol** (mL)	**E10**(mL)	**Toluene**(mL)	**Tol. v/v (%)**
45 mL	5 mL	4.95	0.05	1.0
		4.90	0.10	2.0
		4.85	0.15	3.0
		4.80	0.20	4.0
		4.75	0.25	5.0
		4.70	0.30	6.0

behavior of the characteristic Raman line of toluene at 1003 cm^{-1} according to the proportion present in each sample. The increment of the relative Raman line of toluene has also shown an slightly quadratic demeanor instead of a linear one. This is often the case for the calculating of the calibration curves by using this method [92, p. 47].

A similar monotonically increasing behavior, as in the Raman line of toluene at 1003 cm^{-1}, was also expected on the Raman lines of toluene located at 786 cm^{-1} and 3057 cm^{-1}, as these lines have values of relative intensity larger than 0.30 (see table 5.3). However, due to the noise and to the signal levels generated by other materials present in the sample, this effect on the two Raman lines has been observed only partially.

Despite the increasing proportion, from 1.0 % to 6.0 %, of toluene content in the laboratory E10 samples, the magnitude of relative intensity displayed by the Raman line of gasoline at 1450 cm^{-1} has shown only minor changes in comparison to changes observed in the narrow band of toluene at 1003 cm^{-1}.

By applying the ratio method, described by Larkin [92, p. 46], we have been able to generate a calibration curve using the relative intensities of the characteristic Raman line of toluene at 1003 cm^{-1} and the Raman line of the gasoline at 1450 cm^{-1} observed in the six spectra of the E10 blends. This method basically make use of the bands of two components with intensities A_1 and A_2.

This calibration curve can be used to determine the content of toluene in unknown samples of E10 blends (e.g. the commercial samples of the previous subsection). A similar method has been also reported for the quantitative detection of ethanol in laboratory-prepared gasoline-ethanol samples without extending this measurements to more practical cases [149]. Furthermore, as it was already shown, the conventional proportions of ethanol

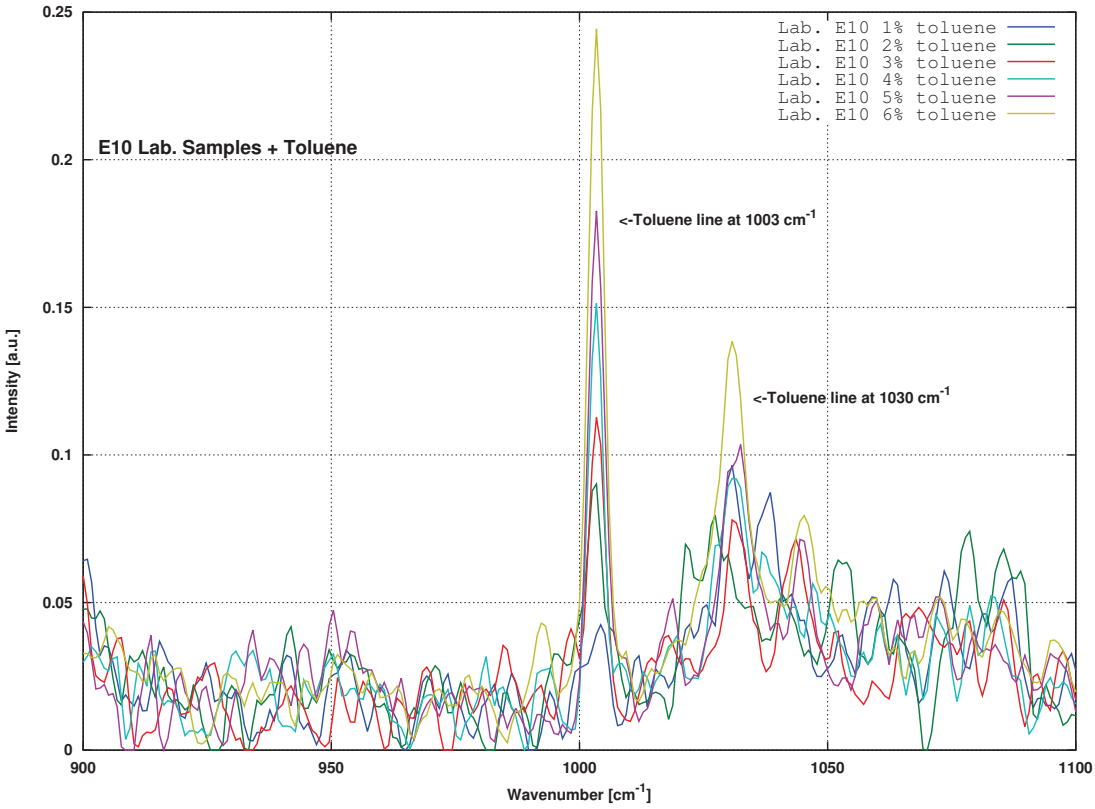

Figure 6.7: Spectral region from 950 cm^{-1} to 1100 cm^{-1} showing the Raman spectra of the samples of laboratory-prepared E10 gasoline-ethanol blend having proportions of toluene between 1 % to 6 %.

present in the commercially-available blends do not produce a large Raman line that could be conveniently used as internal reference, as in the case of toluene. Moreover, the Raman line of toluene is narrower than the Raman line of ethanol, which is relevant in terms of frequency accuracy.

Figure 6.8 shows the Raman spectra of the six E10 gasoline-ethanol samples with proportions of toluene ranging from 1.0 % to 6.0 % in the region from 0 cm^{-1} to 3500 cm^{-1}. This figure also shows a close up of the two Raman peaks used in the rate method. The calibration curve obtained and the data fitted for the samples show a coefficient of determination of about $R = 0.994915$.

Using the rate values obtained from the characteristic and well-defined Raman line from toluene at 1003 cm^{-1} and from the characteristic Raman line of gasoline at 1450 cm^{-1}, it

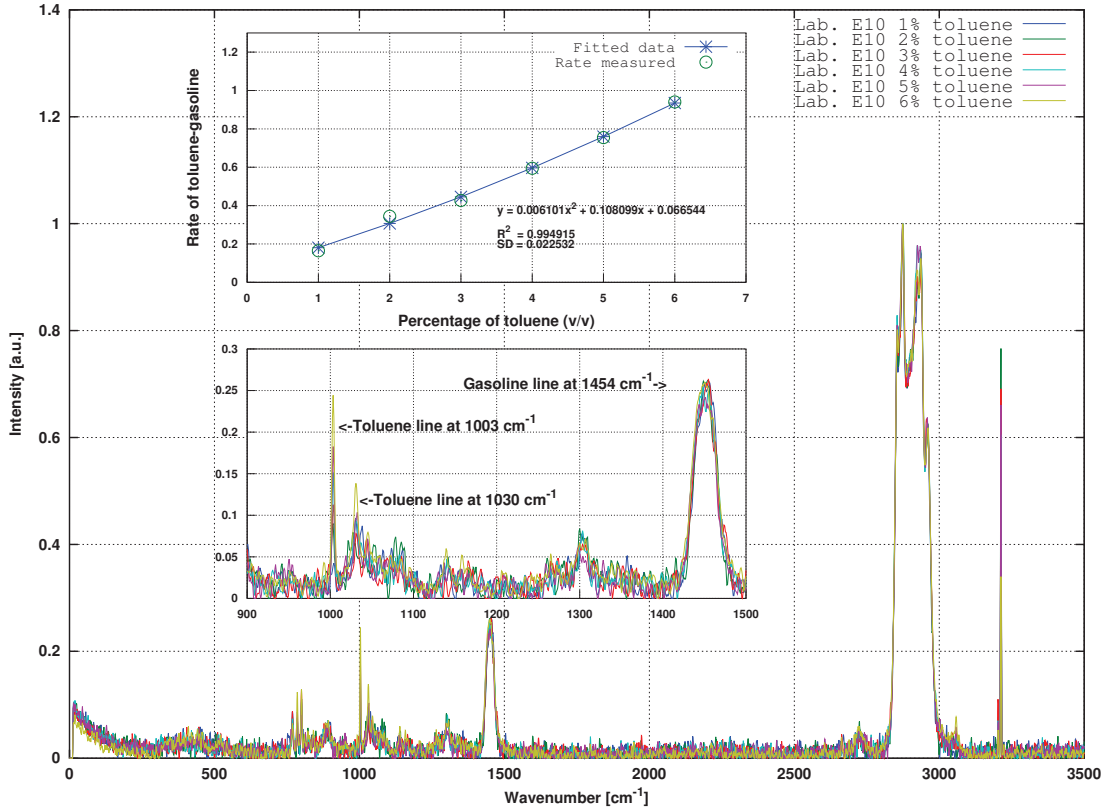

Figure 6.8: Raman spectra of the laboratory-prepared gasoline-ethanol blends having different proportions of toluene. The close up frame belongs to the Raman lines of toluene and gasoline-ethanol blend used for defining the calibration curve. Image taken from [132].

has been possible to generate a calibration curve for these samples containing from 1% to 6% v/v of toluene. A quantitative analysis of the toluene included in commercial gasoline-ethanol blends has been performed by extrapolating the values obtained in this calibration curve.

By removing the spectral wide-band component of the commercial E10 samples from Aral, Shell and Esso, it has been possible to verify the relative intensity of the characteristic Raman lines of toluene and gasoline. The ratio of these two intensities has permitted the estimation of toluene content in these three commercial gasoline-ethanol samples by evaluating the coefficients calculated previously. The determined proportions of toluene in the commercial gasoline samples are in the range from 12.1% to 12.8% v/v. These results are consistent with the qualitative information of their respective Raman spectra, and

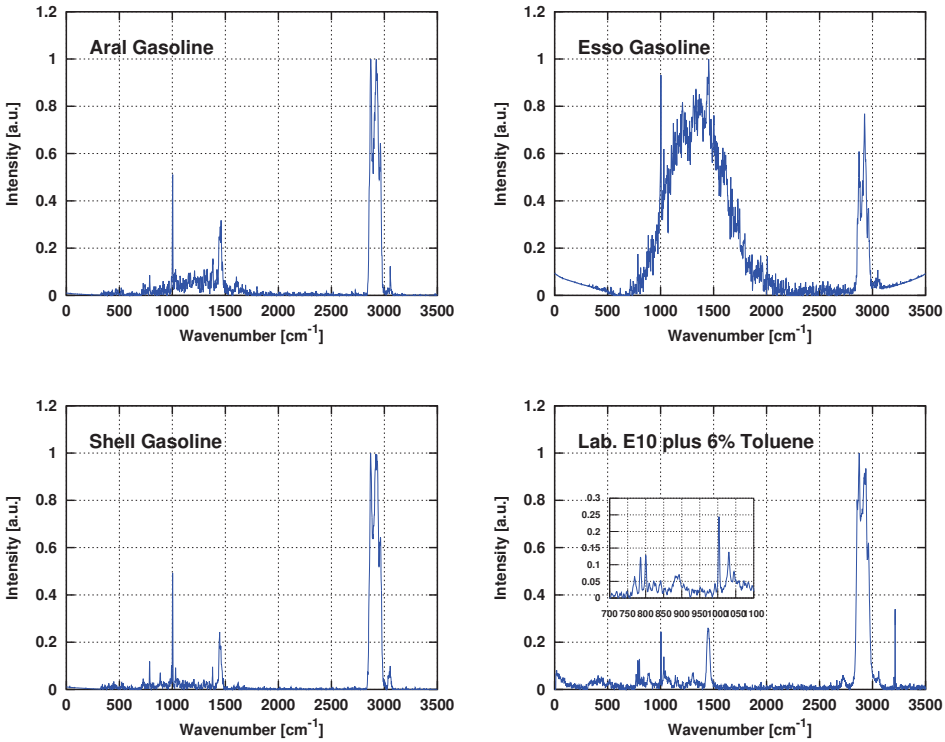

Figure 6.9: Raman spectra of the three commercial and the laboratory-prepared gasoline-ethanol samples.

these proportions are a close approximation to the average value reported by the European Commission and the Environment Agency, despite the presence of additional materials on the samples.

Figure 6.9 depicts the Raman spectra from the three commercial gasoline-ethanol blends and the Raman spectrum from the laboratory-prepapred gasoline-ethanol sample having 6.0 % content of toluene. The later shows a Raman line of toluene (Raman shift at 1003 cm^{-1}) having a relative intensity of about 0.245. The removal of the wide-band elements of the spectra of the commercial samples, allows us to observe a relative intensity between 0.50 to 0.52 in this Raman line (approximately twice the intensity obtained in the sample having 6.0 % toluene content), which is in agreement with the approximated values calculated.

6.2 Monitoring of hydraulic fluids

Lubricants oils are widely used in order to reduce the friction among the parts of mechanical systems and to transmit more power. One of the largest markets of lubricants are oils for engines and automotive industry, as well as for hydraulic systems [215]. The economical relevance of this type of products increases constantly as the reduction in costs in any process includes a proper saving in the energy (also positively regarded from the environmental perspective) that is required. This can be accomplished by reducing the stress and the friction of the mechanical arrangements used [106, p. 1-3] [102, 1-2].

Several efforts have been taking place in the field of lubricants aimed to substitute the large proportion fossil-oil-based [71, p. 1] lubricants by synthetic, vegetables and biodegradable ones in order to reduce the pollutants in case of emissions or accidental spillings [145, p. 242] [105, p. 50] [112, 151]. However, the use of fossil-oil-based lubricants still represent a large portion of the entire market, and these material can cause severe soil pollution and therefore a proper disposal must be provided [199, p. 165]. Mortier et al. have described broadly the different impacts that these lubricant oils can have on the environment from different perspectives [115, p. 435].

We have performed a brief series of Raman measurements of two different sets of hydraulic oil Hyspin (high viscosity index - HVI) from Castrol^{TM} [23] by using our FT-Raman spectrometer prototype [134]. HVI hydraulic oils are obtained conventionally from paraffinic (alkane groups [101, sec. 3.1.2]) mineral oil [71, p. 20]. The refining process of such a hydraulic oils involve paraffinics, aromatics, and solvents. These materials are also considered hazardous to the public health environment [115, p. 14-15].

The objective of these measurement was the observation of the structural changes in the molecules of aging oil inside the machinery, in which this hydraulic oil has been used. By analyzing the spectral information we wanted to determine if the characteristics of the hydraulic fluid, such as: viscosity, corrosion control, fluidity, filterability, water tolerance, etc., could be inferred by observing the different molecular vibrations of the aging the samples. This aging behavior of the hydraulic oil (oxidation, polymerization or enlargement of hydrocarbons, and hydrolysis) causes significant changes of the base fluid [200, sec. 11.3.8]. By properly verifying the working conditions of the hydraulic fluid, it is possible to preserve the appropriate functioning of the machine during longer periods of time, while consuming lesser quantities of hydraulic oil.

Table 6.6: Sets of hydraulic oil Hyspin HVI and the usage time and their corresponding usage time that were used for the Raman measurements.

	Approx. time of usage (h)				
	1	2	3	4	5
set 1	0	576	1008	1368	1680
set 2	0	170	340	510	680

For the Raman analysis, we have acquired two sets of samples that have been used during different periods of time. Each set consists of five samples of hydraulic fluid having different wearing times. One of the sets (set 1) has been filtered by using micrometer paper in order to remove small floating particles that could generate spurious signals in our back-scattered Raman light. The second set has been directly analyzed without additional filtering or preparation whatsoever. Table 6.6 shows the general information about these two sets of hydraulic fluid, as well as the assigned number of the samples. At measuring time, every sample of the two sets of hydraulic fluid has been poured into a 5.0 mL quartz cuvette and subsequently placed in front of a 20X microscope objective in the FT-Raman spectrometer.

Figure 6.10 and figure 6.11 present the Raman spectra of the hydraulic fluid (set 1 and set 2 respectively) obtained by using our FT-Raman prototype. The Raman spectra are presented in the range from $0\,\mathrm{cm}^{-1}$ to $3500\,\mathrm{cm}^{-1}$ with a spectral resolution of $5.0\,\mathrm{cm}^{-1}$. The Raman spectra from these two sets of Castrol Hyspin hydraulic oil have been dominated by a large wide-band component and background noise (fluorescence effects), although every resulting spectra has been calculated by averaging 45 scans, for signal-to-noise ratio improvement, given the noisy nature of these samples. These effects have prevented us from obtaining a proper analysis of the molecular structure. Nevertheless, certain qualitative aspects and molecular changes of the Hyspin oil in the initial phases of the wearing have been observed.

The initial sample of set 1 has clearly shown the Raman lines at $1308\,\mathrm{cm}^{-1}$, $1440\,\mathrm{cm}^{-1}$, $1814\,\mathrm{cm}^{-1}$ and $2853\,\mathrm{cm}^{-1}$. These Raman lines belong to the alkane groups of the strong vibrating modes (CH_2 wag, CH_2 bend, and CH_3 out-of-phase bend and in-phase stretch [92, 74-76]). The spectrum from the sample two of the first set of hydraulic fluid has lost several of the original Raman information and the line at $2380\,\mathrm{cm}^{-1}$ remains as the largest line (line of reduced intensity in the first sample of this set). The third sample of set 1 has also

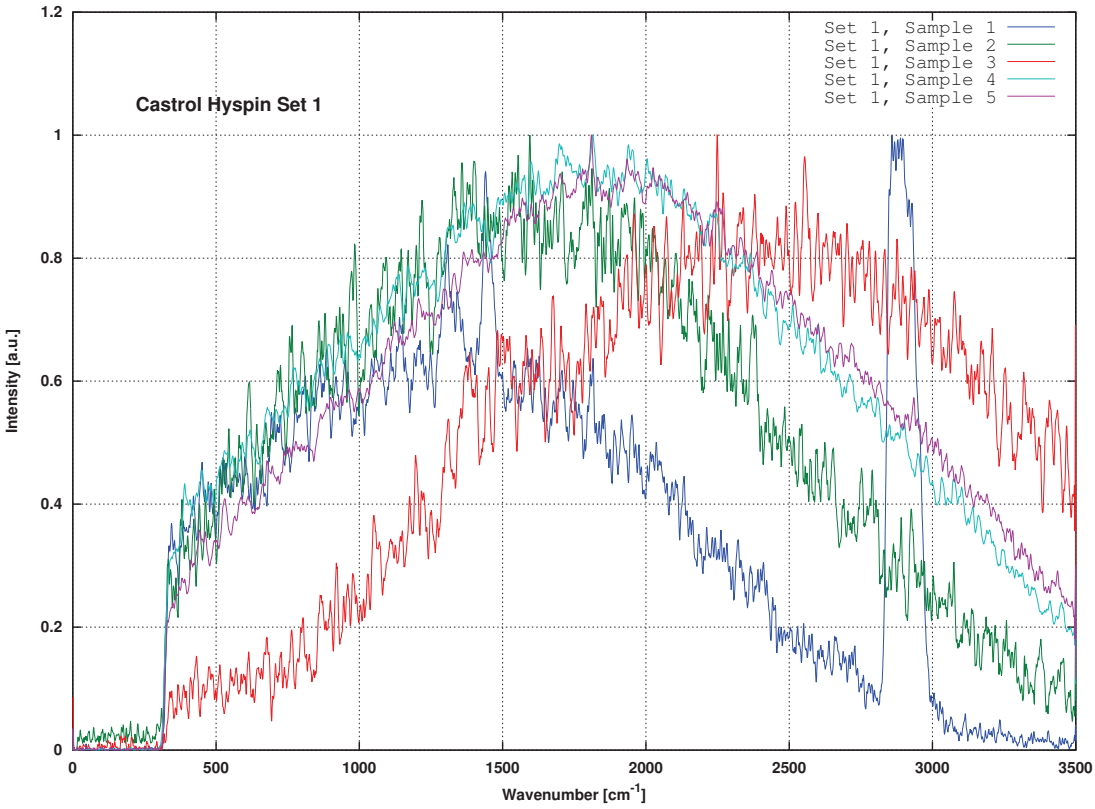

Figure 6.10: Raman spectra of the five hydraulic fluids from the set 1.

shown a shift of the wide-band component into the region of higher wavenumbers of the spectrum. However a conclusive change on the molecular structure of the samples cannot be properly determined beyond the vibrating modes previously mentioned. The last two samples of set 1 have shown no additional information that indicates a clear molecular change. The samples from set 2, with shorter periods of usage, have shown even stronger effects of the wide-band spectral components compared to those from set 1. Therefore, the samples of set 2 offer less suitable information for the molecular analysis of the hydraulic fluid. This artifact can be attributed to the unfiltered characteristic of these specific set of samples.

By using the actual configuration, the measurement capabilities of our FT-Raman spectrometer have been diminished due to the strong effects of the fluorescence. This type of emissions inhibit the proper acquisition of Raman light of our photon counting system. Nevertheless, this weakness of our measurement system, for this particular case, might be

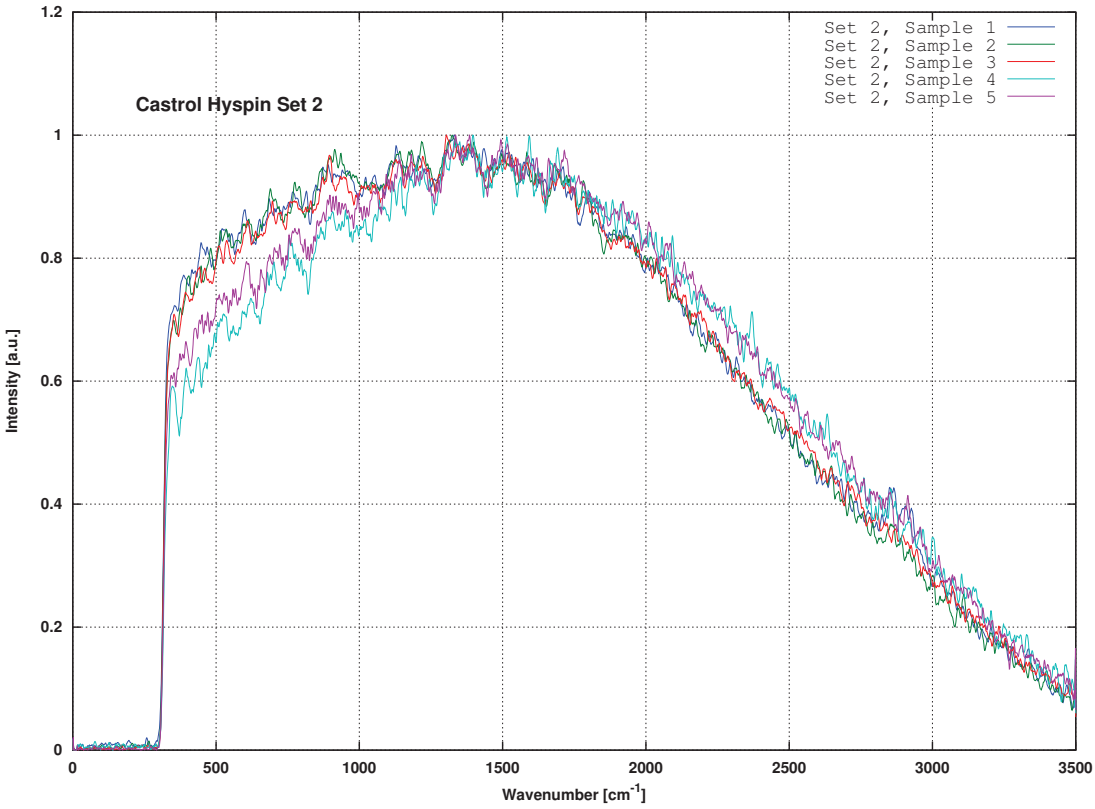

Figure 6.11: Raman spectra of the five hydraulic fluids from the set 2.

overcome by combining our FT-Raman system and the spectral evaluation method with exciting light sources of higher wavelengths (e.g. λ_{source} =1064 nm). At these wavelengths, the levels of fluorescence decreases significantly. By doing that, a better observation of the vibration modes of the samples analyzed can be achieved. Additional treatment such as bleaching, filtering of the samples, etc. can be applied prior to the Raman measurements. However, this last suggestion would represent again a severe drawback to the intrinsic advantage that Raman spectroscopy offers in terms of sample preparation.

6.3 Monitoring of alcoholic beverages

Beverage and food industries have dynamic production processes where a rapid condition of the products must be determined in order to achieve either cost reductions or to improve operations. Raman spectroscopy has been already applied in several fields of these

aforementioned industries due to its intrinsic technical characteristics [78, p. 143][146, p. 946][158]. Moreover, using Raman analysis can be applied in a contact-less fashion to already packaged products (e.g. in glass containers, plastic bottles and blisters), and without applying pre-treatments whatsoever to the samples under observation. These features cannot be offered by several techniques with the level of selectivity that Raman spectroscopy provides.

Raman spectroscopy has been also used in the spectral analysis of alcoholic beverages. In this specific case, Raman analysis also offers an additional advantage over IR spectroscopy since the Raman analysis is normally fully compatible with aqueous samples (since water is a poor Raman scatterer) [161, p. 405][50, p. 295][181, p. 33].

The types of analysis performed to alcoholic beverages by using Raman spectroscopy include: production aid, quality control, quantification of ethanol content, detection of adulterated beverages, authentication of the products, discrimination of similar types of beverages, identification of illegal drugs dissolved in the beverages, detection of harmful materials in the beverages (e.g. methanol, isopropanol, aldehydes), etc [39, p. 93][143, p. 81][89].

Some of these analysis assist on the avoidance, in the consumption, of higher levels of certain materials, as methanol (normally present in distilled beverages in low proportions), that are often related to severe health issues or even death due to the alcoholic beverages having poor quality characteristics [56, 202, 125].

In this section, we present the measurements, performed by using our Raman device and evaluation method of some samples of the Mexican alcoholic beverages bacanora and tequila. These two alcoholic beverages are made from similar agave plants, and their production processes are also similar. However, as tequila has already reach a wider portion of the market, its production relies in more strict norms and standards of quality in comparison with the production of bacanora, which is mostly produced by traditional and rudimentary methods. By using our FT-Raman arrangement we wanted to determine how the chemical structure of these two beverages differ from each other, and also how these two beverages differ from the chemical structure of ethanol.

Table 6.7: Samples of Bacanora used during the Raman spectral measurements.

	Bacanora samples characteristics	
Sample No.	Origin of the sample	Type of preparation
1	Producer 1	sample with sugar
2	Producer 1	sample with no sugar
3	Producer 2	sample unknown

6.3.1 Monitoring of the traditional distilled bacanora with our proposed device and method

Bacanora is a traditional, tequila-like alcoholic beverage produced in the state of Sonora in the north of Mexico. This beverage is distilled from the plant *Agave angustifolia* [162]. The demand of this product has been increasing substantially in recent years due to several factors [40, 55, 159, 162]. Although bacanora has been given recently its *designation of origin*, and legal changes related to this beverage have been approved [60], most of the production still relies on traditional and rudimentary methods without a proper standard of quality and only based on the perception of experienced subjects [64]. Certain studies of content of several agave-derived beverages, including bacanora, have been performed by using ion and gas chromatography, and some other analytical techniques [40, 89]. Some of the results obtained have shown that the amount of methanol and ethanol strongly varies among the samples due to the raw materials used. It is also possible, that the lack of proper methods for monitoring contribute to these findings.

Raman spectroscopy has demonstrated its effectiveness in a vast amount of study fields, including food and beverage industries. However, Raman spectroscopy has not been applied, as of the time of this research project, for the chemical analysis of bacanora, which possesses a chemical structure similar to that of tequila. This spectroscopic technique could be of interest in the elaboration of this traditional beverage.

We have acquired, for the first time[1], the Raman spectra of three samples of bacanora by using the FT-Raman instrument that we propose. These Raman information have been subsequently compared with the Raman spectrum of pure ethanol. Additionally we have compared these Raman spectra with the extracted Raman spectra of some samples of tequila, which has a similar production process and it is extracted from a similar plant.

[1] At the development time of the present thesis report, no previous spectral studies of bacanora have been found by using Raman spectroscopy.

The purpose of the measurements was the qualitative analysis of these distilled beverages. We also wanted to verify if some harmful materials were present in these samples.

The Raman spectra obtained have permitted the observation of certain qualitative characteristics of the samples. In order to validate the measurements, additional analysis of the same samples have been performed by using gas chromatography (Bruker 400-GC Series 1).

For the FT-Raman spectral measurement, we have used three different bacanora samples. Two of the bacanora samples have been obtained from the same producer in the town of Rayon, Sonora. The producer of these two samples claimed to include glucose (in form of conventional sugar) in one of the samples in order to obtain a larger amount of ethanol (C_2H_6O). The third sample has been obtained in the town of Bacoachi, Sonora, from an unknown producer. Additional information about the distilling process, the storage, the raw materials used, etc. have not been provided. Furthermore, the alcohol volume of the samples was not at disposal prior to the measurements. Table 6.7 gives an overview of the samples used in the spectral analysis.

The Raman spectra from the three bacanora samples have been extracted by using our self-designed and realized FT-Raman spectrometer and the adapted method that we have proposed. As expected, the resulting Raman spectra obtained from the bacanora samples have shown a matching similitude to the Raman spectrum of ethanol (C_2H_6O). This spectral information, obtained from the measurements, can be observed in figure 6.12. The spectra have been presented in the range from $0\,\mathrm{cm}^{-1}$ to $3500\,\mathrm{cm}^{-1}$ with a spectral resolution of about $1.66\,\mathrm{cm}^{-1}$. The Raman spectrum of ethanol has been also included as a reference.

Some qualitative differences of the samples can be observed, when the Raman spectra of bacanora are superimposed. Firstly, it can be noticed, that the bacanora samples also contain additional chemical compounds, including water (visible wide band between approximately $3100\,\mathrm{cm}^{-1}$ and $3500\,\mathrm{cm}^{-1}$). In contrast, the sample of pure ethanol shows a reduced amount of noise and a flat line in this same region at the end of the presented spectrum range. Moreover, although the characteristic Raman band of ethanol at $882\,\mathrm{cm}^{-1}$ can be clearly observed in the three samples, the occupied area under the curve at this Raman band of the bacanora with sugar would indicate a larger amount of ethanol than the sample produced without additional sugar.

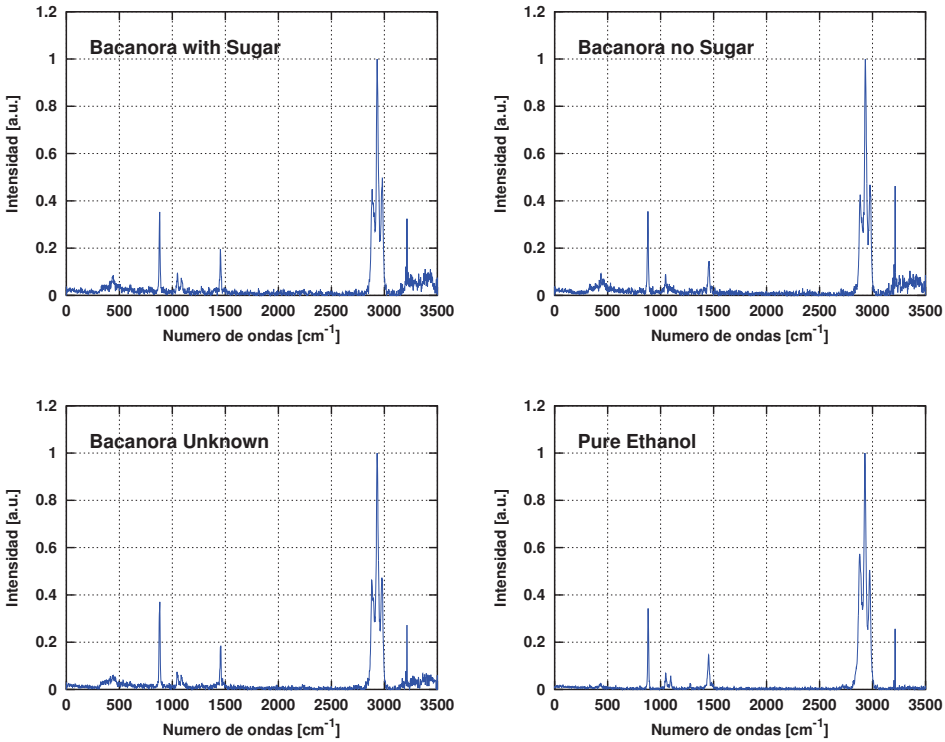

Figure 6.12: Raman spectra from the three samples of bacanora. An additional Raman spectrum of ethanol has been also used as a reference.

The results from the chromatographic analysis of the samples are displayed in table 6.8. The amount of ethanol present in the samples 1 and 2 are consistent with the information given by the producer 1. The levels of methanol content are within the allowed limits for consumption ordered by Mexican official norm of bacanora (a minimum specified content of 30 mg/mL and a maximum of 300 mg/mL)[171]. It is also within the limits ordered by the EU. Additional traces of the following materials have been also found in the chromatographic analysis: 1-propanol (C_3H_8O), 2-methyl-1-propanol ($C_4H_{10}O$), 3-methyl-1-butanol ($C_5H_{12}O$) and acetaldehyde (C_2H_4O).

6.3.2 Monitoring of tequila with our proposed device and method

Unlike bacanora, the production of tequila is accomplished under strict Mexican norms and standards of quality. In comparison to bacanora (regional recognized), tequila has already

gained recognition and consumers at an international level. This alcoholic beverage is obtained from the plant "blue agave" (*Agave tequilana Weber var. azul, Agavaceae*) [33, 51, 89], which is similar to the one used for the production of bacanora.

In the case of tequila, which is a distilled beverage produced by using proper industrial standards, different methods of monitoring, including Raman spectroscopy in a minor proportion in some cases, have been applied for its qualitative analysis and discrimination [24, 53, 107]. Since this combination of Raman spectroscopy and analysis of tequila has not been fully exploited, it presents itself as an appealing opportunity to test the capabilities of our FT-Raman device in this specific field. Furthermore, some of the spectral properties of bacanora exhibited in subsection 6.3.1 can be contrasted to those that can be displayed by tequila.

For the spectral monitoring of this alcoholic beverage we have gathered seven types of tequila (most of them of the *reposado* type that rest for certain period of time in oak barrels [52, p. 1-3][172]). These untreated samples have been obtained from new and sealed bottles of tequila. Table 6.9 shows a listing having the basic characteristics and the name of the tequila, as well as number assigned to each of the samples.

The samples have been analyzed by collecting the Raman back-scattered light of about 50 scans of our FT-Raman spectrometer with a resolution of $5.0\,\mathrm{cm}^{-1}$. The larger amount of scans, in comparison with previous measurements, had as a purpose the improvement of the signal-to-noise ration, and the proper detection of the Raman spectral component of water (H_2O), which is a poor Raman scatterer. We also wanted to avoid the rather moderate levels of fluorescence detected on the samples that could smear the Raman signals of the spectra.

Figure 6.13 shows the spectra of tequila obtained from the seven samples. The characteristic Raman line of ethanol (C_2H_6O) at $882\,\mathrm{cm}^{-1}$ can be clearly observed in all the

Table 6.8: Resulting amount of ethanol and methanol contained in the bacanora samples. These values have been obtained by using gas chromatography.

	Bacanora contents	
Sample No.	Amount of ethanol	Amount of methanol
1 (Producer 1)	52.0%	0.13%
2 (Producer 1)	48.8%	0.14%
3 (Producer 2)	50.8%	0.12%

Table 6.9: Samples of tequila and some of their properties. These samples have been used for the Raman spectral measurements.

	Description and properties of the tequila		
Sample No.	Denomination	Classification	Alcoholic graduation
1	Antiguo de Herradura	Reposado (rested)	38 %
2	Herradura Original	Reposado (rested)	40 %
3	Gran Centenario Azul	Reposado (rested)	35 %
4	José Cuervo Especial	Reposado (rested / mixed)	40 %
5	Don Julio	Reserva (rested)	38 %
6	Cazadores	Reposado (rested)	38 %
7	Leyenda del Milagro	Silver (whtie)	40 %

samples. Samples 1 and 2 ("Antiguo de Herradura" and "Herradura original", from the same producer of tequila) have shown a distinguishing similarity that suggest little or no difference in the steps of the production or the aging processes. As expected, the only sample of white tequila (sample 7) has shown a clear flat Raman spectrum. This type of clear tequilas are commonly bottled directly after the distillation and therefore with less chemical compounds that might generate fluorescence effects by being introduced into the spirit.

With the evident exception in the observed spectra of sample 6 and sample 7 (tequila "Cazadores" and "Leyenda del Milagro" respectively), the Raman spectra of these tequilas have shown a significantly amount of wide-band components (fluorescence). This is because during the aging process of the "rested" (*"reposado"*) tequila, certain materials from the oak barrels are "passed" to this spirits. Another reason is that the Mexican norm for tequila also allows the mixture of caramels and some other materials in order to enhance and influence the flavors and colors of such a beverage.

Despite the smearing effects caused by the fluorescence, and with the solely exception of sample 4 ("José Cuervo especial", that contains a mixture of different tequilas and its visually darker characteristic suggests a larger amount of additional chemical compounds), the Raman spectra of these samples of tequila have shown the Raman signal of water in the wide band section between approximately $3100\,\mathrm{cm}^{-1}$ and $3500\,\mathrm{cm}^{-1}$.

Figure 6.14 shows the Raman spectra of the three samples of bacanora that have been presented in the previous subsection, and the Raman spectra of the seven samples of tequila. The Raman spectra of bacanora have been extracted again by using

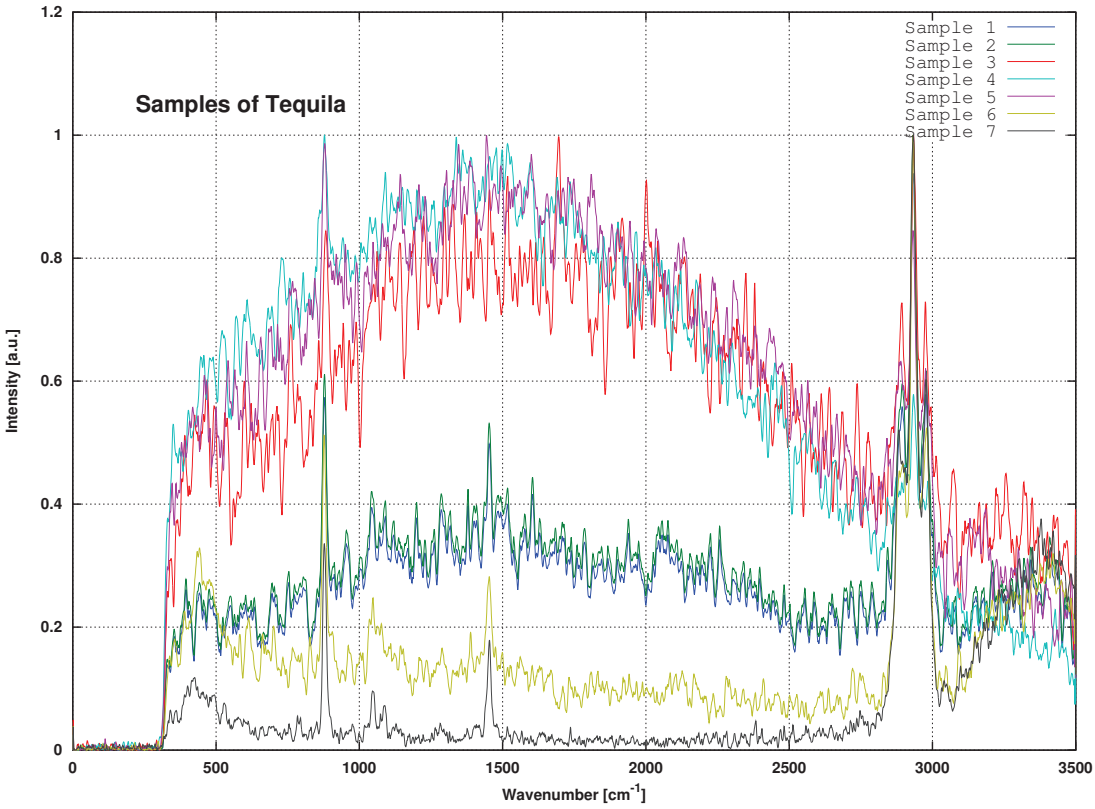

Figure 6.13: Raman spectra of the seven samples of tequilas enumarated in table 6.9. These Raman spectra have been obtained by using our FT-Raman spectrometer.

our FT-Raman spectrometer under the same conditions we have used during the Raman measurements of the samples of tequila in order to reduce acquisition errors.

Due to the strong effects of the fluorescence of most of the samples if tequila, a proper comparison against the Raman spectra of bacanora is not straightforward despite their spectral similitude. However, by taking the clear Raman spectrum from sample 7 ("Leyenda del Milagro Silver"), it is possible to observe a slightly larger intensity of the Raman lines of ethanol in the samples of bacanora. It can also be observed a larger and more pronounced intensity, in the wide-band of water in the Raman spectra from tequila. As previously stated, bacanora has shown an average of about 50 % ethanol content v/v, while tequila has an ethanol content v/v between 38 % to 40 %.

Figure 6.15 displays a two-dimensional projection of the singular value decomposition (SVD) that we have applied to the spectra of tequila, bacanora and pure ethanol. This

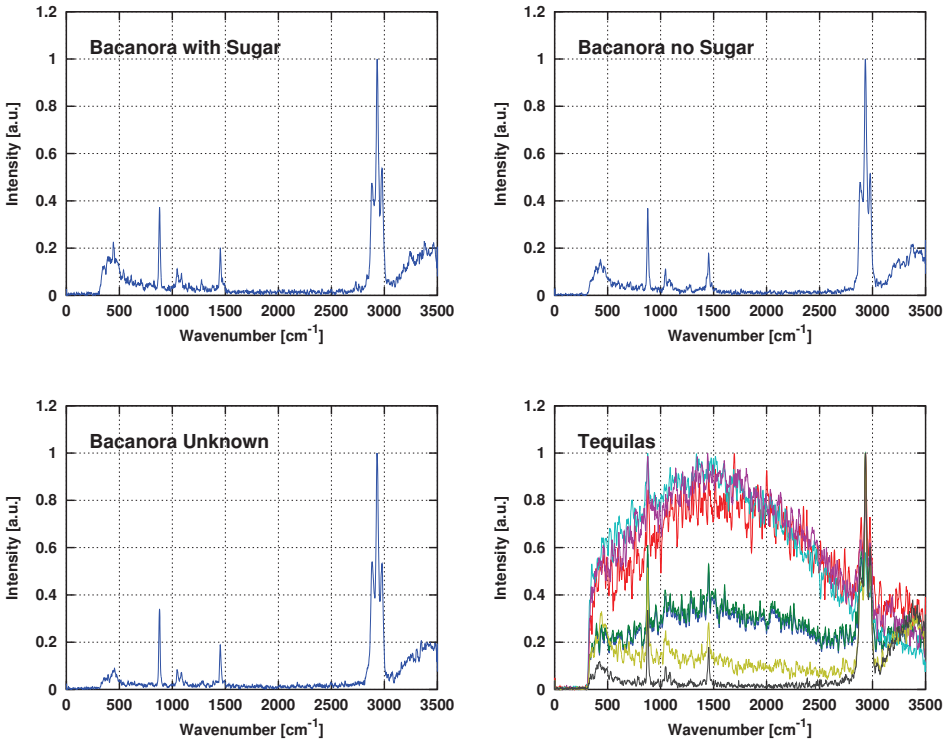

Figure 6.14: Spectral comparison of the Raman spectra obtained from the three samples of bacanora and the seven samples of tequila.

has been performed in order to observe the distribution of the samples, and the similarity among them. Based on the resulting vectorized information of this two-dimensional projection of the SVD, we have also calculated the cosine similarity to the Raman spectrum of ethanol. The results obtained from this operation can be seen in table 6.10.

The visual and numerical results shown in figure 6.15 and in table 6.10 suggest a remarkable resemblance of the three Raman spectra of bacanora and the tequilas samples 1, 6 and 7 (cosine similarities larger than 0.99) to the spectral information of ethanol. The tequila sample 2 shows a relative large value of 0.733610, although its Raman spectrum is qualitatively speaking identical to the one of sample 1. As expected, the noisy spectra from the samples 3, 4 and 5 have shown only a reduced level of similarity to ethanol due to the smearing effect caused by the fluorescence.

The FT-Raman spectrometer with the actual configuration has the capability of ex-

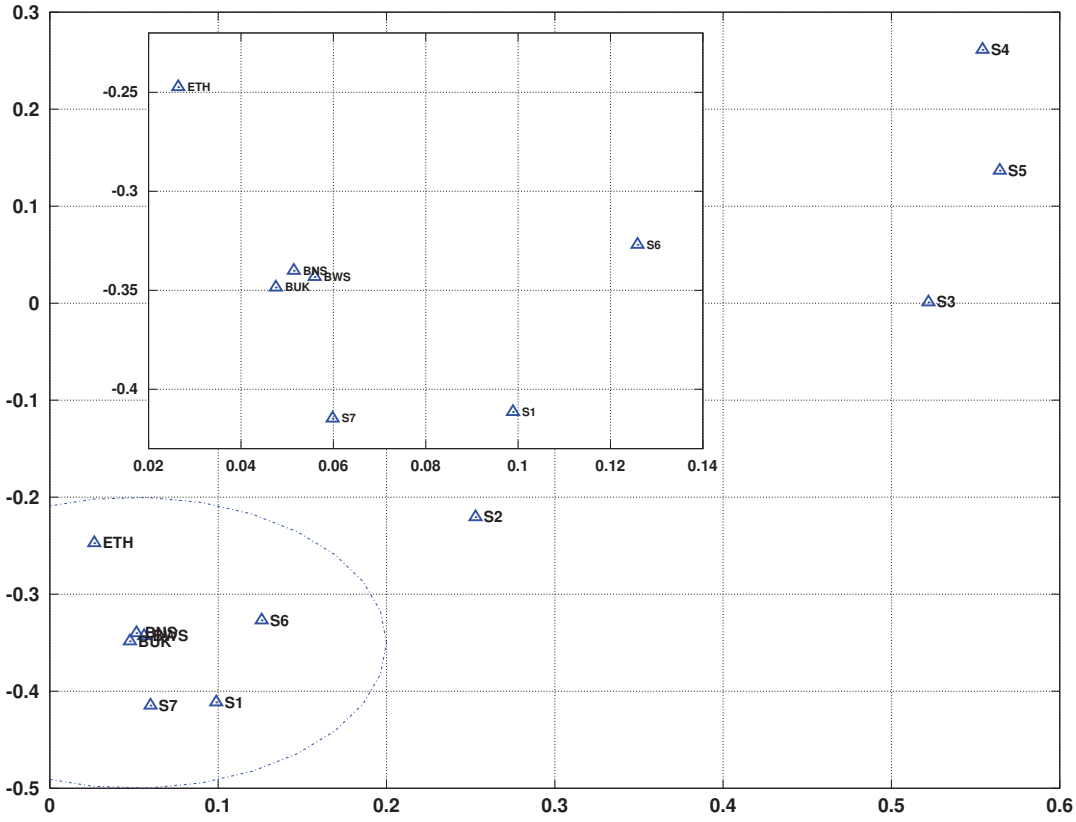

Figure 6.15: Two-dimensional projection of the singular value decomposition (SVD) applied to the samples of tequila, bacanora and ethanol. The close up region shows the clustered values of bacanora and three tequilas.

tracting the Raman spectrum of tequila, even with some degree of smearing influence due to effect of fluorescence (in the case of rested tequila). However, our FT-Raman device seems more appropriate for the monitoring of the production of tequila in the initial phase or in white tequilas. In the case of bacanora, since the product is basically bottled right after the distillation, no additional materials are passed and therefore its Raman spectrum can be collected easily with the actual configuration.

6.4 Miscellaneous spectral measurements

Beside the applications of our FT-Raman system and method in monitoring processes, we have also carried out certain spectral analysis of optical devices and light sources by

Table 6.10: Cosine similarity to ethanol applied to the vectors of the two-dimensional projections of the Raman spectra of tequila and bacanora. The samples marked with "*" have suffered the strong effects of fluorescence.

Sample	Alcoholic graduation	Similarity to Ethanol
Ethanol	100 %	1.000000
Tequila sample 1	38 %	0.991629
Tequila sample 2	40 %	0.733610
Tequila sample 3*	35 %	0.104572
Tequila sample 4*	40 %	-0.327843
Tequila sample 5*	38 %	-0.130722
Tequila sample 6	38 %	0.966131
Tequila sample 7	40 %	0.999320
Bacanora with sugar	52 %	0.998475
Bacanora no sugar	49 %	0.999044
Bacanora unknown	51 %	0.999574

performing only reduced or "no changes at all" in the original instrumental configuration of our FT-Raman spectrometer (e.g. removal of the laser line filter, removal of the notch filter, purposely inserting losses the light coupling, etc.).

These experiments are somehow outside of the main scope of our research goals, as the design and development of the FT-Raman spectrometer were intended for other type of applications. Nevertheless, we were constrained with some technical artifacts, and these spectral measurements have allowed us to accurately characterize certain components in order to optimize the final and operative configuration of our FT-Raman system in a convenient fashion.

The spectral characterization of the optical components have been helpful, specially on the initial phase of the development of our FT-Raman spectrometer. At the initial stage of the development, it was necessary to carefully verify features and parameters such as:

- Bandwidth characteristics of notch filters and laser line filters.
- Distribution of the plasma lines of the discharge lamp of the laser.
- Bandwidth of a variety of light sources.

By closely observing these parameters, we have been able to objectively decide over the best choices, in terms of optical components, photon counting rates and sometimes costs, that we would include in an optimized design of our FT-Raman device. We have

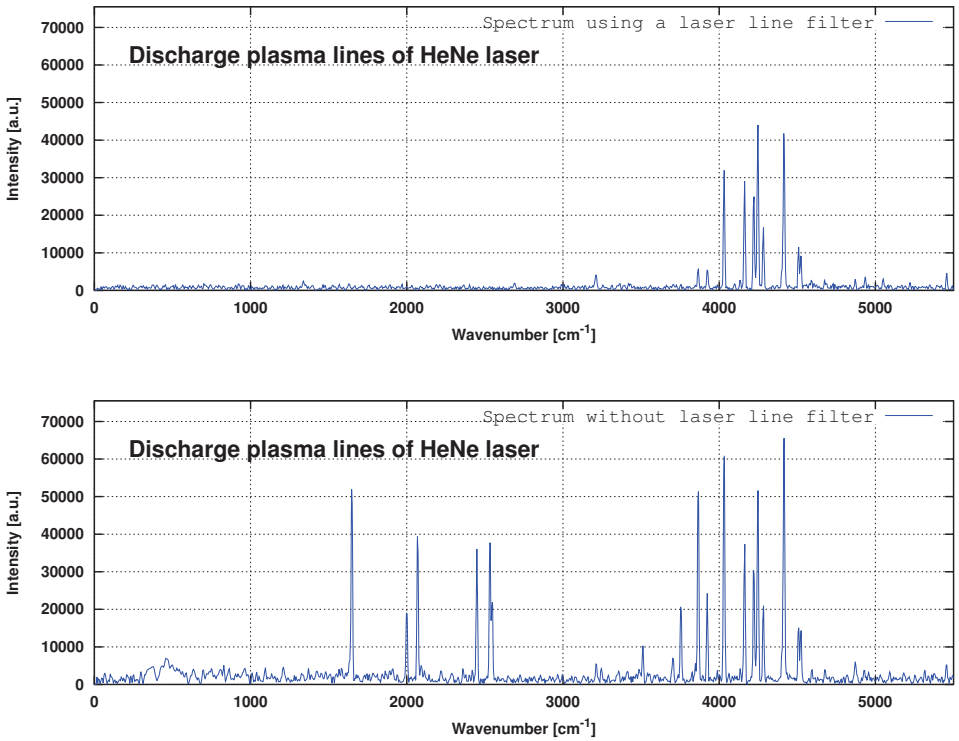

Figure 6.16: Effect of the laser line filter on the spectral components of the plasma lines that are generated by the discharge lamp of the HeNe laser. The range of the wavenumber axis shown is equivalent to a spectral range between 632.8 nm to 970.6 nm.

also been able to discriminate defective and deficient parts that contribute to aggravate the detection of the reduced amount of Raman signals available for the spectral analysis.

Figure 6.16 provides an overview of the possible effects that a deficient laser line filter could have on a Raman spectrum of interest. As it can be seen, some of the plasma lines of the discharge lamp of the laser are located within the range from $0\,\mathrm{cm}^{-1}$ to $3500\,\mathrm{cm}^{-1}$, that we have normally observed in our Raman analysis. The plasma lines in the higher wavenumbers would not have any effect of the spectral calculations. However this would reduce the detection capacity of Raman back-scattered light in our photon counting device.

Figure 6.16 also shows the effect of the laser line filter on the distribution and the amplitude of the plasma lines that are generated by the HeNe laser used in our FT-Raman spectrometer. These lines are normally several orders of magnitudes smaller than

the main output signal (λ =632.8 nm) and their power levels are difficult to determine by conventional measurement techniques. However, an inadequate filtering of these low-intensity signals would affect negatively our measurement system.

Similar examples have been performed with other optical filters and some light sources. From all these devices, we have obtained a great deal of accurate spectral information. As already mentioned, the spectral characterization of these components do not require extensive changes on either the original setup or the evaluation software modules.

6.5 Conclusion of the chapter

In this chapter, by using the low-cost FT-Raman spectrometer and the method that we propose, specific cases of Raman analysis that can be potentially found in some production processes have been introduced. We have concentrated our efforts in the fields of gasoline-ethanol blends, hydraulic fluids and some agave-derived alcoholic beverages. All these fields involve the use materials having a negative connotation in terms of toxicity. We have also made a brief reference to some additional spectral measurements performed in order to determine the characteristics of optical parts and lights sources.

In relation to what we have been able to observe in the analysis performed to the gasoline samples, our low-cost FT-Raman spectrometer and our evaluation method have shown satisfactory results in both laboratory-prepared and commercially-available samples. The latter samples have shown a higher degree of complexity and it has been necessary to applied an extra effort in order to extract the information of interest. However, given the amount of toluene that we could observe and the frequency accuracy that we have achieved, it has been possible to perform some quantitative analysis on the commercial samples of gasoline without applying any additional chemical markers to the samples.

The actual configuration of our FT-Raman spectrometer has shown some weaknesses in the spectral analysis of hydraulic fluids, since these materials are extremely noisy in terms of fluorescence, specially the unfiltered samples. In this type of measurements though, we have been able observe some molecular changes in the first phases of usage of the hydraulic fluid. Nevertheless, we would have to implement some changes, already scheduled, to the actual system, if further measurements of these type of materials are to be performed: excitation light sources of higher wavelength, and an appropriate photon counting detector.

The agave-derived alcoholic beverages have shown an overall satisfactory results. However, our actual system seems to be more adequate in the monitoring processes of the traditional-produced bacanora and in the production of white tequila (or the initial phases in the production of tequila, prior to the "resting" period). These type of distilled beverages have shown a cleaner and simpler to interpret Raman spectra, in comparison with the rested tequilas, that have added materials from the aging containers. Although a significant level of fluorescence has been observed, it was still possible to distinguish the main Raman lines collected from these samples of rested tequila.

In all the presented cases, it would be helpful to apply more and better adapted chemometric techniques, according to the nature of each sample, in order to extract additional information from the Raman data collected. The measurement of harmful materials related to other fields of study would also contribute to the evaluation of the capabilities of our FT-Raman device in monitoring processes.

Chapter 7. General conclusions and outlook

The previous two chapters have shown some of the results related to the experimental validation of our low-cost and flexible FT-Raman system and the evaluation method that we propose by using materials commonly used in Raman spectroscopy. We have also shown some of the possible monitoring applications in which this proposed Raman device can be further exploited. In the present chapter, we extended a final discussion about our findings and contributions, including some of the limitations that we have encountered. We also provided some comments and suggestions about what we consider to be essential for the further developments and directions of this research project.

7.1 Conclusions

The present document reports some of the main validating results related to the conception and the realization of a low-cost FT-Raman spectrometer based on an original combination of conventional hardware parts supported by a spectral evaluation method that allows a good frequency accuracy of the acquired spectrum. We have also justified the reasons behind the choice of the Raman technique over other similar spectroscopic techniques. FT-Raman spectroscopy is a highly selective analytical method and it has a wide range of applications in a large variety of fields of study. This technique can be applied in a clean and practical fashion, as little or no sample preparation is required. This technique has the advantage of perform spectral measurements without having contact to the sample.

The main purpose of the FT-Raman instrument that we propose is to perform, at low cost basis, the monitoring of processes that involve materials having a harmful or dangerous nature that can potentially affect negatively to either public health or environment. We have accomplished satisfactorily most of our initial goals proposed, without significantly affecting the financial aspects that such a FT-Raman device can represent, in terms of acquisition, maintenance and operation. An additional factor that we have considered is strongly related to the flexibility and the freedom and/or ease that the user can have by performing Raman analysis with such an instrument in cases where certain non-regular configurations of the system are required.

In order to obtain effectively a low-cost FT-Raman measurement system with the characteristics and capacities that we initially targeted, it has been necessary to concentrate our efforts in the following key points:

- Elimination and replacement of sophisticated hardware parts and proprietary software applications.
- Analysis and development of an adequate spectral evaluation method that considers all the negative influences on the optical path and still permits an accurate extraction of the spectral information.
- Extensive assessment of the frequency accuracy of the data obtained by using the FT-Raman system that we have conceived and realized (Raman spectra comparison against values of standard Raman spectra, and against Raman spectra obtained by using modern commercially-available FT-Raman spectrometers).
- Analysis of different common materials having a negative connotation in either public health or environment.

In this scientific and technological project we have demonstrated the feasibility of using this novel combination of conventional hardware parts and open-source software applications for the accurate extraction of frequency-accurate Raman spectral information in a clean and sustainable manner. This validating assertion has been obtained by analyzing some calibration materials commonly used in Raman spectroscopy. The resulting Raman spectra of these materials obtained with our device have shown highly resembling spectral values and reduce frequency deviations (only fractions of cm^{-1}) in comparison to the Raman standard values reported by the American Society for Testing and Materials (ASTM).

Likewise, we have explored the monitoring of certain processes in different areas that involve harmful or polluting materials by using our resulting FT-Raman prototype. The results of these experiments have shown an assertive level of success in both qualitative and up to a certain extent quantitative analysis. The less favorable cases were related to high fluorescent materials that cause a significant smearing of the Raman spectrum of interest. This type of light emission is what we consider the main limitation in terms of detection capacity and quantification.

In terms of mechanical stability and robustness, we can claim that the different experimental procedures performed with our FT-Raman spectrometer have been carried out without any assistance of isolation mechanisms for the damping of mechanical vibrations. Moreover, our FT-Raman prototype is located on the top floor of a mechanical workshop in which different heavy tools, such as milling machines and metalworking lathes, operate on a daily basis. None of these mechanical disturbances that are transmitted to the building have been registered on the resulting spectral information obtained by using our FT-Raman spectrometer system.

However, a detailed measurement about the influence of the surrounding mechanical vibration affecting our system has not been formally performed so far. Such a measurement would provide useful information about the limit of the external mechanical noise that our FT-Raman device could tolerate. Nonetheless, the strict simultaneous sampling of the reference and photon counting signals that we have implemented (performed within a few μs) contributes to a certain level of "mechanical noise tolerance" on our FT-Raman system, and makes it suitable for certain harsh environments. The mechanical disturbances normally transmitted to building structures have frequencies in a lower range [147, p. 406] [91, sec. 1.2] compared to our sampling rate and acquisition times.

Although our FT-Raman instrument was developed on a low-cost basis (part costs between approximately 15,000 € and 20,000 € depending on the configuration of the FT-Raman system), and certain financial data related to the different parts that constitute our FT-Raman system have been obtained, a proper assessment of the financial-related parameters has not been properly achieved. Likewise, we have been able to obtain the final market prices of certain commercially-available FT-Raman instruments. However, a fair approximation of the producing price cannot be inferred, as the manufacturers do not disclose these type of detailed data.

Due to these aforementioned reasons, we have not been able to provide a reliable and precise comparison of the financial aspects involved in the development of our FT-Raman system and the one of commercially-available FT-Raman devices. Nevertheless, by merely taking into account the market prices available (or the approximated general cost of production disclosed in the annual reports by Bruker and Thermo Fisher Scientific [37, 194, 195]), we can conclude that the Raman device that we propose can be a legitimate choice for certain applications and environments that require FT-Raman analysis at low costs.

Thereupon, our inexpensive FT-Raman system was achieved by using an original combination of conventional materials and evaluation methods. It could find its way into new sectors and areas of applications, where Raman spectroscopy has been only recalled in the theory, but not in the practical sense, since its costly acquisition, operation and maintenance result unattractive (specially in the case where non-dispersive Raman devices are needed).

As examples for these sectors or areas of applications where low-cost Raman devices can be introduced, we can mention the following cases:

- Small and medium size companies. These types of enterprises commonly are subject to a strict control of their budgets, specially those in countries having emerging or poor economies.
- Geographically isolated regions. In these places, where no proper access to maintenance or support is available, our device can be repaired or operated by using conventional parts easily available.
- Education environments. Such a development would allow more access to non-dispersive Raman spectrometers in laboratories of graduate, undergraduate and secondary levels of schooling, where the maintenance and operation of the device can be performed by a local trained technical personnel.
- Uncontrolled and harsh environments. Application located in places where special facilities for the control of certain conditions are not available (e.g. clean rooms, temperature and humidity control, isolation of certain levels of mechanical vibrations).

The list of possible cases, where this prototype of FT-Raman instrument could be introduced, can be extensive, as well as the combination of factors that could meet the specific requirements of a monitoring application including our technology. The final decision over this matter depends directly on the level of benefit that the user might achieved in his application by using this type of instrument that we have realized.

7.2 Future work and possible improvements

The research work and the corresponding contribution described throughout this report belong basically to the "prototyping phase" and to the validating measurements that can

be achieved with our proposed FT-Raman system. There are several possible improvements and further developments that can be implemented to our prototype in order to make an optimal use of our FT-Raman system technology. The requirements of the applications and the constrains adopted by the end user will shape the final structure of the FT-Raman system. Since there are several fields where the Raman analysis can be applied, the possible changes on the system can be significant.

The actual configuration of the FT-Raman spectrometer that we have presented, can perform better in certain samples, in terms of detection and quantification, by modifying the excitation source (to higher wavelengths) in order to reduce the effects of fluorescence. This type of light emission has been the most critical drawback that we have encountered by combining our system and these type of noisy samples. The modification would require also the replacement of the detector in the photon counting unit that could sense the Raman shift having higher wavelengths.

An additional modification of the instrumental setup that could have a positive impact on the performance of the system, is the replacement of the two flat mirrors of the Michelson interferometer by two cube-corner mirrors. This change would reduced significantly the need for constant, time consuming and sometimes tedious adjustment prior to the scanning process. Moreover, such a components would provide a larger stability to the system in terms of visibility, since the tilting effect of the flat mirror can be overcome in measurements having higher resolutions [79, p. 116][174, p. 138][62, p. 112-114]. These supplemental and substituting device parts can be acquired for relative low costs and they are also well integrated into Michelson interferometers (there are reported measurements having spectral resolutions $\geq 0.5\,\mathrm{cm}^{-1}$, which is three times the required resolution of our measurements).

A further step concerning the miniaturization of the FT-Raman instrument can be achieved by using an all-fiber FT-Raman setup, in which the entire Michelson interferometer is replaced by a Mach-Zehnder interferometer based on single-mode-fiber couplers, gradient-index lenses (selfoc) and a coupled laser diode. This setup would allow a significant reduction of the mechanical components required to operate. The optical path differences required can be produced by generating changes on the refractive index of the fiber arms conforming the Mach-Zehnder interferometer. One method to accomplish this, is to generate controlled temperature changes, by using Peltier elements, in opposite direction on these two arms of single-mode optical fiber. Figure 7.1 depicts the schematic

of a possible version of the previously described all-fiber FT-Raman spectrometer.

The reported thermal coefficient $\frac{dn}{dT}$ for SiO_2 optical fiber is between $2 \times 10^{-5}\,K^{-1}$ to $3 \times 10^{-5}\,K^{-1}$ [49, p. 97][219, p. 241] under conditions of room temperature[170, p. 12]. By developing fiber arms having a length L of approx. 10.0 m and taking the lower value of thermal coefficient of the optical fiber, the generated optical path difference obtained is:

$$\frac{dn}{dT} \cdot L \approx 2 \cdot 10^{-4}/^{\circ}K \approx 200\mu m/^{\circ}K$$

This value is equivalent to around 316 wavelengths, if a λ =632.8 nm HeNe laser is used as a reference. This relation helps out to calculate the temperature difference that needs to be applied, so that a specific optical path difference is produced. The temperature difference applied to the arms of the interferometer depends on the measurement resolution required. To achieve Raman scans having an optical path difference of about 6.0 mm, equivalent to approximately 9500 wavelengths (optical paths commonly used in our measurements), it would be necessary to applied a temperature difference on the arms of the Mach-Zehnder interferometer of about 30.0 °C, which can be easily achieved by using Peltier elements. By increasing two or three times the length L of the Mach-Zehnder arms, the temperature changes required to produce the optical path difference, can be reduced by these same factors and it would not affect significantly the size of the interferometer. It also would contribute to a higher tolerance in the construction of the Mach-Zehnder interferometer, which requires well-balanced arms (L_1 and L_2) of optical fiber having a low difference in length (in the ideal case $\Delta_L = L_1 - L_2 \simeq 0$).

For each arm of the interferometer, a temperature sensor is connected to the controller feedback. In the same way, with the help of the temperature sensors, the control routine programmed inside the micro-controller would transmit the PWM signals to an H-Bridge in order to deliver the current necessary to the Peltier elements.

By using this configuration, it is possible to achieve Raman measurements having very high resolutions, almost 100% interferogram visibility, a far lower effects of the range on the spectrum, and substantial smoothness on the optical path scanning. Furthermore, this type of setup would assist in the reduction of the size of the FT-Raman spectrometer. The main drawback observed by using this type of arrangement is the low amount of Raman light that can be coupled due to the small range of the optical system. However, nowadays

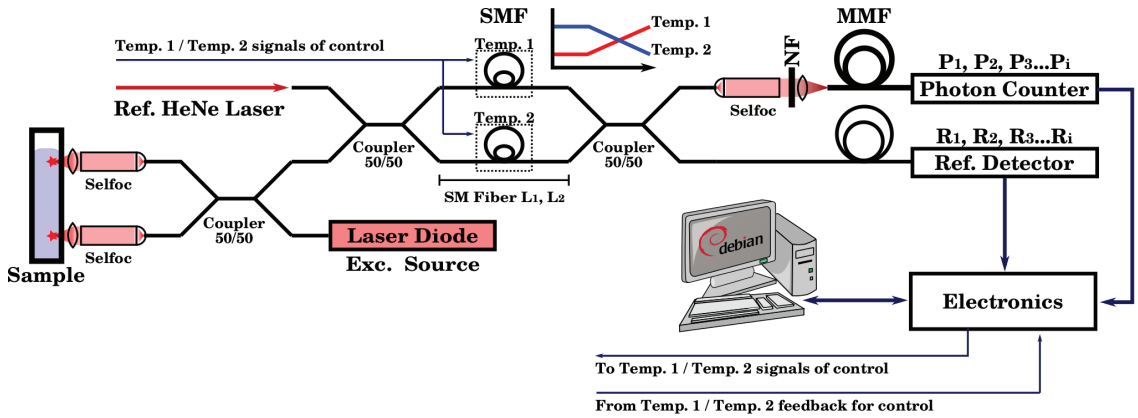

Figure 7.1: All-fiber FT-Raman spectrometer based on a Mach-Zehnder interferometer build by using single mode couplers, gradient-index (selfoc) lenses and coupled laser diode. LF=Laser line filter; NF=Notch filter; SMF=Single-mode fiber; MMF=Multi-mode fiber.

it is possible to find laser modules coupled into single-mode fibers that deliver hundreds of mW of optical power.

The evaluation method that we propose has demonstrated a great deal of frequency accuracy of the Raman spectra obtained with our FT-Raman spectrometer. However, the evaluation method supporting the technology that we propose can be subject of modifications that allow a more efficient measurement system such as:

- Adaptive filtering of signal generated by the optical path difference according to the speed of scanning.
- Analysis of the effects on the optical path difference generated by the mechanical disturbances and the circuitry noise of the system.
- Automatic discrimination of possible defective Raman measurements (single scans out of certain range)
- Incorporation of chemometrical techniques in the analysis of the collected Raman spectra.
- Incorporation of an additional reference photo-detector in order to reduce the effects of the noise present in the circuitry of such a devices.

In terms of data processing, our FT-Raman system can be provided as a future product with additional tools that allow an improvement in the extraction of information form a

specific analyzed sample. For instance, the system can be complemented with a database of spectral information that contains Raman data about the chemical compounds related to process where the FT-Raman system is operating. By using a database and correlation methods, the FT-Raman system would be able to perform tasks like determining the composition of the materials present on the monitoring process.

Likewise, a proper set of algorithms for the compensation of the instrumental effects caused by the Michelson interferometer, which is embedded in our FT-Raman spectrometer, would improve the accuracy and the quality of the collected Raman spectra. All the Raman spectra obtained and introduced in the present report have not been compensated for these aforementioned instrumental effects.

Finally, we consider to be very important for future productions, that our proposed FT-Raman system was tested under practical conditions and under a large range of fields of applications. This approach assists in determining in which type of areas the FT-Raman system that we propose can have rewarding applications with satisfying levels of efficiency.

List of publications related to the thesis (2011-2014)

Peer reviewed (International Journals):

1. Valentin Ortega Clavero, Andreas Weber, Werner Schröder, Patrick Mayrueis, Nicolas Javahiraly. *Qualitative and Quantitative Spectral Analysis of Binary Gasoline-Ethanol Blends Using a Low-Cost FT-Raman Spectrometer Prototype.* Lasers in Engineering ISSN: 0898-1507 (print) ISSN: 1029-029X (online) Volume 25 (2013), Number 3-4, p. 247-253

2. Valentin Ortega Clavero, Andreas Weber, Werner Schröder, Patrick Meyrueis, Nicolas Javahiraly. *Detailed spectral monitoring of different combustible blends based on gasoline, ethanol and methanol using FT-Raman spectroscopy.* Environmental Biotechnology, p-ISSN 1734-4964 8(1):1 - 6, 2012.

Peer reviewed (International Journals) - under review:

1. Valentin Ortega Clavero, Vidal Salazar Solano, Andreas Weber, Werner Schröder, Nicolas Javahiraly, Patrick Meyrueis, Jesús Mario Moreno Dena. *Posible uso de espectroscopia Raman como herramienta de análisis en la producción y el control de calidad de bacanora.* Revista Fitotecnia Mexicana, ISSN 0187-7380, 2014.

2. Valentin Ortega Clavero, Nicolas Javahiraly, Andreas Weber, Werner Schröder, Patrick Meyrueis. *A comparison of the Raman spectral information from toluene and cyclohexane using different FT-Raman devices.* Lasers in Engineering ISSN: 0898-1507 (print) ISSN: 1029-029X (online) Volume XX. 2013,

International conferences with proceedings and refereed:

1. Valentin Ortega Clavero, Andreas Weber, Werner Schröder, Dan Curticapean, Nicolas Javahiraly, Patrick Meyrueis. *Monitoring of the molecular structure of lubricant oil using a FT-Raman spectrometer prototype.* Proc. SPIE 9141, Optical Sensing and Detection III, 91411W, 2014

2. Valentin Ortega Clavero, Andreas Weber, Werner Schröder, Dan Curticapean, Nicolas Javahiraly, and Patrick Meyrueis. *Spectral monitoring of toluene and ethanol in gasoline blends using fourier-transform Raman spectroscopy.* Proc. SPIE Optical Measurement Systems for Industrial Inspection VIII, 8788(8):8788-112, 2013.

3. Valentin Ortega Clavero, Andreas Weber, Werner Schröder, Nicolas Javahiraly, and Patrick Meyrueis. *Spectral observation of fuel additives in gasoline-ethanol blends using a fourier-transform Raman spectrometer prototype.* Proc. SPIE 8720 Photonic Applications for Aerospace, Commercial, and Harsh Environments IV, (4):8720-26, 2013.

4. Valentin Ortega Clavero, Andreas Weber, Werner Schröder, Patrick Meyrueis, and Nicolas Javahiraly. *Comparative spectral analysis of commercial fuel-ethanol blends using a low-cost prototype FT-Raman spectrometer.* Proc. SPIE 8368, Photonic Applications for Aerospace, Transportation, and Harsh Environment III, 83680E, pages-83680E-83680E-7, 2012.

5. Valentin Ortega Clavero, Andreas Weber, Werner Schröder, Patrick Meyrueis, and Nicolas Javahiraly. *Detailed spectral monitoring of different bio-fuels using FT-Raman spectroscopy.* 3rd International Conference on Environmental Best Practices (EBP3), 2011.

6. Valentin Ortega Clavero, Werner Schröder, Patrick Meyrueis, and Andreas Weber. *Robust, precise, high resolution fourier transform Raman spectrometer.* Proc. SPIE 8065, SPIE Eco-Photonics 2011: Sustainable Design, Manufacturing, and Engineering Workforce Education for a Green Future, 806510, 8065(1):806510, 2011.

Miscellaneous

1. Valentin Ortega Clavero, Werner Schröder. *Entwicklung eines FT-Raman - Spektrometers.* Beiträge aus Forschung und Technik 2014. Institut für Angewandte Forschung. Hochschule Offenburg. ISSN 1866-9352

2. Valentin Ortega Clavero. *Método para el monitoreo de procesos utilizando espectroscopía FT-Raman de bajo costo.* II Simposio de becarios y ex-becarios del CONACyT. November 6-8 2013. European Parliament. Strasbourg, France.

3. Valentin Ortega Clavero, Werner Schröder. *Weiterentwicklung des Raman-Spektrometers* Campus - Das Magazin der Hochschule Offenburg, Ausgabe Nr. 30/ Winter 2010/2011.

Appendix A. Calculation of the expected Raman scattering light

For the proper evaluation of the amount of scattering light available at the detector, we have to take into account several factors: intensity of the exciting source, Raman cross section of the materials, density of the material under observation, geometry of the collecting optics, efficiency of the detector, etc. This has allowed determining the characteristics required of the photon detector. According to the information reported by McCreery [109, 110], the generated and the detected amount of Raman scattering light can be calculated using eq. A.1 and eq. A.2:

$$L = P_D \beta D_S(dz) \tag{A.1}$$

$$C = A_D \Omega_D T Q \tag{A.2}$$

$$Signal = LCt_s \tag{A.3}$$

L (in photons $\mathrm{sr}^{-1}\,\mathrm{cm}^{-2}\,\mathrm{s}^{-1}$) in eq. A.1 represents the amount of generated photons per seconds in a surface of $1.0\,\mathrm{cm}^2$ with a theoretical collection over 1 stereoradian of solid angle. P_D is the amount of photons per second per square centimeter of the excitation source, β is the cross section of the material under observation and D_S is the molecular density of the sample.

C (in $\mathrm{cm}^2\,\mathrm{sr\,e\,photon}^{-1}$) represents the collection function. This parameter defines the amount electrons per collected photon per stereoradians in $1.0\,\mathrm{cm}^2$, that are available for spectral evaluation. A_D is the area of the sample observed by the instrument, Ω_D is the solid angle of the optical arrangement, T and Q represent the transmission of the instrument and the quantum efficiency of the photon detector respectively.

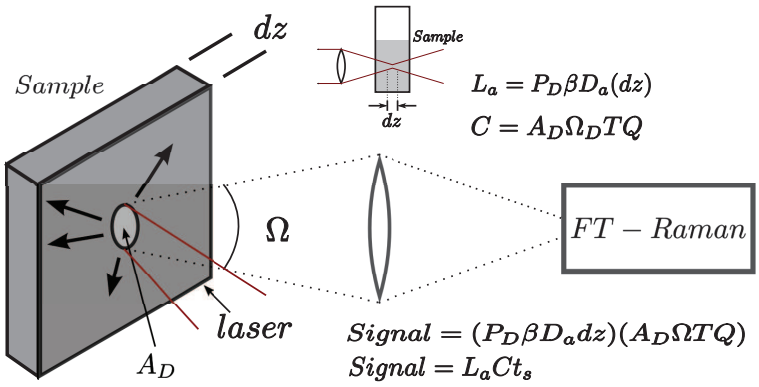

Figure A.1: Diagram of the variables involved in the generation and detection of Raman scattering light in a 180° back-scattering geometry. Figure reproduced from [109, p. 36].

We have estimated the amount of Raman scattering that a single photon avalanche diode (SPAD) would detect if we place a sample of pure cyclohexane (C_6H_{12}) in front of a microscope objective 20x. As excitation light source, we have used a helium-neon laser (HeNe laser, λ =632.8 nm, P =10 mW, ø=1.0 mm).

The smallest area observed (A_D=3.8112 × 10^{-7} cm^2) at the sample has been calculated using the beam waist of the HeNe laser passing through the 20x microscope objective (focal length f=8.2 mm). The 10 mW on this calculated area are equivalent (see eq. A.4 and A.5) to a power density P_D=3.1830 × 10^{16} photons/s/cm^2 [41, p. 319].

$$E_{photon} = h\upsilon = \frac{hc}{\lambda} = \frac{6.626 \times 10^{-34}\text{Js} \times 3 \times 10^{8}\text{m/s}}{632.8 \times 10^{-9}\,\text{m}} = 3.1413 \times 10^{-19}\,\text{J} \qquad \text{(A.4)}$$

$$\text{photons / dt} = \frac{10\,\text{mW}}{3.1413 \times 10^{-19}\,\text{J}} = 3.1834 \times 10^{16}\ \text{photons/s} \qquad \text{(A.5)}$$

The molecular density D_S of cyclohexane can be directly extracted from its density (0.779 g/mL), its molar mass (84.16 g/mol) and the Avogadro's constant (6.022 × 10^{23}/mol).

$$D_S = 0.779\,\text{g}\frac{1\,\text{mol}}{84.16\,\text{g}}6.022 \times 10^{23}/\text{mol} \simeq 5.57 \times 10^{21}\,\text{molecules/cm}^3$$

The Raman cross section reported by McCreery for the Raman line of cyclohexane at 802 cm^{-1}, is given for excitation sources of different wavelengths. The closest value to

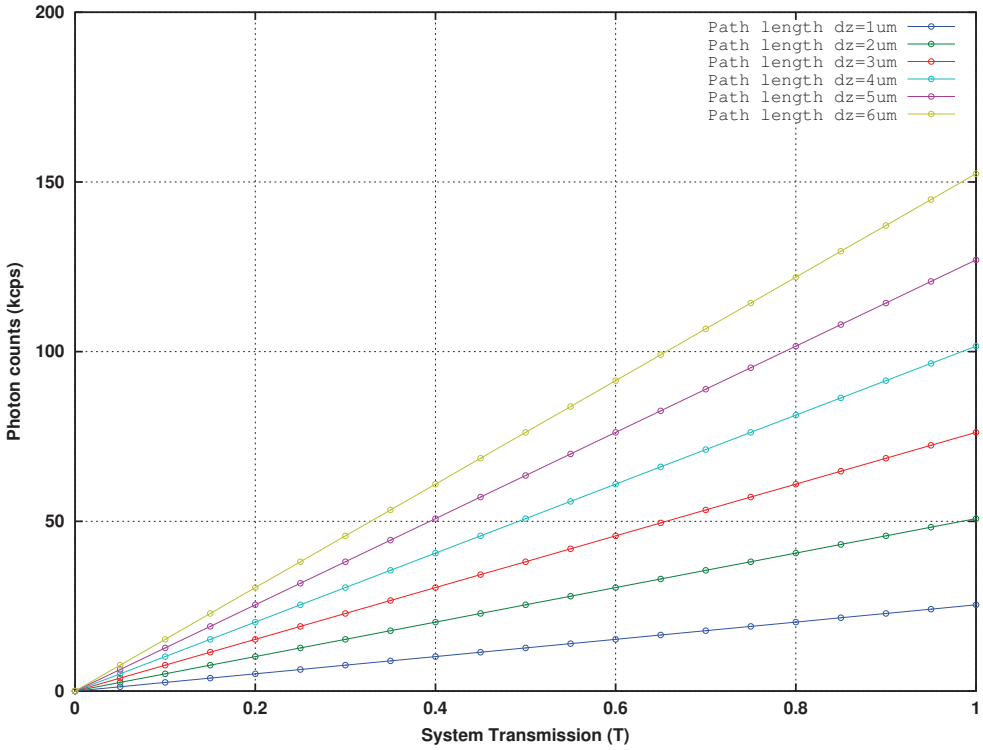

Figure A.2: Expected photon counting rate under different transmission values T of the FT-Raman system and assuming different values of path lenght dz in the observed sample of cyclohexane. A quantum efficiency of 0.70 for the APD has been considered.

the HeNe laser (at λ=632.8 nm) is 647 nm and it corresponds to a Raman cross section of $\beta(\mathrm{cm}^2\,\mathrm{sr}^{-1}\,\mathrm{molecule}^{-1})=2.1\times10^{-30}$. The value of the Raman cross section increases as the wavelength of the excitation source decreases [109, p. 29], so we have considered an approximated value of Raman cross section β=2.43. This value has been obtained by applying interpolation to the four values of β suggested for the Raman line of cyclohexane at 802 cm^{-1}.

The value of dz depends on the actual adjustment of the optics used to excite the sample and collect the Raman back-scattered light. For practical reasons we have taken the value of the depth of field (DOF) of the 20x microscope objective. This variable describe the distance range where the object being observed appears sharp, and hence can be portrayed at the spectrometer entrance or at the collecting waveguide. For the common 20x microscope objectives this value is the range of 1.0 μm to 5.8 μm depending on the conditions of the arrangement.

Combining the four variables ($P_D \beta D_S dz$) the amount of Raman scattering light L produced at the sample of cyclohexane, depending on the observed depth (dz), would be in the range from 1.13×10^{11} photons $\mathrm{sr}^{-1}\,\mathrm{cm}^{-2}$ /s, with the smallest observed depth, to 6.78×10^{11} photons $\mathrm{sr}^{-1}\,\mathrm{cm}^{-2}$ /s.

With the observed area A_D=$3.8112 \times 10^{-7}\,\mathrm{cm}^2$, a solid angle $\Omega_D \simeq 0.84$ (calculated for the 20x microscope objective) and assuming a quantum efficiency $Q = 0.70$ we have generated cuerves with the expected amount of photons per second for different transmission conditions of the system and for different values of dz. Under the less favorable conditions (worst transmission and the shortest path length), we would be able to detect only around 1 kcps to 5 kcps. The optimal scenario, at higher levels of system transmission and longer path lengths in the sample, the counting rate could exceed 150 kcps.

Appendix B. Technical description of the hardware components

In chapter 4 the implementation of the FT-Raman system has been described. However, this description has only included the key points about the composition of the FT-Raman spectrometer that we have developed.

As already explained through chapter 4, the implementation of our FT-Raman spectrometer prototype has been carried out by combining mostly conventional and inexpensive hardware parts. In this appendix we have included additional information about the parts conforming the FT-Raman prototype. All the parts of the FT-Raman spectrometer prototype are on an undamped 80 cm x 120 cm table for optical experiments. Figure B.1 shows an image that has been taken from the top view of the FT-spectrometer prototype. The next sections are dedicated to describe with more detail the main parts of our FT-Raman device.

B.1 Michelson interferometer

The core of our system is a Michelson interferometer (located in the middle of the experiments table in figure B.1). This interferometer has been built by combining a self-designed massive aluminum case and an M-413[1] linear translation stage from Physik Instrumente. The translation stage has a gearing system with a conversion rate of 54.6. The DC-motor that drives the translation stage has a quadrature encoder that generates 400 pulses per turn, and every turn of the shaft generates 0.5 mm of linear shift. These device allows linear translation having a theoretical mechanical resolution of about 23 nm. Figure B.2 shows the diagram and its dimensions, and the catalog image of a linear stage similar to the one used in the implementation of our FT-Raman prototype. We consider that this hardware parts consist of the most sophisticated component present in our Raman system, although this model of linear stage is at least 15 years old.

[1] Predecessor version of the actual model available by PI (Physik Instrumente).

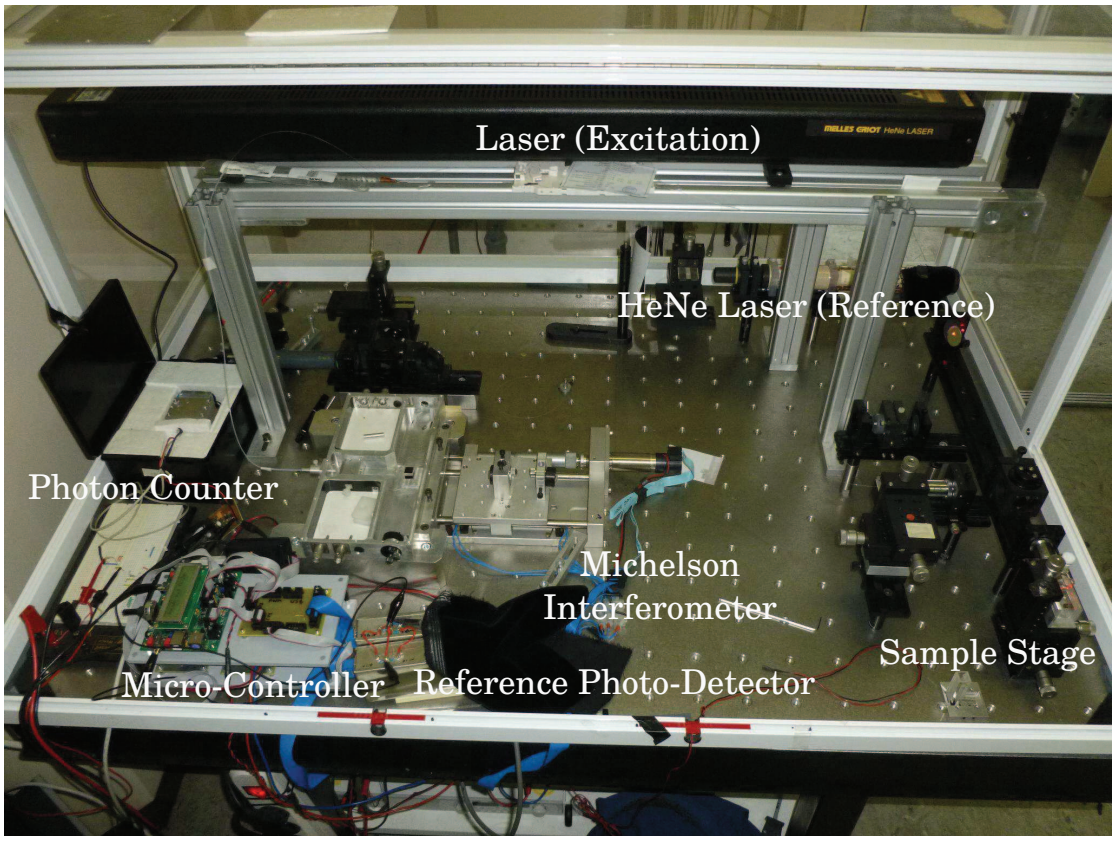

Figure B.1: Overview of the FT-Raman prototype.

The entrance pupil (plan-convex lens, $f = 8.0\,\text{mm}$) of the Michelson interferometer is illuminated by a multi-mode optical fiber, which transport the back-scattered Raman light from the analyzed sample and the HeNe laser light used for generating the reference signal. The aluminum case holds the fixed mirror M_1 on a XY tilting insert and the 50/50 beam-splitter cube. The scanning mirror M_2 is mounted on top of the linear translation stage. Figure B.3 shows the distribution of the main parts conforming the Michelson interferometer.

The modulated light coming out of the Michelson interferometer (upper part of the aluminum case) is transmitted to the photon counting device and to the reference photo-detector by mirror-bending the output beams 45°. The output light is then divided by using a 75/25 beam-splitter cube. This can be better seen in figure 4.1 at the initial part of chapter 4. The two corresponding beams are focused into multi-mode fibers by using conventional 20X microscope objectives. The mechanical support of the optical parts has

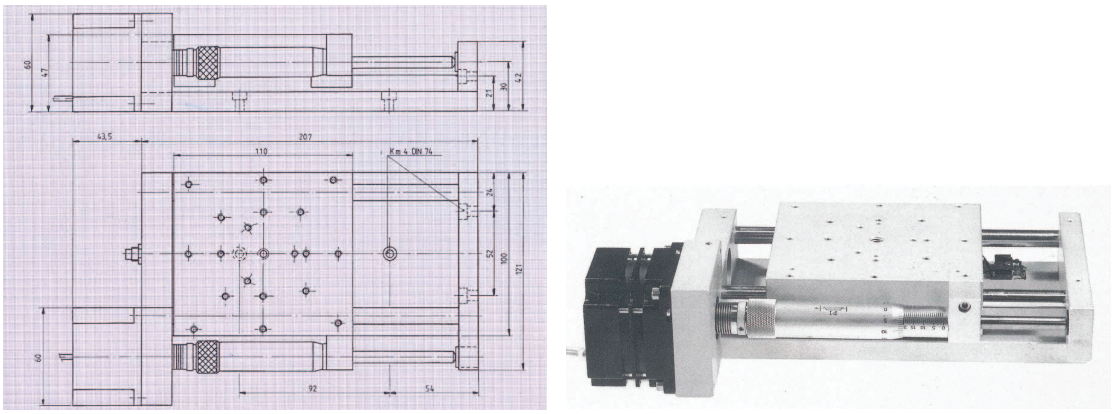

(a) (b)

Figure B.2: Diagram and picture of the translation stage used in the development of the Michelson interferometer.

been accomplished by using holders (Sys 40) and adjusting unis from OWIS and Qioptiq[1].

B.2 Photon counting unit

The photon counting unit (on the center left part of figure B.1) that we use for the detection of Raman scattering light, has been developed by combining a Si C30921SH avalanche photo-diode (APD) from Excelitas Technologies [48][2], and a cooling stage. This type of APD is intended for ultra-low light levels applications (such detection of Raman scattering light). The C30921SH APD has a light pipe, in which a multi-mode fiber has

[1]Previously known as Linos Photonics

[2]Former product of the company PerkinElmer

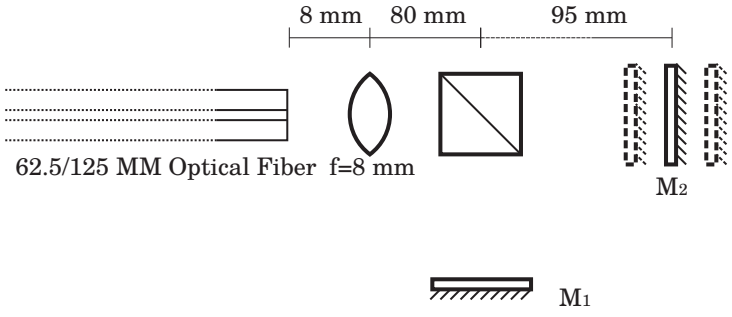

Figure B.3: Representative diagram of the main parts used in the Michelson interferometer and their internal arrangement.

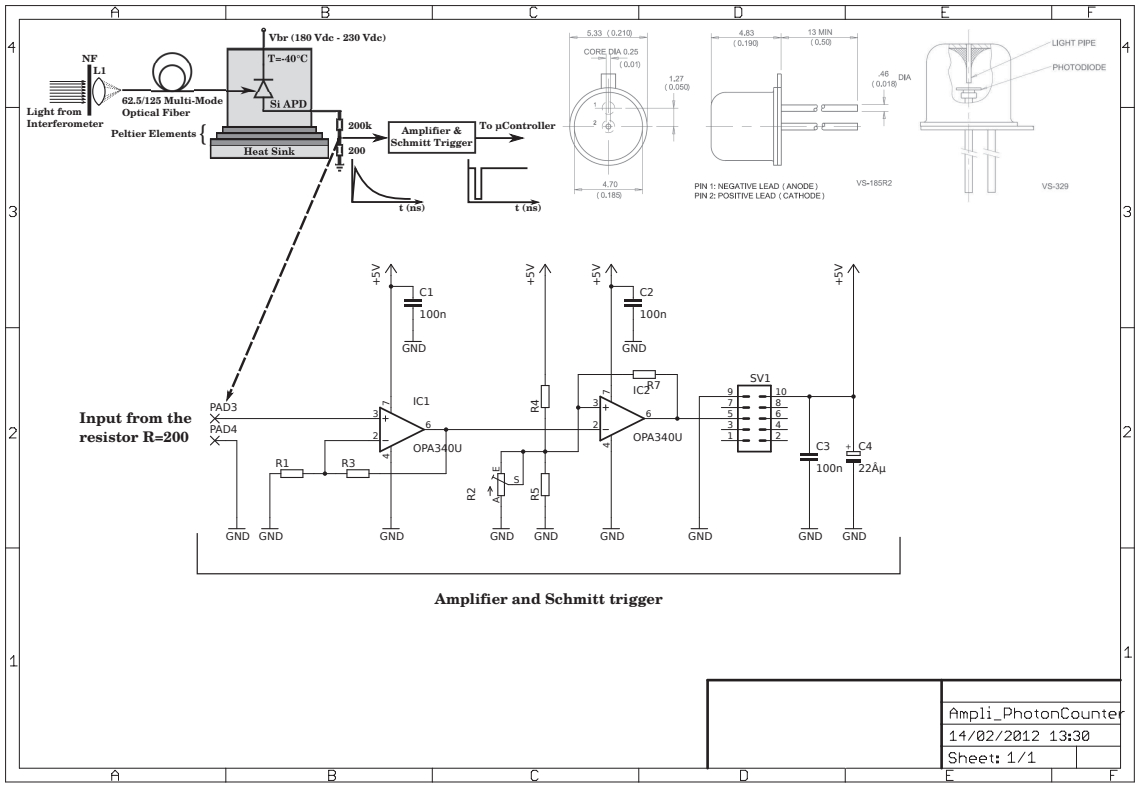

Figure B.4: Circuitry and schematic of the photon counting unit used in the FT-Raman spectrometer. Upper right: dimmension and package outline of the Si C30921SH APD. This package ouline and the corresponding data are courtesy of Excelitas Technologies.

been epoxied in order to direct the light coming out from the Michelson interferometer into the Si detecting surface.

The APD is mounted on the top part of a three-stage of Peltier elements that allow the cooling effect necessary to reduce the dark counting rate generated. The heat generated by the hot face of the Peltier arrangement has been extracted by using a 40 mm x 40 mm water heat-sink. An aluminum case contains the APD and the heat-sink, as well as some of the circuitry of the photon counter unit. The inner free space has been filled up by using thermal isolating foam. This configuration allows the operation of the photon counting unit in under a temperature range between $-35\,^{\circ}\mathrm{C}$ to $-40\,^{\circ}\mathrm{C}$.

Figure B.4 depicts the basic circuitry for the amplification and conditioning of the signal obtained from the APD in our photon counting unit. The signal output from our passive quenching circuit is amplified and conditioned (Schmitt trigger) to a micro-

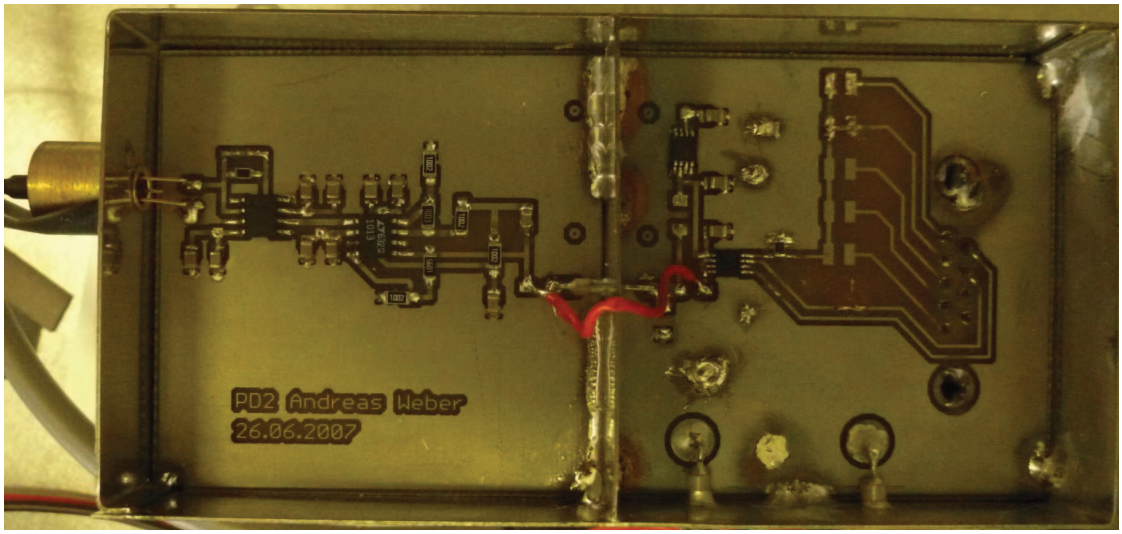

Figure B.5: Top view of the circuitry of the reference photo-detector. The input stage of the circuit consist of a low-noise amplifier and filtering parts, while the second stage perform the analog-to-digital conversion and the serial transmission to the micro-controller.

controller-compatible level of 5.0 V. The output signal of the photon counting unit is connected to an 8-bit counter register of the ATmega32 micro-controller, which is read during the main interrupt service routine (ISR) every 1/16 ms and transmitted every ms.

B.3 Reference photo-detector

The basic composition and functionality of the reference photo-detector has been described and depicted in section 4.1.3. Since the amount HeNe laser power level used to generate the reference signal of our measurements, the printed circuit board of this photo-detector is encapsulated inside a case of thin sheet metal in order to avoid external spurious electromagnetic radiations.

Figure B.5 shows an image from the top view of the reference photo-detector without the case cover. The digital signals obtained are transmitted to the micro-controller through the serial peripheral interface bus (SPI), which is connected to a 9-pin D-sub adapter.

The first part of the reference photo-detector consists of a trans-impedance amplifier (Hamamatsu Si photo-diode as an input with an adapter for the multi-mode optical fiber), a filtering stage, and voltage references.

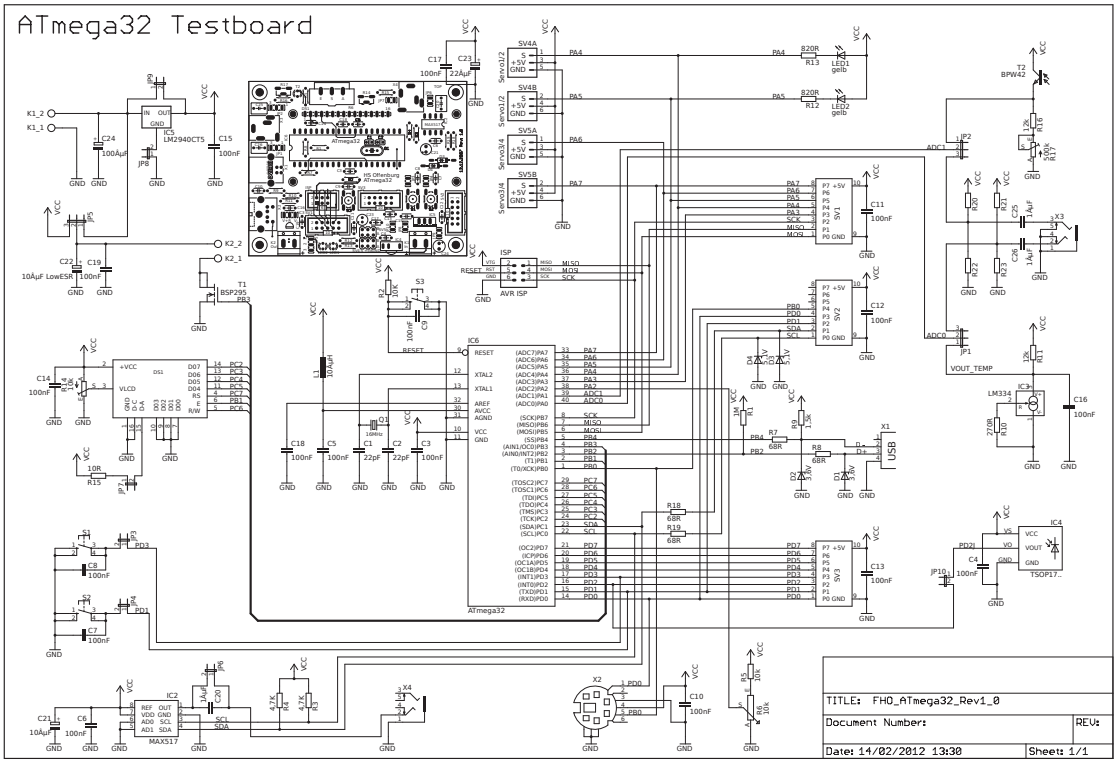

Figure B.6: Schematic and corresponding printed circuit board of the MK Board used to coordinate the different components of the FT-Raman spectrometer. Courtesy of A. Weber, R. Lehmann and S. Steiger from the University of Applied Science Offenburg (Hochschule Offenburg / Faculty E+I / IUAS).

The second part of the circuit consists of the analog-to-digital conversion circuitry and the serial transmission stage (SPI). The serial interface of this last part of the reference photo-detector is called by the micro-controller during the scanning processes (e.g. commands in lines 17 and 18 of the source code snippet shown in figure B.8))

B.4 Micro-controller and H-Bridge

The micro-controller ATmega32 embedded on the evaluation "MK Board" (bottom left in figure B.1) coordinates the low-level functionality of the FT-Raman system. This evaluation board has been designed for general applications purposes in the department of Electrical Engineering and Information Technology (E+I) of the University of Applied Sciences Offenburg (Hochschule Offenburg).

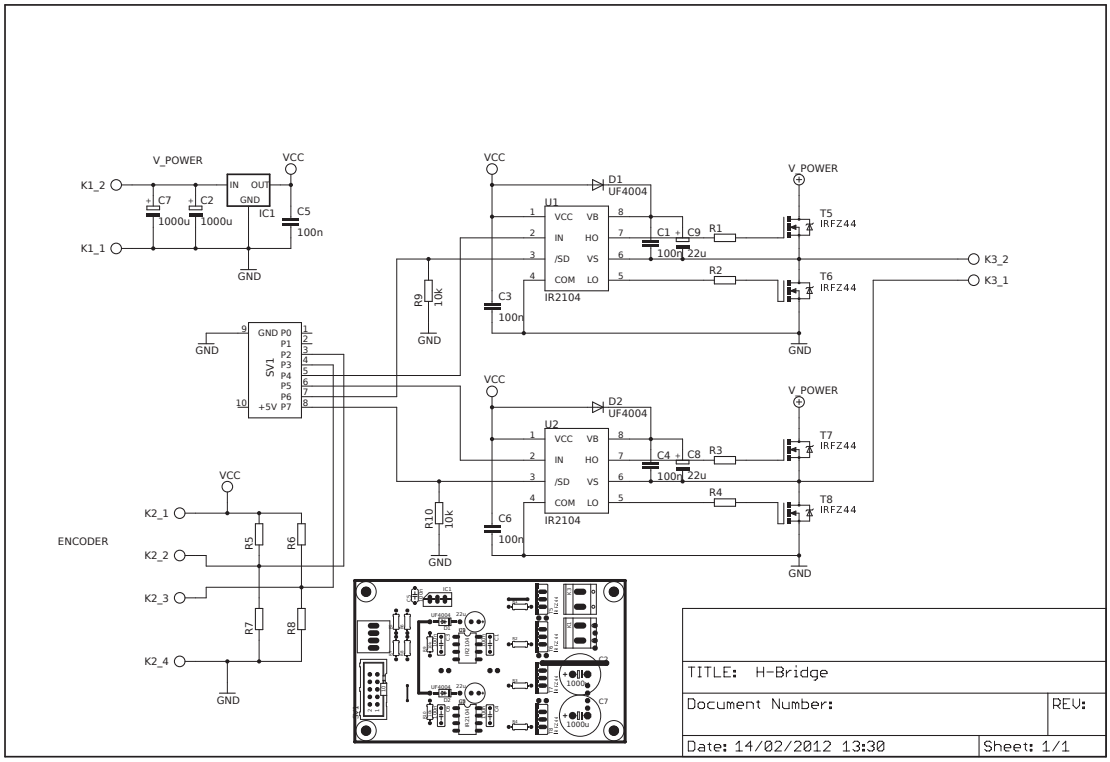

Figure B.7: Schematic and corresponding printed circuit board of the H-Bridge used to drive the DC-Motor connected to the translation stage of the Michelson interferometer.

This evaluation board consist of a printed circuit board (PCB) having dimensions of 100 mm x 80 mm, and around 100 electrical components distributed on its two layers. Most of the components have through-hole terminals, which make this evaluation board suitable for rapid-prototyping and heavy duty. This also permits to perform rapid changes in case of modifications or repairments by only using basic equipments.

The "MK Board" has been adapted to the requirements of our FT-Raman spectrometer. By using this device, we have been able to ensure that during the scanning processes, the samples obtained are strictly time-equally distributed. The routines programmed in the micro-controller also provide communication capabilities with the graphical user interface, and generate a monotonically increasing movement of the scanning mirror M_2 of the Michelson interferometer.

Figure B.6 shows the schematic of this evaluation board and the top-view of the resulting printed circuit board. Figure B.8 shows a source code listing that is programmed to the ATmega32 micro-controller. This code is the initial part of the main interrupt service

```
1  ...
2  ISR(TIMER2_COMP_vect) { //16kHz interrupt
3      static uint8_t speed_divider=0,ISR_Divider_Counter=0;
4      new_quadrature_value=(PINA >> 6) & 0x03;
5      position+=position_table[old_quadrature_value][new_quadrature_value];
6      old_quadrature_value=new_quadrature_value;
7
8      photonold = photon;
9      photon = TCNT0;
10     deltaphoton = ( photon - photonold ) & 0xFF;
11     total_photons += deltaphoton;
12
13     //ISR divider counts 16 times (0 - 15)
14     //to divide the main ISR freq ( freq = 1KHz)
15     if (ISR_Divider_Counter++ >= 15) {
16         if ( streaming_mode==1 && bit_is_clear(PIND,PD3) ) {
17         PORTA &= ~_BV(PA3);     //Chip Select down(chip enable)
18         uart_put_int16(getSPISample());
19         //Reference 1
20
21         PORTA &= ~_BV(PA5);     //Chip Select down(chip enable)
22         uart_put_int16(getSPISample());
23         //Reference 2
24
25         uart_put_int16( (uint16_t)total_photons );
26         //Photon Counter
27
28         uart_put_int16( position );
29         uart_put_int16( position >> 16 );
30         //Position (Motor encoder)
31
32         uart_put_int16( status );
33         total_photons = 0;
34         }
35         ISR_Divider_Counter = 0;
36     }...
```

Figure B.8: Snippet of the interrupt service routine (ISR) that controls the scanning processes of the FT-Raman spectrometer. This piece of C source code performs the time-equally distributed sampling of the photon counting unit and the reference signal within a few μs every ms.

routine (ISR) used to drive the scanning processes during the Raman measurements.

Figure B.7 shows the electrical schematic and the resulting PCB of the H-Bridge. This H-Bridge is used to electrically drive in both directions the DC-Motor of the linear translation table of the Michelson interferometer. The H-Bridge receives the PWM signals from the micro-controller (as a result of the evaluation in the PID control loop).

The PWM signal transmitted to the H-bridge, is generated by using the so called "16-bit Timer/Counter 1" of the micro-controller. This module is able to deliver a phase corrected PWM signals (10-bit resolution). This permits the constant, precise and monotonically positioning of the scanning mirror meeting the required mechanical resolution of the linear translation table.

The main parts of the H-Bridge are two IR2104 half-Bridge drivers, and four IRFZ44 advanced HEXFET power MOSFETs ($V_{DSS} = 55\,\mathrm{V}$, $I_D = 49\,\mathrm{A}$). These components are

manufactured by International Rectifier. Additionally, the H-Bridge circuit also have some fast recovery diodes and capacitors that are used as charging pump for the components from International Rectifier.

The parts included in the circuitry allows the H-Bridge to drive elements having current requirements of some mA up to 49 A, as in the case of larger DC-Motors or arrangements of Peltier elements (as in the case of the all-fiber Mach-Zehnder interferometer).

References

[1] A comparative study of diesel analysis by ftir, {FTNIR} and ft-raman spectroscopy using {PLS} and artificial neural network analysis.

[2] Agilent Technologies, Inc. . Validation of Analytical Methods. `http://www.chem.agilent.com/Library/primers/Public/5990-5140EN.pdf`, February 2010. Accessed: January 2014.

[3] S.N. Ahmed. *Physics and Engineering of Radiation Detection*. Elsevier Science, 2007. ISBN 9780080569642.

[4] J.R. Albani. *Principles and Applications of Fluorescence Spectroscopy*. Wiley, 2008. ISBN 9780470691335.

[5] Vincenzo Amendola and Moreno Meneghetti. Controlled size manipulation of free gold nanoparticles by laser irradiation and their facile bioconjugation. *J. Mater. Chem.*, 17:4705–4710, 2007. doi: 10.1039/B709621F.

[6] Vincenzo Amendola and Moreno Meneghetti. Size Evaluation of Gold Nanoparticles by UV-VIS Spectroscopy. *The Journal of Physical Chemistry C*, 113(11):4277–4285, 2009. doi: 10.1021/jp8082425.

[7] American Society for Testing and Materials (ASTM). Standard Guide for Raman Shift Standards for Spectrometer Calibration (ASTM E1840). `http://www.astm.org/Standards/E1840.htm`, 2007. Accessed: September 2013.

[8] J.E. Anderson, D.M. DiCicco, J.M. Ginder, U. Kramer, T.G. Leone, H.E. Raney-Pablo, and T.J. Wallington. High octane number ethanol-gasoline blends: Quantifying the potential benefits in the United States. *Fuel*, 97(0):585 – 594, 2012.

[9] Rosaleen J Anderson, David J Bendell, and Paul W Groundwater. *Organic Spectroscopic Analysis*. Tutorial Chemistry Texts. The Royal Society of Chemistry, 2004. ISBN 978-0-85404-476-4.

[10] Atmel Corporation. ATmega32. `http://www.atmel.com/devices/atmega32.aspx`, Updated: February 2011. Accessed: January 2014.

[11] W Baeyens, T Vankeirsbilck, A Vercauteren, G Van der Weken, F Verpoort, G Vergote, and J.P Remon. Applications of Raman spectroscopy in pharmaceutical analysis. *TrAC Trends in Analytical Chemistry*, 21(12):869 – 877, 2002.

[12] W.R.G. Baeyens, T.R.M. De Beer, Y. Vander Heyden, J.P. Remon, C. Vervaet, and F. Verpoort. Influence of particle size on the quantitative determination of salicylic acid in a pharmaceutical ointment using FT-Raman spectroscopy. *European Journal of Pharmaceutical Sciences*, 30(3-4):229 – 235, 2007.

[13] W.R.G. Baeyens, T.R.M. De Beer, A. Vermeire, D. Broes, J.P. Remon, and C. Vervaet. Raman spectroscopic method for the determination of medroxyprogesterone acetate in a pharmaceutical suspension: validation of quantifying abilities, uncertainty assessment and comparison with the high performance liquid chromatography reference method. *Analytica Chimica Acta*, 589(2):192 – 199, 2007.

[14] Roman M. Balabin, Ravilya Z. Safieva, and Ekaterina I. Lomakina. Gasoline classification using near infrared (nir) spectroscopy data: Comparison of multivariate techniques. *Analytica Chimica Acta*, 671(1-2):27 – 35, 2010.

[15] Gertie C.A.M. Bokken, Ronald J. Corbee, Frans van Knapen, and Aldert A. Bergwerff. Immunochemical detection of salmonella group b, d and e using an optical surface plasmon resonance biosensor. *FEMS Microbiology Letters*, 222(1):75 – 82, 2003.

[16] Bryan T. Bowie, D. Bruce Chase, and Peter R. Griffiths. Factors Affecting the Performance of Bench-Top Raman Spectrometers. Part I: Instrumental Effects. *Appl. Spectrosc.*, 54(5):164A–173A, May 2000.

[17] Bryan T. Bowie, D. Bruce Chase, and Peter R. Griffiths. Factors affecting the Performance of Bench-Top Raman Spectrometers. Part II: Effect of Sample. *Appl. Spectrosc.*, 54(6):200A–207A, Jun 2000.

[18] Bryan T. Bowie, D. Bruce Chase, Ian R. Lewis, and Peter R. Griffiths. *Anomalies and Artifacts in Raman Spectroscopy in Handbook of Vibrational Spectroscopy*, chapter 3. John Wiley & Sons, Ltd, 2006. ISBN 9780470027325.

[19] L. Brand and M.L. Johnson. *Fluorescence Spectroscopy*. Methods in enzymology. Elsevier Science, 2011. ISBN 9780080923345.

[20] Charles T. Campbell and Gibum Kim. SPR microscopy and its applications to high-throughput analyses of biomolecular binding events and their kinetics. *Biomaterials*, 28(15):2380 – 2392, 2007.

[21] B. Carter and R. Mancini. *Op Amps for Everyone*. Elsevier Science, 2009. ISBN 9780080949482.

[22] J.K. Casper. *Fossil Fuels and Pollution: The Future of Air Quality*. Global warming. Facts On File, Incorporated, 2010. ISBN 9781438127415.

[23] Castrol Industrial. Castrol Hyspin HVI - Product Data. `http://www.castrol.com/liveassets/bp_internet/castrol/castrol_switzerland/STAGING/local_assets/downloads/h/Castrol_Hyspin_HVI_DE_2011_06.pdf`, May 2011. Accessed: March 2014.

[24] Silvia Guillermina Ceballos-Magaña, José Marcos Jurado, María Jesús Martín, and Fernando Pablos. Quantitation of twelve metals in tequila and mezcal spirits as authenticity parameters. *Journal of Agricultural and Food Chemistry*, 57(4):1372–1376, 2009. doi: 10.1021/jf803626k.

[25] Sharon Lai-Fung Chan, Yu-He Kan, Ka-Lai Yip, Jie-Sheng Huang, and Chi-Ming Che. Ruthenium complexes of 1,4,7-trimethyl-1,4,7-triazacyclononane for atom and group transfer reactions. *Coordination Chemistry Reviews*, 255(7-8):899–919, 2011. ISSN 0010-8545.

[26] L. Chaparro. *Signals and Systems using MATLAB*. Elsevier Science, 2010. ISBN 9780080879338.

[27] Chi-Ming Che and Tai-Chu Lau. Ruthenium and osmium: High oxidation states. In J. A. McCleverty and T. J. Meyer, editors, *Comprehensive Coordination Chemistry II*, pages 733 – 847. Pergamon, Oxford, 2003. ISBN 978-0-08-043748-4.

[28] Chi-Ming Che, Chi-Ming Ho, and Jie-Sheng Huang. Metal-carbon multiple bonded complexes: Carbene, vinylidene and allenylidene complexes of ruthenium and osmium supported by macrocyclic ligands. *Coordination Chemistry Reviews*, 251(17-20):2145 – 2166, 2007. ISSN 0010-8545.

[29] Steven J. Choquette, Stephen N. Chesler, David L. Duewer, Shuwen Wang, and Thomas C. O'Haver. Identification and Quantitation of Oxygenates in Gasoline Ampules Using Fourier Transform Near-Infrared and Fourier Transform Raman Spectroscopy. *Analytical Chemistry*, 68(20):3525–3533, 1996.

[30] Steven J. Choquette, Stephen N. Chesler, David L. Duewer, Shuwen Wang, and Thomas C. O'Haver. Identification and Quantitation of Oxygenates in Gasoline Ampules Using Fourier Transform Near-Infrared and Fourier Transform Raman Spectroscopy. *Analytical Chemistry*, 68(20):3525–3533, 1996.

[31] Mustafa H. Chowdhury, Krishanu Ray, Chris D. Geddes, and Joseph R. Lakowicz. Use of silver nanoparticles to enhance surface plasmon-coupled emission (SPCE). *Chemical Physics Letters*, 452 (1-3):162 – 167, 2008. ISSN 0009-2614. doi: 10.1016/j.cplett.2007.12.047.

[32] John M. Coffin. Interferometer of an infrared spectrometer with dynamic moving mirror alignment / US patent 5,883,712, March 1999. Accessed: October 2013.

[33] Ulises Contreras, O. Barbosa-García, J.L. Pichardo-Molina, G. Ramos-Ortíz, J.L. Maldonado, M.A. Meneses-Nava, N.E. Ornelas-Soto, and P.L. López de Alba. Screening method for identification of adulterate and fake tequilas by using UV-VIS spectroscopy and chemometrics. *Food Research International*, 43(10):2356 – 2362, 2010. ISSN 0963-9969.

[34] John B. Cooper, Philip E. Flecher, Thomas M. Vess, and William T. Welch. Remote fiber optic Raman analysis of benzene, toulene, and ethylbenzene in mock petroleum fuels using partial least squares regression analysis. *Spectrochimica Acta Part A: Molecular and Biomolecular Spectroscopy*, 52(10):1235 – 1244, 1996.

[35] John B. Cooper, Philip E. Flecher, William T. Welch, and Sacharia Albin. Determination of octane numbers and Reid vapor pressure in commercial gasoline using dispersive fiber-optic Raman spectroscopy. *Spectrochimica Acta Part A: Molecular and Biomolecular Spectroscopy*, 53(2):199 – 206, 1997.

[36] Bruker Corporation. 2012 Annual Report, April 2013. URL `http://www.sec.gov/Archives/edgar/data/1109354/000104746913001958/a2213258z10-k.htm`. Document of the U.S. Securities and Exchange Commission (SEC). Accessed: February 2014.

[37] Bruker Corporation. 2012 Annual Report, April 2013. URL `http://ir.bruker.com/phoenix.zhtml?c=121496&p=irol-IRHome`. Accessed: February 2014.

[38] Ruchita S. Das and Y.K. Agrawal. Raman spectroscopy: Recent advancements, techniques and applications. *Vibrational Spectroscopy*, 57(2):163 – 176, 2011.

[39] M. de la Guardia and S. Garrigues. *Handbook of Green Analytical Chemistry*. Wiley, 2012. ISBN 9780470972014.

[40] Antonio De León-Rodríguez, Pilar Escalante-Minakata, María I. Jiménez-García, Leandro G. Ordonez-Acevedo, José L. Flores Flores, and Ana P. Barba de la Rosa. Characterization of volatile compounds from ethnic agave alcoholic beverages by gas chromatography-mass spectrometry. *Food Technol. Biotechnol*, 46:448–455, 2008.

[41] B. Dörband, H. Gross, and H. Müller. *Handbook of Optical Systems, Metrology of Optical Components and Systems*. Wiley, 2012. ISBN 9783527403813.

[42] John W. Eaton, David Bateman, and Søren Hauberg. *GNU Octave Manual Version 3*. Network Theory Limited, 2008. ISBN 0-9546120-6-X.

[43] David I. Ellis, Victoria L. Brewster, Warwick B. Dunn, J. William Allwood, Alexander P. Golovanov, and Royston Goodacre. Fingerprinting food: current technologies for the detection of food adulteration and contamination. *Chem. Soc. Rev.*, 41:5706–5727, 2012.

[44] Environment Agency. Soil Guideline Values for toluene in soil - Science Report SC050021 / toluene SGV, March 2009. URL `http://www.environment-agency.gov.uk/research/planning/64015.aspx`. Accessed: September 2013.

[45] S.K. Eswaramoorthy, Y. Wang, L.J. Sherry, J.A. Dieringer, J.P. Camden, G.C. Schatz, R.P. Van Duyne, and L.D. Marks. A method to correlate optical properties and structures of metallic nanoparticles. *Ultramicroscopy*, 109(9):1110 – 1113, 2009.

[46] European Chemicals Agency (ECHA). Risk Assessment Report CAS No: 71-43-2 EINECS No: 200-753-7 benzene, 2008. URL `http://echa.europa.eu/documents/10162/be2a96a7-40f6-40d7-81e5-b8c3f948efc2`. Accessed: January 2014.

[47] European Commission. Risk Assessment Report CAS No: 108-88-3 EINECS No: 203-625-9 toluene, 2002. URL `http://esis.jrc.ec.europa.eu/`. Joint Research Center - Institute for Health and Consumer Protection, Accessed: September 2013.

[48] Excelitas Technologies Corp. Silicon Avalanche Photodiodes C30902 Series - Datasheet, September 2011. URL `http://www.excelitas.com/downloads/DTS_C30902.pdf`. Accessed: December 2013.

[49] Z. Fang, K. Chin, R. Qu, H. Cai, and K. Chang. *Fundamentals of Optical Fiber Sensors*. Wiley Series in Microwave and Optical Engineering. Wiley, 2012. ISBN 9781118381755.

[50] John R. Ferraro, Kazuo Nakamoto, and Chris W. Brown. *Introductory Raman Spectroscopy*. Elsevier, second edition, 2003.

[51] Jose-Axel Flores, Anne Gschaedler, Lorena Amaya-Delgado, Enrique J. Herrera-López, Melchor Arellano, and Javier Arrizon. Simultaneous saccharification and fermentation of agave tequilana fructans by kluyveromyces marxianus yeasts for bioethanol and tequila production. *Bioresource Technology*, 146(0):267 – 273, 2013. ISSN 0960-8524.

[52] R. Foley. *Tequila 1000*. Bartender Magazine. Sourcebooks, Incorporated, 2008. ISBN 9781402247965.

[53] C. Frausto-Reyes, C. Medina-Gutiérrez, R. Sato-Berrú, and L.R. Sahagún. Qualitative study of ethanol content in tequilas by Raman spectroscopy and principal component analysis. *Spectrochimica Acta Part A: Molecular and Biomolecular Spectroscopy*, 61(11-12):2657 – 2662, 2005.

[54] Yi Fu, Jian Zhang, and Joseph R. Lakowicz. Metal-enhanced fluorescence of single green fluorescent protein (GFP). *Biochemical and Biophysical Research Communications*, 376(4):712 – 717, 2008. ISSN 0006-291X. doi: 10.1016/j.bbrc.2008.09.062.

[55] Alfonso A. Gardea, Lloyd T. Findley, J. Antonio Orozco-Avitia, and Noemí Banuelos. Bacanora and sotol: So far, so close. *Estudios Sociales - Revista de Investigación Científica*, 20(2):149 – 168, 2012.

[56] J.M Garrigues, A Pérez-Ponce, S Garrigues, and M de la Guardia. Direct determination of ethanol and methanol in liquid samples by means of vapor phase-Fourier transform infrared spectroscopy . *Vibrational Spectroscopy*, 15(2):219 – 228, 1997. ISSN 0924-2031.

[57] Salvador Garrigues and Miguel de la Guardia. Non-invasive analysis of solid samples. *TrAC Trends in Analytical Chemistry*, 43(0):161–173, 2013. ISSN 0165-9936.

[58] S.G. Gilbert. *A Small Dose of Toxicology: The Health Effects of Common Chemicals*. Taylor & Francis, 2004. ISBN 9780203461730.

[59] Bruker Optik GmbH. MultiRAM FT-Raman Spectrometer - Specifications, 2013. URL `http://www.bruker.com/fileadmin/user_upload/8-PDF-Docs/OpticalSpectrospcopy/Raman/MultiRAM/Flyers/MultiRAM_Flyer_EN.pdf`. Accessed: January 2014.

[60] Gobierno del Estado de Sonora. Ley de fomento para la producción, industrialización y comercialización del bacanora del Estado de Sonora. b.o. no. 46 secc. iii, 12 2008.

[61] Ana Gonzalvez, Salvador Garrigues, Miguel de la Guardia, and Sergio Armenta. The ways to the trace level analysis in infrared spectroscopy. *Anal. Methods*, 3:43–52, 2011.

[62] P. Griffiths and J.A. De Haseth. *Fourier Transform Infrared Spectrometry*. Chemical Analysis: A Series of Monographs on Analytical Chemistry and Its Applications. Wiley, 2007. ISBN 9780470106297.

[63] Peter R. Griffiths. "Trading rules" in infrared Fourier transform spectroscopy. *Analytical Chemistry*, 44(11):1909–1913, 1972.

[64] M. L. Gutiérrez-Coronado, E. Acedo-Félix, and A. I. Valenzuela-Quintanar. Industria del bacanora y su proceso de elaboración. *Ciencia y Tecnología Alimentaria*, 5:394–404, 2007.

[65] Maryam Hajbabaei, Georgios Karavalakis, J. Wayne Miller, Mark Villela, Karen Huaying Xu, and Thomas D. Durbin. Impact of olefin content on criteria and toxic emissions from modern gasoline vehicles. *Fuel*, (0):–, 2012. ISSN 0016-2361.

[66] K. Harding. *Handbook of Optical Dimensional Metrology*. Series in Optics and Optoelectronics. Taylor & Francis, 2013. ISBN 9781439854815.

[67] P. Hariharan. *Optical Interferometry*. Elsevier, San Diego, second edition, 2003.

[68] P. Hariharan. *Basics of Interferometry*. Elsevier, second edition, 2007.

[69] D. Harvey. *Modern Analytical Chemistry*. McGraw-Hill, 1999. ISBN 9780072375473.

[70] A.W. Hayes. *Principles and Methods of Toxicology, Fifth Edition*. Pharmacology and Toxicology. Taylor & Francis, 2007. ISBN 9780849337789.

[71] P. Hodges. *Hydraulic Fluids*. Elsevier Science, 1996. ISBN 9780080523897.

[72] B. Holtsnider and B.D. Jaffe. *IT Manager's Handbook: Getting your new job done*. IT Manager's Handbook Series. Elsevier Science, 2010. ISBN 9780080465746.

[73] Jirí Homola. Sensors based on spectroscopy of guided waves. In F. Baldini, A.N. Chester, J. Homola, and S. Martellucci, editors, *Optical Chemical Sensors*, volume 224 of *NATO Science Series II: Mathematics, Physics and Chemistry*, pages 179–192. Springer Netherlands, 2006. ISBN 978-1-4020-4609-4.

[74] Jirí Homola, Sinclair S. Yee, and David Myszka. Chapter 4 - surface plasmon resonance biosensors. In Frances S. Ligler and Chris Rowe Taitt, editors, *Optical Biosensors (Second Edition)*, pages 185 – 242. Elsevier, Amsterdam, second edition edition, 2008.

[75] HORIBA Scientific. Horiba Fluorescence Application Notes, 2013. URL `http://www.horiba.com/us/en/scientific/products/fluorescence-spectroscopy/application-notes/`. Accessed: March 2013.

[76] HORIBA Scientific. HORIBA Raman Application Notes and Articles, 2013. URL `http://www.horiba.com/scientific/products/raman-spectroscopy/applications/`. Accessed: August 2013.

[77] HORIBA Scientific. HORIBA Raman Microscopes, 2014. URL `http://www.horiba.com/scientific/products/raman-spectroscopy/raman-spectrometers/raman-microscopes/`. Accessed: January 2014.

[78] J. Irudayaraj and C. Reh. *Nondestructive Testing of Food Quality*. Institute of Food Technologists Series. Wiley, 2008. ISBN 9780470388280.

[79] John James. *Spectrograph Design Fundamentals*. Cambridge University Press, 2007. ISBN 9781139462792.

[80] E. Jorgensen. *Ecotoxicology*. Elsevier Science, 2010. ISBN 9780444536297.

[81] Carlos R. Kaiser, Joana L. Borges, Anderson R. dos Santos, Débora A. Azevedo, and Luiz A. D'Avila. Quality control of gasoline by 1H NMR: Aromatics, olefinics, paraffinics, and oxygenated and benzene contents. *Fuel*, 89(1):99 – 104, 2010. ISSN 0016-2361.

[82] Kaiser Optical Systems, Inc. Raman Applications / Solutions , 2013. URL `http://www.kosi.com/Raman_Spectroscopy/applications.php?ss=100`. Accessed: August 2013.

[83] J.J. Kaluarachchi. *Groundwater Contamination by Organic Pollutants: Analysis and Remediation*. ASCE manuals and reports on engineering practice. American Society of Civil Engineers, 2001. ISBN 9780784405277.

[84] Jyrki Kauppinen and Jari Partanen. *Fourier Transforms in Spectroscopy*. Wiley-VCH Verlag GmbH, Berlin, first edition, 2001.

[85] A. Keens and N. Rapp. Method of obtaining an optical ft spectrum / US patent 5,923,422, February 1998. Accessed: January 2014.

[86] M. Khanna, J. Scheffran, and D. Zilberman. *Handbook of Bioenergy Economics and Policy*. Natural Resource Management and Policy. Springer, 2009. ISBN 9781441903693.

[87] V. Koubová, E. Brynda, L. Karasová, J. Skvor, J. Homola, J. Dostálek, P. Tobiska, and J. Rosický. Detection of foodborne pathogens using surface plasmon resonance biosensors. *Sensors and Actuators B: Chemical*, 74(1-3):100 – 105, 2001.

[88] B. Kwabi-Addo and T.L. Lindstrom. *Cancer Causes and Controversies: Understanding Risk Reduction and Prevention*. ABC-CLIO, 2011. ISBN 9780313379284.

[89] Dirk W. Lachenmeier, Eva-Maria Sohnius, Rainer Attig, and Mercedes G. López. Quantification of selected volatile constituents and anions in mexican agave spirits (tequila, mezcal, sotol, bacanora). *Journal of Agricultural and Food Chemistry*, 54(11):3911–3915, 2006. doi: 10.1021/jf060094h.

[90] J.R. Lakowicz. *Principles of Fluorescence Spectroscopy*. Springer London, Limited, 2009. ISBN 9780387463124.

[91] C. Lalanne. *Mechanical Vibration and Shock Analysis, Sinusoidal Vibration*. Mechanical Vibration and Shock Analysis. Wiley, 2013. ISBN 9781118618905.

[92] P. Larkin. *Infrared and Raman Spectroscopy; Principles and Spectral Interpretation*. Elsevier Science, 2011. ISBN 9780123870186.

[93] Ian R. Lewis and Howell G.M. Edwards. *Handbook of Raman Spectroscopy: From the Research Laboratory to the Process Line*. Marcel Dekker, New York, 2001.

[94] E. Li-Chan. *Macromolecular Interactions of Food Proteins Studied by Raman Spectroscopy*, chapter 3, pages 15–36. American Chemical Society, 1996.

[95] E. Li-Chan, J. Chalmers, and P. Griffiths. *Applications of Vibrational Spectroscopy in Food Science*. Number v. 1. John Wiley & Sons, 2011. ISBN 9780470742990.

[96] E.C.Y. Li-Chan. The applications of Raman spectroscopy in food science. *Trends in Food Science & Technology*, 7(11):361 – 370, 1996.

[97] Eunice C. Y. Li-Chan and Judy C. K. Chan. Production of lactoferricin and other cationic peptides from food grade bovine lactoferrin with various iron saturation levels. *Journal of Agricultural and Food Chemistry*, 55(2):493–501, 2007.

[98] Eunice C. Y. Li-Chan, Nooshin Alizadeh-Pasdar, and Shuryo Nakai. Principal component similarity analysis of Raman spectra to study the effects of pH, heating, and k-Carrageenan on Whey protein structure. *Journal of Agricultural and Food Chemistry*, 50(21):6042–6052, 2002.

[99] Eunice C.Y. Li-Chan and Soo-Yeun Moon. Assessment of added ingredient effect on interaction of simulated beef flavour and soy protein isolate by gas chromatography, spectroscopy and descriptive sensory analysis. *Food Research International*, 40(10):1227 – 1238, 2007.

[100] M. Lippmann. *Environmental Toxicants: Human Exposures and Their Health Effects*. Wiley, 2009. ISBN 9780470442883.

[101] P.M. Lugt. *Grease Lubrication in Rolling Bearings*. Tribology in Practice Series. Wiley, 2012. ISBN 9781118483978.

[102] T.R. Lynch. *Process Chemistry of Lubricant Base Stocks*. Chemical Industries. Taylor & Francis, 2007. ISBN 9781420020540.

[103] Lotte B. Lyndgaard, Frans van den Berg, and Anna de Juan. Quantification of paracetamol through tablet blister packages by Raman spectroscopy and multivariate curve resolution-alternating least squares. *Chemometrics and Intelligent Laboratory Systems*, 125(0):58 – 66, 2013.

[104] P. Maddaloni, M. Bellini, and P. De Natale. *Laser-Based Measurements for Time and Frequency Domain Applications: A Handbook*. Series in Optics and Optoelectronics. Taylor & Francis, 2013. ISBN 9781439841518.

[105] S. Majumdar. *Oil Hydraulic Systems: Principles and Maintenance*. McGraw-Hill, 2002. ISBN 9780074637487.

[106] T. Mang and W. Dresel. *Lubricants and Lubrication*. Wiley, 2007. ISBN 9783527610334.

[107] G. Martínez-López, D. Luna-Moreno, D. Monzón-Hernández, and R. Valdivia-Hernández. Optical method to differentiate tequilas based on angular modulation surface plasmon resonance. *Optics and Lasers in Engineering*, 49(6):675 – 679, 2011.

[108] B. McCarty. *Learning Red Hat Linux*. O'Reilly, 2003. ISBN 9780596004699.

[109] Richard L. McCreery. *Raman Spectroscopy for Chemical Analysis*. Wiley-Interscience, New York, 2000.

[110] Richard L. McCreery. *Photometric Standards for Raman Spectroscopy*. John Wiley & Sons, Ltd, 2002. ISBN 9780470027325.

[111] McCreery Research Group. Standard Spectra - Raman Materials, 2012. URL `http://www.chem.ualberta.ca/~mccreery/ramanmaterials.html`. Accessed: September 2013.

[112] Philip Mercurio, Kathryn A. Burns, and Joanne Cavanagh. Testing the ecotoxicology of vegetable versus mineral based lubricating oils: 2. induction of mixed function oxidase enzymes in barramundi, lates calcarifer, a tropical fish species. *Environmental Pollution*, 129(2):175 – 182, 2004. ISSN 0269-7491.

[113] Satyendra K. Mishra and Banshi D. Gupta. Surface plasmon resonance based fiber optic pH sensor utilizing Ag/ITO/Al/hydrogel layers. *Analyst*, 138:2640–2646, 2013.

[114] Valentina Morandi, Franco Marabelli, Vincenzo Amendola, Moreno Meneghetti, and Davide Comoretto. Light Localization Effect on the Optical Properties of Opals Doped with Gold Nanoparticles. *The Journal of Physical Chemistry C*, 112(16):6293–6298, 2008. doi: 10.1021/jp711040r.

[115] R.M. Mortier, M.F. Fox, and S.T. Orszulik. *Chemistry and Technology of Lubricants*. SpringerLink: Springer e-Books. Springer, 2011. ISBN 9781402086625.

[116] National Center for Biotechnology Information (NCBI). Benzene - Compound Summary (CID 241), September 2004. URL http://pubchem.ncbi.nlm.nih.gov/summary/summary.cgi?cid=241&loc=ec_rcs. Accessed: October 2013.

[117] National Center for Biotechnology Information (NCBI). Cyclohexane - Compound Summary (CID 8078), September 2004. URL http://pubchem.ncbi.nlm.nih.gov/summary/summary.cgi?cid=8078&loc=ec_rcs. Accessed: October 2013.

[118] National Center for Biotechnology Information (NCBI). Toluene - Compound Summary (CID 1140), September 2004. URL http://pubchem.ncbi.nlm.nih.gov/summary/summary.cgi?cid=1140&loc=ec_rcs. Accessed: October 2013.

[119] National Institute of Advanced Industrial Science and Technology (AIST / SDBS). Spectral Database for Organic Compounds (SDBS), 2013. URL http://sdbs.riodb.aist.go.jp/sdbs/cgi-bin/direct_frame_top.cgi. Accessed: September 2013.

[120] National Institute of Standards and Technology (NIST). NIST Chemistry WebBook - Benzene, 2011. URL http://webbook.nist.gov/cgi/cbook.cgi?ID=C71432&Mask=800. Accessed: January 2014.

[121] David A. Naylor, Trevor R. Fulton, Peter W. Davis, Ian M. Chapman, Brad G. Gom, Locke D. Spencer, John V. Lindner, Nathan E. Nelson-Fitzpatrick, Margaret K. Tahic, and Gary R. Davis. Data processing pipeline for a time-sampled imaging Fourier transform spectrometer. *Proc. SPIE*, 5546:61–72, 2004. doi: 10.1117/12.560096.

[122] Yasushi Numata and Hiroyuki Tanaka. Quantitative analysis of quercetin using Raman spectroscopy. *Food Chemistry*, 126(2):751 – 755, 2011.

[123] Yasushi Numata, Yoshiyuki Iida, and Hiroyuki Tanaka. Quantitative analysis of alcohol-water binary solutions using Raman spectroscopy. *Journal of Quantitative Spectroscopy and Radiative Transfer*, 112(6):1043 – 1049, 2011.

[124] Ocean Optics, Inc. North American Retail Price List, June 2013. URL http://www.oceanoptics.com/pricelist.pdf. Accessed: February 2014.

[125] Office of Pollution Prevention and Toxics U.S. Environmental Protection Agency (EPA). Chemicals in the environment: Methanol (CAS NO. 67-56-1), August 1997. URL http://www.epa.gov/chemfact/f_methan.txt. Accessed: February 2014.

[126] Flavia C.C. Oliveira, Christian R.R. Brandão, Hugo F. Ramalho, Leonardo A.F. da Costa, Paulo A.Z. Suarez, and Joel C. Rubim. Adulteration of diesel/biodiesel blends by vegetable oil as determined by Fourier transform (FT) near infrared spectrometry and FT-Raman spectroscopy. *Analytica Chimica Acta*, 587(2):194 – 199, 2007.

[127] V. Ortega Clavero, A. Weber, W. Schröder, P. Meyrueis, and N. Javahiraly. Detailed spectral monitoring of different combustible blends based on gasoline, ethanol and methanol using FT-Raman spectroscopy. *Environmental Biotechnology*, 8(1):1 – 6, 2012. ISSN 1734-4964.

[128] V. Ortega Clavero, A. Weber, W. Schröder, P. Meyrueis, and N. Javahiraly. Comparative spectral analysis of commercial fuel-ethanol blends using a low-cost prototype ft-raman spectrometer.

Proc. SPIE 8368, Photonic Applications for Aerospace, Transportation, and Harsh Environment III, 83680E, pages 83680E–83680E–7, 2012.

[129] V. Ortega Clavero, Andreas W., W. Schröder, N. Javahiraly, and P. Meyrueis. Spectral observation of fuel additives in gasoline-ethanol blends using a fourier-transform raman spectrometer prototype. *Proc. SPIE 8720 Photonic Applications for Aerospace, Commercial, and Harsh Environments IV*, (4):8720–26, 2013.

[130] V. Ortega Clavero, A. Weber, W. Schröder, D. Curticapean, N. Javahiraly, and P. Meyrueis. Spectral monitoring of toluene and ethanol in gasoline blends using fourier-transform raman spectroscopy. *Proc. SPIE Optical Measurement Systems for Industrial Inspection VIII*, 8788(8):8788–112, 2013.

[131] V. Ortega Clavero, A. Weber, W. Schröder, D. Curticapean, P. Meyrueis, and N. Javahiraly. Spectral monitoring of toluene and ethanol in gasoline blends using Fourier-Transform Raman spectroscopy. *Proc. SPIE*, 8788:878834–878834–8, 2013.

[132] V. Ortega Clavero, A. Weber, W. Schröder, N. Javahiraly, and P. Meyrueis. Use of the characteristic Raman lines of toluene (C7H8) as reference on the analysis of gasoline blends. *Environmental Biotechnology*, 9(2):under review, 2013. ISSN 1734-4964.

[133] V. Ortega Clavero, A. Weber, W. Schröder, P. Meyrueis, and N. Javahiraly. Qualitative and Quantitative Spectral Analysis of Binary Gasoline-Ethanol Blends Using a Low-Cost FT-Raman Spectrometer Prototype. *Lasers in Engineering*, 25(3-4):247–253, 2013. ISSN 0898-1507.

[134] V. Ortega Clavero, A. Weber, W. Schröder, D. Curticapean, P. Meyrueis, and N. Javahiraly. Monitoring of the molecular structure of lubricant oil using a FT-Raman spectrometer prototype. *Proc. SPIE Photonics Europe*, 9141:9141–71, 2014.

[135] M. Palmer. *Guide to UNIX Using Linux*. Networking (Course Technology). Cengage Learning, 2007. ISBN 9781418837235.

[136] M. Palocz-Andresen. *Decreasing Fuel Consumption and Exhaust Gas Emissions in Transportation: Sensing, Control and Reduction of Emissions*. Green Energy and Technology. Springer, 2012. ISBN 9783642119767.

[137] D.L. Pavia. *Introduction to Spectroscopy*. International student edition. Brooks/Cole, 2009. ISBN 9780495114789.

[138] José Luis Pérez Pavón, Miguel del Nogal Sánchez, Ma Esther Fernández Laespada, Carmelo García Pinto, and Bernardo Moreno Cordero. Determination of naphthalene and total methylnaphthalenes in gasoline using direct injection-mass spectrometry. *Talanta*, 72(1):256 – 262, 2007. ISSN 0039-9140.

[139] W. D. Perkins. Fourier transform infrared spectroscopy. Part II. Advantages of FT-IR. *Journal of Chemical Education*, 64(11):A269, 1987.

[140] C. Perrotton, N. Javahiraly, M. Slaman, B. Dam, and P. Meyrueis. Fiber optic surface plasmon resonance sensor based on wavelength modulation for hydrogen sensing. *Opt. Express*, 19(S6):A1175–A1183, Nov 2011.

[141] Cedric Perrotton, Martin Slaman, Nicolas Javahiraly, Herman Schreuders, Bernard Dam, and Patrick Meyrueis. Wavelength response of a surface plasmon resonance palladium-coated optical fiber sensor for hydrogen detection. *Optical Engineering*, 50(1):014403–014403–8, 2011.

[142] Cédric Perrotton, Ruud. J. Westerwaal, Nicolas Javahiraly, Martin Slaman, Herman Schreuders, Bernard Dam, and Patrick Meyrueis. A reliable, sensitive and fast optical fiber hydrogen sensor based on surface plasmon resonance. *Opt. Express*, 21(1):382–390, Jan 2013.

[143] Y. Picó. *Chemical Analysis of Food: Techniques and Applications*. Chemical Analysis of Food: Techniques and Applications. Academic Press, 2012. ISBN 9780123848628.

[144] M Piliarik, J Homola, Z Mańíková, and J Ctyroký. Surface plasmon resonance sensor based on a single-mode polarization-maintaining optical fiber. *Sensors and Actuators B: Chemical*, 90(1-3):236 – 242, 2003.

[145] L.Z. Pillon. *Surface Activity of Petroleum Derived Lubricants*. Chemical industries. Taylor & Francis, 2010. ISBN 9781439803417.

[146] V.R. Preedy. *Beer in Health and Disease Prevention*. Elsevier Science, 2011. ISBN 9780080920498.

[147] T. Proulx. *Rotating Machinery, Structural Health Monitoring, Shock and Vibration, Volume 5: Proceedings of the 29th IMAC, A Conference on Structural Dynamics, 2011*. Conference Proceedings of the Society for Experimental Mechanics Series. Springer, 2011. ISBN 9781441994288.

[148] Paul D.A. Pudney and Thomas M. Hancewicz. *The Role of Confocal Raman Spectroscopy in Food Science*. John Wiley & Sons, Ltd, 2006. ISBN 9780470027325.

[149] Qing Ye, Qinfeng Xu, Yongai Yu, Ronghui Qu, and Zujie Fang. Rapid and quantitative detection of ethanol proportion in ethanol-gasoline mixtures by Raman spectroscopy. *Optics Communications*, 282(18):3785 – 3788, 2009. ISSN 0030-4018.

[150] Qing Ye, Qinfeng Xu, Haiwen Cai, and Ronghui Qu. Determination of methanol ratio in methanol-doped biogasoline by a fiber Raman sensing system. *Sensors and Actuators B: Chemical*, 146(1):75 – 78, 2010.

[151] L.A. Quinchia, M.A. Delgado, C. Valencia, J.M. Franco, and C. Gallegos. Viscosity modification of different vegetable oils with (EVA) copolymer for lubricant applications. *Industrial Crops and Products*, 32(3):607 – 612, 2010. ISSN 0926-6690.

[152] C. V. Raman. A new radiation. *Indian Journal of Physics*, 2:387 – 398, 1928.

[153] C. V. Raman and K. S. Krishnan. A new type of secondary radiation. *Nature*, 121:501 – 502, 1928.

[154] J. Ries, T. Weidemann, and P. Schwille. 2.11 fluorescence correlation spectroscopy. In Editor in Chief: Edward H. Egelman, editor, *Comprehensive Biophysics*, pages 210 – 245. Elsevier, Amsterdam, 2012. ISBN 978-0-08-095718-0.

[155] J.W. Robinson, E.M.S. Frame, and G.M. Frame. *Undergraduate Instrumental Analysis, Sixth Edition*. Taylor & Francis, 2004. ISBN 9780849306501.

[156] Voirrey L. Robinson, Christopher A. Hunter, and Michael D. Ward. An improved synthesis, crystal structures, and metallochromism of salts of [ru(tolyl-terpy)(cn)3]-. *Inorganica Chimica Acta*, 363 (12):2938 – 2944, 2010. ISSN 0020-1693.

[157] E. J. Rosenbaum. Raman spectroscopy. *Analytical Chemistry*, 28(4):596–597, 1956.

[158] Joel C. Rubim, Leornardo S. Mendes, Flavia C.C. Oliveira, and Paulo A.Z. Suarez. Determination of ethanol in fuel ethanol and beverages by Fourier transform (FT)-near infrared and FT-Raman spectrometries. *Analytica Chimica Acta*, 493(2):219 – 231, 2003.

[159] Vidal Salazar Solano and Alejandro Mungaray Lagarda. La industria informal del mezcal bacanora. *Estudios sociales (Hermosillo, Son.)*, 17:163 – 198, 06 2009. ISSN 0188-4557.

[160] B.E.A. Saleh and M.C. Teich. *Fundamentals of Photonics*. Wiley Series in Pure and Applied Optics. Wiley, 2007. ISBN 9780471358329.

[161] R. Salzer and H.W. Siesler. *Infrared and Raman Spectroscopic Imaging*. Wiley, 2009. ISBN 9783527626748.

[162] F. Sánchez-Teyer, S. Moreno-Salazar, M. Esqueda, A. Barraza, and M.L. Robert. Genetic variability of wild Agave angustifolia populations based on AFLP: A basic study for conservation. *Journal of Arid Environments*, 73(6-7):611 – 616, 2009.

[163] V. Saptari. *Fourier Transform Spectroscopy Instrumentation Engineering*. SPIE Press monograph. SPIE Optical Engineering Press, 2004. ISBN 9780819451644.

[164] S. Sasic and S. Ekins. *Pharmaceutical Applications of Raman Spectroscopy*. Wiley Series on Technologies for the Pharmaceutical Industry, v.2. Wiley, 2008. ISBN 9780470225875.

[165] Slobodan Sasic. *Pharmaceutical Applications of Raman Spectroscopy*. Wiley, New Jersey, 2008.

[166] R.Ysacc Sato-Berrú, Jorge Medina-Valtierra, Cirilo Medina-Gutiérrez, and Claudio Frausto-Reyes. Quantitative {NIR} Raman analysis in liquid mixtures. *Spectrochimica Acta Part A: Molecular and Biomolecular Spectroscopy*, 60(10):2225 – 2229, 2004.

[167] M. Sauer, J. Hofkens, and J. Enderlein. *Handbook of Fluorescence Spectroscopy and Imaging: From Ensemble to Single Molecules*. Wiley, 2010. ISBN 9783527633524.

[168] R.B.Richard B.M. Schasfoort and Anna.J. Tudos. *Handbook Of Surface Plasmon Resonance*. Royal Society of Chemistry, 2008. ISBN 9780854042678.

[169] Robert A. Schoonheydt. UV-VIS-NIR spectroscopy and microscopy of heterogeneous catalysts. *Chem. Soc. Rev.*, 39:5051–5066, 2010.

[170] SCHOTT Corporation. Optical Glass, April 2013. URL `http://www.schott.com/advanced_optics/english/download/schott-optical-glass-collection-datasheets-february-2014-eng.pdf`. Accessed: February 2014.

[171] Secretaria de Economía - Gobierno del Estado de Sonora. NORMA Oficial Mexicana NOM-168-SCFI-2004, Bebidas alcohólicas-Bacanora-Especificaciones de elaboración, envasado y etiquetado, December 2005.

[172] Secretaria de Gobernación. NORMA Oficial Mexicana NOM-006-SCFI-2012, Bebidas alcohólicas-Tequila-Especificaciones., December 2012. URL {http://www.dof.gob.mx/nota_detalle.php?codigo=5282165&fecha=13/12/2012}.

[173] H.M. Shapiro. *Practical Flow Cytometry*. Wiley, 2005. ISBN 9780471434030.

[174] G.G. Shepherd. *Spectral Imaging of the Atmosphere*. International Geophysics. Elsevier Science, 2002. ISBN 9780080517513.

[175] H.W. Siesler, Y. Ozaki, S. Kawata, and H.M. Heise. *Near-Infrared Spectroscopy: Principles, Instruments, Applications*. NetLibrary, Inc. Wiley, 2008. ISBN 9783527612673.

[176] A. Simon, J. Gast, and A. Keens. Fourier spectrometer / US patent 5,309,217, May 1994. Accessed: July 2013.

[177] B.K. Simpson. *Food Biochemistry and Food Processing*. Wiley, 2012. ISBN 9781118308042.

[178] Sarika Singh, Satyendra K. Mishra, and Banshi D. Gupta. Sensitivity enhancement of a surface plasmon resonance based fibre optic refractive index sensor utilizing an additional layer of oxides. *Sensors and Actuators A: Physical*, 193(0):136 – 140, 2013.

[179] R.A. Smiley and H.L. Jackson. *Chemistry and the Chemical Industry: A Practical Guide for Non-Chemists*. Taylor & Francis, 2002. ISBN 9781420031775.

[180] B.C. Smith. *Fundamentals of Fourier Transform Infrared Spectroscopy, Second Edition*. Taylor & Francis, 2011. ISBN 9781420069303.

[181] Ewen Smith and Geoffrey Dent. *Modern Raman Spectroscopy: A Practical Approach*. Wiley, West Sussex, 2005.

[182] Sachin K. Srivastava, Roli Verma, and Banshi D. Gupta. Surface plasmon resonance based fiber optic sensor for the detection of low water content in ethanol. *Sensors and Actuators B: Chemical*, 153(1):194 – 198, 2011.

[183] T.L. Sterling. *Beowulf Cluster Computing with Linux*. Scientific and Computational Engineering Series. MIT Press, 2002. ISBN 9780262692748.

[184] J A Stone, J E Decker, P Gill, P Juncar, A Lewis, G D Rovera, and M Viliesid. Advice from the CCL on the use of unstabilized lasers as standards of wavelength: the helium-neon laser at 633 nm. *Metrologia*, 46(1):11, 2009.

[185] Ernane Ribeiro Streva, Vanya Márcia Duarte Pasa, and José Ricardo Sodré. Aging effects on gasoline-ethanol blend properties and composition. *Fuel*, 90(1):215 – 219, 2011. ISSN 0016-2361.

[186] B.H. Stuart. *Infrared Spectroscopy: Fundamentals and Applications*. Analytical Techniques in the Sciences (AnTs) *. Wiley, 2004. ISBN 9780470011133.

[187] Mark C. Abrams Sumner P. Davis and James W. Brault. *Fourier Transform Spectrometry*. Academic Press, first edition, 2001.

[188] Raymond Wai-Yin Sun and Chi-Ming Che. The anti-cancer properties of gold(iii) compounds with dianionic porphyrin and tetradentate ligands. *Coordination Chemistry Reviews*, 253(11-12):1682–1691, 2009. ISSN 0010-8545.

[189] H.H. Szmant. *Organic Building Blocks of the Chemical Industry*. Wiley, 1989. ISBN 9780471855453.

[190] Roman Szostak and Sylwester Mazurek. A quantitative analysis of liquid hydrocarbon mixtures on the basis of FT-Raman spectra registered under unstable conditions. *Journal of Molecular Structure*, 704(1-3):235 – 245, 2004.

[191] Rana Tabassum, Satyendra K. Mishra, and Banshi D. Gupta. Surface plasmon resonance-based fiber optic hydrogen sulphide gas sensor utilizing Cu-ZnO thin films. *Phys. Chem. Chem. Phys.*, pages –, 2013.

[192] Gary R. Takeoka and Susan E. Ebeler. *Progress in Authentication of Food and Wine*, chapter 2, pages 3–11. American Chemical Society, 011.

[193] ThermoFisher Scientific. Application Note: 50771. Advantages of Fourier-Transform Near-Infrared Spectroscopy, 2006. URL `http://www.thermoscientific.com/ecomm/servlet/techresource?resourceId=89646&storeId=11152&from=search#`. Accessed: July 2013.

[194] ThermoFisher Scientific. 2012 Annual Report, February 2013. URL `http://www.sec.gov/Archives/edgar/data/97745/000009774513000007/tmok12.htm`. Document of the U.S. Securities and Exchange Commission (SEC). Accessed: February 2014.

[195] ThermoFisher Scientific. 2012 Annual Report, February 2013. URL `http://ir.thermofisher.com/files/doc_financials/annual/TMO_2012AnnualReport.pdf`. Accessed: February 2014.

[196] L. Thévenaz. *Advanced Fiber Optics: Concepts and Technology*. Engineering sciences. EFPL Press, 2011. ISBN 9782940222438.

[197] Michael Thompson, Stephen L R Ellison, and Roger Wood. Harmonized guidelines for single-laboratory validation of methods of analysis. *Pure and Applied Chemistry*, 74(5):835–855, 2002.

[198] Nancy L Thompson, Alena M Lieto, and Noah W Allen. Recent advances in fluorescence correlation spectroscopy. *Current Opinion in Structural Biology*, 12(5):634 – 641, 2002. ISSN 0959-440X.

[199] J. Toedt, D. Koza, and K. Van Cleef-Toedt. *Chemical Composition of Everyday Products*. ABC-Clio ebook. Greenwood Press, 2005. ISBN 9780313325793.

[200] G.E. Totten. *Handbook of Lubrication and Tribology: Volume I Application and Maintenance, Second Edition*. Handbook of Lubrication and Tribology. Taylor & Francis, 2006. ISBN 9781420003840.

[201] Md. Jamal Uddin, Nicolas DiCesare, and Joseph R. Lakowicz. Photoinduced electron transfer quenching and sugar effects on the electrostatic interaction between an anionic Ru(II) complex and cationic bipyridinium derivatives functionalized with boronic acids. *Inorganica Chimica Acta*, 381 (0):104 – 110, 2012. ISSN 0020-1693.

[202] UNITED NATIONS ENVIRONMENT PROGRAMME. ENVIRONMENTAL HEALTH CRITERIA 196 - Methanol, 1997. URL `http://www.inchem.org/documents/ehc/ehc/ehc196.htm`. Accessed: February 2014.

[203] United States Environmental Protection Agency. Clean Air Act. 42 USC 7545 - Regulation of fuels , 2012. URL http://www.law.cornell.edu/uscode/text/42/7545. Accessed: August 2013.

[204] US Environmental Protection Agency (EPA). Benzene (CASRN 71-43-2), January 2000. URL http://www.epa.gov/iris/subst/0276.htm. Accessed: January 2014.

[205] US Environmental Protection Agency (EPA). Toluene 108-88-3 Hazard Summary, July 2012. URL http://www.epa.gov/ttn/atw/hlthef/toluene.html. Accessed: January 2014.

[206] U.S. National Library of Medicine - Toxicology Data Network (TOXNET). Benzene - Human Health Effects, December 2011. URL http://toxnet.nlm.nih.gov/cgi-bin/sis/search/r?dbs+hsdb:@term+@rn+@rel+71-43-2. Accessed: January 2014.

[207] R.P. Van Duyne, L.B. Sagle, L.K. Ruvuna, and J.A. Ruemmele. Advances in localized surface plasmon resonance spectroscopy biosensing. *Nanomedicine (Lond)*, 6(8):1447–62, 2011.

[208] Nanna Viereck, Tina Salomonsen, Frans van den Berg, and Soren Balling Engelsen. *Raman applications in food analysis*, chapter 8, pages 199–224. Wiley, 2008.

[209] O. Wada. *Optoelectronic Integration: Physics, Technology and Applications: Physics, Technology, and Applications*. The Springer International Series in Engineering and Computer Science. Springer US, 1994. ISBN 9780792394532.

[210] Mark Wall, Joe Hodkiewicz, and Patricia Henson. Polymorph Characterization using Raman Spectroscopy in High Throughput Crystallization Studies, 2007. ThermoFisher Scientific, Application Note: 50873.

[211] Siegfried Wartewig. *IR and Raman Spectroscopy: Fundamental Processing*. Wiley-VCH, Weinheim, first edition, 2003.

[212] John Waswa, Joseph Irudayaraj, and Chitrita DebRoy. Direct detection of E. Coli O157:H7 in selected food systems by a surface plasmon resonance biosensor. *LWT - Food Science and Technology*, 40(2):187 – 192, 2007.

[213] Andreas Weber. Dipl. Entwicklung der Ansteuerung und Signalverarbeitung für interferometrische Faserkreisel und dessen Anwendung zur Messung des Faraday-Effekts. University of Applied Sciences Offenburg, August 2007.

[214] M.N. Wernick and J.N. Aarsvold. *Emission Tomography: The Fundamentals of PET and SPECT*. Elsevier Science, 2004. ISBN 9780080521879.

[215] Andreas Willing. Lubricants based on renewable resources - an environmentally compatible alternative to mineral oil products. *Chemosphere*, 43(1):89 – 98, 2001. ISSN 0045-6535.

[216] Dominik Wöll, Bente M. I. Flier, Moritz Baier, Johannes Huber, Klaus Mullen, Stefan Mecking, and Andreas Zumbusch. Single molecule fluorescence microscopy investigations on heterogeneity of translational diffusion in thin polymer films. *Phys. Chem. Chem. Phys.*, 13:1770–1775, 2011. doi: 10.1039/C0CP01801E.

[217] Dominik Wöll, Bente M. I. Flier, Moritz C. Baier, Johannes Huber, Klaus Müllen, Stefan Mecking, and Andreas Zumbusch. Heterogeneous diffusion in thin polymer films as observed by high-temperature single-molecule fluorescence microscopy. *Journal of the American Chemical Society*, 134(1):480–488, 2012.

[218] Dominik Wöll, Beate Stempfle, Maren Dill, Martin J. Winterhalder, and Klaus Mullen. Single molecule diffusion and its heterogeneity during the bulk radical polymerization of styrene and methyl methacrylate. *Polym. Chem.*, 3:2456–2463, 2012. doi: 10.1039/C2PY20268A.

[219] S. Yin, P.B. Ruffin, and F.T.S. Yu. *Fiber Optic Sensors, Second Edition*. Optical Science and Engineering. Taylor & Francis, 2010. ISBN 9781420053661.

[220] Jong Seol Yuk, Sun-Ju Yi, Se-Hui Jung, Jeong-A Han, Young-Myeong Kim, and Kwon-Soo Ha. Ex situ analysis of protein arrays by SPR spectroscopy for the application of immunosensors. *Journal of the Korean Physical Society*, 44(4):967 – 972, 2004.

[221] C. Zhang. *Fundamentals of Environmental Sampling and Analysis*. Wiley, 2007. ISBN 9780470120675.

[222] Jian Zhang, Yi Fu, and Joseph R. Lakowicz. Enhanced Förster resonance energy transfer (FRET) on a single metal particle. *The Journal of Physical Chemistry C*, 111(1):50–56, 2007. doi: 10.1021/jp062665e.

[223] Jian Zhang, Yi Fu, Ge Li, Kazimierz Nowaczyk, Richard Y. Zhao, and Joseph R. Lakowicz. Direct observation to chemokine receptor 5 on T-lymphocyte cell surface using fluorescent metal nanoprobes. *Biochemical and Biophysical Research Communications*, 400(1):111 – 116, 2010. ISSN 0006-291X.

Declaration

I herewith declare that I have produced this document without the prohibited assistance of third parties and without making use of aids other than those specified; notions taken over directly or indirectly from other sources have been identified as such. This paper has not previously been presented in identical or similar form to any other foreign examination board. The thesis work was conducted from November 2010 to April 2014 under the supervision of Prof. Patrick Meyrueis (University of Strasbourg, Thesis Director) and Prof. Werner Schröder (Offenburg University of Applied Sciences, Thesis Co-Director).

Illkirch, France; Offenburg, Germany.

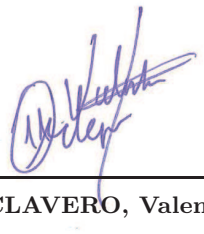

July 11th, 2014

ORTEGA CLAVERO, Valentin **Date**